SLOVAK GEOLOGICAL MAGAZINE

SLOVAK GEOLOGICAL MAGAZINE

Periodical journal of Geological Survey of Slovak Republic is a quarterly presenting the results of investigation and researches in a wide range of topics:

- regional geology and geological maps
- lithology and stratigraphy
- petrology and mineralogy
- paleontology
- geochemistry and isotope geology
- geophysics and deep structure
- geology of deposits and metallogeny

- tectonics and structural geology
- hydrogeology and geothermal energy
- environmental geochemistry
- engineering geology and geotechnology
- geological factors of the environment
- petroarcheology

The journal is focused on problems of the Alpine-Carpathian region.

3902001018511

SLOVAK GEOLOGICAL MAGAZINE

SGEOLOGICAL MAGAZINE

3-4/2002

Ore mineralization on the Pezinok – Trojárová deposit in the Malé Karpaty Mts., Slovakia: mineralogical and geochemical characterization

MARTIN CHOVAN[1], STANISLAVA TRTÍKOVÁ [2], VOJTECH VILINOVIČ[3], MILOŠ KHUN[4], PETER HANAS[5]

[1]Dept. of Mineralogy and Petrology, Faculty of Natural Sciences, Comenius University, Mlynská dolina G, 842 15 Bratislava
[2]Geological Institute, Slovak Academy of Sciences, Severná 5, 974 01 Banská Bystrica
[3]GEOTEST Bratislava, Ltd., Vlčie hrdlo, 821 07 Bratislava.
[4]Dept. of Geochemistry, Faculty of Natural Sciences, Comenius University, Mlynská Dolina G, 842 15 Bratislava
[5]Slovak Ministry of Environment, Nám. Ľ. Štúra 1, 812 35 Bratislava.

Abstract: Ore mineralization on the Trojárová deposit is hosted in metamorphosed black shales, embraced by complex of metabasics and metatuffs. Following ore mineralizations were discerned: 1) metamorphosed exhalation-sedimentary pyrite mineralization, 2) molybdenite mineralization in granitoides; and 3) hydrothermal Sb-Fe-As-Au mineralization. Geochemical investigation of ore bearing black shales revealed intensive pyritization of black shales, close association of Sb-Fe-As-Au sulphidic mineralization with carbonates and Au binding to arsenopyrite. Five successive stages of hydrothermal Sb-Fe-As-Au mineralization were distinguished, with stibnite mineralization in 3rd and 4th stage. Main factor controlling the stibnite deposition was probably the decreasing temperature.

Key words: black shales, carbonatization, arsenopyrite, stibnite

Introduction

The Trojárová locality is situated northwards from Sb-Au deposit Kolársky vrch in one of productive zones of larger area between the towns Pezinok and Pernek in Malé Karpaty Mts. (Fig. 1). Positive geochemical anomalies were detected in exploration boreholes and subsequently the Trojárová adit was drilled in order to investigate the Au-As and Sb mineralizations. This study summarizes main results of detailed mineralogical, petrological and geochemical research performed on samples from the drillcores and from the Trojárová adit.

Geological setting and ore mineralization

Variscan crystalline in surroundings of studied area consists of two granitoid bodies (southern Bratislava massive and northern Modra massive) and a zone of metamorphites inbetween, stretching in the NW-SE direction across the mountain ridge (Pezinok-Pernek crystalline). Three lithologic units were recognized in the metamorphic belt (Pezinok, Pernek and Harmónia succession), each one composed of two formations. Lower pelitic-psamitic flysch-like formation of silurian–lower devonian age gradually passes into upper volcanosedimantary formation of lower–middle devonian age (Planderová & Pahr, 1983) with black shales, basalts and basaltic tuffs, carbonates, gabros and gabbrodiorites. Intrusives of the Bratislava massive are represented by peraluminous monzogranites and granodiorites with high quartz contents (Cambel & Vilinovič, 1987) classified as Ca-alkaline granitoids to granites. Modra granitoids are shifted towards Ca-alkaline-trondhjemitic series, represented by metaaluminous-peraluminous biotitic granodiorites and tonalites. Both

granitoid massives exhibit Rb-Sr age 348 ±4 Ma (Cambel et al., 1990). Putiš (1987) and Plašienka et al. (1991) distinguished four stages of variscan tectonometamorphic evolution of related area:

1. regional metamorphism;
2. peripluthonic metamorphism with distinctive zonality, related to intruding of the Bratislava massive;
3. contact metamorphism caused by the intrusion of Modra massive
4. late variscian fold tectonics of the metamorphic belt between the towns Pezinok and Pernek.

Alpine evolution of studied area started by epivariscan clastic sedimentation in upper permian and evolved through different tectonic regimes (rifting – areal extension – pre-compressional subsidence – compression; each accompanied by its characteristic sedimentation) to the thrusting and nappe emplacement, which took place in middle Cretaceous and determined the present day geological structure of Malé Karpaty Mts. Neogene brittle tectonics has slightly rearranged this paleoalpine structure and caused uplift of the horst of present-day mountain ridge along major normal- and strike-slip faults.

The ore mineralizations in Malé Karpaty Mts. were subject of numerous studies, among others Cambel (1959), Polák (1974), Kantor (1974), Žákovský (1962), Andráš (1984). Reader could find good review in Chovan et al. (1992), who distinguished the following mineralization types in four productive zones in the Malé Karpaty Mts. crystalline:

I. Metamorphosed exhalation-sedimentary mineralization with pyrite;

II. Hydrothermal mineralization, with following subtypes: 1. – molybdenum in granitoids; 2. – copper-base

Slovak Geol. Mag., 8, 3– 4 (2002), 179 – 193

180
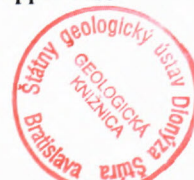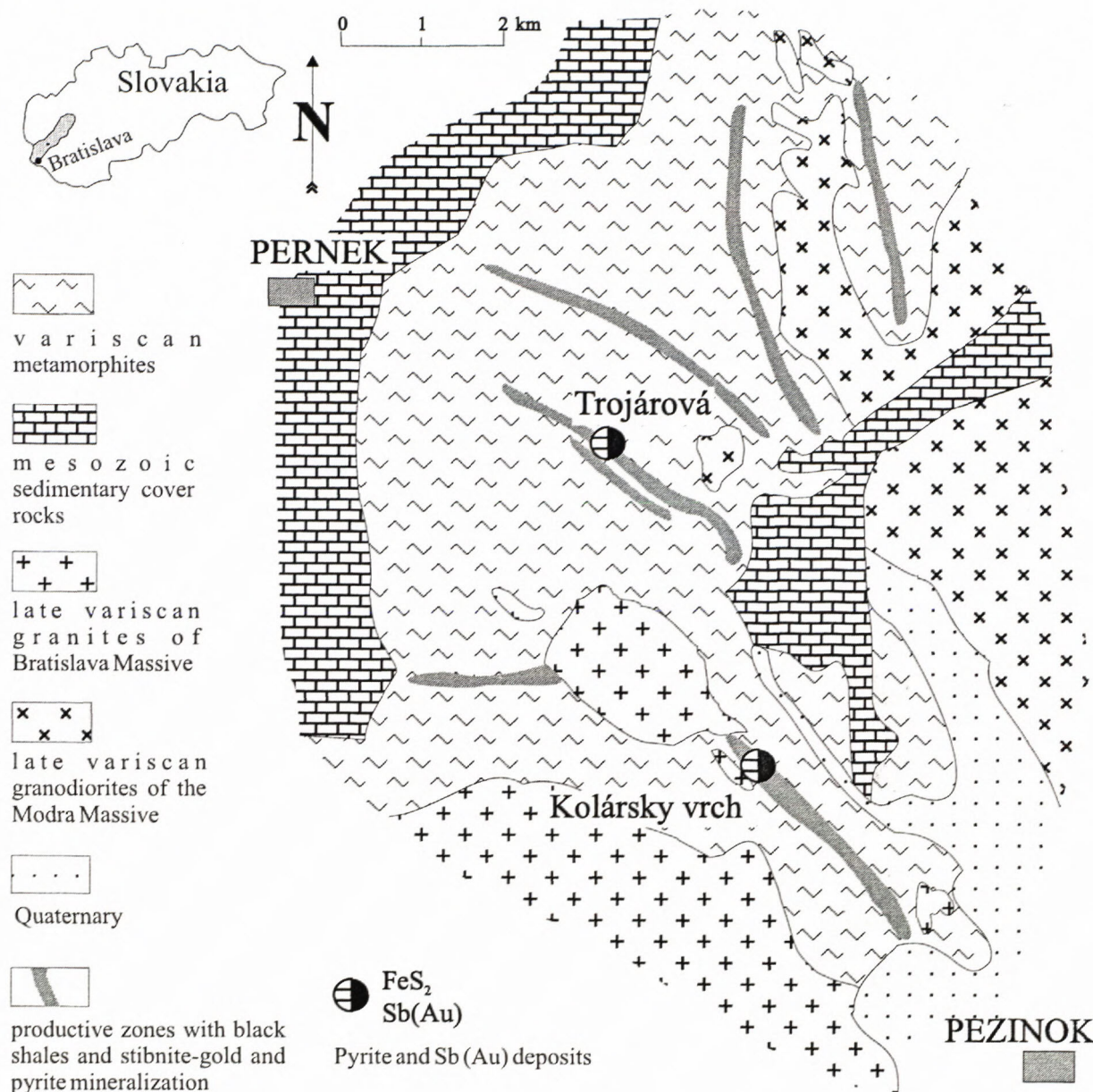
Fig. 1 Simplified geological map of the Malé Karpaty Mts., region between Pezinok and Pernek (after Cambel 1959; Polák & Rak 1980).

III. metal with silver: (a) Cu-Pb, Ag, (Ni); (b) Pb-Zn; (c) Pb-Ag; 3. – antimony-gold: (a) gold-sulphidic; (b) gold-quartz; (c) stibnite.

Sampling and analytical methods

The material for mineralogical, petrological and geochemical study was obtained from the cores of exploratory boreholes and from the prospection adit on Trojárová locality. Several samples of nearly identical mineralization from adit Antimonitová (Kolársky vrch deposit) were collected for comparison.

Optical microscopic observations were carried out on the microscope Jenapol. Electron WDS microanalyses were performed on JEOL, JXA 840 A (Faculty of Natural Sciences, Comenius University) (analyst Krištín) and by JEOL SUPERPROBE 733 (Geological Survey of Slovak Republic), accelerating voltage 20 KeV, 15 nA, beam diameter 5.10^{-6} m, standards Sb_2S_3, GaAs, FeS_2, FeAsS, HgS-Hg, PbS-Pb, Ag, Sb, Zn, Cu, Bi, Co, Ni, Au, Mn a Cd (analysts Caňo and Siman). Semiquantitative EDS and scanning electron microprobe images were performed by JSM 840 (Geological Survey of Slovak Republic).

Following spectral analytical methods were used to determine the concentrations of individual elements (laboratories of Geological Institute of Faculty of Natural Sciences, Comenius University, and Institute of Geological Exploration in Spišská Nová Ves): Au - AAS; As and Sb - AAS with hydride generation technique; trace elements – OES; C_{org} and C_{min} quantitative analysis. AAS analyses of Au were performed by Philips PU 9000 with deuterium background corrector using electrothermic

atomization PV 9095 Video Furnace in Ar atmosphere (Geological Institute of Slovak Academy of Sciences, Banská Bystrica). Manometric, thermometric analysis and X-ray powder diffraction analysis were carried out in Geological Institute of Faculty of Natural Sciences, Comenius University.

The samples of black shales from cores of boreholes PT-13, PT-55, PT-57 were studied by means of Infrared Absorption Spectroscopy where Soxhlet's method was applied for organic component extraction and method of column chromatography for organic material fractionation. The contents of C, H, N, S was determined by Element Analyser Carlo Erba 1106 (Department of Organic Chemistry, Faculty of Natural Sciences Comenius University). Chemical separation of graphite was performed in the laboratory of analytical chemistry (Geological Survey of Slovak Republic). Contents of trace and metal elements in bulk samples was determined by means of quantitative SPA and AAS (Geological Institute of Faculty of Natural Sciences Comenius University). The contents of P_2O_5 was estimated photocolorimetrically (Dept. of Economic Geology, Faculty of Natural Sciences, Comenius University).

Results

Surrounding rocks

The black shales form narrow strips within the "belts" of actinolitic schists. These are embraced by amphibolites. This complex is underlain by by staurolite-biotite paragneisses and granitoids of the Bratislava massive. Their contact is accompanied by a cataclastic zone of thickness up to 2 m.

"Actinolitic" schists exhibit prevailingly nematoblastic structure. Their ground mass consists of collumnar to spicular "actinolite", chlorite, quartz and sphene. According to classification of Leake et al. (1997) the previously mentioned actinolite corresponds to Mg-hornblendite – tchermakite (Moravanský et al., 2001). Carbonates, pyrite and "actinolite" are arranged into coarse-grained layers. Heterogranular porfyroblastic texture and granonematoblastic texture with blasts of plagioclase and quartz occurs sporadically. A graphitic substance is present in zones adjacent to the black shales, which indicates gradual transitions between the two lithotypes. This is well documented by presence of the amphibole in black shales.

Amphibolites are characterized by heterogranular porphyroblastic texture, their matrix is composed of amphiboles, finegrained light sphene, pyrite and carbonates. Blasts of plagioclase, carbonate, "actinolite", quartz and minerals of epidote-zoisite group occur in this matrix.

Tectonic breccias occur on the contact of the complex of metabasites and granitoid rocks and were formed mostly on the expense of granitoids. Their textures indicate transition between mylonitization and brittle cataclasis. The observations in our material are in agreement with the concept of Putiš (1987) about the overthrust of metabasite complex over the paragneisses.

Granitoid rocks are affected by cataclasis / mylonitization, which is mostly localized at the contact with metabasites.

Staurolite-biotite paragneiss are affected by regional-periplutonic metamorphism (staurolite-sillimanite zone) caused by the intrusion of granitoids (Korikovskij et al., 1984).

Hydrothermal alterations

Moravanský (2000) distinguished three alteration zones: carbonitization and illitization zone, muscovitization zone and chloritization zone. The altered rock is characteristic by the association carbonate-sericite-quartz-pyrite. "Actinolitic" schists are affected by carbonatization, which is most intense at their contact with black shales and it fades out with the distance from the contact. Carbonatization is localized 1) in the foliation; and 2) in veins cutting the foliation, filled by carbonates, quartz, ±albite and ore minerals.

Hydrothermal alterations of granitoids comprise sericitization and in lesser extent carbonatization of plagioclases, muscovitization and chloritization (Moravanský, 2000; Moravanský et al., 2001).

Ti-Fe oxides in hydrothermally altered black and actinolithic shales form anhedral grains with low reflectance, arranged concordantly with foliation.

V-Cr garnet was recorded in actinolithic-tremolitic schists on the localities Trojárová and Rybníček (Uher et al., 1994).

Black shales

Ore mineralization is hosted in the black shales which form zones with thickness up to 20 m in the actinolitic schists (Fig. 2). Their weak rheology designated them to deform much more intensively than surrounding rock during orogenic processes, which is pronounced in subtly-folded structure. Black shales consist of quartz, sericitic matrix, organic matter and biotite of two generations. Plagioclase, chlorites, carbonates, actinolite, Ti-oxides(?), rutile and apatite occurs as accessory minerals. Black shales are impregnated with pyrite, arsenopyrite is rare.

The average contents of C_{org} in black shales is 5.5 %. Infrared spectra of organic compounds extracted in benzene show for occurrence of absorption bands which are assigned to valence vibrations of C-H bands of CH_3, CH_2, or CH groups. The C-O-C bands in esteric and etheric compound and C=O bands of saturated kethon and unsaturated ester of karboxylum acid are abundant. Two samples were analysed for contents of H, C and S, following results were obtained: H – 10-0.30 %; C – 5.46-5.48 %; S – 5.95-7.82 % (Oružinský et al., 1990).

The samples from boreholes and adits were analysed for contents of accessory and trace elements, whereby enrichment in S_{tot}, C_{org}, C_{min}, Sb, Au, and As compared to surrounding rocks was revealed (Fig. 3). Contents of Au, As and Sb represent significant anomaly (sensu Judovič et al., 1990; Judovič & Kertis, 1991). From comparison of these values with those from other black shales productive zones of Malé Karpaty Mts. (Cambel & Khun, 1983) follows 4.9x enrichment for Au, 38.7x for Sb and 21.2x for As.

Remarkably high contents of Mo in the samples from boreholes are presumably connected with greisenized granitoids with molybdenite in the underlier. An increased contents of V in black shales samples was determined too.
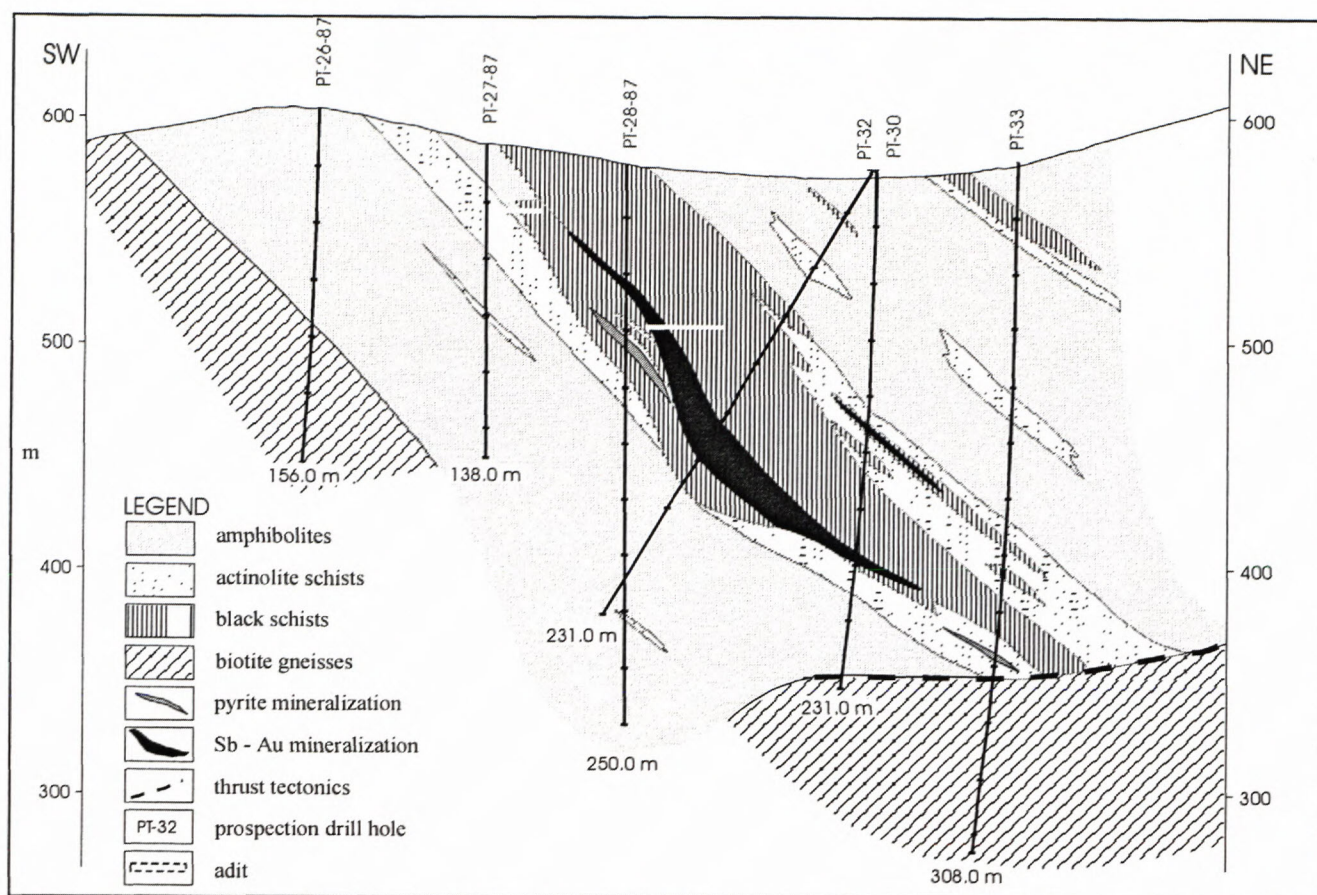
Fig. 2 Geological profile across the complex of crystalline schists with position of boreholes and prospection adits on the Trojárová deposit, Malé Karpaty Mts. (after Hanas et al., 1989).

An Sb and arsenopyrite mineralization was detected in black shales from boreholes on the Trojárová locality. Negative correlation between C_{org} and C_{min} ($r = -0.661$) follows from the statistical analysis of geochemical data from these samples, affinities of other elements to C_{org} are as follows: V 0.799; Zr 0.724; Y 0.69; Ni 0.656; Sb 0.589, indistinct positive correlations show Pb, Mo, Cu, and Ag. Sr (0.706), Sc (0.67), and Cr (0.606) have significant positive correlation with C_{min}. V (-0.717), Ni (-0.569), Cu (-0.498), Mo (-0.498) (Fig.4) show negative correlation with C_{min}. Elements Co, Ba, Bi, and B have very weak positive correlation with both C_{org} and C_{min}. The contents of As, Au, and S_{tot} were not determined in the borehole samples. These correlation coefficients are in compliance with other published data from black shales (e.g. Judovič & Kertis, 1991).

The fully evolved Sb-Fe-As-Au mineralization (see below) proved in boreholes was not attained during the exploration works in the Trojárová adit, and drilling stopped in its marginal zone. Therefore arsenopyrite and pyrite are dominant here and Sb-minerals occur in accessory amounts. Studied samples of this mineralization exhibit affinity of Au, As and Sb to C_{min} (0.847, 0.617 and 0.519, respectively) (Fig. 5). This indicates the correlation of these elements with the intensity of carbonatization. Correlation of S_{tot} with C_{org} (0.526) shows for synsedimentary pyritization in black shales. Arsenic has a negative correlation with C_{org} (-0.593). Close association

of Au and As (0.703) is related to Au-enrichment in arsenopyrite which is bound to carbonatic layers in black shales. Sb positive correlation with Au and As can point to the presence of an Au alloy in Au bearing arsenopyrite.

Graphite was identified and investigated in several samples from boreholes. Those samples were grinded and treated by chemical agents - carbonates were removed in HCl (by 60°C), silicates in HF (60°C), fluorides by powdered Zn after mechanical processing (see Janků, 1991). Separated graphite exhibits slice morphology, euhedral grains are scarce (Fig. 6). Grain size ranges up to 10 μm (Fig. 6), exceptionally up to 50 μm, which ranks the studied samples to microcrystalline graphite (1 μm - 100 μm). Value of *c*-parameter, calculated from the *d(001)* spacing of X-ray diffraction patterns (Tab.1) of graphite is 6.735 x 10^{-10} m.

Ore mineralization

Three mineralization types were distinguished on the Trojárová locality:
1. metamorphosed pyrite-pyrrhotite Fe-S mineralization of volcano-sedimentary origin,
2. molybdenite mineralization,
3. hydrothermal Sb-Fe-As-Au mineralization.

Fe-S mineralization

Mineralization is hosted in amphibolite layers, "actinolitic" schists and black shales.
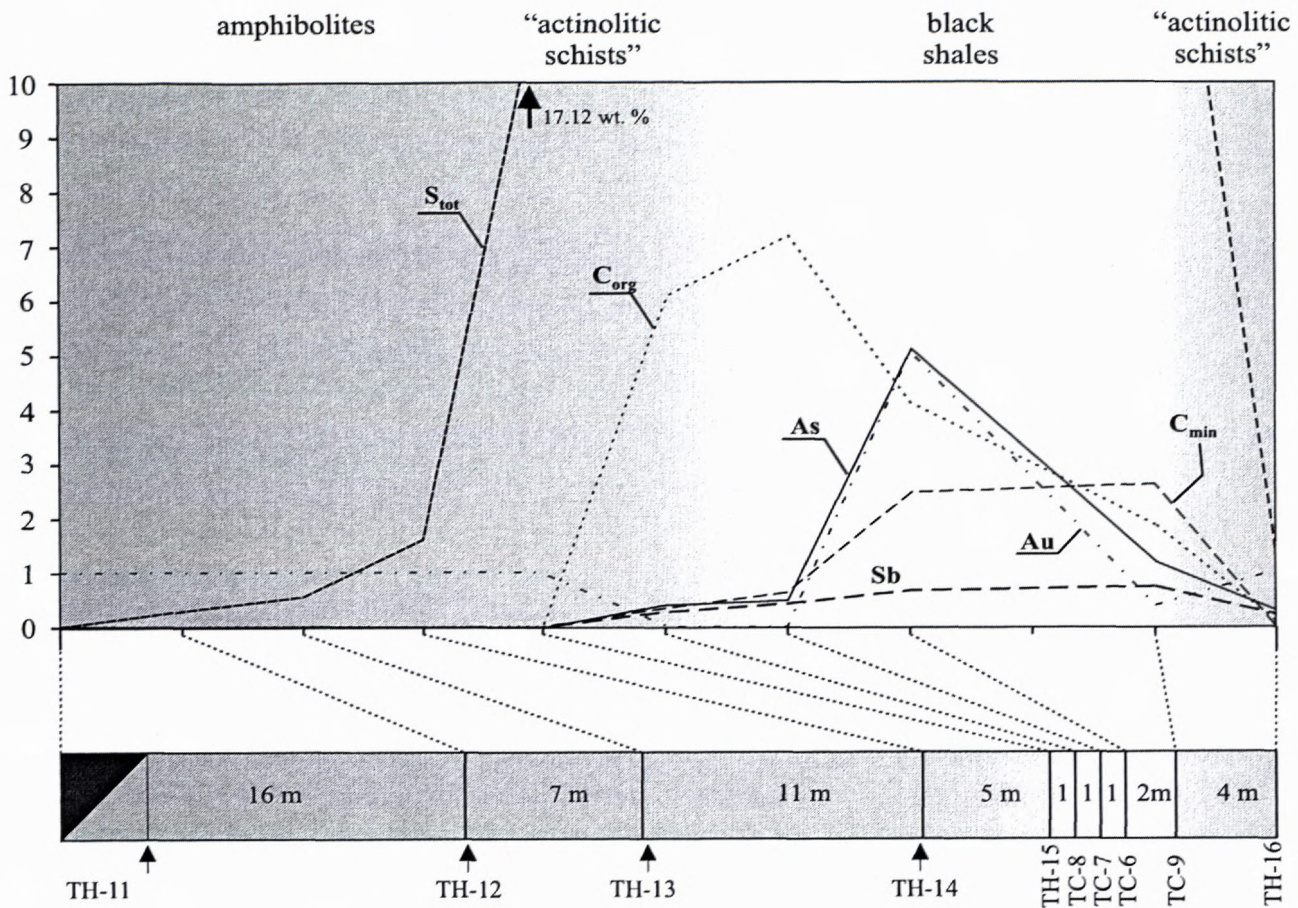
Fig. 3 Schematic profile of PT5 gallery in the Trojárová adit with plot of S_{tot}, C_{org}, C_{min}, Sb, As, and Au contents in amphibolites, actinolitic schists and black shales. Strong increase in contents of these elements is bound to black shales. The contents of Au in ppm x 10, contents of S_{tot}, C_{org}, C_{min} in wt.%, Sb and As content in wt.% x 10. Position of sampling sites TH11-TH16 and TC6-TC9 is shown on the bottom of the picture.
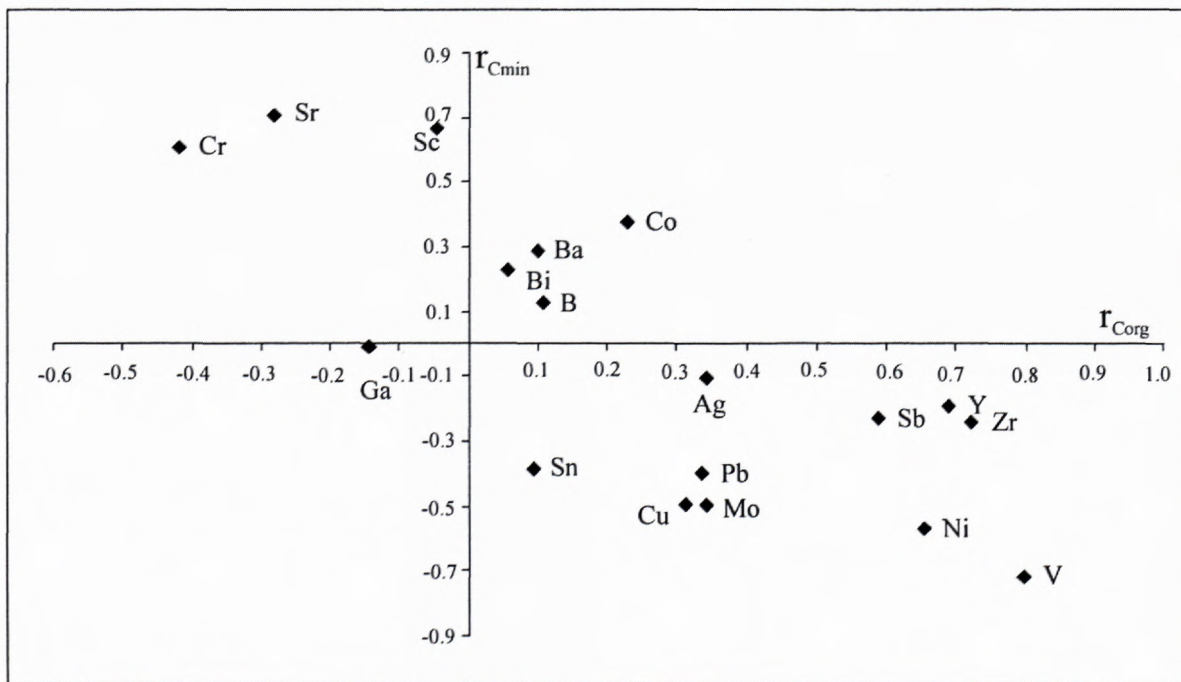
Fig. 4 Plot of correlation coefficients of analysed elements in black shales from boreholes (12 samples), r_{Corg} and r_{Cmin} are correlation coefficients of C_{org} and C_{min} with corresponding elements.

184
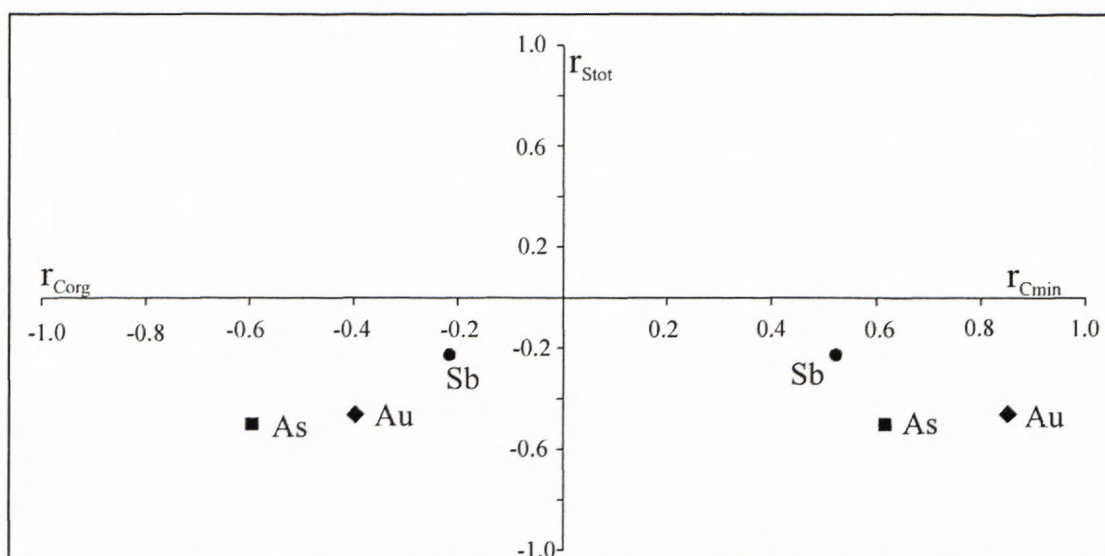
Fig. 5 Plot of correlation coefficients of As, Au, and Sb in black shales samples from Trojárová adit (14 samples), r_{Stot}, r_{Corg}, r_{Cmin} are correlation coefficients of S_{tot}, C_{org}, and C_{min} with corresponding metal elements.

Tab. 1 X-ray diffraction data of graphite from Trojárová black shales (Janků, 1991).

dm sample7	I/Imax	dtab graphite	I	hkl	d pyrite	I	d arsenopyrite	I
3.85	15	-	-	-	-	-	-	-
3.351	**100**	**3.36**	**100**	002	-	-	-	-
3.22	5	-	-	-	-	-	-	-
3.121	10	-	-	-	3.128	35	-	-
2.998	10	-	-	-	-	-	-	-
2.965	5	-	-	-	-	-	-	-
2.706	20	-	-	-	2.709	85	-	-
2.423	20	-	-	-	2.423	65	2.418	95
2.212	15	-	-	-	2.219	50	2.204	25
2.112	5	2.13	10	100	-	-	-	-
1.914	15	2.03	50	101	1.915	40	1.943	25
1.813	8	1.80	5	102	-	-	1.814	90
1.758	5	-	-	-	-	-	1.759	20
1.687	10	1.678	80	004	-	-	-	-
1.631	30	-	-	-	1.633	100	1.631	30
1.502	5	1.544	10	103	1.5025	-	-	-
1.450	5	-	-	-	1.445	25	-	-

Pyrite (Tab. 2, analyses 1, 2) as dominant mineral of this mineralization forms impregnations, layers and thin lenses arranged concondantly with foliation. Usually it forms anhedral grains and their aggregates, often intensively corroded and cataclassed (Fig. 7). In fine grained aggregates pyrite also occurs in intergrowths with quartz and pyrrhotite. Mineralization was metamorphosed and intensively folded, whereby the new generation of recrystallized pyrite originated.

Pyrrhotite is abundant mineral and probably represents product of metamorphism of pyrite mineralization. (Tab. 2, analyses 3, 4)

Chalcopyrite is rare, it forms anhedral grains in pyrrhotite aggregates (Tab. 2, analysis 5).

Sphalerite occurs frequently but in small amounts in the form of tiny grains in pyrite-pyrrhotite aggregates. Its increased contents of Fe - 7.9 wt.% average is notable (Tab. 2, analysis 6).

Mo mineralization

A molybdenite specimen of size 3x3 cm was found in the drillhole PT 45 in depth 271 m (Hanas et al., 1989) in almost monomineral muscovite rock of greizen appearance (Fig. 8). Its host rock - muscovitic leucogranite – forms the underlier of the complex of metatuffs and metabasites. From geochemical viewpoint molybdenite is pure, almost without admixtures (Tab. 5, analysis 1). Thermoelectric voltage measurements revealed the P-type conduction (hole type), values of thermoelectric voltage coefficient are typical for molybdenite from greizens (Ďurža & Chovan, 1995).

Sb-Fe-As-Au mineralization

Carbonate and quartz veins with hydrothermal Sb-Fe-As-Au mineralization are hosted in the black shales.

Tab. 2 Electron microprobe analyses of minerals of pyrite-pyrrhotite mineralization (wt. %), the Pezinok – Trojárová deposit, pyrite (1,2), pyrrhotite (3,4), chalcopyrite (5), sphalerite (6).

Analyse num.	1	2	3	4	5	6
Sample	45/9	45/9	45/9	45/9	45/9	45/9
Fe	47.11	47.78	60.14	58.17	30.42	7.85
Bi	-	-	-	0.00	-	0.19
S	51.05	55.42	39.04	39.72	35.44	32.91
As	0.34	0.03	0.01	-	0.00	-
Ni	0.08	0.07	0.42	-	0.03	-
Co	0.08	0.09	0.07	-	0.03	-
Cu	0.03	0.03	0.00	-	34.13	-
Zn	-	-	-	0.38	-	59.17
Hg	-	-	-	0.32	-	0.00
Mn	-	-	-	0.00	-	0.06
Cd	-	-	-	0.04	-	0.38
Ag	-	-	-	0.02	-	0.00
Σ	98.69	99.04	99.68	98.65	100.05	100.56
recaltulated on the Σ of atoms						
	3	3	2	2	4	2
Fe	1.04	0.99	0.94	0.91	1.00	0.14
Bi	-	0.00	-	0.00	-	0.00
S	1.95	2.00	1.06	1.08	2.02	0.99
As	0.01	-	0.00	-	0.00	-
Ni	0.00	-	0.01	-	0.00	-
Co	0.00	-	0.00	-	0.00	-
Cu	0.00	-	0.00	-	0.98	-
Zn	-	0.00	-	0.01	-	0.87
Hg	-	0.00	-	0.00	-	0.00
Cd	-	0.00	-	0.00	-	0.00
Ag	-	0.00	-	0.00	-	0.00

Arsenopyrite is the m ost abundant ore mineral in the Trojárová adit. It forms crystallic aggregates in carbonate-quartz lenses and veins in black shales, in minor extent also in carbonate veins in actinolitic shists adjacent to black shales. Arsenopyrite treats in two morphological types:
1. The enhedral, severely cataclased arsenopyrite forms crystalline aggregates with grainsize ranging from <10 μm to 100 μm (samples: T-24, T-39, T-40, Tab. 3, analyses 1 to 7). It often intergrows with coarse-grained pyrite. The sectional zonality due to the irregular distribution of Sb (bright zones) and As in arsenopyrite grains is shown on SEM images (Fig. 9). Grains with exceptionally high Au concentration up to 6700 ppm occur in T-24 sample, (Tab. 3, analyses 1 to 4).
2. Euhedral (sometimes subhedral) arsenopyrite forms crystallic aggregates and isolated crystals of size up to 150 μm in carbonate and quartz. The inner grain texture is heterogenous, oscillatory zonation is frequent (Fig. 10). The alternation of bright and dark zones is again related to differences in As and Sb distribution. Arsenopyrite with diffuse zonality occurs rarely (sample T-20). Increased contents of Au was scarcely detected in several grains by means of electron microprobe (up to 800 ppm, Tab. 3, analysis 8).

According to electron microanalyses arsenopyrite has high contents of S, decreased contents of As and adequate contents of Fe - $Fe_{1.005}As_{0.85}S_{1.135}$ considering theoretical arsenopyrite composition. Contents of As is 27 at. % in average, which is too low for implementation of the Kretschmar & Scott´s (1976) arsenopyrite thermometer. As is replaced by Sb in samples where value of correlation coefficient is -0.8. Younger carbonatic veins with Sb mineralization leak into this arsenopyrite mineralization. Arsenopyrite is replaced by stibnite and it contains extremely Sb rich zones with contents of Sb up to 11 wt. %.

Besides these two types some other arsenopyrite morphological varieties were discerned: (a) Extremely cataclased and corroded arsenopyrite occurs in zone of intensive deformation between black shales and actinolitic schists. Arsenopyrite impregnated the rock along the schistosity and was subject to superimposed deformation. (b) Tiny isolated euhedral crystals of arsenopyrite, often accompanied by stibnite, occur in thin carbonatic veins. These crystals were not affected by deformation and thus represent the youngest generation of arsenopyrite.

Pyrite of hydrothermal origin forms subhedral, scarcely euhedral crystals and their aggregates, often intergrown with cataclased arsenopyrite (Fig. 11). Age relations in such aggregates are ambiguous and crystallization intervals of the two minerals seem to overlap. Aggregates with gudmundite were observed as well. (Fig. 11). Pyrite grains often enclose quartz and carbonate inclusions. Typical is slight optical anisotropy of pyrite due to admixture of As, zonality is rare. The Au contents of up to 10 ppm were detected in pyrite (see analyses in table 3).

Gudmundite is rather abundant ore mineral in the samples from the Trojárová adit. We distinguished two generations. Gudmundite-I occurs as disseminated clusters of subhedral and anhedral crystals in arsenopyrite and arsenopyrite-pyrite aggregates or it forms monomineral aggregates and veins in pyrite and arsenopyrite (Fig. 11). It often encloses relict grains and fragments of arsenopyrite. Pyrrhotite either penetrates into gudmundite aggregates (Fig. 12) or occurs along with gudmundite as isolated clusters in carbonates. Gudmundite-I is usually present in boundary zones of carbonatic veins with Sb-mineralization (Fig. 13), where it directly contacts quartz crystals and often also pyrrhotite. Gudmundite II associates with stibnite, berthierite, native Sb or with Sb oxides/sulphooxides. Cataclased gudmundite is often replaced by stibnite. Admixtures of other elements were not detected (Tab. 4, analyses 1-3).

Pyrrhotite occurs in two morphological types. 1. Veins of pyrrhotite intrude into the arsenopyrite-gudmundite aggregates (Fig. 12). 2. Pyrrhotite of younger generation is euhedral or subhedral, occurs as a component of carbonate veins, where it is accompanied by berthierite and native antimony (Fig. 14), intergrows with native antimony (Fig. 15) or gudmundite (Fig. 16), rarely with arsenopyrite (Fig. 17). The mineral pairs gudmundite–pyrrhotite, resp. native antimony–pyrrhotite exhibit equilibrium microstructures. On the other hand, pyrrhotite is intensively replaced by stibnite (Fig. 16) and berthierite, often even pseudomorphed by the later.
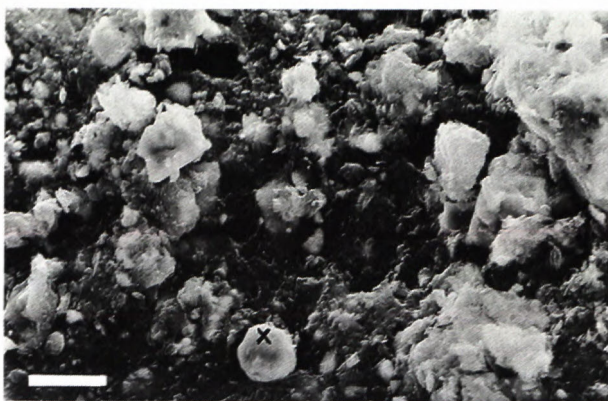
Fig. 6
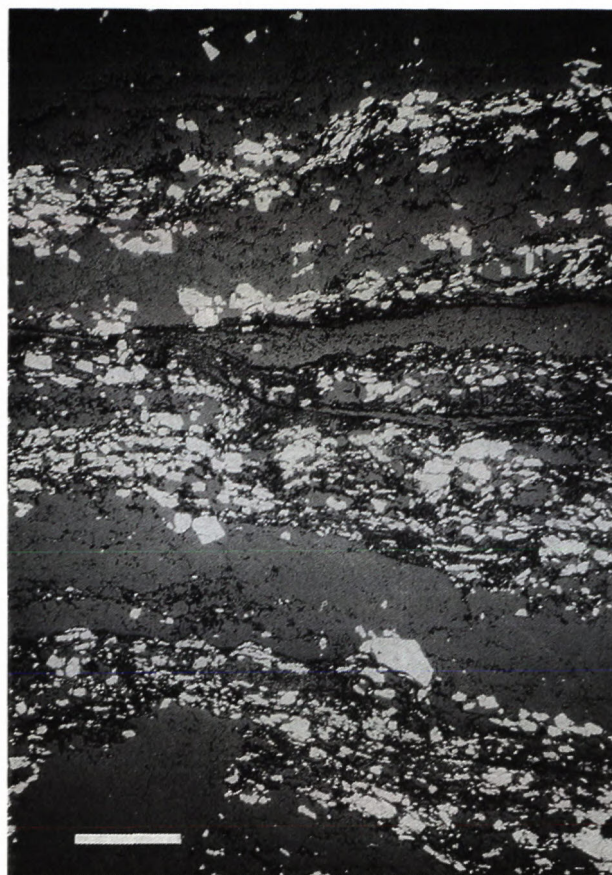
Fig. 7
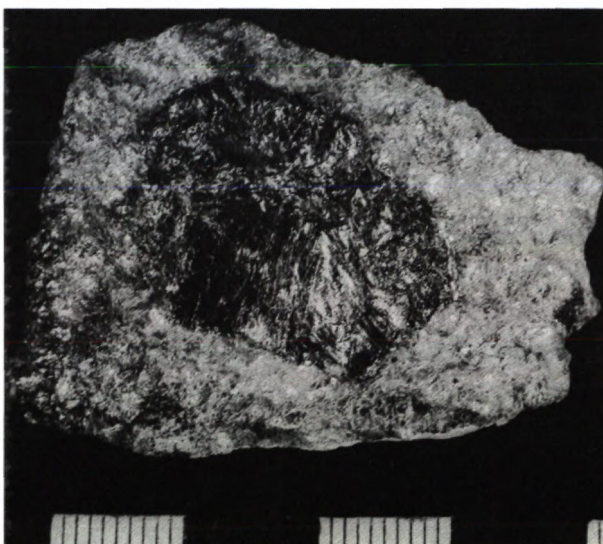
Fig . 8

Fig. 9

Fig. 10

Fig. 6 Morphology of graphite from the concentrate, graphite grain is marked with character "x", SEM image, scale bare corresponds to 10 μm.

Fig. 7 Typical texture of synsedimentary pyrite (white) from pyrite-pyrrhotite mineralization in black shales of Trojárová deposit, reflected light, scale bar is 500 μm.

Fig. 8 Crystal of molybdenite from greisenized granite, borehole sample PT 45/271.1. 1 unit is 1 cm.

Fig. 9 Irregular sectorial zonation of inhomogeneous, cataclased arsenopyrite grains in black quartz from the first stage of hydrothermal mineralization, SEM image, scale bar is 100 μm.

Fig. 10 Typical laminar zonation of fine-grained euhedral arsenopyrite, the first stage of hydrothermal mineralization, SEM image, scale bar is 10 μm.
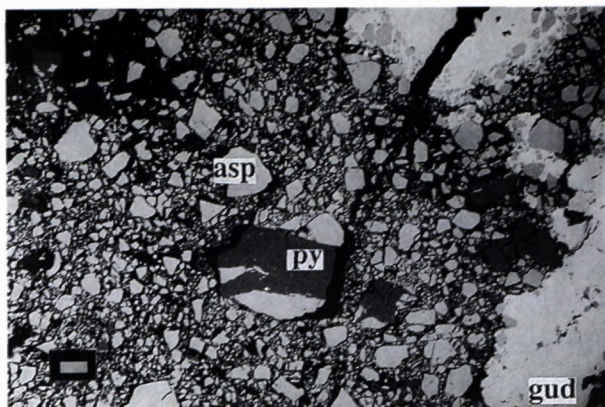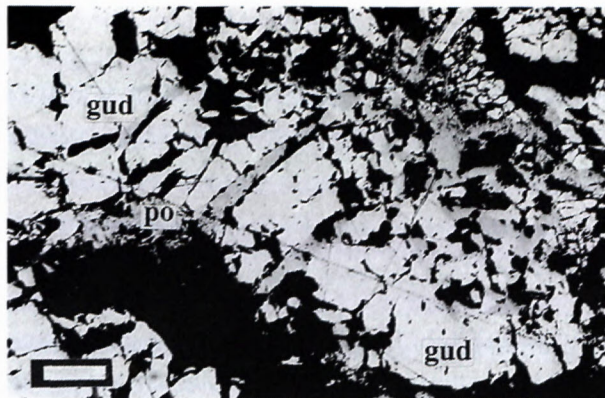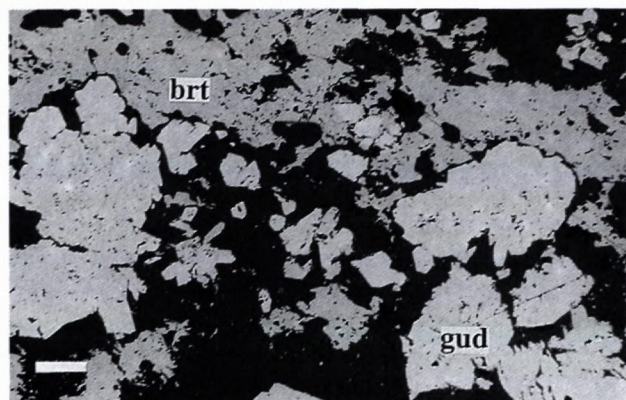
Fig. 11

Fig. 12

Fig. 13
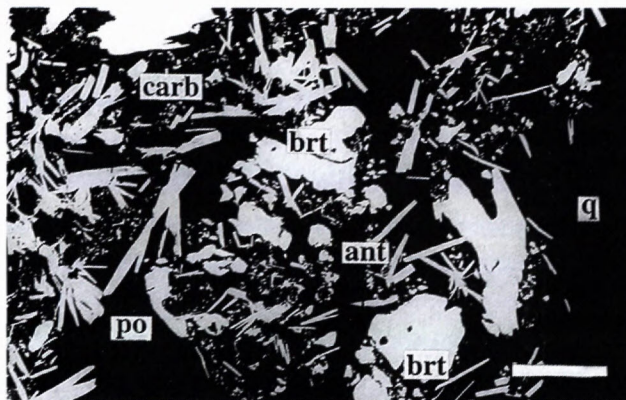
Fig. 14
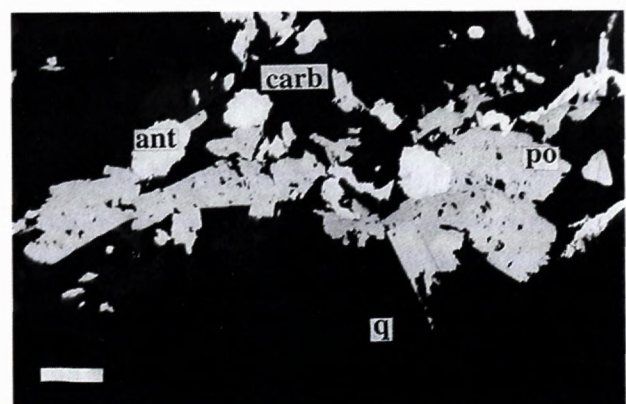
Fig. 15
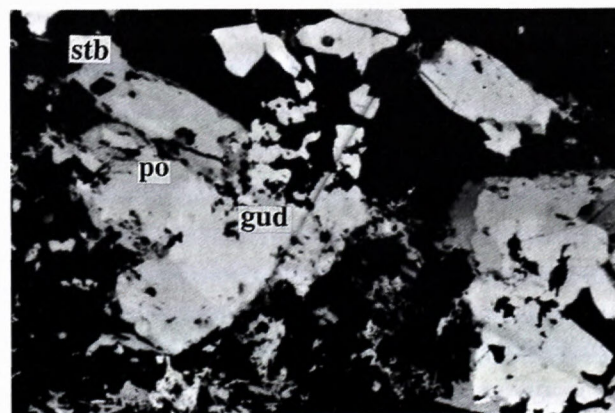
Fig. 16

Fig. 11 Sample with gudmundite (gud) penetrating the arsenopyrite (asp) - pyrite (py) aggregate affected by cataclasis, SEM image, scale bar is 100 μm.

Fig. 12 Reflected light microphotograph of pyrrhotite (po) penetrating the brecciated gudmundite (gu) aggregate, scale bar is 100 μm.

Fig. 13 Vein of younger berthierite (brt) penetrating the gudmundite (gud) aggregate of older stage, borehole sample PT - 52/7, reflected light, scale bar is 100 μm.

Fig. 14 Reflected light microphotograph of relationship between of needle-shape pyrrhotite (po), berthierite (brt) and fine aggregates of native antimony (ant) in a carbonate (carb) vein penetrating voids in quartz (q) aggregate, borehole sample PT – 57/137.4. SEM image, scale bar is 100 μm.

Fig. 15 Textural relationship between pyrrhotite (po) and native antimony (ant) in carbonate vein (carb), ore minerals are in sharp contact. This mineralization is in contact with older quartz crystals (q), scale bar is 100 μm (reflected light).

Fig. 16 Intergrowth of pyrrhotite (po) and gudmundite (gud) – an equilibrium association, stibnite (stb) replaces the pyrrhotite, reflected light, scale bar is 100 μm.

Slovak Geol. Mag., 8, 3–4 (2002), 179–193

188

Tab. 3 Electron microprobe analyses of arsenopyrite (wt.%), the Pezinok – Trojárová deposit.

Analyse number	1	2	3	4	5	6	7	8	9	10	11	12	13	14
Sample	T-24	T-24	T-24	T-24	T-39	T-39	T-39	T-20A	T-29	T-29	T-29	T-30	T-30	T-30
Fe	33.19	33.18	34.16	33.83	35.35	35.18	35.69	35.61	35.09	34.31	35.87	36.81	35.60	36.03
Sb	0.04	0.06	0.07	0.06	0.00	0.00	0.00	1.52	1.12	0.35	0.99	0.00	0.41	0.00
Bi	0.13	0.12	0.03	0.07	0.00	0.00	0.00	0.00	0.00	0.00	0.04	0.00	0.00	0.00
S	22.08	23.17	21.46	22.89	22.64	23.97	22.93	20.05	24.58	23.71	23.45	22.30	24.99	23.92
Au	0.67	0.54	0.04	0.00	0.00	0.00	0.00	0.01	0.00	0.00	0.00	0.00	0.00	0.00
As	42.06	41.69	42.80	42.25	41.30	40.14	41.18	42.73	38.46	41.19	39.87	41.80	39.42	40.63
Ni	0.15	0.00	0.24	0.00	0.00	0.00	0.00	0.00	0.00	0.00	0.00	0.00	0.00	0.00
Co	0.00	0.00	0.00	0.00	0.00	0.00	0.00	0.00	0.00	0.00	0.00	0.00	0.00	0.00
Σ	98.32	98.76	98.80	99.10	99.29	99.29	99.80	99.92	99.24	99.55	100.22	100.91	100.42	100.58
recaltulated on the 3 of atoms														
Fe	0.96	0.95	0.99	0.96	1.00	0.99	1.01	1.04	0.98	0.97	1.01	1.03	0.98	1.00
Sb	0.00	0.00	0.00	0.00	0.00	0.00	0.00	0.02	0.01	0.00	0.01	0.00	0.01	0.00
Bi	0.00	0.00	0.00	0.00	0.00	0.00	0.00	0.00	0.00	0.00	0.00	0.00	0.00	0.00
S	1.12	1.16	1.08	1.14	1.12	1.17	1.13	1,02	1.20	1.16	1.15	1.09	1.2	1.16
Au	0.01	0.00	0.00	0.00	0.00	0.00	0.00	0.00	0.00	0.00	0.00	0.00	0.00	0.00
As	0.91	0.89	0.92	0.90	0.87	0.84	0.87	0.93	0.80	0.87	0.83	0.88	0.81	0.84
Ni	0.00	0.00	0.00	0.00	0.00	0.00	0.00	0.00	0.00	0.00	0.00	0.00	0.00	0.00
Co	0.00	0.00	0.00	0.00	0.00	0.00	0.00	0.00	0.00	0.00	0.00	0.00	0.00	0.00

Stibnite is a component of carbonate veins cutting the arsenopyrite-pyrite paragenesis and filling fractures in cataclased arsenopyrite and pyrite crystals. These veins also penetrate into surrounding actinolithic shales. The contents of stibnite is generally low. Several textural types were determinated:

1. Massive monomineral stibnite aggregates show evidences of superimposed dynamic recrystallization, such as deformation twins, shape-preferred orientation and even features of crystallographically preferred orientation of aggregates. Stibnite encloses quartz and older gudmundite with signs of corrosion and replacement. Stibnite of this type often intergrows with massive native antimony, however, their contact is rarely direct – Sb oxides/sulphooxides occur as an interface instead. (This applies mostly on the Antimonitová adit samples, Kolársky vrch). Stibnite associates with pyrrhotite and berthierite (Fig. 14) and also occurs in mixtures of Sb oxides/sulphooxides, probably as a relict (Fig.18).

2. The vein-filling stibnite, (likewise berthierite), often replaces pyrrhotite in its aggregates with gudmundite or with native antimony (Fig. 16, 17, respectively). Sometimes stibnite was observed to cement aggregates of these minerals.

3. Radial stibnite aggregates crystallized in cavities of Sb oxides/sulphooxides as well as along fissures in the host rock likely represent the youngest stibnite generation remobilized in the latest mineralization stage. The thin stibnite veins often seal hydraulically brecciated oxide aggregates. Stibnite identification was confirmed by electron microprobe analyses (Tab. 4, analyses 4-6).

Berthierite is rare and it's occurrence is related to Sb mineralization in carbonate veins (Fig. 14). It forms thin veinlets in pyrrhotite, sometimes also monomineral aggregates. Berthierite replaces and pseudomorphs pyrrhotite. In its intergrows with tetraedrite and arsenopyrite berthierite forms cores of these aggregates. Berthierite is more abundant in association with stibnite and kermesite within carbonates, where it forms veins and spicular crystals (Tab. 4, analyses 7 and 8).

Native antimony is scarce, it seldom occurs in larger clusters of anhedral isometric grains or aggregates with mosaic structure (Fig. 14, 15, Tab. 4, analysis 9). Significant accumulations of native antimony were observed in samples from the Antimonitová adit (Kolársky vrch deposit), where it often dominates over Sb sulphides and forms massive monomineral aggregates. Study of the Trojárová locality supplemented by the samples from Kolársky vrch deposit, revealed, that native antimony, accompanied by pyrrhotite, gudmundite, berthierite and stibnite, is a component of carbonatic mineralization. Native antimony intergrows with pyrrhotite, forming equilibrium microstructures. It is frequently corroded and replaced by kermezite, valentinite and senarmontite, which commonly occurs along the boundaries with quartz grains.

Galenite and *sphalerite* are very rare. Galenite seals the fissures in *sphalerite* aggregates. Fe contents in the sphalerite is about 5 wt. % (Tab. 4, analysis 11). It also associates with gudmundite and pyrrhotite.

Chalcopyrite, as very rare mineral, occurs in parageneses with tetrahedrite and gudmundite or it forms individual anhedral grains in carbonate veins, which penetrate into cataclased arsenopyrite-pyrite aggregates.

Tab. 4 Electron microprobe analyses of minerals of stibnite mineralization (wt. %), the Pezinok – Trojárová deposit, gudmundite (1-3), stibnite (4-6), berthierite (7, 8), native antimony (9), galena (10), sphalerite (11), tetrahedrite (12), pyrite (13, 14).

| Analyse number	1	2	3	4	5	6	7	8	9	10	11	12	13	14
Sample	T-39	45/8	45/8	36/10	45/2	T-20A	57/171.9	45/8	57/137.4	11/139.8	11/139.8	45/8	T-39	T-30
Fe	28.32	24.39	25.39	0.21	0.02	0.24	12.54	12.67	0.24	0.03	5.83	5.92	46.96	45.66
Sb	55.77	61.52	60.15	73.27	73.65	73.36	58.57	58.51	99.98	-	-	31.86	0.00	0.00
Bi	-	0.03	-	-	0.22	-	0.80	-	0.00	-	-	-	0.00	0.00
S	16.56	15.27	15.54	26.88	25.28	27.80	28.97	28.49	0.02	12.98	31.84	25.41	54.92	53.02
Au	0.00	-	-	-	-	0.00	-	-	-	-	-	-	0.00	0.00
As	0.00	0.35	-	-	0.12	0.00	0.02	0.70	0.00	-	-	-	0.00	2.55
Ni	-	-	-	0.02	-	-	-	0.02	-	-	-	-	0.00	0.00
Co	-	0.02	-	0.01	0.03	-	-	-	-	-	-	-	0.00	0.00
Cu	-	0.14	-	-	0.02	-	-	0.15	-	-	-	36.98	-	-
Zn	-	-	-	0.01	0.01	-	-	-	-	0.09	61.08	0.80	-	-
Hg	-	0.06	-	0.33	0.19	-	0.32	0.09	0.38	-	-	0.71	-	-
Mn	-	-	-	-	-	-	-	-	-	0.07	0.03	-	-	-
Cd	-	-	-	-	-	-	-	-	-	0.03	0.45	-	-	-
Ag	-	0.02	-	0.05	0.01	-	-	0.02	-	0.04	-	0.07	-	-
Pb	-	-	-	-	-	-	-	-	-	86.61	-	-	-	-
Σ	100.71	101.80	101.08	100.78	99.55	101.40	101.22	100.65	100.62	99.85	99.23	101.75	101.89	101.22
recaltulated on the Σ of atoms	3	3	3	5	5	5	7	7	-	2	2	29	3	3
Fe	1.02	0.92	0.95	0.01	0.00	0.01	0.97	0.99	-	0.00	0.10	1.83	0.99	0.98
Sb	0.93	1.07	1.03	2.11	2.16	2.04	2. 09	2.09	-	-	-	4.33	0.00	0.00
Bi	-	0.00	-	-	0.00	-	0.02	-	-	-	-	-	0.00	0.00
S	1.04	1.01	1.01	2.88	2.82	2.94	3.92	3.87	-	0.98	0.98	13.17	2.01	1.98
Au	0.00	-	-	-	-	0.00	-	-	-	-	-	-	0.00	0.00
As	0.00	0.00	-	-	0.12	0.00	0.23	0.04	-	-	-	-	0.00	0.04
Ni	-	-	-	0.00	-	-	-	0.00	-	-	-	-	0.00	0.00
Co	-	0.00	-	0.00	0.00	-	-	-	-	-	-	-	0.00	0.00
Cu	-	0.00	-	-	0.00	-	-	0.01	-	-	-	9.67	-	-
Zn	-	-	-	0.00	0.00	-	-	-	-	0.09	0.92	0.16	-	-
Hg	-	0.00	-	0.00	0.00	-	0.01	0.00	-	-	-	0.00	-	-
Mn	-	-	-	-	-	-	-	-	-	0.00	0.00	-	-	-
Cd	-	-	-	-	-	-	-	-	-	0.00	0.00	-	-	-
Ag	-	0.00	0.00	0.00	0.00	-	-	0.00	-	0.00	-	0.00	-	-
Pb	-	-	-	-	-	-	-	-	-	1.01	-	-	-	-
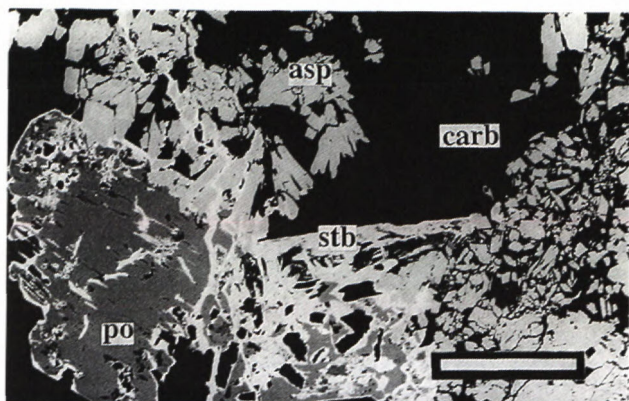
Fig. 17 Pyrrhotite (po), arsenopyrite (asp), stibnite (stb) in carbonate (carb) vein. Pyrrhotite is replaced by stibnite, arsenopyrite appears to be in equilibrium with pyrrhotite, adit sample, SEM image, scale bar is 100 μm.

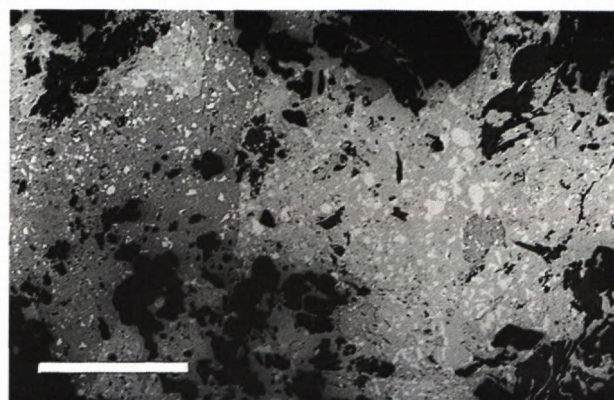*Fig. 18 SEM image of replacement texture of hypogene kermesite (dark grey), valentinite (grey) and native antimony (white), scale bar is 100 μm.*

Tetrahedrite is rare, it associates with chalcopyrite, berthierite, eventually with native antimony. From the chemical composition follows its classification as an Sb member of the tetrahedrite-tenantite series with minor As contents and increased Fe contents. Contents of Zn, Hg, and Ag are low (Tab. 4, analysis 12).

Ullmanite was recorded in calcite veins with gudmundite, chalcopyrite, tetrahedrite, and berthierite. Detailed description and data for this mineral are summarised in Andráš & Chovan (1995).

Gold is chemically bonded preferentially to arsenopyrite and pyrite with contents up to 230 ppm (Andráš et al., 1995, 2000). Its distribution is irregular and Au bonding in sulphides is not satisfactorily explained. No visible gold was recorded on the Trojárová deposit.

Sb oxides and sulphooxides represent a unique stage in the Sb-Fe-As-Au mineralization, characterized by shift from sulphidic towards oxidic conditions. Abundant *kermesite* forms aggregates or spicular crystals, often radially arranged. In massive ores it intergrows with stibnite and also associates with gudmundite, berthierite and native antimony. Kermesite also forms intergrowths with other Sb oxides/sulphooxides (Fig. 18). *Valentinite* was identified optically and microchemically (Tab. 5, analyses 2, 3). *Senarmontite* is isotropic and intergrows with kermesite and valentinite. *Cervantite* was also identified macroscopically. Sb oxides/sulphooxides replace native antimony and stibnite, especially along boundaries between the two minerals or along their boundaries with quartz. Relics of the primary phases often occur in the aggregates of Sb oxides/sulphooxides (Fig. 18). Aggregates of Sb oxides/sulphooxides were intersected by veins of younger generation of stibnite, which has also sealed hydraulic fractures in these aggregates (samples from Antimonitová adit, Kolársky vrch).

Gangue minerals

Carbonates are dominant gangue minerals on the Trojárová deposit. They form lenses and veins in black shales of thickness ranging from centimetres up to several decimetres but rarely they also occur in adjacent "actinolitic" schists and amphibolites. Fine- to medium grained carbonate aggregates of grey or yellowish-white colour are usually intergrown with quartz and host As-, Sb-, and Fe-sulphides. According to DTA and manometric analyses dolomite-ankerite predominate, calcite is more seldom. The younger (several mm thick) carbonate veins of white colour, intersecting older massive carbonatic aggregates and upright penetrating the schistosity, consist exclusively of calcite. Marcasite is present in these calcite veins.

Quartz accompanied by arsenopyrite and pyrite forms cataclased lenses and short veinlets in black shales. Quartz of younger generation, associated with Sb sulphidic mineralization, occurs very rarely.

Discussion and conclusions

Trends of enrichment factors of metallic elements in ore-bearing black shales of the Trojárová deposit are similar to those in other productive zones in wider Pezinok area. This concerns mainly C_{org}, C_{min}, As, Sb, Au, S, Mo, and V. High contents of S is due to intensive pyritization in black shales and surrounding rocks. The contents of Sb, Au and As in black shales are markedly increased in comparison with weekly altered and unaltered rocks. Variations in the S concentration depend on the intensity of pyritization. Sb and As enrichments in black shales are negligible and show negative correlation with C_{org}. As, Sb, and S contents are slightly increased in hydrothermally altered rocks.

Correlation relations between elements indicate 1) binding of Au to arsenopyrite; 2) close association of ore minerals with carbonates and 3) intensive pyritization of black shales. Since the Sb mineralization is hosted in carbonate veins, often cutting the black shale foliation, it is considered as epigenetic. However, significant positive correlation of Sb and C_{org} and weak negative correlation of Sb and C_{min} in 12 samples from boreholes (Fig.4) contradict to this statement. The explanation is problematic. Macroscopical crystals of Sb minerals and their variable

Tab. 5 Electron microprobe analyses of molybdenite (1) and Sb oxides (2,3) and sulphooxides (4-6), the Pezinok – Trojárová deposit.

Analyses number	1	2	3	4	5	6
Sample	45/271	57/171.9	57/171.9	57/171.9	57/171.9	57/171.9
As	-	0.10	0.00	0.00	0.17	0.00
Bi	-	0.00	0.05	0.39	0.00	0.00
Fe	-	0.01	0.03	1.47	0.00	1.13
Hg	-	0.61	0.00	0.90	0.17	0.41
Mo	60.54	-	-	-	-	-
S	39.20	0.09	0.03	20.14	18.68	18.37
Sb	-	80.22	80.51	73.18	74.99	73.72
W	0.20		-	-	-	-
Σ	99.94	81.03	80.62	96.08	94.01	93.63
Recalculated on	2 atoms	3 oxygens	3 oxygens	1 oxygen	1 oxygen	1 oxygen
Mo	1.02	-	-	-	-	-
S	1.98	-	-	2.16	1.88	1.85
Sb	-	1.78	1.79	2.07	1.99	1.96
O	-	3.20	3.27	0.84	1.20	1.23
Σ	-	4.98	5.06	5.07	6.07	6.04

content in carbonate veins can devalue results of statistical analysis. Association of Sb minerals with carbonate veins was confirmed by statistical analysis of 42 samples from borehole, with positive correlation between C_{min} and Sb (r = 0.51) (Chovan et al., 1990), as well as in samples of black shales form Trojárová adit (Fig. 5).

Three ore mineralizations types were distinguished (Table 6). The oldest *exhalation-sedimentary pyrite* mineralization has evolved in black shales and was subsequently metamorphosed. Dominant association pyrite-pyrrhotite is accompanied by accessory chalcopyrite and sphalerite. In the same environment the later superimposed *hydrothermal Sb-Fe-As-Au* mineralization took place. The occurence of the *molybdenite mineralization* is restricted to the leucogranite.

Arsenopyrite is the most abundant ore mineral in samples of hydrothermal mineralization from the Trojárová deposit, pyrite is less frequent. Gudmundite, pyrrhotite and stibnite are rather abundant in samples from Sb-mineralization. Sphalerite, berthierite, native antimony, tetrahedrite, chalcopyrite, and ullmanite are rare. The Au- enrichment was detected in all textural varietes of arsenopyrite and pyrite. Pyrite from surrounding rocks is depleted in Au. Native gold does not occur. Gangue minerals involves predominantly ankerite, minor calcite and quartz.

Despite that complete succession scheme could not be figured out, five evolution periods of hydrothermal mineralization were discerned (see Table 6). The Sb-Fe-As-Au mineralization encompasses several mineral stages.

Pyrite-arsenopyrite stage (1st stage, table 6) associates with carbonates and with dark quartz. Low As contents in studied arsenopyrites does not permit application of the arsenopyrite geothermometer of Kretschmar & Scott (1976), nevertheless, analogical samples from the Kolársky vrch deposit yielded temperature ranges 350-410 °C and 350-450 °C (using geothermometers of

Kretschmar & Scott, 1976 and Sundblad et al., 1984, respectively) for crystallization of arsenopyrite (published in Andráš & Horváth, 1985, Andráš et al., 1999). Increased influx of Sb in the 3rd stage probably caused the observed anomalous Sb contents in arsenopyrite.

Younger **gudmundite I** (2nd stage, table 6) often penetrates the pyrite-arsenopyrite aggregates. Such mineral association is stable at increased fS_2 or increased fO_2 (Williams-Jones & Normand, 1997).

Other mineralization stages are characteristic by intensive carbonatization and presence of Sb minerals.

Paragenesis **gudmundite–berthierite–pyrrhotite–native antimony–stibnite** (3rd stage, table 6) is abundant in a carbonatic veinstone from boreholes. Carbonate veins with Sb sulphides and veins with pyrrhotite intensively penetrate the arsenopyrite and arsenopyrite-pyrite aggregates. Pyrrhotite frequently intergrows with gudmundite or with native antimony. **Pyrrhotite** coexists in a stable association with **native antimony**, which is a rather uncommon. According to Borodaev et al. (1985) and Williams-Jones & Normand (1997) such association is stable at high temperatures (Fig. 19). Other example of similar textural relations between the two minerals is described from the stibnite deposit Quebec Antimony in Canada (Normand et al., 1996). The observed association **pyrrhotite-gudmundite**, which also appears in textures indicating a stable coexistence, is, on the contrary, stable at lower temperatures than pyrrhotite-native antimony paragenesis (Fig. 19).
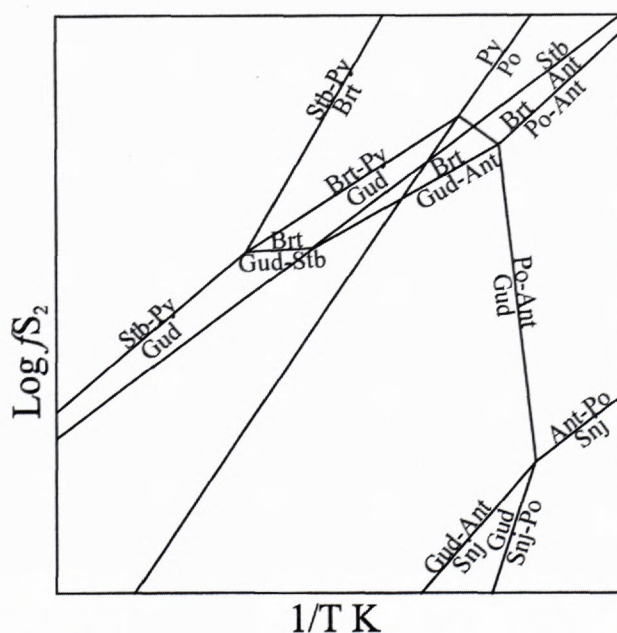
Fig. 19 Topology of the system Fe-Sb-S among the phases stibnite (Stb), native antimony (Ant), gudmundite (Gud), berthierite (Brt), seinäjokite (Snj), pyrite (Py) and pyrrhotite (Po). (After Williams-Jones and Normand 1997).

Pyrrhotite of both associations (with gudmundite and with native antimony, respectively) is intensively replaced by stibnite and berthierite. According to phase diagrams of the system Fe-Sb-S-O proposed by Williams-Jones & Normand (1997) this phase transition indicates a decrease of temperature (Fig. 19).

192

Tab. 6 Succession, mineral assemblages and elements addition, the Pezinok – Trojárová deposit

MINERALIZATION	MINERAL ASSAMBLAGES	ELEMENTS
metamorphosed exhalation-sedimentary	**pyrite, pyrrhotite**, sphalerite, chalcopyrite	Fe, S
hydrothermal in granitoids	**molybdenite**	Mo, S
hydrothermal Sb-Fe-As-Au in black shales, stages:		
1.	ankerite, calcite, quartz **arsenopyrite and pyrite** with invisible gold	Ca, Mg S, As, Fe, Au
2.	gudmundite I, pyrrhotite I, pyrite, quartz	Sb, Fe, S Si, O
3.	ankerite, calcite pyrrhotite II, native antimony, **gudmundite** II, berthierite, **stibnite I,** kermesite, valentinite, uullmanite, tetrahedrite, chalcopyrite	Ca, Mg, C S, Sb, Fe, Ni, Cu, O
4.	stibnite II, (arsenopyrite, gudmundite) (recrystallised)	As, Fe, Sb, S
5.	**calcite**, marcasite	Ca, C, O, Fe, S

Gudmundite appears to have coexisted stably with berthierite. Gudmundite crystallizes at relatively wide spread of fS_2, however, its association with berthierite is stable at higher values of fS_2 (Fig. 19, Williams-Jones & Normand 1997). On the contrary, overgrowths of gudmundite with stibnite show features of corrosion.

In our samples berthierite is far less abundant than stibnite. Williams-Jones & Normand (1997) explained that if cooling is a controlling factor of mineral deposition, at the state of unbuffered fO_2 (resp. fS_2) berthierite is replaced by stibnite on the cooling path.

Mineral association **stibnite-hypogene kermesite–valentinite-senarmontite** is stable at increased fO_2 and high Sb activity (Williams-Jones & Normand, 1997). However, the coeval crystallization of stibnite and Sb oxides / sulfooxides is not evident from textures. The native antimony, stibnite of the 3rd stage (see Table 6), berthierite and gudmundite occur as relics after oxidation in hypogene Sb oxides/sulfooxides. The occurence of native antimony was previously commented by Cambel (1959) who considered it as a transition element on the oxidation path from gudmundite to Sb oxides/ sulfooxides.

The recrystallised euhedral arsenopyrite, tetrahedrite, chalcopyrite and ullmanite are probably connected with 3rd stage (Table 6) mineralization stage.

Late stage stibnite – stibnite II (4th stage, table 6) (thin veinlets, radial aggregates and cements in aggregates of Sb oxides/sulfooxides) appears to be younger than Sb oxides/sulfooxides and coexist with them in a direct contact. It fills fissures and cavities in the Sb oxides/ sulfooxides and native antimony, often crystallized along boundaries between quartz and massive native antimony. The youngest recrystallised stibnite fills the fissures in host rocks. According to Williams-Jones & Normand (1997) stibnite formation is favored by reductive conditions in a course of cooling.

Mineral associations on the deposit Trojárová are analogous to those on the Quebec Antimony deposit, Canada (Williams-Jones & Normand, 1997) where gudmundite and native antimony are dominant ore minerals (Normand et al., 1996) and probably experienced similar evolution, comparable also with other Sb deposits, such as Mari Rosa and El Juncalón deposits in Spain (Ortega & Vindel, 1995), deposits in Montagne Noire region, France (Munoz & Shepherd, 1987), or the Moretons Hratbour deposit in Canada (Kay & Strong, 1983). According to Williams-Jones & Normand (1997) the main factor controlling the stibnite deposition is decreasing temperature.

References

Andráš P., 1984: Questions of antimonite and gold mineralization on the Pezinok deposit. Manuscript, GÚ SAV, Bratislava 154 (in Slovak).

Andráš P., Dubaj D.& Kotulová J., 1999: Arsenopyrite geothermometer application at Pezinok Sb-Au deposit. Miner. Slovaca, 31, 322-324 (in Slovak).

Andráš P. & Horvát I., 1985: Thermoanalytical study of the metamorphism grade in Malé Karpaty Mts. region. Geol. Zbor. Geol. Carpathica, 36, 1, 75-84.

Andráš P. & Chovan M., 1995: Ullmanite from the Trojárová deposit (Malé Karpaty Mts.). Miner. Slovaca 27, 75-77 (in Slovak).

Andráš P., Chovan M., Stankovič J., Paulínyová E. & Svitáčová A., 2000: Distribution of "invisible gold" in gold-bearing sulphides from the West Carpathians Tatrikum, Sovakia, Uhlí Rudy, 2, 16-25 (in Slovak).

Andráš P., Wagner F., Ragan M., Friedl J., Marcoux E., Caňo F. and Nagy G., 1995: Gold in arsenopyrites from the Pezinok deposit (W.Carpathians, Slovakia). Geol. Carpathica, 46, 6, 335-342.

Borodaev Y. S., Mozgova N. N., Ozerova N. A., Slusarev V., Oivanen P & Yletyinen V., 1985: Typomorphic mineral associations of antimony deposits with native antimony in the Baltic Shield. Geol. zbor. (Bratislava), 36, 305-313.

Cambel B., 1959: Hydrotermal deposits in the Malé Karpaty Mts. - mineralogy and geochemistry of their ores. Acta Geol. Geogr. Univ. Comenianae (Bratislava), 3, 338.

Cambel B., Miklós J., Khun M. & Veselský J., 1990: Geochemistry and petrology of clay-metamorphic rocks of the Malé Karpaty Mts. Crystalline complex. Geol. Instit. Slovak. Acad. Sci., Bratislava, 1-267.

Cambel B. & Khun M., 1983: Geochemical characteristic of black shales from the ore-bearing complex of the Malé Karpaty Mts. Geol. Zbor. – Geol. Carpath., 34, 1, 15-44.

Cambel B. & Vilinovič V.,1987: Geochemistry and petrology of granitoids of Malé Karpaty Mts. Veda, Bratislava, 248 (in Slovak).

Ďurža O. & Chovan M., 1995: Thermoelectrical power of molybdenite from Western Carpathian granitoid massives. Miner. Slovaca, 27, 283-286 (in Slovak).

Hanas P., Stupák J. & Tréger M., 1989: The preliminary report Pezinok - Trojárová. Manuscript, Geofond, Bratislava, 101 (in Slovak).

Chovan M. (ed.), 1990: Mineralogical, geochemical and petrographical study of borehole on the Pezinok-Trojárová deposit. Manuscript, Comenius University, Bratislava, 119 p. (in Slovak).

Chovan M., Rojkovič I., Andráš P. & Hanas P., 1992: Ore mineralization of the Malé Karpaty Mts. Geol. Carpathica, 43, 275-286.

Janků H., 1991: Graphite in the Pezinok - Pernek crystalline complex. Manuscript, PriF UK, Bratislava, 59 (in Slovak).

Judovič J. E., Ketris M. P. & Merc A. V., 1990: Geochimija i rudogenez zolota v čornych slancach. IGCP 254, Syktyvar, 61.

Judovič J. E. & Ketris M. P., 1991: Geochimija i rudogenez toksičnych elementov - primesej (Cd, Hg, As, Sb, Se) v čornych slancach. IGCP 254, Syktyrkar, 80.

Kantor J., 1974: Sulphur isotopes of the stratiform pyrite deposit Turecký vrch and stibnite deposit Pezinok, in Malé Karpaty Mts. crystalline, Czechoslovakia. Geol. Zbor. SAV, 25, 2, 331 - 334.

Kay A. & Strong D.F., 1983: Geologic and fluid controls on As-Sb-Au mineralization in the Moretons Harbour area, Newfoundland. Econ. Geol., 78, 1590-1604.

Korikovskij S. P., Cambel B., Miklóš J. & Janák M., 1984: Metamorphose of the Malé Karpaty Mts. crystalline: stages, zonality, connection with the granitoids. Geol. Zbor. Geol. Carpathica, 35, 4, 437-462 (in Russian).

Kretschmar U. & Scott S. D., 1976: Phase relation involving arsenopyrite in the system Fe-As-S and their application. Canad. Mineralogist, 14, 363-386.

Leake B.E., Woolley A.R., Arps Ch.E.S., Birch W. D., Gilbert M. Ch., Grice J.D., Hartworne F. C., Kato A., Kisch H.J., Krivovichet V.G., Linthout K., Laird J., Mandarino J. A., Maresch W.V., Nickel E.H., Rock N. M.S., Schumacher J.C., Smith D.C., Stephenson N. C. N., Ungaretti L., Whittaker E.J.W. & Youzhi G., 1997: Nomenclature of amphibolites: report of the subcommitee on amphiboles of the international mineralogical association, commission on new minerals and mineral names. The Canadian Mineralogists, 35,219-237.

Maheľ M., 1983: Beziehung Westkarpaten-Ostalpen, Position der Ubergangs-Abschnites-Deviner Karpaten. Geol. Zbor. Geol. Carpathica, 34, 2, 131-149.

Moravanský D., 2000: Chemical composition of selected minerals and it's changes in hydrotermal alteration processes of γδ and metahasites (philosilicates and amphibolites). Manucript, RNDr. thesis, PriF UK, Bratislava, 74.

Moravanský D., Chovan M. & Lipka J., 2001: Phyllosilicates form hydrothermally altered granitoid rocks in the Pezinok Sb-Au deposit, Western Carpatians, Slovakia. Geol. Carpathica, 52, 3, 127-138.

Munoz M. & Shepherd T. J., 1987: Fluid inclusion study of the Bournac polymetallic (Sb-As-Pb-Zn-Fe-Cu...) vein deposit (Montagne Noire, France). Mineral. Deposita, 22, 11-17.

Normand CH., Gauthier M. & Jébrak M,. 1996: The Québec Antimony Deposit: An Example of Gudmundite-Native Antimony Mineralization in the Ophiolitic Mélange of the Southeastern Québec Appalachians. Economic Geology, 91, 149 - 163.

Ortega L. & Vindel E., 1995: Evolution of ore forming fluid associated with late Hercynian antimony deposits in Central/Western Spain: case study of Mari Rosa and El Juncalón. Eur. J. Mineral., 7, 655-673.

Oružinský V., Chovan M. & Hanas P., 1990: Black shales and Sb, Fe mineralization at the Pezinok - Trojárová deposit. Geol. Prusk., Praha, 9/10, 290-291 (in Slovak).

Planderová E. & Pahr A., 1983: Biostratigraphical evaluation of weakly metamorphosed sediments of Wechsel series and their possible correlation with Harmónia Group in Malé Karpaty Mts. Miner. Slovaca, 15, 5, 358-436.

Plašienka D., Michalík J., Kováč M., Gross P. & Putiš M., 1991: Paleotectonic evolution of Malé Karpaty Mts. - an overview. Geol. Carpathica, 42, 4, 195-208.

Polák S., 1974: Antimony ores of the Malé Karpaty Mts. - a new insight into prospecting problematic. Geol. Pruskum, 16, 97-99 (in Slovak).

Polák S. & Rak D., 1980: Prognostication problem of antimony mineralization in the Malé Karpaty Mountains. In: Ilavský (Ed.): Antimony ore mineralizations of Czechoslovakia, GÚDŠ, 69-88 (in Slovak).

Putiš M., 1987: Geology and tectonics of SW and N part of the crystalline in Malé Karpaty Mts. Miner. Slovaca, 19, 2, 135-157 (in Slovak).

Uher P., Chovan M. & Majzlan D., 1994: Vanadian-chromian garnet in mafic pyroclastic rocks of the Malé Karpaty Mts., Western Carpathians, Slovakia. Candian Mineralogist, 32, 319-326.

Sundblad K., Zachrison E., Smers, S. H., Berglund S. & Alinder C., 1984: Sphalerite geobarometry and arsenopyrite geothermometry applied to metamorphoused sulfide ores in the Swedish Caledonides. Econ. Geol., 79, 1660-1668.

Williams-Jones A. E. & Normand Ch., 1997: Controls of Mineral Parageneses in the System Fe-Sb-S-O. Econ. Geol., 92, 308 - 324.

Tennantite from the vein Mayer, baňa Mária deposit in Rožňava, Spišsko-gemerské rudohorie Mts.

ANTAL BORIS

Department of Geology of Mineral Deposits, Faculty of Natural Sciences, Comenius University,
Mlynská dolina, 842 15 Bratislava

Abstract: Tennantite has been determined at the deposit Rožňava, located at the eastern margin of the southern belt of deposits in the Spišsko-Gemerské Rudohorie Mts., formed by deposits of the siderite-sulphide formation. Tennantite was not described from deposits of this belt so far.

This mineral was determined from the vein Mayer, located in the eastern part of the deposit Rožňava at the mine Mária in the chalcopyrite-pyrite aggregate. Here it forms a fine network of veinlets associated with mixed phases of tetrahedrite composition. These veinlets consist of phases that form three generations, based on textural-structural relations and different chemical composition. The youngest generation cements older part of the aggregate. It is predominantly homogeneous with high As (3.57-4.08 atoms) and Fe (1.6-1.86 atoms) contents and low scatter of their values - this is Fe-tennantite. Older generation is formed by zoned, crushed aggregate with variable concentrations of both As and Fe, increasing towards the margin of the aggregate. It is formed by a mixed Fe-type of tetrahedrite-tennantite (1.06<As<3.14; 1.26<Fe<1.61 atoms). A fragment (crystalline core) in the previous phase of mixed composition represents the oldest generation. Typically, it has an excess of S and PMe, lower Fe content from 1.25 to 1.37 atoms and high Sb content – this is Fe-tetrahedrite. Its chemical composition is similar to tetrahedrites from other samples from the vein Mayer. These represent Sb-member of the mineral series with lower Fe content compared to other analyses (1.34-1.60 atoms), with significant excess of PMe and Me at the expense of S and with the presence of minor elements, such as Hg (0.8-2.31 wt.%), Bi (0.06-0.73 wt.%) and Ag (0.27-0.81 wt.%).

Keywords: Spišsko-Gemerské Rudohorie Mts., hydrothermal mineralisation, Fe-tetrahedrite to Fe-tennantite.

Introduction

Rožňava is the most important ore deposit region in the southern belt of deposits in the Spišsko-Gemerské Rudohorie Mts., formed by deposits of the siderite-sulphide formation.

This region consists of a dense cluster of vein structures having a lens-like form of veins, both in their direction and dip. The course of veins is conformable to the general direction of rocks and their cleavage planes formed by Alpine tectonics. Vein structures are of interfoliaceous, intercleavageous type (Bernard, et al., 1981; Ilavský, et al., 1979; Rozložník, 1982; Slavkovský, 1978; Varček, 1973; 1973a; Varček, et al., 1968).

The deposit region is divided into two parts: the western part formed by a fan of veins in the massif of the ground elevation Turecká, and the eastern one, formed by a number of veins located N from the town Rožňava in the area of Rožňava spa. The vein Maria, with the parallel segment called Mayer or Mária II, is the most important vein in the eastern part. Recently, blind lodes called Strieborná and less important vein Pallag in SE have been discovered here too (Babčan & Novák, 1961; Fusán, et al., 1963; Mesarčík, 1986, 1991, 1996; Paholič, 1969).

The vein Mária occurs here in a complex of rocks of the Gelnica group, formed by alternating quartzites, quartz-sericite phyllites and porphyroids of the Drnava group of beds (Bernard, et al., 1969; 1981; Ilavský, et al.,

1964; Novák, 1959; Rozložník, 1973, 1981; Slávik, et al., 1967; Varček, 1954, 1954a; Varček, 1959; Varček, 1973; 1973a; Varček, et al., 1968).

According to studies of Varček (1953 - 1961), Novák (1960), Rozložník (1981) and Mesarčík et al. (1986) the vein has a simple mineralisation. In siderite, veinlets with quartz and abundant tetrahedrite, minor pyrite and rare chalcopyrite occur. In this study a range of other primary and secondary minerals has been determined (fig. 1).

The vein Mayer is considered as a SW segment of the vein Mária, duplicated by tectonics (Abonyi et al., 1977). Before, it was regarded as a separate vein cropping out in the area of the hill Kalvária, where Cu and Ag ore used to be mined. The mineralisation is similar to the vein Mária, but it contains less tetrahedrite.

Strieborná vein structure was opened at 13th level during the exploration of the SE vicinity of the deposit. Nowadays, the deposit is opened also on the 10th and 8th levels, it has the average thickness of 4.9 m and a variable screw-shaped inclination alike the vein Mária.

Mineralogy of tetrahedrite

Tetrahedrite, the most abundant mineral of ore veins at the deposit, together with chalcopyrite form the main components of the primary copper ores. Together with chalcopyrite and quartz it forms a network of thin veinlets, penetrating siderite, or irregular massive aggregates

Slovak Geol. Mag., 8, 3– 4(2002), 195– 204

196
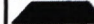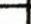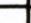
Stage	Siderite	Quartz-ankerite siderite		Quartz-sulphide			Quartz-stibnite	Supergenne minerals
Substage		1	2	1	2	3		
Quartz		▬		▬	▬	▬	▬	
Sericite		▬		▬				
Turmaline				▬			▬	
Albite				▬				
Hydromica				▬				Allophane
Apatit				▬				Aragonite
Siderite	▬		▬		▬		▬	Annabergite
Ankerite			▬			▬		Barite
Pyrite	▬	▬		▬	▬		▬	Covellite
Arsenopyrite					▬		▬	Delafossite
Gersdorffite				▬				Erythrite
Ullmanite				▬				Goethite
Kobellite				▬				Halloysite
Pyrhotite				▬				Gibbsite
Marcasite					▬			Calcite
Sphalerite					▬			Cuprite
Chalcopyrite					▬			Malachite
Tetrahedrite					▬			Mn-Oxides
X-mineral					▬			Cinnabar
Nativ Bi					▬			Native Ag
Nativ Gold					▬			Native Hg
Galena						▬	▬	Native Cu
Stibnite							▬	Gypsum
Jamesonite							▬	
Cinnabar						▬		
Barite					▬	▬		
Hematite						▬		
Calcite						▬		

Fig. 1. Succession scheme of mineralisation at the deposit Mária in Rožňava (Rozložník, 1981).

and clusters, several centimetres in size. Tetrahedrite also occurs in the form of idiomorphic crystals of tetrahedrite habit, 2-4 mm, max. 2 cm in size, associated with columnar crystals of quartz. In the past it was mined at upper levels of the deposit due to the increased Ag content that gradually decreased with depth. It intimately intergrows with kobellite. According to the published chemical composition only tetrahedrite - Sb-end member of the isomorphous tehrahedrite-tennantite mineral series with As content up to 2.35 wt.% (Cu 30.81-36.95; Ag 0.49-0.60; Fe 5.23-6.64; Zn 0.95-1.03; Hg 1.37-2.24; Sb 25.53-29.06; As 0.74-2.35; S 24.74-25.52; Bi 0.31-1.55 wt.%; vein Mária) has been described yet at the deposit (Bernard, 1958; Bernard, et al., 1969; 1981; Kupčík, Matherny & Varček, 1961; Novák, 1959; 1961; 1967; Slávik, et al., 1967; Varček, 1959).

Tennantite, the As-end member of the isomorphous tetrahedrite-tennantite mineral series, was described only from deposits of the northern siderite-sulphide belt, namely from the deposit Dobšiná (Ni-Cu veins, Kašpar, 1970),

Hnilčík - district of Gretla (Bernard, et al., 1981; Macko & Ondrejkovič, 1965; Slávik, et al., 1967; Varček, 1973a), Košická Belá – Vodná Baňa (Ďuďa, 1976), Mlynky – district of Havrania dolina (Rieder, 1963), Slovinky (Regásek, 1968), Spišská Nová Ves – Cu-sandstones and from the deposit Novoveská Huta (Háber, Krištín & Rojkovič 1993).

Methodology

A study using a scanning electron microscope (JEOL JSM - 840 and EDAX, Geol. Survey of the Slovak Rep. Bratislava, D. Dubík) preceded quantitative microchemical analyses.

Quantitative analyses were carried out on the instrument JEOL SUPERPROBE 733 (Geol. Survey of the Slovak Rep. Bratislava) using a correlation program ZAF-M, 20nA beam current, 25kV accelerating voltage and LiF crystal. The following standards were used: pure Cu, Ag, Fe, Zn, Co, Ni, Bi, Sb, Te, Au, cinnabar for Hg,

Tab. 1. Quantitative microchemical analyses of tetrahedrite-tennantite aggregates (wt. %) from the vein Mayer in Rožňava, mine Mária. m - homogeneous aggreg., br – bright phase, dk – dark phase, xx – fragment of bright phase; other measured elements, such as Au, Ni, Co, Pb, Te and Se did not reach detectable concentrations (JEOL SUPERPROBE 733, Geol. Survey of the Slovak Rep. Bratislava, P. Konečný, P. Siman and D. Ozdín.).

Samp. No.	Phase	Anal. No.	(Cu	Ag)	(Fe	Zn	Hg)	(Sb	As	Bi)	S	Total
9	m	12	36,58	0,81	4,59	1,39	1,92	30,04	0,55	0,39	24,21	100,48
9	m	13	37,23	0,76	4,68	1,36	1,67	29,46	0,93	0,46	23,94	100,49
10	m	14	36,61	0,39	4,57	1,13	1,64	30,43	0,73	0,51	23,05	99,06
10	m	15	37,26	0,48	4,86	1,07	1,41	29,36	0,79	0,39	24,05	99,67
11	m	16	38,02	0,31	4,72	1,07	1,57	29,28	1,07	0,09	23,82	99,95
11	m	17	37,69	0,27	4,81	1,07	2,08	29,43	0,87	0,32	23,85	100,39
13	m	18	36,71	0,52	4,65	1,24	1,63	30,44	0,71	0,73	23,2	99,83
13	m	19	37,64	0,51	4,61	1,39	0,8	29,81	0,79	0,29	22,44	98,28
14	m	20	37,82	0,32	4,36	1,33	1,35	31,12	0,35	0,19	23,29	100,13
14	m	21	37,26	0,32	4,81	1,18	1,44	31,14	0,41	0,13	21,88	98,57
14	m	22	38,56	0,28	4,79	1,21	1,72	29,39	0,4	0,27	23,35	99,97
14	m	23	37,65	0,42	4,86	1,08	2,02	30,37	0,41	0,06	23,92	100,79
15	m	24	37,31	0,66	4,68	1,05	1,74	29,73	0,48	0,45	23,62	99,72
15	m	25	36,89	0,74	4,62	0,83	2,31	29,34	0,7	0,25	21,46	97,14
16	m	26	37,76	0,72	5,06	0,86	1,33	28,28	1,05	0,55	21,97	97,58
16	m	27	38,48	0,61	5,01	0,99	1,44	28,69	1,05	0,56	23,44	100,27
16	m	28	36,99	0,6	5,03	0,49	2,18	28,35	0,92	0,69	22,26	97,51
17	br	2	40,68	0	5,62	1,19	0	15,1	10,3	0	26,84	99,73
17	br	3	40,77	0	5,82	0,99	0	11,16	12,82	0	27,28	98,84
17	br	7	41,44	0	5,58	1,58	0	8,72	14,53	0	28,77	100,62
17	br	8	41,33	0	5,6	1,58	0	9,34	14,42	0	27,92	100,19
17	br	51	40,53	0	5,21	1,53	0	8,66	14,4	0	27,95	98,28
17	br	52	41,23	0	5,26	1,77	0	9,13	13,9	0	28,04	99,33
17	br	53	41,41	0	5,29	1,61	0	9,34	13,98	0	27,69	99,32
17	br	59	40,64	0	5,66	1,02	0	10,14	13,17	0	28,28	98,91
17	br	60	38,98	0	4,87	1,87	0	21,43	4,93	0	26,66	98,74
17	br	61	39,13	0	4,5	2,23	0	18,33	7,66	0	27,08	98,93
17	br	62	39,94	0	4,54	2,12	0	15,76	9,89	0	27,69	99,94
17	br	4	41,64	0	5,75	1,52	0	7,27	15,76	0	28,48	100,42
17	dr	5	42,56	0	6,85	0,84	0	0,18	19,51	0	29,35	99,29
17	dr	6	42,15	0	6,05	1,11	0	2,86	18,08	0	29,08	99,33
17	dr	54	42,13	0	6,31	0,87	0	0	19,44	0	29,39	98,14
17	dr	55	41,82	0	6,44	0,82	0	0	20,42	0	29,45	98,95
17	dr	56	42,06	0	6,99	0,65	0	0	20,24	0	28,93	98,87
17	dr	57	42,37	0	6,91	0	0	0	20,56	0	29,46	99,30
17	dr	58	42,25	0	7,11	0	0	0	20,25	0	29,51	99,12
17	dr	63	41,33	0	6,51	0,75	0	2,68	18,24	0	29,46	98,97
17	dr	64	41,69	0	6,71	0,5	0	0	20,68	0	29,36	98,94
17	dr	65	42,09	0	6,53	0,45	0	0	20,92	0	29,49	99,48
17	xx	x	37,39	0	4,62	2,33	0	27,56	1,17	0	25,84	98,91
17	xx	x/1	37,04	0,06	4,19	2,13	0	29,09	1,23	0	25,51	99,25
	m	min	36,58	0,27	4,36	0,49	0,80	28,28	0,35	0,06	21,46	97,14
	m	avg	37,44	0,51	4,75	1,10	1,66	29,69	0,72	0,37	23,16	99,40
	m	max	38,56	0,81	5,06	1,39	2,31	31,14	1,07	0,73	24,21	100,79
	br	min	38,98	0,00	4,50	0,99	0,00	7,27	4,93	0,00	26,66	98,28
	br	avg	40,64	0,00	5,31	1,58	0,00	12,03	12,15	0,00	27,72	99,44
	br	max	41,64	0,00	5,82	2,23	0,00	21,43	15,76	0,00	28,77	100,62
	dr	min	41,33	0,00	6,05	0,00	0,00	0,00	18,08	0,00	28,93	98,14
	dr	avg	42,05	0,00	6,64	0,60	0,00	0,57	19,83	0,00	29,35	99,04
	dr	max	42,56	0,00	7,11	1,11	0,00	2,86	20,92	0,00	29,51	99,48

arsenopyrite for As and S, Bi_2Se_3 for Se. Operators were P. Konečný, P. Siman and D. Ozdín.

Measurements were performed on polished, degreased and ultrasonic-cleaned sections, coated by carbon. Apart from elements shown in tables 1 and 2 also some other elements, such as Au, Ni, Co, Pb, Te and Se were measured, but they did not reach detectable concentrations.

Crystallochemical formulas of tetrahedrites were recalculated according to the basic structure of the cell Me^{+1}_{10}, Me^{+2}_2, $PMe4$, S_{13}. This represents 29 atoms per unit cell.

Results

Mineralogical study of ore vein filling from the deposit Baňa Mária detected tennantite in chalcopyrite aggregate, associated with mixed phases of tetrahedrite composition (sample no. A-17, vein Mayer, 11th level; fig. 2).

The massive aggregate of chalcopyrite, occurring in siderite veinstone, is relatively heavily intergrown with "chains" of allotriomorphic pyrites. In the aggregate
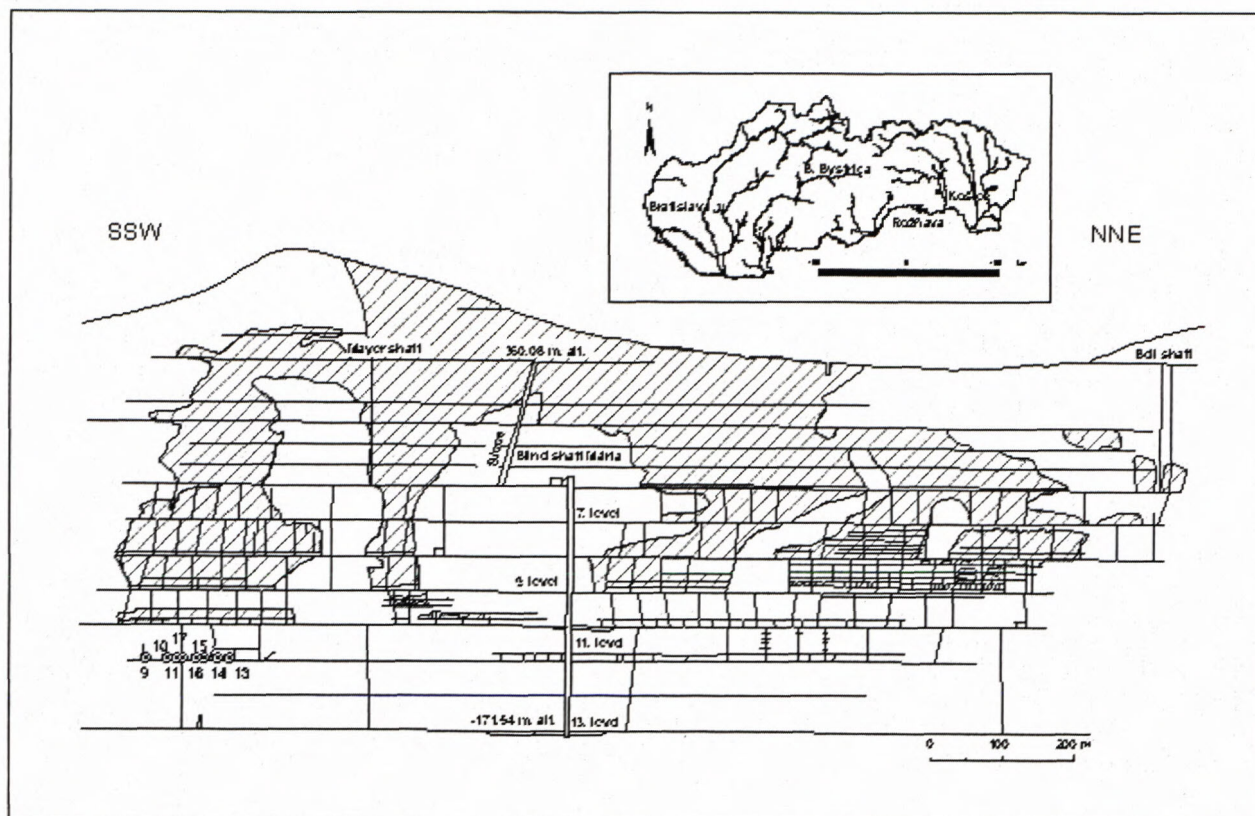
Fig. 2. The mine Mária, layout of veins Mária and Mayer with location of analysed samples. Cross-hatched area represents worked-out spaces.

irregular inclusions of quartz and phenocrysts – metacrysts of carbonates of rhombohedral section also occur. A network of fine veinlets of tetrahedrite-tennantite composition cuts the whole aggregate. Locally breccias of chalcopyrite, cemented by tetrahedrite, occur (fig. 3. A, B).

Homogenity of tetrahedrite – tennantite veinlets

A variable degree of homogenity was recognised during the SEM study of tetrahedrite aggregates, forming veinlets. Thin veinlets cutting the „chains" of pyrite appear to be completely homogeneous (fig. 3. A).

A coarser veinlet in chalcopyrite proved to be inhomogeneous (fig. 3. B). It consists of two phases with a cataclastic mutual relationship. Older (bright) phase is broken, cemented and overprinted by younger (dark) phase (fig. A, C, D). Older phase has a banded – colloform texture. The alternating zones penetrate across the whole aggregate (fig. 4. A, C), while the brighter component diminishes in direction from assumed cores of crystals to the margin of the aggregate. The cores of crystals are formed by fragments of even brighter phase (fig. 4. B).

Younger (darker) phase, that cements the crushed aggregate of brighter phase, is usually homogeneous, only in the proximity of fragments of brighter phase it locally forms a diffuse to banded texture (fig. 4. D).

Chemical composition of aggregates of tetrahedrite – tennantite veinlets

The chemical composition of analysed mineral phases, forming veinlets in chalcopyrite, varies from mineral aggregates of mixed composition (bright phase) with tetrahedrite number from 72.79 to 22.11 up to As end-member of the tetrahedrite-tennantite isomorphous series (dark phase) with tetrahedrite number from 8.87 up to 0.00. On the other hand, the fragment of brighter phase represents an Sb end-member (As<1 atom.) with tetrahedrite number 93.6 (tab. 1, 2).

These phases (dark and bright) typically have an excess of S compared to the theoretical composition and a lack of monovalent (Me^{+1}) and bivalent (Me^{+2}) metals (fig. 5. A, B). The number of atoms of mettaloids (PMe) is mostly close to the theoretical composition (fig. 5. C, D).

The dark phase has higher As content with low scatter of values around the theoretical composition of four atoms. The bright phase has higher content of Sb (0.89 – 2.83 atoms) and the scatter of values varies in the range of up to 2 atoms (fig. 6. A, B, C, D).

Concentrations of mono- and bivalent metals form a smaller scatter of values (about 0.2 – 0.3 atoms). The concentrations of Me^{+1}, formed by Cu only, reach higher values in the bright phase than in the dark one. Zn content values form similar relations. So the dark phase has higher number of As and Fe atoms, while the dark one has higher number of Sb, Zn and Cu atoms, reciprocally (fig. 6. B, C, D).

The described chemical composition of As phases (dark and bright ones) is markedly contrast compared to other analysed mineral aggregates of tetrahedrite samples from the vein Mayer. The presence of minor elements, such as Ag, Hg, Bi and Sb is a characteristic for these aggregates. The high concentration of Sb (4 – 4.51 atoms)

Tab. 2. Composition of tetrahedrite-tennantite aggregates (number of atoms) from the vein Mayer in Rožňava, mine Mária. m – homogeneous aggreg., br – bright phase, dk – dark phase, xx – frag-fragment of bright phase, TD/TN – tetrahedrite number; recalculated for 29 atoms (JEOL SUPERPROBE 733, Geol. Survey of the Slovak Rep. Bratislava, P. Konečný, P. Siman and D. Ozdín.).

Samp. No.	Phase	Anal. No.	Cu	Ag	A 10	A/10	Fe	Zn	Fe+Zn	Hg	B 2	B/2	Sb	As	Bi	C 4	C/4	S	S/13	TD/TN
9	m	12	9,78	0,13	9,91	0,99	1,40	0,36	1,76	0,16	1,92	0,96	4,19	0,12	0,03	4,35	1,09	12,83	0,99	97,1
9	m	13	9,94	0,12	10,06	1,01	1,42	0,35	1,77	0,14	1,92	0,96	4,11	0,21	0,04	4,35	1,09	12,67	0,97	95,1
10	m	14	10,02	0,06	10,08	1,01	1,42	0,30	1,72	0,14	1,87	0,93	4,35	0,17	0,04	4,56	1,14	12,50	0,96	96,2
10	m	15	9,97	0,08	10,05	1,00	1,48	0,28	1,76	0,12	1,88	0,94	4,10	0,18	0,03	4,31	1,08	12,76	0,98	95,8
11	m	16	10,16	0,05	10,21	1,02	1,43	0,28	1,71	0,13	1,85	0,92	4,08	0,24	0,01	4,33	1,08	12,61	0,97	94,4
11	m	17	10,07	0,04	10,12	1,01	1,46	0,28	1,74	0,18	1,92	0,96	4,11	0,20	0,03	4,33	1,08	12,64	0,97	95,4
13	m	18	9,98	0,08	10,06	1,01	1,44	0,33	1,77	0,14	1,91	0,95	4,32	0,16	0,06	4,54	1,14	12,50	0,96	96,3
13	m	19	10,34	0,08	10,42	1,04	1,44	0,37	1,81	0,07	1,88	0,94	4,27	0,18	0,02	4,48	1,12	12,22	0,94	95,9
14	m	20	10,21	0,05	10,26	1,03	1,34	0,35	1,69	0,12	1,80	0,90	4,38	0,08	0,02	4,48	1,12	12,46	0,96	98,2
14	m	21	10,34	0,05	10,39	1,04	1,52	0,32	1,84	0,13	1,96	0,98	4,51	0,10	0,01	4,62	1,15	12,03	0,93	97,9
14	m	22	10,36	0,04	10,40	1,04	1,46	0,32	1,78	0,15	1,93	0,96	4,12	0,09	0,02	4,23	1,06	12,43	0,96	97,8
14	m	23	10,04	0,07	10,11	1,01	1,47	0,28	1,75	0,17	1,93	0,96	4,23	0,09	0,00	4,32	1,08	12,64	0,97	97,9
15	m	24	10,07	0,10	10,17	1,02	1,44	0,28	1,71	0,15	1,86	0,93	4,19	0,11	0,04	4,33	1,08	12,63	0,97	97,4
15	m	25	10,42	0,12	10,55	1,05	1,49	0,23	1,71	0,21	1,92	0,96	4,33	0,17	0,02	4,52	1,13	12,02	0,92	96,3
16	m	26	10,47	0,12	10,59	1,06	1,60	0,23	1,83	0,12	1,95	0,97	4,09	0,25	0,05	4,39	1,10	12,08	0,93	94,3
16	m	27	10,29	0,10	10,39	1,04	1,52	0,26	1,78	0,12	1,90	0,95	4,00	0,24	0,05	4,29	1,07	12,42	0,96	94,4
16	m	28	10,30	0,10	10,40	1,04	1,59	0,13	1,73	0,19	1,92	0,96	4,12	0,22	0,06	4,40	1,10	12,29	0,95	95,0
17	br	2	9,99	0,00	9,99	1,00	1,57	0,28	1,86	0,00	1,86	0,93	1,94	2,15	0,00	4,08	1,02	13,07	1,01	47,4
17	br	3	9,93	0,00	9,93	0,99	1,61	0,23	1,85	0,00	1,85	0,92	1,42	2,65	0,00	4,07	1,02	13,16	1,01	34,9
17	br	7	9,75	0,00	9,75	0,98	1,49	0,36	1,86	0,00	1,86	0,93	1,07	2,90	0,00	3,97	0,99	13,42	1,03	27,0
17	br	8	9,85	0,00	9,85	0,98	1,52	0,37	1,88	0,00	1,88	0,94	1,16	2,91	0,00	4,08	1,02	13,19	1,01	28,5
17	br	51	9,79	0,00	9,79	0,98	1,43	0,36	1,79	0,00	1,79	0,90	1,09	2,95	0,00	4,04	1,01	13,38	1,03	27,0
17	br	52	9,88	0,00	9,88	0,99	1,43	0,41	1,85	0,00	1,85	0,92	1,14	2,82	0,00	3,97	0,99	13,31	1,02	28,8
17	br	53	9,96	0,00	9,96	1,00	1,45	0,38	1,82	0,00	1,82	0,91	1,17	2,85	0,00	4,02	1,01	13,20	1,02	29,1
17	br	59	9,77	0,00	9,77	0,98	1,55	0,24	1,79	0,00	1,79	0,89	1,27	2,69	0,00	3,96	0,99	13,48	1,04	32,1
17	br	60	9,87	0,00	9,87	0,99	1,40	0,46	1,86	0,00	1,86	0,93	2,83	1,06	0,00	3,89	0,97	13,38	1,03	72,8
17	br	61	9,77	0,00	9,77	0,98	1,28	0,54	1,82	0,00	1,82	0,91	2,39	1,62	0,00	4,01	1,00	13,40	1,03	59,6
17	br	62	9,76	0,00	9,76	0,98	1,26	0,50	1,77	0,00	1,77	0,88	2,01	2,05	0,00	4,06	1,02	13,41	1,03	49,5
17	br	4	9,80	0,00	9,80	0,98	1,54	0,35	1,89	0,00	1,89	0,94	0,89	3,14	0,00	4,04	1,01	13,28	1,02	22,1
17	dr	5	9,80	0,00	9,80	0,98	1,79	0,19	1,98	0,00	1,98	0,99	0,02	3,81	0,00	3,83	0,96	13,39	1,03	0,6
17	dr	6	9,81	0,00	9,81	0,98	1,60	0,25	1,85	0,00	1,85	0,93	0,35	3,57	0,00	3,92	0,98	13,42	1,03	8,9
17	dr	54	9,78	0,00	9,78	0,98	1,67	0,20	1,86	0,00	1,86	0,93	0,00	3,83	0,00	3,83	0,96	13,53	1,04	0,0
17	dr	55	9,65	0,00	9,65	0,97	1,69	0,18	1,88	0,00	1,88	0,94	0,00	4,00	0,00	4,00	1,00	13,47	1,04	0,0
17	dr	56	9,75	0,00	9,75	0,97	1,84	0,15	1,99	0,00	1,99	0,99	0,00	3,98	0,00	3,98	0,99	13,29	1,02	0,0
17	dr	57	9,75	0,00	9,75	0,97	1,81	0,00	1,81	0,00	1,81	0,90	0,00	4,01	0,00	4,01	1,00	13,43	1,03	0,0
17	dr	58	9,72	0,00	9,72	0,97	1,86	0,00	1,86	0,00	1,86	0,93	0,00	3,95	0,00	3,95	0,99	13,46	1,04	0,0
17	dr	63	9,61	0,00	9,61	0,96	1,72	0,17	1,89	0,00	1,89	0,95	0,33	3,60	0,00	3,92	0,98	13,58	1,04	8,3
17	dr	64	9,63	0,00	9,63	0,96	1,76	0,11	1,88	0,00	1,88	0,94	0,00	4,05	0,00	4,05	1,01	13,44	1,03	0,0
17	cr	65	9,68	0,00	9,68	0,97	1,71	0,10	1,81	0,00	1,81	0,90	0,00	4,08	0,00	4,08	1,02	13,44	1,03	0,0
17	xx	x	9,72	0,00	9,72	0,97	1,37	0,59	1,96	0,00	1,96	0,98	3,74	0,26	0,00	4,00	1,00	13,32	1,02	93,5
17	xx	x/1	9,70	0,01	9,71	0,97	1,25	0,54	1,79	0,00	1,79	0,90	3,98	0,27	0,00	4,25	1,06	13,25	1,02	93,6
	m	min	9,78	0,04	9,91	0,99	1,34	0,13	1,69	0,07	1,80	0,90	4,00	0,08	0,00	4,23	1,06	12,02	0,92	94,31
	m	avg	10,16	0,08	10,24	1,02	1,47	0,29	1,76	0,14	1,90	0,95	4,21	0,17	0,03	4,40	1,10	12,45	0,96	96,21
	m	max	10,47	0,13	10,59	1,06	1,60	0,37	1,84	0,21	1,96	0,98	4,51	0,25	0,06	4,62	1,15	12,83	0,99	98,21
	br	min	9,75	0,00	9,75	0,98	1,26	0,23	1,77	0,00	1,77	0,88	0,89	1,06	0,00	3,89	0,97	13,07	1,01	22,11
	br	avg	9,84	0,00	9,84	0,98	1,46	0,37	1,84	0,00	1,84	0,92	1,53	2,48	0,00	4,02	1,00	13,31	1,02	38,24
	br	max	9,99	0,00	9,99	1,00	1,61	0,54	1,89	0,00	1,89	0,94	2,83	3,14	0,00	4,08	1,02	13,48	1,04	72,79
	dr	min	9,61	0,00	9,61	0,96	1,60	0,00	1,81	0,00	1,81	0,90	0,00	3,57	0,00	3,83	0,96	13,29	1,02	0,00
	dr	avg	9,72	0,00	9,72	0,97	1,75	0,13	1,88	0,00	1,88	0,94	0,07	3,89	0,00	3,96	0,99	13,44	1,03	1,77
	dr	max	9,81	0,00	9,81	0,98	1,86	0,25	1,99	0,00	1,99	0,99	0,35	4,08	0,00	4,08	1,02	13,58	1,04	8,87
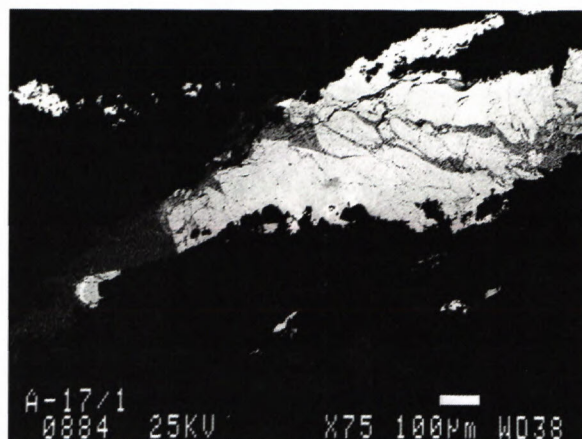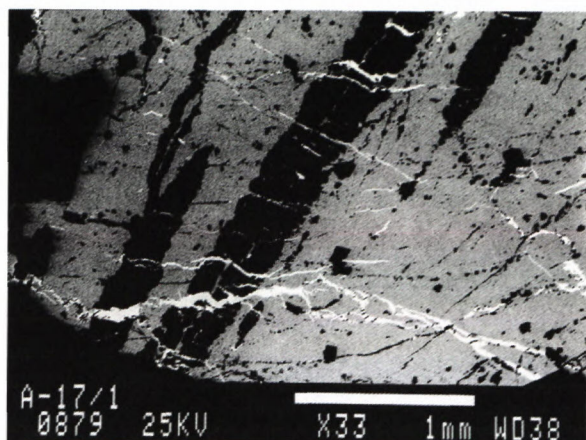
Fig.3. A. Chalcopyrite (pale grey) – pyrite (dark) aggregate with tennantite veinlets (white). B. Tetrahedrite-tennantite vienlet (white and grey) in chalcopyrite (black). SEM images

assigns them to the Sb end-member. An excess of PMe is also typical, formed by Sb itself as well as by the presence of Bi (fig. 5. C, D; 6. C; tab. 1, 2).

Compared to As phases tetrahedrite aggregates have an excess of Me^{+1} but a lack of Me^{+1}, despite interesting concentrations of Hg (0.8 – 2.31 wt.%) (fig. 5. A, B). The excess of Me^{+1} (predominantly Cu; fig. 8. B) is so high, that in spite of the lack of Me^{+2} the total of mono- and bivalent elements exceeds the theoretical value for tetrahedrites.

Interestingly, chemical composition of analyses of "crystalline core – fragment" occur among the analyses of described mineral aggregates. This is an Sb-member of the tetrahedrite-tennantite series with the absence of minor elements (Hg, Bi and negligible Ag content – 0.06 wt.%).

According to the excess of S, high concentrations of PMe, Zn and small concentrations of Me^{+1}, Cu, Ag and Fe they are similar to the bright phase of a mixed composition, but according to Sb and As contents below 1 atom they belong to tetrahedrite (fig. 5, 6).

According to mineralogical observations and chemical analyses the given mineral aggregates are possible to divide into several generations.

A/ The youngest generation is formed by the dark phase, cementing the oldest part of the aggregate and thin veinlets cutting chalcopyrite-pyrite part of the sample. Typically, it has mainly homogeneous composition with high concentrations of As (3.57-4.08 atoms) and Fe (1.6-1.86 atoms) and low scatter of their values. This is an As end-member of the mineral series - tennantite (fig. 3. A, 4. A, C, D).

B/ The "bright" phase forms older generation compared to the earlier. It consists of zoned, crushed aggregate with variable As and Fe contents, with a trend of increasing concentrations in direction towards the margin of the aggregate (fig. 4, A, B, C). It is formed by mixed type of tetrahedrite – tennantite series (1.06<As<3.14; 1.26<Fe<1.61 atoms).

C/ The fragment (crystalline core) in bright phase (B) represents the next generation. This generation has probably homogeneous composition, but the very small size of the fragment does not allow an unambiguous

evaluation. The chemical composition is substantially different from previous phases even if some trends are identical with As phases (excess of S and PMe, lower Fe content from 1.25 to 1.37 atoms and high amount of Sb). This is an Sb end-member – tetrahedrite with the As content markedly below 1 atom. Its chemical composition is close to tetrahedrites from other samples from the vein Mayer (fig. 4. B).

Other samples represent Sb-members of the mineral series with lower content of Fe compared to other analyses (1.34-1.60 atoms) and significant excess of PMe and Me at the expense of S. Low but still present concentrations of minor elements, such as Hg (0.8-2.31 wt.%), Bi (0.06-0.73 wt.%) and Ag (0.27-0.81 wt.%) are the next characteristic (tab. 1).

The chemical composition of tetrahedrite aggregates is not identical to analyses of the "crystalline core – fragment". Neither a direct contact with mineral aggregates of As-phases has been determined, but we suppose that this is a generation older than the As-phases.

All members of the mineral series have substantial prevalence of Fe (above 1 atom), consequently it is possible to say that at the vein Mayer mineral aggregates composed of Fe-tetrahedrite to Fe-tennantite are present.

Conclusions

According to the structural-textural composition of tetrahedrite-tennantite aggregates forming veinlets in chalcopyrite aggregate and based on their different chemical composition we suppose that in the studied sample three generations of minerals of the tetrahedrite-tennantite series are present detached by repeated tectonic movements.

1st generation is formed by Fe-tetrahedrite with Hg, Bi and Ag contents. It represents the major generation widespread along the whole studied part of the vein Mayer and this is in agreement with the data from various authors. Analyse of the "crystalline core – fragment" could be preliminary also assigned to this generation.

2nd generation is formed by Fe-mixed type with a broad spectrum of concentrations of major structural elements.
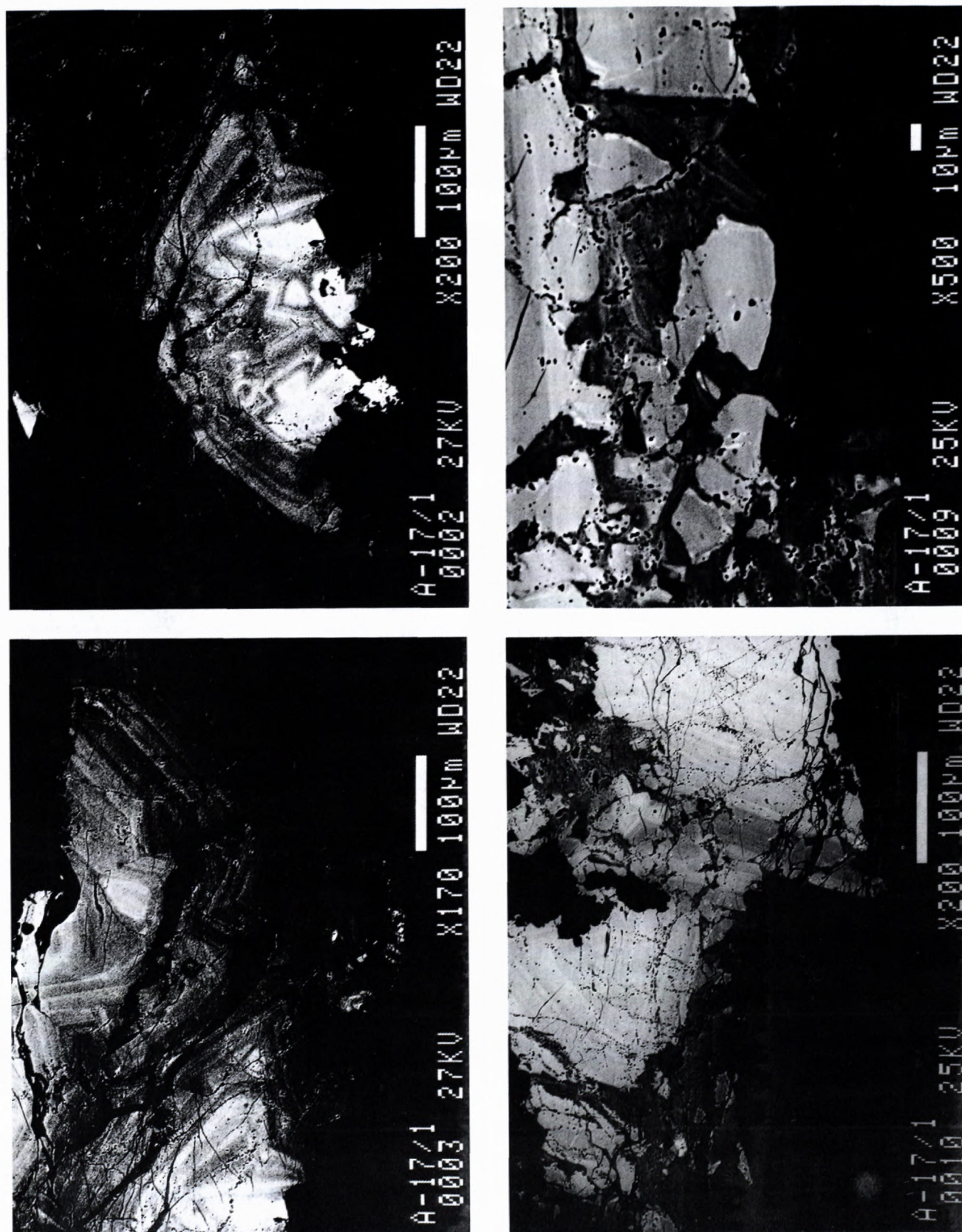
Fig. 4. A. Tetrahedrite-tennantite aggregate, older phase – grey, younger phase – black (detail from fig. 3. B). B. Aggregate of mixed composition composed of older phase with crystalline core – fragment (anal. no. x, x/1) in lower part of the photograph (detail from fig. 3. B). C. Crushed aggregate of mixed composition (pale grey) cemented by younger phase, formed by tennantite (grey). D. Detail of mutual relationship of older (pale grey) and younger phase (grey to black). Numbers show location of microanalyses. SEM images.

Slovak Geol. Mag., 8, 3– 4(2002), 195– 204

202
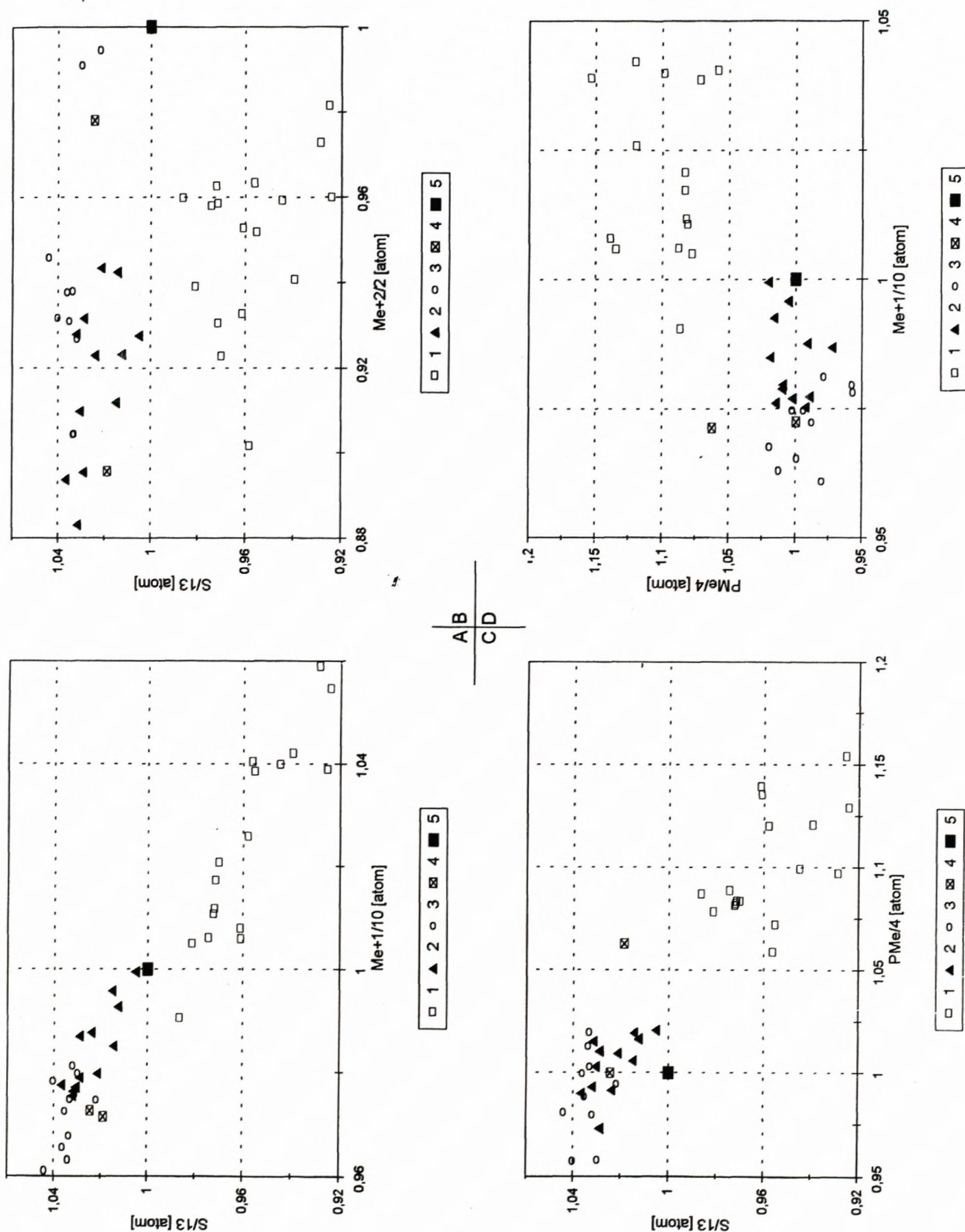
Fig. 5. Correlation diagrams of S, PMe, mono- and bivalent metals in tetrahedrite-tennantite aggregates (1 – homogeneous aggregates, 2 – bright phase, sample no. 17, 3 – dark phase, sample no. 17, 4 – fragment of bright phase, sample no. 17, 5 – theoretical composition).
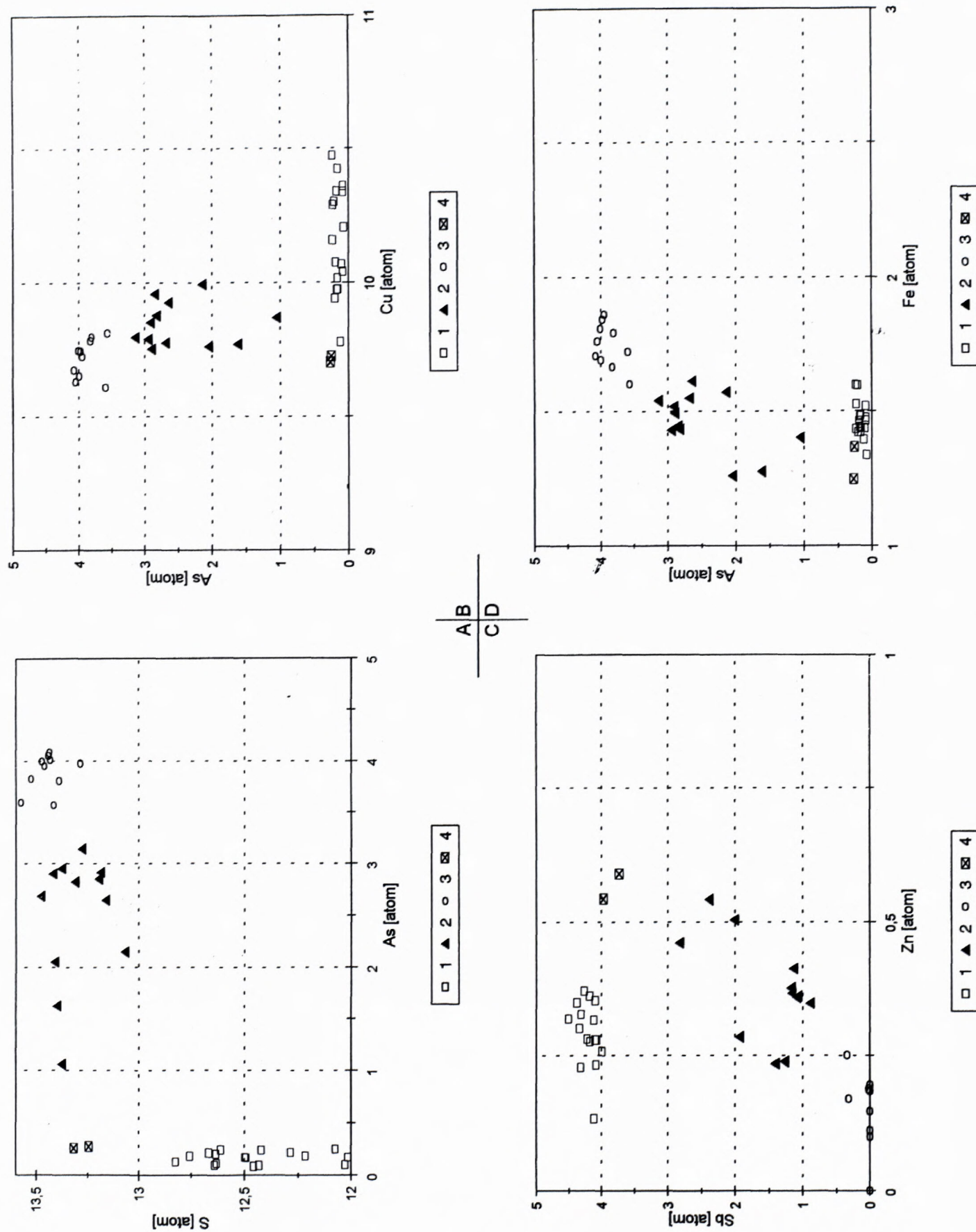
Fig. 6. Correlation diagrams of S, As, Sb, Zn, Fe and Cu in tetrahedrite-tennantite aggregates (1 – homogeneous aggregates, 2 – bright phase, 3 – dark phase, 4 – fragment of bright phase).

3rd generation is the youngest one, represented by Fe-tennantite with narrow spread of values of structural element concentrations.

We suppose that 2nd and 3rd generations originated at the end of the mineralisation process, approximately during the 3rd substage of the quartz-sulphide stage (fig. 1). The occurrence of these generations at the deposit is probably just limited but this does not exclude their presence also at other veins or parts of the deposit.

References

Abonyi, A. edit., 1977: Final report - calculation reserves Rožňava - Mária. Detailed exploration. MS Archiv GSSR. 215p. (in Slovak)

Babčan, J. & Novák, F., 1961: Allophane and hydrargillite from Mária vein at Rožňava. Acta Univ. Carol. (Praha), Geol. No. 1, 21-33. (in Czech)

Bernard, J. H., 1958: Chemical and seiz latticed constants of tetra-hedrites from Spišsko-gemerské rudohorie Mts. Rozpr. Čs. Akad. Věd, Ř. mt. přír. Věd, (Praha), 68, 14, 1-74. (in Czech)

Bernard, J. H. edit., 1969: Mineralogy of Czechoslovakia. 1. edition, Praha, Academia, 396 p. (in Czech)

Bernard, J. H. edit., 1981: Mineralogy of Czechoslovakia. 2. edition, Praha, Academia, 648 p. (in Czech)

Fusán, O. edit., 1963: Legend to clear geological map CzSSR 1 : 200 000, Vysoké Tatry Mts. Bratislava, Geofond, 215 p. (in Slovak)

Háber, M., Krištín, J. & Rojkovič, I., 1993: The tennantite - tetrahedrite series in permian formations of the Western Carpathians. Geol. Carpathica, (Bratislava) 45, 1, 11-28.

Ilavský, J. edit., 1964: Legend to map raw materials CzSSR 1 : 200 000 M-34-XXVII Vysoké Tatry Mts. Bratislava, Geol. ústav D. Štúra, 81 p. (in Slovak)

Ilavský, J. edit., 1979: Metallogenése de l'Europe alpine central et du sud-est. Bratislava, Geologický ústav D. Štúra, 413.

Ďuďa, R., 1976: Ore occurrences and mineral and paragenetic conditions in region Košické Hámre - Košice - Hýľov. Miner. slov. (Sp. N. Ves), 8, 5, 447-468. (in Slovak)

Kašpar, P., 1970: Beitrag zum Studium der Mikrohärte von Hg-Tetredriten. Neu. Jb. Mineral., Mh. (Stuttgart), 1, 29-33.

Kupčík, V., Matherny, M. & Varček, C., 1961: Contribution to structural problem of mineral "lilianit". Geol. Sbor. Slov. Akad. Vied. (Bratislava), 12, 1, 103-111. (in Slovak)

Macko, J. & Ondrejkovič, K., 1965: Ores occurrences in Permian-Wefénian stripe Spišsko - gemerské rudohorie Mts. (Cu-sandstone). Zpr. geol. Výsk. v Roku 1964, part 2 (Bratislava), 41-42. (in Slovak)

Mesarčík, I. edit., 1986: Rožňava - center, complex Cu-Fe ores, Prospecting exploration. MS Archiv GSSR. 165 p. (in Slovak)

Mesarčík, I. edit., 1991: Final report Rožňava - Strieborná vein. MS Archiv GSSR, 133 p. (in Slovak)

Mesarčík, I. edit., 1996: Final report - calculation reserves Rožňava - Strieborná vein II. MS Archiv GSSR, 175 p. (in Slovak)

Novák, F., 1959: Tetrahedrite from Mária deposit at Rožňava. Geol. Práce, Zoš. (Bratislava), 56, 217-246. (in Czech)

Novák, F., 1960: Ullmanite (NiSbS) from Sadlovská vein at Rožňava. Věst. Ústř. Úst. geol. (Praha), 35, 1, 77-79. (in Czech)

Novák, F., 1961: Kobellite from Mária vein at Rožňava, Věst. Ústř. Úst. geol. (Praha), 36, 2, 97-107. (in Czech)

Novák, F., 1967: Chemical composition of tetrahedrite from VII. to X. level Mária vein at Rožňava. Čas. Mineral. Geol. (Praha), 12, 1, 49-57. (in Czech)

Paholič, Ľ., 1969: Depth development of Mária deposit at Rožňava. Geol. Prúzk. (Praha), 4, 210-215. (in Czech)

Regásek, F., 1968: Mineralogy and geochimisty of tetrahedrite from Slovinky deposit in Spišsko-gemerské rudohorie Mts. Sbor. geol. Vied, Západ. Karpaty, (Bratislava), 9, 7-48. (in Slovak)

Rieder, M., 1963: Enargite from Havrana dolina valley of north from Mlynky in Spišsko-gemerské rudohorie Mts. Čas. Mineral. Geol. (Praha), 8, 1, 43-48. (in Czech)

Rozložník, L., 1982: Structural types metalogenetic units of siderite formation in Spišsko-gemerské rudohorie Mts. Hornícka Příbram ve věde a technice (Příbram), sek. Prognóza nerast. sur. v ČSSR, 52-68. (in Slovak)

Rozložník, O., 1973: Summary of geologic and deposits conditions of environs Rožňava. In: Zborník Banícky Gemer, 70 rokov baníckeho múzea v Rožňave. Martin, 105-206. (in Slovak)

Rozložník, O., 1981: Mineralogical report from Mária-Rožňava deposit. MS Archiv GSSR, 215 p. (in Slovak)

Slávik, J. edit., 1967: Raw materials of Slovakia. Bratislava, SVTL, 510 p. (in Slovak)

Slavkovský, J., 1978: Structural analysis Rožňava ore district. Miner. slov. (Sp. N. Ves), 10, 6, 505-526. (in Slovak)

Varček, C., 1953: Geological and paragenetic conditions of siderite mineral deposite Malý Vrch at Krásnohorské Podhradie. Geol. Sbor. Akad. Vied (Bratislava), 4,3-4,751-765. (in Slovak)

Varček, C., 1954: Preliminary report at recherch of metalogenetic conditions of environts Rožňava. Geol. Práce, Zpr. (Bratislava), 1, 71-74. (in Slovak)

Varček, C., 1954a: Preliminary report at study siderite formation at Rožňava. Geol práce, Zpr. (Bratislava), 1, 74-76. (in Slovak)

Varček, C., 1955: To questin of origin and distribution albite on siderites vein in regin Rožňava. Geol práce, Zpr. (Bratislava), 4, 86-92. (in Slovak)

Varček, C., 1956: Contribution to knowledge of metalogenetic condition in south part Spišsko-gemerské rudohorie Mts. Geol. Sbor. Akad. Vied (Bratislava), 7, 1-2, 58-65. (in Slovak)

Varček, C., 1959: Paragenetic condition of Mária vein in Rožňava. Geol. Práce, Zoš. (Bratislava), 55, 181-213. (in Slovak)

Varček, C., 1961: Zonale Verteilung der hydrothermalen Vererzung im Zips-Gömörer und Einfluss des geologischen Milieu auf Charakter der Mineralisation. Geol práce, Zoš. (Bratislava), 60, 281-301.

Varček, C., 1973: Deposits of mineral raw materials of the West Carpathians. In: Guide to excursion. X. Congress of Carpathian - Balkan Geological Association. Bratislava, Geologický ústav D. Štúra, 62.

Varček, C., 1973a: Paragenetic and geochemic condition of hydrothermal mineral deposits in Spišsko-gemerské rudohorie Mts. Kap. III/c. In: Geologicko-ložisková štúdia SGR. MS Archiv GSSR 122 p. (in Slovak)

Varček, C. edit., 1968: Ore deposits of the West Carpathians. In: Guide to excursion 24 AC. XXIII. Session of International Geological Congress, Praha, Ústřední ústav geol., 1-48. (in Slovak)

Trends in chemical composition of tetrahedrite from the deposit Jeďovec (Fichtenhübel), Spišsko-gemerské rudohorie Mts.

ANTAL BORIS

Department of Geology of Mineral Deposits, Faculty of Natural Sciences, Comenius University,
Mlynská dolina, 842 15 Bratislava

Abstract. The deposit Jeďovec with veins Konštancia, Krištof and Michal, located in the central part of the Spišsko-Gemerské Rudohorie Mts., hosts hydrothermal siderite-sulphide mineralisation. Studied samples of tetrahedrite come from veins Konštancia and Krištof. Analyses determined Sb-end member of tetrahedrite with 100 to 83.67 % of tetrahedrite component with substantial Fe content (3.69-6.01 wt.%). Minor elements reach the following maximum values: Ag-1.47, Zn-2.69, Hg-0.51, Bi-0.65 wt.%. According to the chemical composition and textural relations tetrahedrite aggregates were divided into two generations. The older one contains two types of phases typical by Cu-As and Ag-Sb contents. The younger generation is typical by the presence of Hg and Bi, S deficiency and higher concentrations of Cu, PMe and Me^{+2} compared to the older one. Phases of selected generations form a geochemical zoning. Phases of the older generation with typical Cu-As contents are located in the central and lower parts of veins (Konštancia). Phases of older generation, typical by Ag-Sb contents, are present at outskirts and in upper parts of veins (Konštancia, Krištof). Aggregates of the younger generation are located in the narrow, central part of veins (Konštancia).

Keywords: Spišsko-gemerské rudohorie Mts., hydrothermal mineralisation, Fe-tetrahedrite, geochemistry, zoning.

Introduction

Sulphosalts of the tetrahedrite-tennantite series are common minerals at deposits of siderite-sulphide formation of Spišsko-gemerské rudohorie Mts., including the deposit Jeďovec. Bernard (1958) and in particular Trdlička (1967) studied this mineral from the deposit in more details.

Tetrahedrite is a common mineral at the deposit. It forms steel-grey irregular aggregates, penetrating together with chalcopyrite into siderite and quartz in the form of veinlets or a network. It also occurs in the form of small lenses and nests (Konštancia vein) penetrating also into ankerite together with abundant pyrite. In cavities in siderite and quartz it forms tiny, max. 1 cm big crystals of tetrahedral form (Raky, Krištof and Konštancia adits). Older sulphides, such as arsenopyrite, pyrite, marcasite, pyrrhotite and sphalerite are replaced by tetrahedrite. It also penetrates into kobellite and jamesonite. In tetrahedrite, apart from needle-shaped grains of kobellite, small grains of gold are locally present. Tetrahedrite aggregates are overgrown by bournonite and bornite. In the mineral succession it is described as the youngest mineral along with chalcopyrite (Bartalský et al., 1962, Bernard, 1958, Matula, 1969, Trdlička, 1963, 1963a, 1963b, 1967, 1967a, Trdlička – Kupka, 1957, Trdlička – Kvaček – Kupka, 1962).

The yet published chemical composition of tetrahedrite from the deposit varies in the following range: Cu 34.77-36.61; Zn 1.15 – 1.76; Fe 6.22 – 7.33; Hg 0.0 – 0.18; Cd tr – 0.01; Sb 26.73 – 29.45; As 0.05 – 0.71; Bi 0.32 – 0.93; S 24.78 – 25.75 wt %; (Konštancia vein); Cu 35.45 – 37.22; Zn 2.93 – 4.73; Fe 3.62 – 4.79; Hg 0.03 – 0.1; Cd 0 – 0.1; Sb 27.72 – 29.06; As 0.51 – 0.59; Bi 0 – 0.14; S 24.5 – 25.53 wt. %; (Krištof vein) (Trdlička, 1967b). Se content was determined in following ranges: 54 – 82 g/t (Babčan, 1966); 0.0054 – 0.0082 wt % (Trdlička, 1963a); 0.002 – 0.0042 wt.% (Kvaček, 1980).

Springer (1969), Hall (1972), Pattrick – Hall (1983), Miller Craig (1983) and others have studied problems of tetrahedrites and tennantites. According to chemical and structural analyses Sack – Loucks (1985) determined the following formula of chemical composition:

$(Cu,Ag)_6$ $([Cu]_{2/3}$ $[Fe, Zn, Cd, Hg, Pb]_{1/3})_6$ $(Sb, As, Bi)_4$ $(S, Se)_{13}$

In this study a general formula:

$$Me^{10}Me^{+2}{}_2(PMe)_4\ S_{13}$$
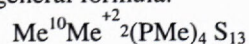
and the recalculation on the bases of 29 atoms were used. Cu and Ag are considered as monovalent metals (Me^{+1}), Fe, Zn, Hg, Pb, Cd as bivalent metals (Me^{+2}) and Sb, As, Bi, Te as metalloids (PMe) (Charlat – Levy, 1974; Mozgova – Cepin, 1983).

Results of tetrahedrite and tennantite structural study of natural samples were followed by the research of synthesis in systems Cu-Sb-S, Cu-As-S, Cu-Ag-Sb-S, Cu-Fe-Sb-S, performed particularly by Maske – Skinner (1971), Tatsuka – Morimoto (1977), Makovický – Skinner (1978), Sack – Ebel (1993). These authors determined the structure of tetrahedrites and tennantites in an artificial system, along with temperatures of origin and stability of tetrahedrites-tennantites in the range 200 – 500°C.

Geology and mineralogy of the deposit

The deposit Jedľovec (Fichtenhübel) is located in the central part of the Spišsko-gemerské rudohorie Mts. between the rocks of the Drnava Formation of the Gelnica group (Bartalský et al., 1962; Maheľ, 1954; Reichwalder, 1970). Parallel ore veins form a fan-type stockwork with general direction E-W and steep dip toward south (Fig. 1).

The vein thickness is variable, it changes from 10 cm to 7 m. The vein is known to continue up to 500 m into depth. The ore field Jedľovec forms a system of 8 - 9
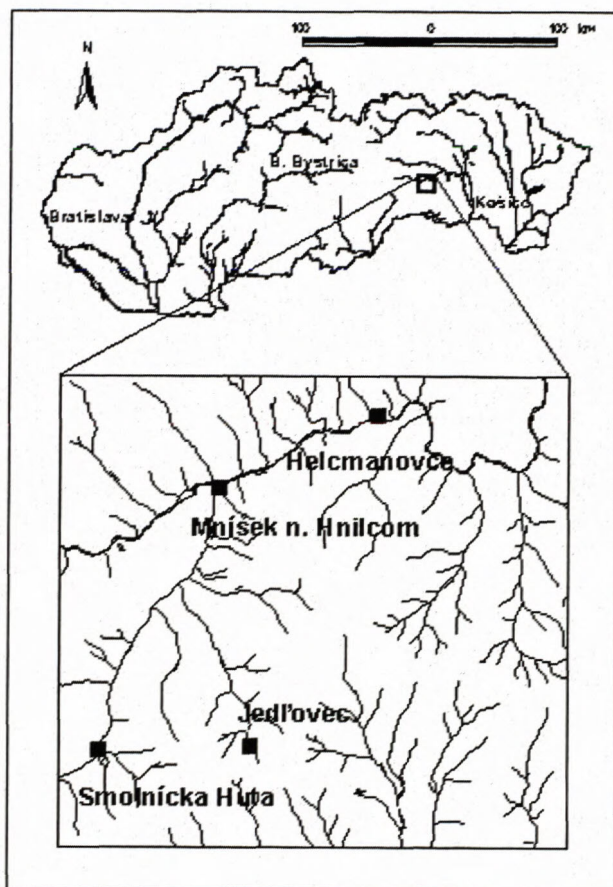
Fig. 1. Location of the deposit Jedľovec.

Fig.2.Simplified succession scheme of mineralisation at the deposit Jedľovec (veins Krištof, Konštancia, Michal I), Macinský (1992).

siderite-sulphidic veins (dykes) with quartz, such as, from north to south, Kornélia, Konštancia Lower and Upper, Krištof (available by cross cut Raky), Johana, Michal I, II, Daniel I, II, Jozef and a quartz-arsenopyrite vein with Co (Grecula, 1966).

The mineral content of vein filling is quite variegated. It was studied mainly by Drnzíková (in: Grecula – Grosz, 1968; Návesňák, 1967) and Trdlička (1963, 1963a, 1967, 1967a, Trdlička et al., 1962). Coarse-crystalline siderite is the major mineral (Antal, 1996), in which very irregularly located sulphides are present, such as chalcopyrite (Antal, 1997), pyrite, tetrahedrite, arsenopyrite, löllingite, cobaltite, glaucodot, pyrhotite, sphalerite, galena, marcasite, hematite, magnetite, calcite, ankerite, stannite, gold and Bi-sulphosalts (bismuth, aikinite, kobellite, galenobismutite, bournonite, boulangerite, jamesonite) (Macinský and Antal, 1993). Sulphides form irregular veinlets, aggregates, nests, impregnations and disseminations accompanied by milk-white quartz (Fig. 2).

A zonal arrangement of the ore mineralisation was described for the deposit. At the vein Krištof, located in the middle of the fan-type structure of the deposit, the sulphidic mineralisation dominates. In direction to the margin of the fan, formed by veins Konštancia, Daniel and Kornélia, this mineralisation is replaced by the siderite mineralisation. Decrease in sulphides and quartz in direction to margins of these veins manifests the horizontal zoning. The vertical zoning is manifested by the predominance of siderite in upper parts of veins, while sulphides are focused more to the centre. In direction to depth the proportion of ankerite increases simultaneously with sulphide decrease (Matula, 1969; Návesňák et al., 1982).

Veins Konštancia (its western part), Krištof, Michal I and Daniel I. had bigger economic importance. The vein filling of the vein Konštancia is formed by coarse-crystalline siderite with high proportion of quartz. Chalcopyrite and tetrahedrite dominate among sulphides. The vein filling of the vein Krištof is composed of pale-brown siderite, extensively crushed, with breccia-type and impregnation-clustered textures, sealed by sulphides and quartz, with a high chalcopyrite content. The main part of the vein filling of the vein Michal I is formed by siderite with minor amount of sulphides, located in nests. Veins Daniel I and II are formed by coarse- to medium-grained siderite with rare sulphide nests (Fusan – Kantor, 1954; Slávik at al., 1967).

Methodology

A study using a scanning electron microscope (JEOL JSM-840, Geol. Survey of the Slovak Rep. Bratislava, J. Stankovič, D. Dubík) and using an energy dispersive X-ray spectrometer (EDAX, Geol. Survey of the Slovak Rep. Bratislava) preceded quantitative microchemical analyses.

Analyses were carried out on the instrument JEOL SUPERPROBE 733 (Geol. Survey of the Slovak Rep. Bratislava) using a correlation program ZAF-M, 30nA

Tab. 1. Results of microchemical analyses of tetrahedrite [wt.%] from the deposit Jedľovec. Other analysed elements, such as Au, Ni, Co, Pb, Te and Se did not reach detectable concentrations. TD/TN - tetrahedrite number (JEOL SUPERPROBE 733, Geol. Survey of the Slovak Rep. Bratislava, F. Caňo, P. Konečný and P. Siman.)

Veins	Anal. No.	Phase	Samp. No.	(Cu	Ag)	(Fe	Zn	Hg)	(Sb	As	Bi)	S	Total	TD/TN
			min.	36,43	0,00	3,69	0,00	0,00	24,98	0,00	0,00	21,94	96,28	83,67
			avg.	37,63	0,44	5,05	1,46	0,06	28,49	1,04	0,07	25,25	99,51	94,41
			max.	38,85	1,47	6,01	2,69	0,51	30,11	3,00	0,65	30,02	101,51	100,00
Konštancia	1	3	1	37,93	0,66	4,76	1,47	0,14	29,71	1,03	0,06	23,61	99,37	94,67
Konštancia	2	3	1	37,55	0,74	4,83	1,33	0,19	29,11	1,22	0,00	23,99	98,96	93,62
Konštancia	3	2	1	36,74	0,55	4,85	1,47	0,00	29,93	0,75	0,02	24,82	99,13	96,09
Konštancia	4	1	1	36,95	0,64	5,10	1,26	0,51	27,67	1,96	0,00	24,85	98,94	89,68
Konštancia	5	3	2	37,78	0,20	4,61	1,63	0,29	29,46	0,73	0,02	24,20	98,92	96,13
Konštancia	6	1	2	37,71	0,18	4,97	1,41	0,00	27,38	1,81	0,04	24,59	98,09	90,30
Konštancia	7	1	2	36,66	0,22	5,01	1,38	0,00	27,53	1,83	0,14	25,64	98,41	90,25
Konštancia	8	3	5	36,69	0,53	5,83	0,55	0,00	26,64	0,10	0,39	30,02	100,75	99,39
Konštancia	9	3	6	38,22	0,36	3,84	2,69	0,23	28,39	0,67	0,17	24,59	99,16	96,31
Konštancia	10	undeterm.	6	37,09	0,30	3,69	2,41	0,00	28,27	0,86	0,00	24,97	97,59	95,29
Konštancia	11	3	6	37,83	0,33	3,81	2,59	0,15	28,35	0,65	0,05	25,19	98,95	96,41
Konštancia	12	2	10	38,40	0,00	5,06	1,34	0,00	28,83	0,98	0,00	25,87	100,48	94,77
Konštancia	13	2	10	38,06	0,00	4,97	1,51	0,00	28,87	0,77	0,00	25,56	99,74	95,85
Konštancia	14	3	21	37,61	0,64	5,85	0,63	0,29	30,11	0,00	0,24	23,15	98,52	100,00
Konštancia	15	3	21	36,99	0,72	5,70	0,56	0,23	30,04	0,04	0,06	21,94	96,28	99,78
Konštancia	16	2	25	37,90	0,00	4,69	1,73	0,00	29,00	0,83	0,00	26,05	100,20	95,56
Konštancia	17	2	25	38,32	0,00	4,64	1,92	0,00	29,04	1,05	0,00	25,64	100,61	94,45
Konštancia	18	1	27	38,59	0,00	5,69	0,48	0,00	28,11	1,31	0,00	25,53	99,71	92,96
Konštancia	19	1	27	38,85	0,00	6,01	0,00	0,00	28,18	1,96	0,00	26,51	101,51	89,85
Konštancia	20	2	27	38,36	0,00	6,01	0,51	0,00	29,02	0,91	0,00	25,38	100,19	95,15
Konštancia	21	1	27	38,10	0,00	5,94	0,19	0,00	27,50	2,02	0,00	26,02	99,77	89,34
Konštancia	22	1	28	38,29	0,00	5,31	0,98	0,00	26,96	1,66	0,00	26,16	99,36	90,90
Konštancia	23	1	28	38,52	0,00	5,43	0,97	0,00	27,01	1,64	0,00	26,08	99,65	91,02
Konštancia	24	1	28	38,79	0,00	5,29	1,01	0,00	28,20	1,15	0,00	26,00	100,44	93,78
Konštancia	25	3	37	38,01	0,37	5,19	1,36	0,21	26,76	2,47	0,65	24,49	99,51	86,96
Konštancia	26	3	37	38,15	0,38	5,23	1,33	0,21	29,51	0,56	0,51	23,90	99,78	97,01
Konštancia	27	3	37	38,12	0,37	4,88	1,74	0,33	29,64	0,46	0,39	24,04	99,97	97,54
Konštancia	28	3	37	38,36	0,36	4,77	1,87	0,21	29,29	0,56	0,42	24,49	100,33	96,99
Konštancia	29	3	37	38,80	0,40	5,40	1,40	0,12	26,64	2,70	0,55	24,31	100,32	85,86
Konštancia	30	1	38	37,62	0,36	4,69	1,92	0,00	27,07	1,72	0,00	26,25	99,63	90,64
Konštancia	31	1	38	38,49	0,24	4,60	1,90	0,00	24,98	3,00	0,00	26,34	99,55	83,67
Konštancia	32	1	55	37,54	0,00	5,00	1,70	0,00	28,92	1,56	0,00	25,83	100,55	91,94
Konštancia	33	1	55	37,86	0,02	4,94	1,75	0,00	27,67	1,37	0,00	25,81	99,42	92,55
Krištof	34	1	4	37,65	0,00	5,37	2,22	0,00	25,11	2,80	0,00	26,38	99,53	84,66
Krištof	35	undeterm.	4	37,22	0,00	5,06	2,52	0,00	27,36	1,19	0,00	25,76	99,11	93,40
Krištof	36	2	18	37,08	0,42	4,23	2,30	0,00	29,04	0,45	0,00	25,60	99,12	97,54
Krištof	37	2	18	36,97	0,51	4,12	2,57	0,00	29,76	0,48	0,00	25,31	99,72	97,45
Krištof	38	2	18	37,43	0,42	4,24	2,66	0,00	29,11	0,45	0,00	25,65	99,96	97,55
Krištof	39	2	40	36,43	1,16	5,89	0,38	0,00	28,72	0,73	0,00	25,85	99,16	96,03
Krištof	40	2	40	37,36	1,18	5,65	0,63	0,00	28,84	0,73	0,00	26,18	100,57	96,05
Krištof	41	3	45	38,25	0,43	5,63	0,97	0,00	29,91	0,71	0,09	22,41	98,40	96,29
Krištof	42	3	45	37,70	0,44	5,63	1,01	0,04	29,35	0,91	0,01	23,59	98,68	95,20
Krištof	43	2	46	37,29	0,14	5,47	0,72	0,00	28,83	0,19	0,00	25,73	98,37	98,94
Krištof	44	2	46	37,17	0,12	5,68	0,77	0,00	29,93	0,31	0,00	25,61	99,59	98,34
Krištof	45	2	49	36,83	1,05	5,16	1,72	0,00	28,50	0,84	0,00	25,83	99,93	95,43
Krištof	46	2	49	36,60	1,47	4,88	1,69	0,00	29,73	0,66	0,00	25,33	100,36	96,52
Krištof	47	2	49	37,07	1,36	5,01	1,69	0,00	28,77	0,64	0,00	25,25	99,79	96,51
Krištof	48	2	49	36,75	1,22	4,83	1,90	0,00	29,16	0,20	0,00	25,24	99,30	98,90
Krištof	49	2	49	36,50	1,33	4,32	2,34	0,00	29,49	0,29	0,00	24,91	99,18	98,43
Krištof	50	2	49	37,25	1,38	4,90	1,56	0,00	28,74	0,71	0,00	26,37	100,91	96,14
Krištof	51	2	49	36,78	1,31	4,98	1,66	0,00	28,94	0,55	0,00	25,18	99,40	97,00
Konštancia			avg.	37,91	0,26	5,05	1,36	0,09	28,30	1,22	0,11	25,21	99,51	93,48
Krištof			avg.	37,13	0,77	5,06	1,63	0,00	28,85	0,71	0,01	25,34	99,50	96,13

Tab. 2. Calculated atomic ratios of crystallochemical formulas of tetrahedrite from the deposit Jedľovec. (A – Me+1, B – Me+2, A+B – total Me, C – PMe)

Veins	Anal. No.	Phase	Samp. No.	Cu	Ag	A	Fe	Zn	Fe+Zn	Hg	B	A+B	Sb	As	Bi	C	S	ABCD	TD/TN
Konštancia	1	3	1	10,15	0,00	10,25	1,45	0,38	1,83	0,01	1,84	12,09	4,15	0,23	0,00	4,39	12,52	29	94,7
Konštancia	2	3	1	10,03	0,00	10,14	1,47	0,35	1,81	0,02	1,83	11,97	4,06	0,28	0,00	4,33	12,70	29	93,6
Konštancia	3	2	1	9,73	0,00	9,82	1,46	0,38	1,84	0,00	1,84	11,66	4,14	0,17	0,00	4,31	13,03	29	96,1
Konštancia	4	1	1	9,75	0,00	9,85	1,53	0,32	1,85	0,04	1,90	11,75	3,81	0,44	0,00	4,25	13,00	29	89,7
Konštancia	5	3	2	10,07	0,00	10,10	1,40	0,42	1,82	0,02	1,85	11,95	4,10	0,17	0,00	4,27	12,79	29	96,1
Konštancia	6	1	2	9,99	0,00	10,02	1,50	0,36	1,86	0,00	1,86	11,88	3,79	0,41	0,00	4,20	12,92	29	90,3
Konštancia	7	1	2	9,61	0,00	9,65	1,49	0,35	1,85	0,00	1,85	11,49	3,77	0,41	0,01	4,19	13,32	29	90,3
Konštancia	8	3	5	9,03	0,00	9,11	1,63	0,13	1,76	0,00	1,76	10,88	3,42	0,02	0,03	3,47	14,65	29	99,4
Konštancia	9	3	6	10,11	0,00	10,16	1,16	0,69	1,85	0,02	1,87	12,03	3,92	0,15	0,01	4,08	12,89	29	96,3
Konštancia	10	undeterm.	6	9,89	0,00	9,93	1,12	0,62	1,74	0,00	1,74	11,68	3,93	0,19	0,00	4,13	13,19	29	95,3
Konštancia	11	3	6	9,95	0,00	10,00	1,14	0,66	1,80	0,01	1,82	11,82	3,89	0,15	0,00	4,04	13,14	29	96,4
Konštancia	12	2	10	9,89	0,00	9,89	1,48	0,34	1,82	0,00	1,82	11,71	3,87	0,21	0,00	4,09	13,20	29	94,8
Konštancia	13	2	10	9,89	0,00	9,89	1,47	0,38	1,85	0,00	1,85	11,74	3,92	0,17	0,00	4,09	13,17	29	95,8
Konštancia	14	3	21	10,19	0,00	10,29	1,80	0,17	1,97	0,02	1,99	12,29	4,26	0,00	0,02	4,28	12,43	29	100,0
Konštancia	15	3	21	10,34	0,00	10,46	1,81	0,15	1,97	0,02	1,99	12,45	4,38	0,01	0,01	4,40	12,16	29	99,8
Konštancia	16	2	25	9,78	0,00	9,78	1,38	0,43	1,81	0,00	1,81	11,59	3,91	0,18	0,00	4,09	13,32	29	95,6
Konštancia	17	2	25	9,89	0,00	9,89	1,36	0,48	1,84	0,00	1,84	11,74	3,91	0,23	0,00	4,14	13,12	29	94,5
Konštancia	18	1	27	10,00	0,00	10,00	1,68	0,12	1,80	0,00	1,80	11,80	3,80	0,29	0,00	4,09	13,11	29	93,0
Konštancia	19	1	27	9,83	0,00	9,83	1,73	0,00	1,73	0,00	1,73	11,56	3,72	0,42	0,00	4,14	13,30	29	89,8
Konštancia	20	2	27	9,94	0,00	9,94	1,77	0,13	1,90	0,00	1,90	11,84	3,92	0,20	0,00	4,12	13,04	29	95,2
Konštancia	21	1	27	9,81	0,00	9,81	1,74	0,05	1,79	0,00	1,79	11,59	3,69	0,44	0,00	4,13	13,27	29	89,3
Konštancia	22	1	28	9,86	0,00	9,86	1,56	0,25	1,80	0,00	1,80	11,66	3,62	0,36	0,00	3,99	13,35	29	90,9
Konštancia	23	1	28	9,90	0,00	9,90	1,59	0,24	1,83	0,00	1,83	11,73	3,62	0,36	0,00	3,98	13,29	29	91,0
Konštancia	24	1	28	9,95	0,00	9,95	1,54	0,25	1,80	0,00	1,80	11,75	3,78	0,25	0,00	4,03	13,22	29	93,8
Konštancia	25	3	37	9,99	0,00	10,05	1,55	0,35	1,90	0,02	1,92	11,97	3,67	0,55	0,05	4,27	12,76	29	87,0
Konštancia	26	3	37	10,14	0,00	10,20	1,58	0,34	1,93	0,02	1,94	12,14	4,09	0,13	0,04	4,26	12,59	29	97,0
Konštancia	27	3	37	10,11	0,00	10,17	1,47	0,45	1,92	0,03	1,95	12,12	4,10	0,10	0,03	4,24	12,64	29	97,5
Konštancia	28	3	37	10,08	0,00	10,14	1,43	0,48	1,90	0,02	1,92	12,06	4,02	0,12	0,03	4,18	12,76	29	97,0
Konštancia	29	3	37	10,13	0,00	10,19	1,60	0,36	1,96	0,01	1,97	12,16	3,63	0,60	0,04	4,27	12,57	29	85,9
Konštancia	30	1	38	9,68	0,00	9,74	1,37	0,48	1,85	0,00	1,85	11,59	3,64	0,38	0,00	4,01	13,39	29	90,6
Konštancia	31	1	38	9,83	0,00	9,87	1,34	0,47	1,81	0,00	1,81	11,68	3,33	0,65	0,00	3,98	13,34	29	83,7
Konštancia	32	1	55	9,68	0,00	9,68	1,47	0,43	1,89	0,00	1,89	11,57	3,89	0,34	0,00	4,23	13,20	29	91,9
Konštancia	33	1	55	9,81	0,00	9,81	1,46	0,44	1,90	0,00	1,90	11,71	3,74	0,30	0,00	4,04	13,25	29	92,6
Krištof	34	1	4	9,60	0,00	9,60	1,56	0,55	2,11	0,00	2,11	11,71	3,34	0,61	0,00	3,95	13,34	29	84,7
Krištof	35	undeterm.	4	9,66	0,00	9,66	1,49	0,64	2,13	0,00	2,13	11,79	3,70	0,26	0,00	3,97	13,25	29	93,4
Krištof	36	2	18	9,72	0,00	9,78	1,26	0,59	1,85	0,00	1,85	11,63	3,97	0,10	0,00	4,07	13,30	29	97,5
Krištof	37	2	18	9,70	0,00	9,78	1,23	0,66	1,88	0,00	1,88	11,66	4,07	0,11	0,00	4,18	13,16	29	97,4
Krištof	38	2	18	9,73	0,00	9,80	1,25	0,67	1,93	0,00	1,93	11,73	3,95	0,10	0,00	4,05	13,22	29	97,5
Krištof	39	2	40	9,52	0,00	9,69	1,75	0,10	1,85	0,00	1,85	11,54	3,92	0,16	0,00	4,08	13,38	29	96,0
Krištof	40	2	40	9,62	0,00	9,80	1,65	0,16	1,81	0,00	1,81	11,61	3,87	0,16	0,00	4,03	13,36	29	96,0
Krištof	41	3	45	10,41	0,00	10,48	1,74	0,26	2,00	0,00	2,00	12,48	4,25	0,16	0,01	4,42	12,09	29	96,3
Krištof	42	3	45	10,10	0,00	10,17	1,72	0,26	1,98	0,00	1,98	12,16	4,11	0,21	0,00	4,31	12,53	29	95,2
Krištof	43	2	46	9,79	0,00	9,81	1,63	0,18	1,82	0,00	1,82	11,62	3,95	0,04	0,00	3,99	13,38	29	98,9
Krištof	44	2	46	9,70	0,00	9,72	1,69	0,20	1,88	0,00	1,88	11,60	4,08	0,07	0,00	4,15	13,25	29	98,3
Krištof	45	2	49	9,56	0,00	9,72	1,52	0,43	1,96	0,00	1,96	11,67	3,86	0,18	0,00	4,04	13,28	29	95,4
Krištof	46	2	49	9,57	0,00	9,79	1,45	0,43	1,88	0,00	1,88	11,67	4,06	0,15	0,00	4,20	13,12	29	96,5
Krištof	47	2	49	9,70	0,00	9,91	1,49	0,43	1,92	0,00	1,92	11,83	3,93	0,14	0,00	4,07	13,10	29	96,5
Krištof	48	2	49	9,67	0,00	9,86	1,45	0,49	1,93	0,00	1,93	11,79	4,00	0,04	0,00	4,05	13,16	29	98,9
Krištof	49	2	49	9,67	0,00	9,88	1,30	0,60	1,90	0,00	1,90	11,78	4,08	0,07	0,00	4,14	13,08	29	98,4
Krištof	50	2	49	9,56	0,00	9,77	1,43	0,39	1,82	0,00	1,82	11,59	3,85	0,15	0,00	4,00	13,41	29	96,1
Krištof	51	2	49	9,67	0,00	9,87	1,49	0,42	1,91	0,00	1,91	11,79	3,97	0,12	0,00	4,09	13,12	29	97,0

beam current, 25kV accelerating voltage, LiF crystal and following standards: pure Cu, Ag, Fe, Zn, Co, Ni, Bi, Sb, Te, Au, cinnabar for Hg, arsenopyrite for As and S, Bi_2Se_3 for Se. Operators were F. Caňo, P. Konečný and P. Siman.

Measurements were performed on polished, degreased and ultrasonic-cleaned sections and polished sections, coated by carbon. Apart from elements shown in tables 1 and 2 also some other elements, such as Au, Ni, Co, Pb, Te and Se were measured, but they did not reach detectable concentrations.

Crystallochemical formulas of tetrahedrites were recalculated according to the basic structure of the cell $Me^{+1}10$, $Me^{+2}2$, PMe4, S13. This represents 29 atoms per unit cell.

Mineralogy and geochemistry of tetrahedrites

In the studied samples tetrahedrite forms irregular aggregates, often associated with chalcopyrite in quartz or siderite veinstone. It contains tiny grains of arsenopyrite or pyrite, often idiomorphous, locally with a slightly cataclastic texture. Tetrahedrite as one of the youngest minerals (Fig. 2) cuts older minerals by a network of veinlets, or it seals cataclased minerals along fractures.

The chemical composition, determined by microanalyses, showed that the studied tetrahedrite is an Sb-end member of the tetrahedrite-tennantite isomorphous series, containing from 83.67 to 100 % of the tetrahedrite component. Fe reaches more significant concentrations (from 1.81 at.%, respect. 6.01 wt.%) at the expense of Zn (from 0 to 0.69 at.%, respect. from 0 to 2.69 wt.%).

Maximum concentrations of minor elements vary around 1.47 wt.% for Ag, 0.65 wt.% for Bi and 0.51 wt.% for Hg (Tab. 1 and 2).

Generally, the chemical composition of tetrahedrite from the deposit Jedľovec (from veins – Konštancia and Krištof) can be characterised as Fe-tetrahedrite.

Nearly all analyses showed an excess of metalloids (PMe) and a significant predominance of Sb over As and a lack of bivalent metals compared to the theoretical composition (Me^{+2}, Fe>Zn). Concentration of metalloids (represented by sulphur only) and monovalent metals (Me^{+1}, Cu>>Ag) also ranges over the theoretical composition of tetrahedrite.

Mutual relationship among groups of elements forming aggregates of tetrahedrite (Me^{+1}, Me^{+2}, PMe, S) and elements themselves are diverse. In the literature discussed negative relationships are preserved between Sb : As, Fe : Zn and Cu : Ag only (Johnson, Craig & Rimstidt, 1986; Mozgova & Cepin, 1983).

Negative mutual relationship, expressed also by the coefficient of correlation, have also two major groups of tetrahedrite elements PMe and S. An increase in PMe content, resulting in PMe excess, is simultaneous to the decrease of S concentration, that gets below the theoretical value of S concentration in tetrahedrite (Fig. 3A). This trend is the result of relatively different behaviour of Sb and As to S. A higher concentration of the earlier (Sb) is accompanied by a decrease of the S content (Fig. 3B) and on the contrary, an increase in As content is accompanied

by an increase in S concentration. Because Sb contents in absolute values are significantly higher, a negative relationship of Sb to S prevails in the total of PMe.

A negative relationship occurs also between S content and contents of metals, monovalent (Me^{+1} – Cu, Ag, Fig. 3C) and partly also bivalent ones (Me^{+2} – Fe, Zn).

The relationship between Ag and S values is preserved apart from samples with high concentration of Ag (samples no. 40, 49) (Fig. 3D). Cu and S values (Fig. 4A) form a less apparent negative relationship. Even positive trends are possible to reach, if the field of data points is divided according to samples from individual veins.

In the mutual relationship between S and Me^{+1} (r – 0.99) these relatively conflicting relationships of studied elements were manifested in a not very clear negative trend (r –0.5) in samples with S content over, and Me^{+1} below the theoretical composition, compared to the significant trend outside these values (r –0.9) (Fig. 3C).

Equally negative relationship between Me^{+2} and S (r – 0.43) is more apparent if the individual elements are confronted with sulphur. When the data field is divided according to sulphur values, two types of values (samples) are possible to assign at Fe : S and Zn : S diagrams. One group has a stable concentration of S and an increasing or decreasing content of Fe or Zn. The second group has decreasing concentration of S and increasing Fe or decreasing Zn contents (Fig. 4C). These relationships are included also in a comprehensive diagram S : Me^{+2}, where a field of samples with a constant S content is possible to assign (slightly in excess, r –0.13), together with a field of samples with decreasing S content (r –0.72) and relatively increasing values of Me^{+2} (Fig. 4B).

Me and PMe contents show a positive relationship (Fig. 4. D). This trend is preserved in the relationship between PMe and Me^{+1} (r 0.76), but in the relationship with Me^{+2} a spread of values occurs (r 0.25), while just one sample exceeds the value of the theoretical composition (sample no. 4). The positive trend between Me^{+1} and PMe is formed by the predominance of Cu values and by the positive trend of As and Ag to Sb (Fig. 5A). The relationship between Cu and Sb is not distinct and it is more characterised by a large scatter of values. The relationship between As and Ag is negative (Fig. 5B), but due to significantly lower values of Ag compared to Cu the positive relationship between PMe and Me^{+1} was not affected.

Very weak mutual relationship between PMe and Me^{+2} is preserved also in relations of individual elements.

Me^{+1} values with Me^{+2} values form a weak positive relationship (r 0.,07) (Fig. 5C). Relatively larger spread of values is the result of weak positive relationship of majority metals (Cu and Fe) and relatively neutral relationship between Cu and Zn, Ag and Fe, Ag and Zn.

Concernig minor elements, tetrahedrites from the Jedľovec deposit contain smaller amount of Ag and Hg. Hg shows usually zero content and its maximum concentration reaches 0.51 wt.%. Because at such low concentration a relatively high analytical error occurs a work with absolute values is not possible.

The concentration of silver varies from 0 to 1.47 wt. %, while the average value is higher in samples from the

Fig. 3. Correlation diagrams of chemical composition of tetrahedrite from the deposit Jedľovec. (1 – first phase of the I. generation Cu-As, 2 – second phase of the I. generation Sb-Ag, 3 – phases of the II. generation Hg-Bi, 4 – not assigned phases, 5 – theoretical composition).

Fig. 4. Correlation diagrams of chemical composition of tetrahedrite from the deposit Jedľovec. (1 – first phase of the I. generation Cu-As, 2 – second phase of the I. generation Sb-Ag, 3 – phases of the II. generation Hg-Bi, 4 – not assigned phases, 5 – theoretical composition).
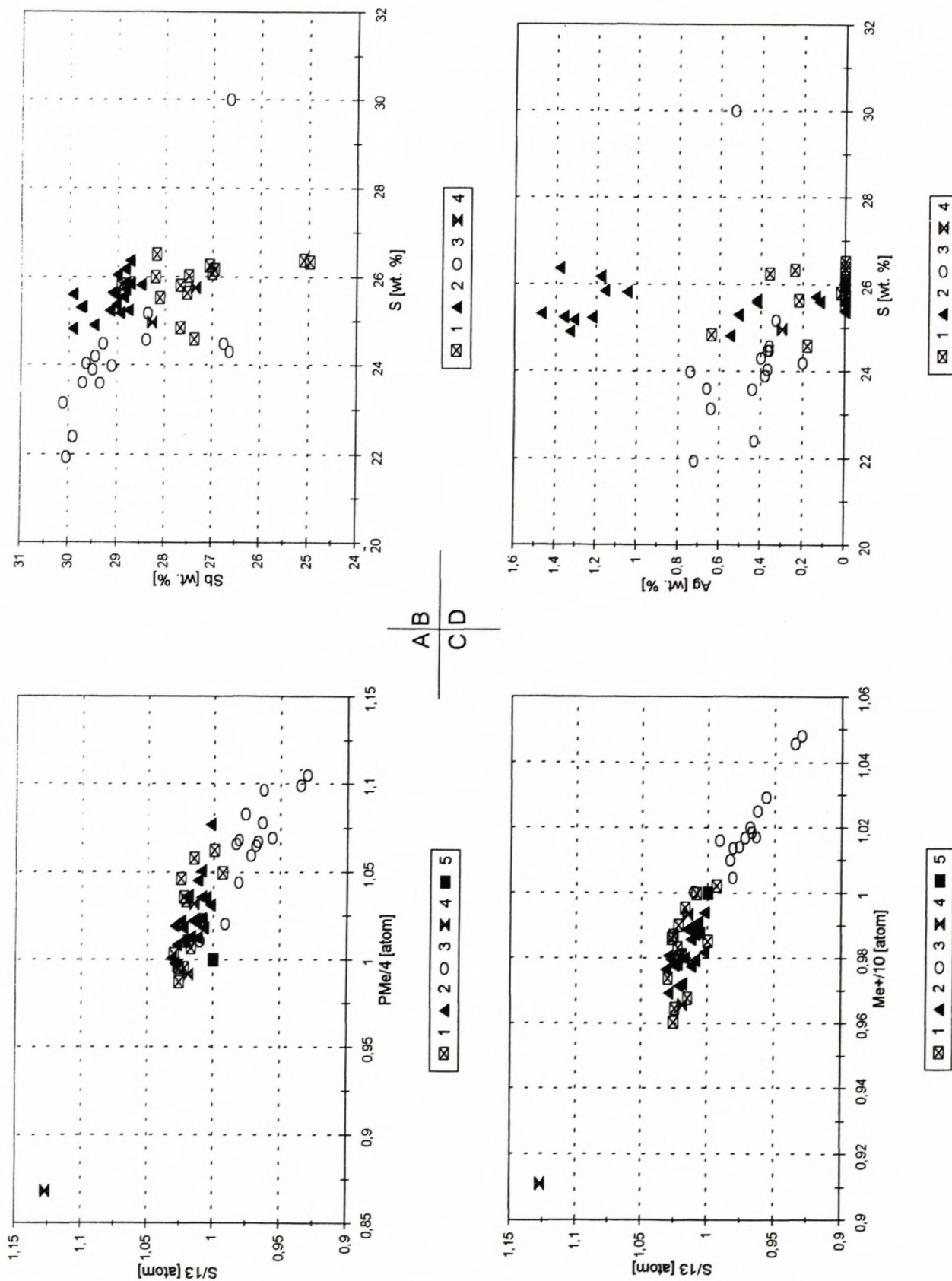
Slovak Geol. Mag., 8, 3–4(2002), 205–217

212

Fig. 5. Correlation diagrams of chemical composition of tetrahedrite from the deposit Jedľovec. (1 – first phase of the I. generation Cu-As, 2 – second phase of the I. generation Sb-Ag, 3 – phases of the II. generation Hg-Bi, 4 – not assigned phases, 5 – theoretical composition).
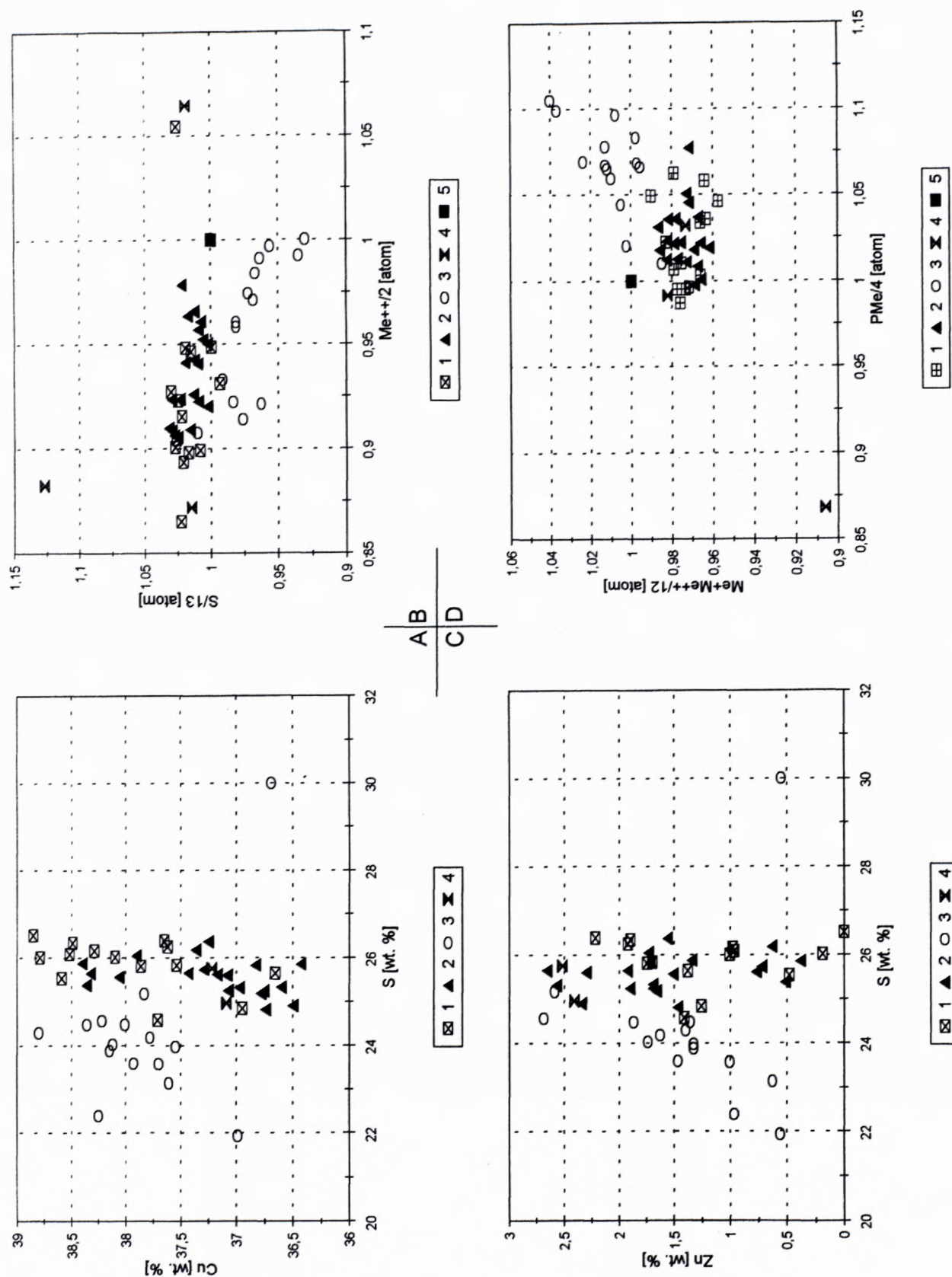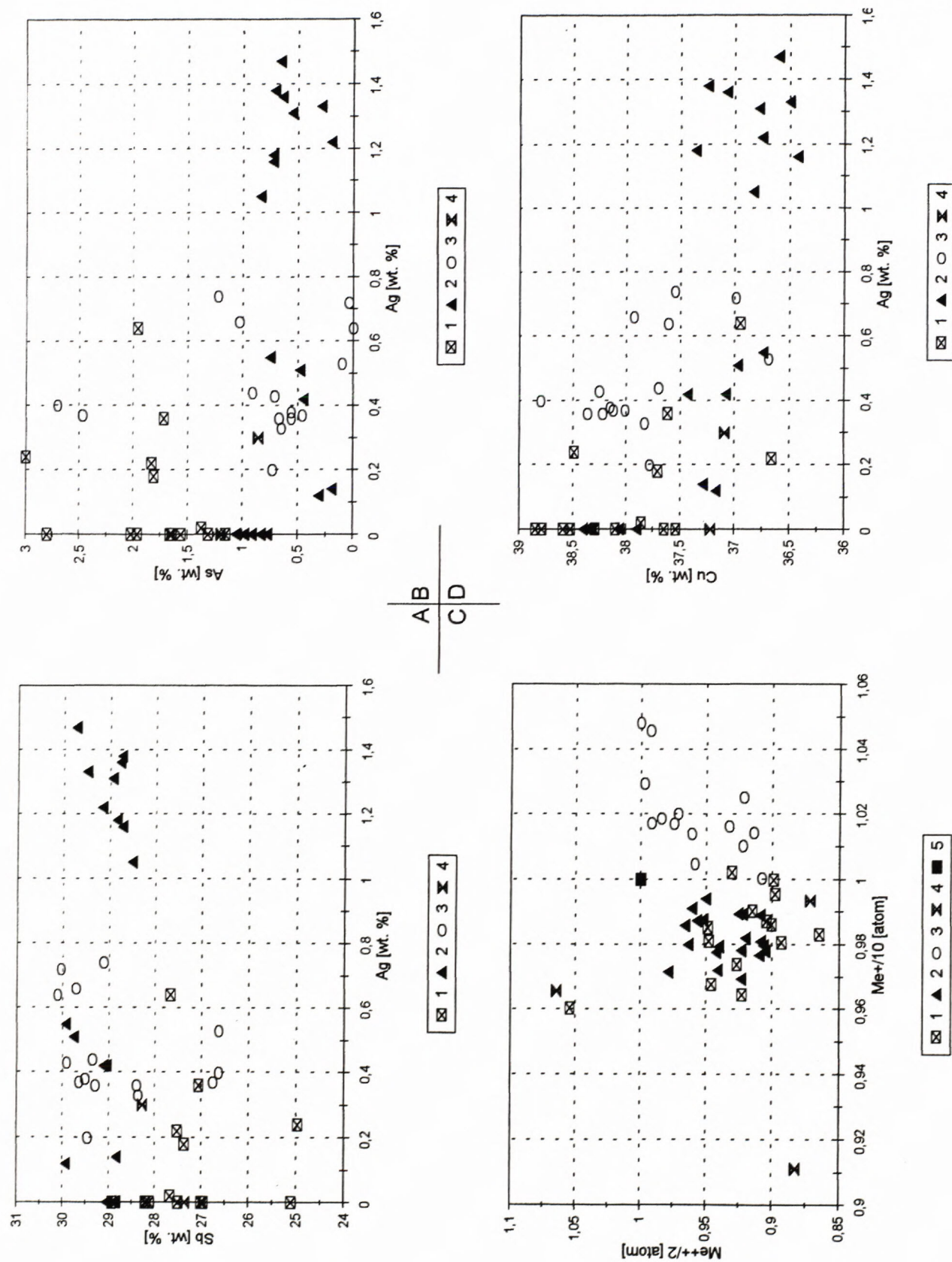
vein Krištof (0.77 wt. %) than from the vein Konštancia (0.26 wt. %) (Tab. 1).

The relationship of Ag and Me^{+2} is not possible to define unambiguously. Values have a large spread, while only samples with high Ag content from the vein Krištof are more distinctly detached.

Apart from samples with high Ag content, a negative trend between concentrations of Ag and S occurs within the frame of the analytical set (Fig. 3D). The relatively increasing concentration of Ag is accompanied by a decrease of S content.

Values of S concentration in samples from the vein Krištof vary around 26 wt. % (apart from samples no. 45; 22.41 – 23.59 wt. %).

The relationship between Ag and As also show a negative trend, accompanied by the selection of samples with high content of Ag (samples no. 40, 49) and low concentration of As. Ag and Sb show a reverse mutual relationship (Fig. 5A, B).

Generally it is possible to say that an increase in Ag concentration is accompanied also by an increase of Sb and decrease of Cu. Fe, Zn and S concentrations are variable – over and below theoretical values. Tetrahedrites with high concentration of Ag are possible to characterise as mineral aggregates with high contents of S and Sb and low contents of As and Cu (Fig. 5D). These samples with higher concentration of Ag are located at the vein Krištof.

The data field, representing chemical composition of analysed phases of tetrahedrites from the deposit Jedľovec, is possible to divide into 3 groups, according to the following typical features:

The 1st group of phases, in majority of samples, has typically higher concentration of Cu (cca over 37.5 wt. %) and As (cca over 1.25 wt. %) within the frame of studied set of analyses. Simultaneously lower concentration of Sb (cca < 28.5 wt. %) and Ag (cca < 0.4 wt. %) is typical, while the 2nd group of phases again has higher Sb and Ag contents (over the values shown, figs. 3B, 4A, 5A, D).

Compared to the 3rd group of phases the 1st and 2nd groups contain high concentration of S, that is always over the theoretical value and they show a low scatter of values (Fig. 3A, B, 4 A). The total of monovalent metals is always below the theoretical value, similar is the concentration of Me^{+2} (Fig. 3C, 4B).

3rd group of phases shows a lack of S and a high scatter of other elements concentrations. The total of Me^{+1}, represented predominantly by Cu, is mostly in excess and over the theoretical value of 10 atoms (Fig. 3C, 4D). Compared to the 1st and 2nd group of phases it contains higher values of PMe total (Fig. 3A). Furthermore, among several elements an apparent correlation occurs, either positive (Zn : S, Me : PMe, Me^{+1}: Me^{+2}) or negative (Fe : S).

Ag and relatively also As reach higher concentrations in the 1st and the 2nd group of elements (Fig. 5B). Hg and Bi contents are bounded to the 3rd group.

Samples with tetrahedrite phases belonging to the 1st and 2nd group are present in both studied veins. At the vein Krištof only two phases from the 2nd group are characterised by Sb and Ag contents (apart from the sample no. 4). At the vein Konštancia phases of this composition

are present in upper parts of the vein and in its E part. Phases typical by Cu and As contents are located in W margin, central and lower parts of the vein.

Phases representing the 3rd group (with Hg and Bi) markedly occur at the vein Konštancia. Here they concentrate mainly in the central part of the vein, forming a narrow zone that reaches from the centre of the vein up to its upper part in vertical direction. Just one sample from the vein Krištof belongs to the 3rd group (Fig. 6).

Homogenity of tetrahedrite aggregates

The variability of tetrahedrite aggregates composition is manifested in their inhomogenity too. Inhomogeneous aggregates with several types of structures occur among relatively large number of homogeneous aggregates. Cloddy and stockwork textures are the most common types of textures (Fig. 7). Both textures consist of phases forming irregular bodies or a network of tetrahedrite veinlets of variable thickness, irregularly cutting the basic phase of the tetrahedrite aggregate. Rarely, regular, banded-laminated structures occur, representing incremental zones of variable composition. These zones rim the aggregates with cloddy texture and simultaneously they are cut by a network of tetrahedrite veinlets. Cloddy textures were observed in samples from both studied veins, but the stockwork texture just in samples from the vein Konštancia and its central part.

Discussion

Apart from textural-structural features, we suppose that two generations of tetrahedrite formation occurred. The younger generation corresponds to the 3rd group of phases with Hg, Bi contents (Spiridonov – Badalov, 1983; Spiridonov et al., 1990), high concentrations of Me^{+1} (Tarkian – Breskovskaja 1990; Spiridonov – Badalov, 1983; Spiridonov et al., 1990) and low S content (Lynch, 1989). Sulphur deficiency as well as an excess of Me^{+1} can correspond to an increase in redox potential of the environment (Spiridonov – Badalov, 1983;), while a part of Cu becomes bivalent.

Based on the frequent similarity of chemical composition proportions to phases of the 1st generation we suppose that phases of the 2nd generation included also the chemical composition of older phases. Alternatively, younger solutions with Hg, Bi, Cu and Sb contents were „contaminated" by these phases.

Only the chemical composition of the sample no. 6 does not show any relation to elements of older phases. Its position in the centre of the zone formed by phases of the 2nd generation could be understood as a representative of this generation with a non-affected chemical composition.

Different chemical composition of the selected generations is manifested also in mutual relationships of individual major elements forming the studied tetrahedrites. The biggest differences occur in relations with sulphur. The biggest difference between the selected generations was determined in the relationship of Me^{+2} (1. gen. r –0.13, 2. gen. r –0.72) and Me^{+1} (1. gen. r –0.13, 2. gen. r –0.72).
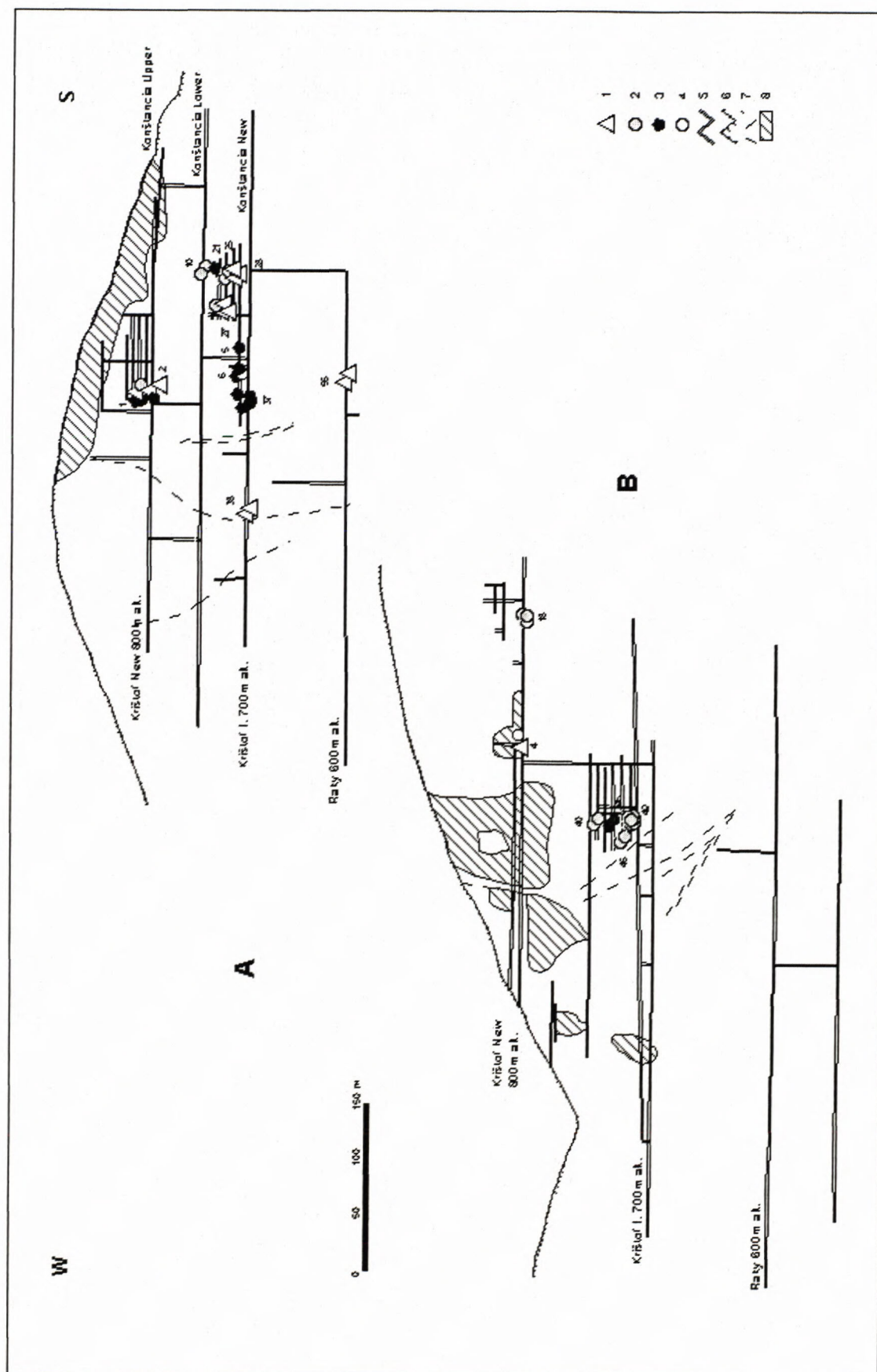
Fig. 6. Map of location of samples with analysed phases from the deposit Jedľovec. A – vein Konštancia, B – vein Krištof (1 – first phase of the I. generation Cu-As, 2 – second phase of the I. generation Sb-Ag, 3 – phases of the II. generation Hg-Bi, 4 – not assigned phases, 5 – mining galleries, 6 – surface line, 7 – faults, 8 – worked-out spaces).
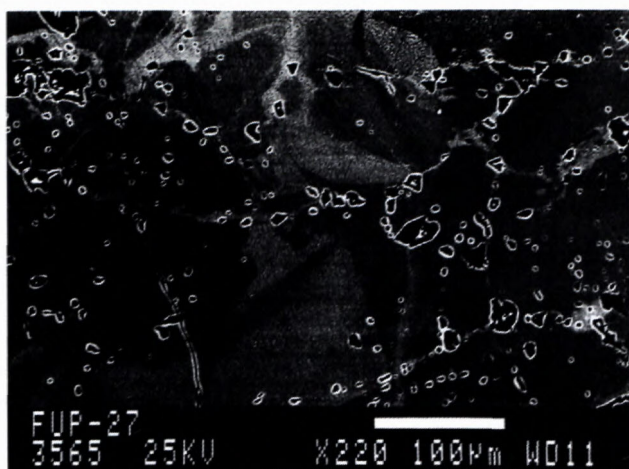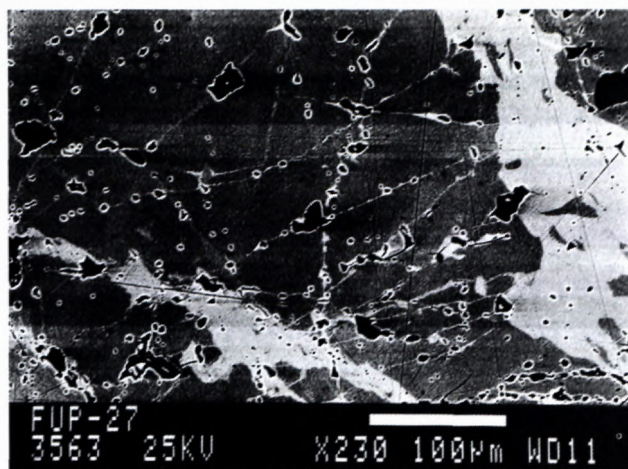
Fig. 7. Examples of inhomogenity textures of tetrahedrite aggregates from the deposit Jedľovec. A – spotty texture; A, B, C – stock-work texture; D, E – spotty "cloddy" texture; F – an aggregate with spotty texture rims a zone formed by banded texture.

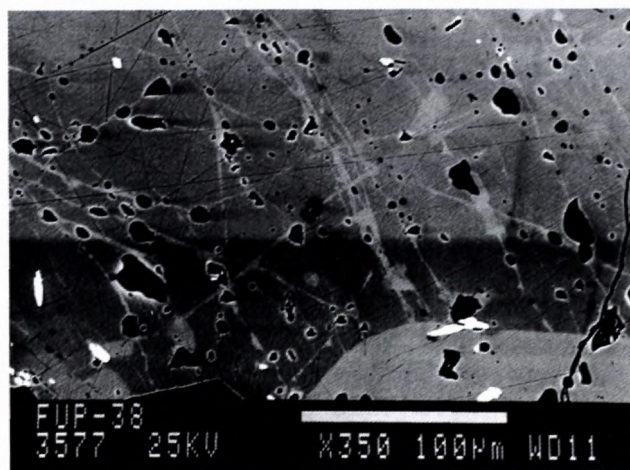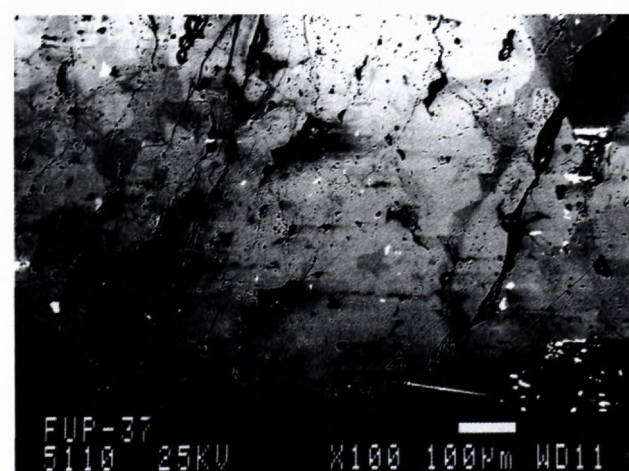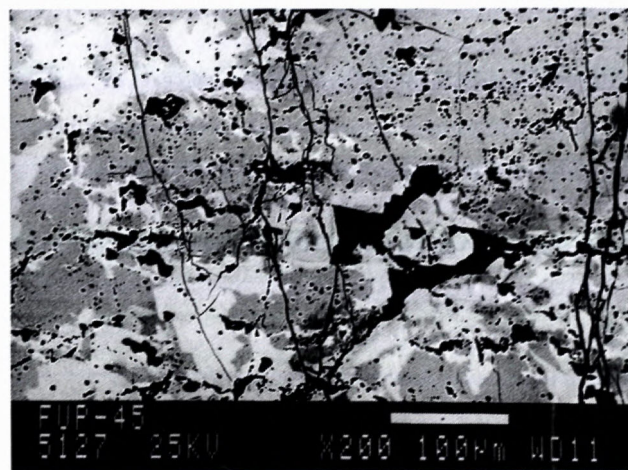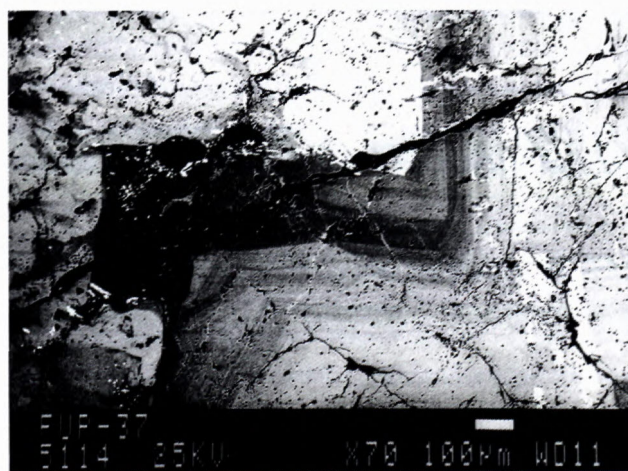Similar differences occur also in relationships of PMe and Me^{+1} (1. gen. r –0.01, 2. gen. r +0.67) as well as Me^{+2} (1. gen. r –0.1, 2. gen. r +0.44). Differences between generations occur also in Me^{+1} and Me^{+2} relationship (1. gen. r +0.05, 2. gen. r 0.6).

Older generation, composed of phases of the 1st and the 2nd group, forms a geochemical zoning represented by phases typical of Cu, As and Sb + Ag contents. The position of phases with increased concentrations of Cu and As should be close to the source of solutions (Hackbarth – Petersen, 1984; Mishra – Mookherjee, 1991; Petersen et al., 1990). Phases with Sb and Ag contents should originate in peripheral parts of veins, in zones remote from the source of solutions.

As shown above, mining works at the vein Krištof reached its peripheral part with Sb, Ag phases. At the vein Konštancia probably also an area was accessed, where solutions were introduced into the structure. This is supported also by the location of the younger 2nd generation with Hg and Bi contents (fig 6).

Conclusions

1. At the deposit Jedľovec (veins Krištof, Konštancia) Fe-tetrahedrite was determined, containing from 100 to 83,67% of the tetrahedrite component with negligible concentration of accompanying metals.

2. Based on chemical composition of individual phases, forming aggregates, two generations of tetrahedrite have been distinguished:

2. a. older, with high and stable concentration of S and lower contents of PMe, Me^{+1} and Me^{+2}, higher concentration of Sb and the presence of high concentrations of Ag within the frame of the set of analyses. This generation is formed by two geochemically dicriminable phases that are typical by the presence of the following metal associations: 1 – Cu, As and 2 – Sb, Ag.

2. b. younger generation typically has present Hg and Bi, sulphur deficiency and high concentrations of Cu. The total of PMe reaches higher values compared to the older generation.

3. Selected generations form geochemical zoning at the deposit. Phases of the older generation, typical by Cu and As contents, are present in the central and lower parts of the veins (Konštancia), accessible by mining works. Phases, typical by Sb and Ag contents at outskirts and upper part of veins (Konštancia, Krištof), and aggregates of younger generation are present within the frame of the open part of the vein (Konštancia) in its narrow central part.

Acknowledgement:

References

Antal, B., 1996: Composition of siderite from the Jedľovec (Fichten-hübel) deposit, Spišsko-gemerské rudohorie Mts. Acta geologica Univers. Comenianae, Nr. 51, 59 – 67.

Antal, B., 1997: Chalkopyrite chemistry in Jedľovec (Fichtenhübel) deposit, Spišsko-gemerské rudohorie Mts. Acta geologica Univers. Comenianae, Nr. 52, 29 – 37.

Babčan, J., 1966: Zur Geochemie des Selens des slowakischen Teils der Westkarpaten. Geol. sbor. Geol. carpath. Bratislava, 17, 1, 1 – 6.

Bartalský, J. & Grecula, P., edit., 1973: Study of geologic-deposit of Spišsko-gemerské rudohorie Mts. MS Archiv GSSR. (in Slovak)

Bartalský, J., Drnzíková, L., Grecula, P. & Návesňák, J., 1962: Vein deposits Cu-ores in easternal region of Spišsko-gemerské rudohorie Mts. Geol. Práce, Zošity, 61, 215 – 220. (in Slovak)

Bernard, J. H., 1958: Chemical and seiz latticed constants of tetra-hedrites from Spišsko-gemerské rudohorie Mts. Rozpr. Čs. Akad. Věd, Ř. mt. přír. Věd, (Praha), 68, 14, 1 – 74. (in Czech)

Charlat, M. & Levy, C., 1974: Substitutions multiples dans la serie tennantite - tetrahedrite. Bull. Soc. Franc. Minéral. Cristallogr., 97, 241 – 250.

Fusan, O. & Kantor, J., 1954: Report at geological recherch in map Švedlár. Geol. Práce, Spr. 1, 40-42. (in Slovak)

Grecula, P., 1965: Geological interpretation of results geophysicals measurements in region Mníšek nad Hnilcom. Geol. Průzkum, 7, 2, 39 - 42. (in Slovak)

Grecula, P., 1966: Contemporaneous stratigraphic and tectonic problems of Gelnica group of Gemericum. Geol. Průzkum, 8, č. 7, 219 – 221. (in Slovak)

Grecula, P. & Grosz, J., 1968: Final report and calculation reserves Fichtenhübel deposit - Fe, Cu impregnation, state to 31.12.1968. MS Archiv GSSR.147 p. (in Slovak)

Hackbarth,C. J. & Petersen, U., 1984: A fractional crystallization model for the deposition of argentian tetrahedrite. Econom. Geology, Vol. 79, 448 – 460.

Hall, A. J., 1972: Substitution of Cu by Zn, Fe and Ag in synthetic tetrahedrite. Bulletin de la Société francais de Mineralogie et de Petrologie, 95, 583 – 594.

Johnson, N. E., Craig, J. R. & Rimstidt, J. D., 1986: Compositional trends in tetrahedrite. Canadian Minerl., 24, 385 – 397.

Kvaček, M., 1980: Selenium distribution in the minerals from some ore deposits of Slovakia. In: Materialy XI. kongressa Karpato-Balkanskoi geologicheskoi associacii, sek. Mineralogia i geochimia. Kyjev, Naukova Dumka, 173 – 178.

Lynch, J. V. G., 1989: Large-scale hydrothermal zoning reflected in the tetrahedrite - freibergite solid solution, KenoHill Ag-Pb-Zn district, Yukon. Canad. Mineralogist, Vol. 27, 383 – 400.

Macinský, P. (1992): Paragenetic and geochemic recherch in Fichten-hübel deposit. MS Archiv Dep. of econ. geol., Comenius University, Bratislava, 82 p. (in Slovak)

Macinský, P. & Antal, B., 1993: Bi-sulphosalts from the Fichtenhübel deposit. Acta Geologica Univ. Comen. 49, 16.

Maheľ, M., 1954: Contribution to stratigraphic of south part the Spišsko -gemerské rudohorie Mts. Notes to territory SE from Železník deposit. Geol. Práce, Zpr. 1, 49 – 53. (in Slovak)

Makovický, E. & Skinner, B. J., 1978: Studies of the sulfosalts of copper. VI. Low - temperature exsolution in synthetic - tetrahedrite solid solution; $Cu_{12+x}Sb_{4+y}S_{13}$. Canad. Mineral., 16, 611 – 623.

Maske, S. & Skinner, B. J., 1971: Studies of the sulphosalts of copper. I. Phase and relations in the system Cu-As-S. Econ. geology, 66, 901 – 918.

Matula, L., 1969: Contribution to geochemistry of the pyrites on the Fichtenhübel deposits. Geol. Práce, Spr. 48, 81 – 90. (in Slovak)

Miller, J. W. & Craig, J. R., 1983: Tetrahedrite-tennantite series compositional variations in the Cofer deposit, Mineral District, Virginia. Amer. Mineralog., 68, 227 – 234.

Mishra, B. & Mookherjee, A., 1991: Tetrahedrite mineral chemistry and metal zoning: A thermodynamic assessment from the Rajpura - Dariba polymetallic deposit, India. Econ. Geology, Vol.. 86, 1529 – 1538.

Mozgova, N. N. & Cepin, A. I., 1983: Bleklye rudy, osobenosti chimicseskogo sostava i svoistv. Nauka, Moskva, 278 p. (in Russian)

Návesňák, J., 1967: Final report - calculation reserves. Detailed exploration. Fichtenhübel deposit Cu-Fe ore, state to 1. 1. 1967. MS Archiv GSSR, 328 p. (in Slovak)

Návesňák, J. edit., 1982: Final report - calculation reserves on the Fichtenhübel deposit - Detailed exploration, complex Cu-Fe ore, state to 1.1.1982. MS Archiv GSSR, 431 p. (in Slovak)

Pattrick, R. A. D. & Hall, A. J., 1983: Silver substitution into synthetic zinc, cadmium and iron tetrahedrites. Mineralog. Magaz., 47, 441 – 451.

Reichwalder, P., 1970: Sketch origin of structurs deposits in region Jeďovec deposit. Geol. Práce, Spr. 51, 109 – 113. (in Slovak)

Petersen, E., Petersen, U. & Hackbarth, C. J., 1990: Ore zoning and tetrahedrite compositional variation at Orcopampa, Peru. Econ. Geology, Vol. 85, 1491–1503.

Sack, R. O. & Ebel, D. S., 1993: As-Sb exchange energies in tetrahedrite - tennantite fahlores and bournonit-seligmanite solid solutions. Mineralogical Magaz., 57, 635 – 642.

Sack, R. O. & Loucks, R. R., 1985: Thermodynamic properties of tetrahderite-tenantites: constraints on the interdependence of the Ag=Cu, Ge=Zn, Cu=Fe and As=Sb exchange reactions. Amer. Mineral., 70, 1270 – 1289.

Slávik, J. edit., 1967: Raw materials of Slovakia. Bratislava, SVTL, 510 p. (in Slovak)

Spiridonov, E. M. & Badalov, A. S., 1983: Evolucia sostava bleklych rud vulkanogennogo mestorojdenia Kairagach v vostochnom Uzbekistane. Geologia rudnych mestorojd. No. 4, 108 – 114. (in Russian)

Spiridonov, E. M., Ignatov, A. I. & Šubina, E. V., 1990: Evolucia bleklych rud vulkanogennogo mestorojdenia Ozernovskoe (Kamchatka). Izvest. Akad. Nauk SSSR, serija geologičeskaja. No. 9, 1990, 82 – 94. (in Russian)

Springer, G., 1969: Elektron probe analyses of tetrahedrite. Neues jahr. Mineral. Mh., 24 – 32.

Tarkian, M. & Breskovskaja, V., 1990: Arsenic minerals and their genetic significance in the Madjarovo ore field, Estern Rhodope, Bulgaria. N. Jb. Miner. Mh. No. 10, 1990, 433 – 442.

Tatsuka, K. & Morimoto, N., 1977: Tetrahedrite stability relations in the Cu - Fe - Sb - S system. Americ. Mineralog. 62, 1101 – 1109.

Trdlička, Z., 1960: Recherch characteristic of ore from deposit district Smrekový vrch -- Hummel. MS Archiv GSSR, 256 p. (in Czech)

Trdlička, Z., 1963: Supergen origin of marcaite and pyrite from pyrhotite on Fichtenhübel deposit (SGR). Čas. Mineral. Geol. (Praha), 8, č. 3, 289 – 290. (in Czech)

Trdlička, Z., 1963a: Selenium in sulphides minerals in Fichtenhübel deposit district. Vest. Ústr. Úst. Geol. 38, č. 1, 37 – 39. (in Czech)

Trdlička, Z., 1963b: To geochemic gold on siderite veins of Spišsko - gemerské rudohorie Mts. Věst. Ústř. Úst. geol., 38, 2, 129 – 131s. (in Czech)

Trdlička, Z., 1967: Mineral and chemic recherch of siderite from Fichtenhübel deosit district. Čas. Mineral. Geol. (Praha), 12, č. 1, 27 – 36. (in Czech)

Trdlička, Z., 1967a: Occurrence Co-arsenopyrite in Fichtenhübel a Smolník deosit districts (SGR). Čas. Nár. Muz. odd. Prirodoved. (Praha), 136, 97 – 102. (in Czech)

Trdlička, Z., 1967b: Mineral study of tetrahedrite from Fichtenhübel deosit (SGR). Čas. Mineral. Geol. (Praha), 12, č. 2, 115 – 121. (in Czech)

Trdlička, Z. & Kupka, F., 1957: Cobellite and virgin bismuth from locality Fichtenhübel on Slovakia. Sbor. Ústr. Úst. Geol. (Praha), 453 – 464. (in Czech)

Trdlička, Z., Kvaček, M. & Kupka, F., 1962: Mineral and chemic recherch of cobellite from siderites veinsl Fichtenhübel deosit districts (SGR). Čas. Mineral. Geol. (Praha), 7, č. 4, 432 – 433. (in Czech)

Trdlička, Z. & Potužák, V., 1962: Contribution to study of ore laboratory dressing from Fichtenhübel deposit districts. Rudy (Praha), 10, 347 – 350. (in Czech)

Trdlička, Z. & Kupka, F., 1966: Zum studium der temperatur der sideritbildung aus dem Fichtenhübel - lagerstättegbiet (Zips-gömörer erzgebirge). Acta Univ. Carol. (Praha), Geol, č. 1, 77– 80.

Volcanic activity in Late Variscan Krkonoše Piedmont Basin: petrological and geochemical constraints

JAROMÍR ULRYCH[1], JANA ŠTĚPÁNKOVÁ[1], JIŘÍ K. NOVÁK[1], EDVÍN PIVEC[1] and VLADIMÍR PROUZA[2]

[1]Institute of Geology, Academy of Sciences of the Czech Republic, Rozvojová 135, 165 02 Praha 6, Czech Republic, ulrych@gli.cas.cz
[2]Czech Geological Survey, Klárov 3/131, 118 21 Praha 2, Czech Republic

Abstract. Three groups of Late Palaeozoic volcanic rocks can be distinguished in the Krkonoše Piedmont Basin: (I) trachyandesites, andesites > trachytes, trachydacites, (II) basaltic trachyandesites, basaltic andesites > basalts, trachybasalts, and (III) rhyolites. Volcanic activity started in the Late Carboniferous, producing calc-alkaline (basic) to intermediate volcanics of group I in the southern part of the Krkonoše Piedmont Basin, and migrated north during the Permian, producing calc-alkaline transitional (mildly alkaline ?) intermediate and acid volcanics of groups II and III. Volcanic rocks of intermediate composition are of Carboniferous and Permian ages, whereas acid volcanics prevailed in the Permian. Basic to intermediate rock members (groups I and II) represent mantle-derived products affected by crustal contamination during the assimilation-fractional crystallization (AFC) process. Although the primary magma composition is obscured by pervasive crustal assimilation, DM or HIMU sources are more probable than the EM source. Heat input into the crust from the ascending basic to intermediate magmas and from the upper mantle led to the formation of anatectic crustal melts represented by rhyolites of the group III. Geochemical similarity of rhyolites of the group III with some late Variscan granites suggests their common source. Although the Late Palaeozoic volcanic rocks in individual basins in N Bohemia come from similar sources and are basically of the same origin, they probably evolved in separate crustal magmatic chambers.

Key words: Late Palaeozoic volcanism, Krkonoše Piedmont Basin, petrology, geochemistry, Sr-Nd isotopes

Introduction

The Bohemian Massif has a unique position within the central Europe as the largest exposed part of the Variscan Orogeny. In the last years, several attempts have been made to characterize the late- to post-collisional volcanic activity and its role in the late stages of the Variscan Orogeny (W. Franke, 1989; D. Franke, 1995). The Variscan Orogeny, a major continental collision episode culminating at about 360 Ma, was accompanied by the emplacement of a range of subduction- and extension-related magmas between 360 and 260 Ma (Lorenz & Nicholls, 1984; Downes & Duthou, 1988; Wilson & Downes, 1991). The mantle beneath the western and central Europe was metasomatized as a consequence of plate subduction during the Variscan Orogeny and especially during late phases of the Late Palaeozoic (LP) extension (Wilson & Downes, 1991). In the Late Carboniferous, the Bohemian Massif became dissected by a conjugate system of wrench faults associated with the accumulation of continental, often coal-bearing volcano-sedimentary sequences. Variscan continent-continent collision in the central Europe was followed by periods of magmatic activity both within the orogeny and in its foreland. Compositional differences between the volcanic rocks were controlled by different tectonic regimes and by the heterogeneity of the basement. Crustal thickening and southward-increasing depths of origin of basic magmas in

the North German Basin may reflect the presence of a pre-existing subduction-influenced basaltic magma source (Benek et al., 1996).

Alkaline (rather transitional!) volcanic activity in marginal parts of the Variscan Orogeny is closely associated with pull-apart structures (Ziegler, 1990). Nevertheless, integrated studies on the Upper Palaeozoic (UP) volcanics of western and central Europe, considering both their structural position and geochemical signatures, have been published only rarely (Eigenfeld & Schwab, 1974; Seckendorf, 1989; Hoth et al., 1993; Korich, 1989, 1992; Benek et al., 1993, 1995, 1996; Kölbl-Ebert 1995). Volcanic series in the basins generally started with a minor basaltic phase and terminated with a voluminous rhyolitic one.

Late Variscan intramontane troughs of central Europe are aligned along old structural discontinuities and tectonic lineaments of the basement (e.g., E-W, NE-SW and/or NW-SE). The broad zone of the above-mentioned basins, together with intensive volcanism, implies a substantial tension and thinning of the crust (Benek et al., 1996). However, Jindřich (1971) related the UP volcanics associated with the graben and half-graben structures along Precambrian lineaments and/or strike-slip faults with the taphrogenic movements induced by updoming of the Bohemian Massif in the Late Palaeozoic and Cenozoic. The responsibility of the Variscan and Alpine orogenies for these phenomena is considered doubtful by

Slovak Geol. Mag., 8, 3– 4(2002), 219 – 234

220
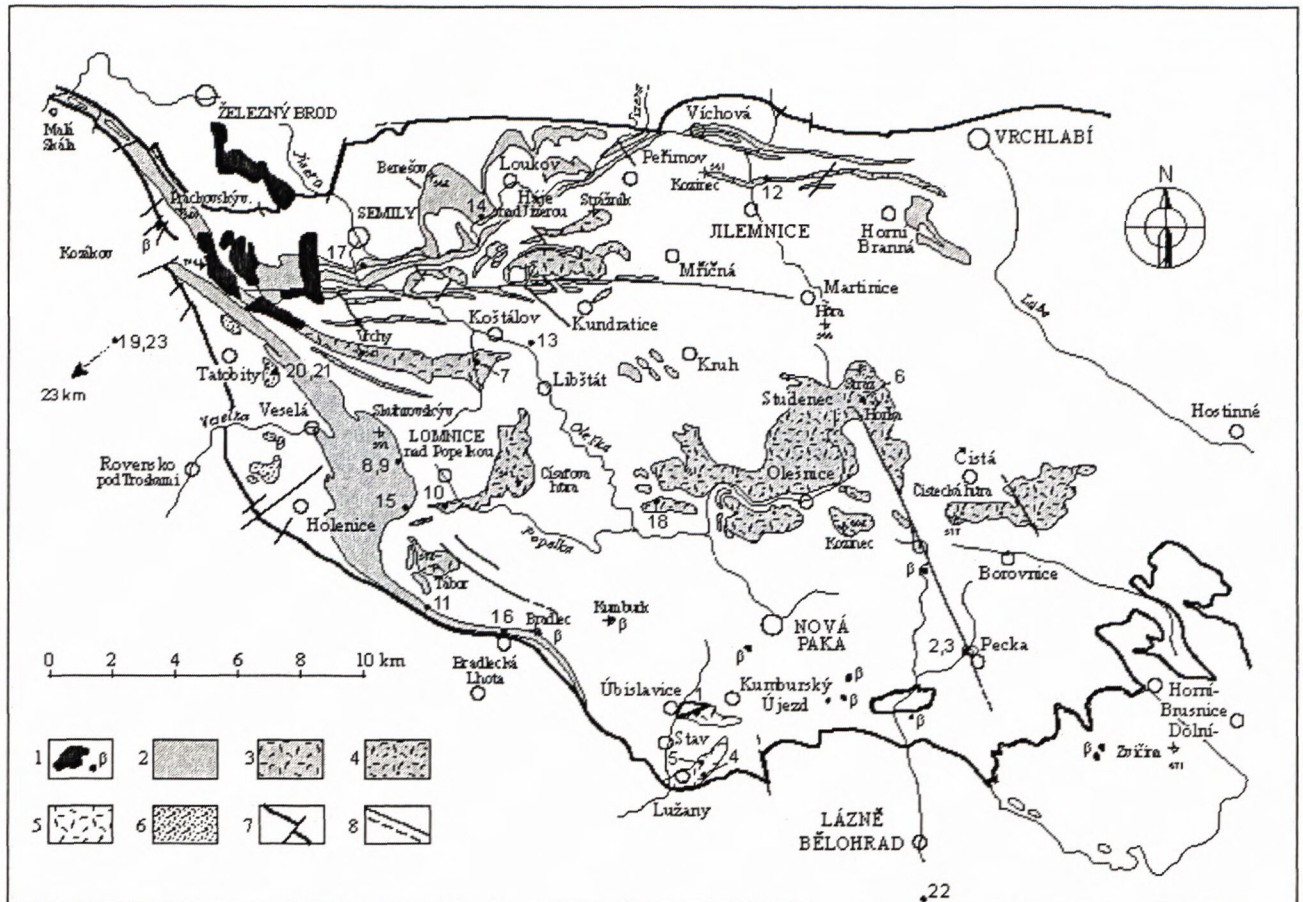
Fig. 1 A sketch of the Late Palaeozoic volcanic rocks within the Krkonoše Piedmont Basin with sample locations (Prouza & Tásler, 2001). Cenozoic: 1 – basaltic volcanics β; Permo-Carboniferous: 2 – basaltic andesites (effusions, locally with small bodies of subvolcanics), 3 – subvolcanics (sills and dykes, volcanic stocks), 4 – volcanic bodies formed by effusives, pyroclastics and subvolcanics, 5 – andesite, dacite, rhyodacite, 6 – rhyolitic ignimbrite, 7 – boundary of the Krkonoše Piedmont Basin with crystalline complexes and Upper Cretaceous sediments, 8 – reverse fault, normal fault, proved and assumed.

Jindřich (1971), as indicated by the taphrogenic character of tectonics and volcanic activity in the Bohemian Massif.

The aim of the study was to extend the knowledge of the geochemical character of the LP volcanism in space and time in the key regions of the Bohemian Massif (Ulrych et al., in prep.): in the Krkonoše Piedmont Basin (KPB) and the associated Mnichovo Hradiště (MHB), and the Česká Kamenice (CKB) basins. A special attention is paid to the study of the source of primary magmas and of the crustal control of the AFC process using trace element and Sr-Nd isotope constraints.

Geological setting of the Late Palaeozoic volcanism in the Bohemian Massif

Products of intensive volcanic activity associated with the late phases of Variscan Orogeny are abundant in the sedimentary fill of the LP basins. Accumulations of largely synchronous volcanic rocks are present in basins of North Bohemian (Lusatian) region (KPB, MHB, CKB and the Intra-Sudetic Basin) and Central Bohemian basins filled with Upper Carboniferous to Lower Permian continental ("limnic") sediments (Fig. 1). The LP volcanism in the Bohemian Massif (Pešek & Tásler, 1989) is characterized by predominance of acid volcanics including tuffs and tuffites over intermediate and basic rocks (except for the MHB).

Volcanic activity in the LP basins occurred in two phases: the first phase dates to the Carboniferous, mostly to Westphalian B and C, and the second phase to the Early Permian, especially Late Autunian (Pešek & Tásler, 1989; Pešek /Ed./, 2001). Products of coeval volcanism outside the LP basins occur in particular in the Altenberg-Teplice caldera (Benek et al., 1995; Breiter et al., 2001).

Although the diverse chemical composition of the UP volcanics (in particular the "melaphyre group") was recognized already by Fediuk (1965, 1967, 1973), no systematic study of this group has been conducted. The scarce unpublished geochemical data (Schovánková, 1985a, b; Bouška, 1985; Rutšek, 1995) indicate a wide range of chemical compositions, especially among the basic and intermediate members of the UP rocks.

Geochemical studies of the LP volcanism have been separated from the study of the relation between the magma composition and tectonomagmatic settings till the present (Pearce, 1982; Pearce et al., 1984). This approach led to the conservation of the classic pet-

rographical interpretation of the volcanics as products of "subsequent" Variscan volcanism (Gotthard, 1933).

Only the latest studies of volcanic products in the Intra-Sudetic Basin by Dziedzic & Teissere (1990), Dziedzic (1996, 1998) and Awdankiewicz (1999a, b) represent modern trends in the study of the LP volcanism in the Bohemian Massif. Three volcanic suites have been recognized by Awdankiewicz (1999b): (i) the Early and the Late Carboniferous calc-alkaline suites, and (ii) the Late Carboniferous and Early Permian weakly alkaline volcanic suite.

Products of the Late Palaeozoic volcanism in the Krkonoše Piedmont Basin

The areal extent of volcanics represents about 10 % of the KPB, 30-50 % of the MHB and 25 % of the CKB. However, the areal extent of volcanic products in the narrow strip of UP rocks along the Lusatian (Lužice) Fault reaches 60-80 %.

Schovánková (1985a, b, 1989) presented the latest results of a comprehensive petrological study of the UP volcanics of the KPB, MHB and CKB. She proposed a collective term andesitoids for intermediate rocks, classified as "melaphyres" in older publications. Andesitoids prevail over other volcanic rocks in the basins, forming up to 90 % of the volume of the KPB. Rhyolitic rocks are abundant only in the upper part of the basin fill of the Upper Autunian age. Andesitoids are placed among potassic sub-route varieties (shoshonites) by their chemical composition.

The oldest products of the LP volcanism are known from the Kumburk Fm. (Westphalian D – Barruelian), and the youngest volcanic rocks are preserved in the Chotěvice Fm. of the Late Autunian age. Volcanic activity culminated in the Late Autunian by the Vrchlabí Fm. where volcanic rocks are the most widespread. The andesitic Kozákov Hill Complex (Fediuk, 1972) and bodies of the Levín Highland (Ponikelská, 1982), Čistecká hůra and Císařova hůra hills are present at this stratigraphic level. Andesitoid volcanics most frequently occur in the form of lava flows but rarely form subvolcanic bodies such as sills and dykes. Andesitic tuffs, tuffites and agglomerates occur only rarely.

Schovánková (1989) suggested that the basaltic andesites of the KPB originated from several independent magmatic chambers. The root zone of the basaltic trachyandesite volcanism may be associated with the E-W-striking first-order fault zone (Kundratice-Javorník Zone – Prouza & Tásler, 2001), accompanied by a series of dykes and subvolcanic bodies. Results of measurements of elliptical vesicles of amygdaloidal parts of andesitoids (Prouza et al., 2000) indicate that the lava flows were reaching out from several volcanic centres near Semily, Lomnice n. P., Nová Paka and the Kozákov Hill Complex, i.e., from centres associated with a fault zone lying near the present Lusatian Fault.

The largest effusive body is that of basalt andesite exposed in the upper part of the SW slope of the Kozákov Hill, and extending to Malá Skála and the N part of the MHB in the NW and to Tužín in the SE (Fediuk, 1972).

Its minimum thickness is 160 m and its total length is about 46 km. Volcanic bodies of the Levín Highland and Čistecká hůra Hill near Nová Paka are interpreted as products of a stratovolcano (Schovánková, 1989) due to the relatively high abundance of andesitic tuffs, tuffites and agglomerates alternating with lava flows.

The largest subvolcanic body (max. 100 m in thickness, about 8 km in length) is the Košťálov sill, followed by the laccolith N of Kundratice (Schovánková, 1989), a.o.

Multiple superimposed bodies (up to several hundreds of metres thick) of basaltic andesite effusions, largely in the Vrchlabí, Prosečné and Chotěvice formations, were proved by boreholes drilled to the basement of the Late Cretaceous sediments in the MHB. The presence of pyroclastics of andesitic composition is sporadic. As an exception, two elongated effusive bodies of andesitoids accompanied by pyroclastics (Středa, 1971; Prouza, 1993) occur in the MHB in a strip of outcrops along the Lusatian Fault.

However, different types of volcanic rocks (dacite sensu Schovánková, 1985b) in the Upper Carboniferous Kumburk Fm. are present in the southern part of the KPB between Stav, Kumburský Újezd and Lužany. A small body of a similar rock is present near Pecka (andesite sensu Schovánková, 1985b).

Acid volcanism is represented by rhyolite ignimbrites (flows), rare rhyolites, rhyolite pyroclastics (tuffs) and mixed rock types such as tuffites and volcaniclastic sediments.

Ignimbrites are the most abundant volcanics, particularly in the MHB (Schovánková, 1985a) with the thickness exceeding 200 m. Ignimbrites form an elongated body (about 8 km long with a thickness of >250 m) between Proseč p. J. and the area S of Pelíkovice. Small bodies of ignimbrites (maximum thickness of ca. 50 m) at Tatobity, Žlábek and Rovensko p. T. and the elongated body S of Kozákov Hill and W of Prackovice Hill lie within the Chotěvice Fm. of the KPB.

Intrusions of rhyolites, partly porphyritic, forming lens-like bodies in phyllites on Mlázovice Chlum Hill SW of Šárovcova Lhota, are probably also products of the LP volcanism.

Methods of investigation

Bulk chemical analyses of rocks were performed using wet method in the Institute of Rock Structure and Mechanics, Academy of Sciences of the Czech Republic, Praha (analyst J. Švec). Trace element concentrations were determined using XRF (J. Štrublová, Gematest, Praha-Černošice) and INAA analytical methods (J. Frána, Nuclear Physics Institute, Academy of Sciences of the CR, Řež). The precision of XRF analyses varies about 5 % as checked by a series of duplicate analyses. The precision of INAA analyses is comparable with the data published by Řanda et al. (1970). The accuracy of individual element INAA determinations was tested against the rock standard B-1.

The analyses of Sr and Nd isotopes were performed in the Isotope Laboratory of the Department of Earth and

KRKONOŠE PIEDMONT BASIN				
Stage		**Lithostratigraphic Unit**		**Character and thickness of volcanic products**
Autunian		Chotěvice Fm.		rhyolite tuffs and tuffites near Mladé Buky, Libeč and in boreholes at Ratibořice
				bodies of ignimbrites near Tatobity, Rovensko p.T., W of Kozákov Hill, NE of Smrčí
		Prosečné Fm.	U	rhyolite tuffs and tuffites in the neighbourhood of the Arkose Horizon, effusive bodies of andesitoids at Kruh, Horní and Dolní Branná and Holenice; Horní Branná and Mladé Buky horizons
			L	
		Vrchlabí Fm.	U	effusives and pyroclastics of the Levín Highland and the Čistecká hůra Hill
			L	andesitoid effusives among Komárov, Loukov and Vrchlabí
Stephanian	C	Semily Fm.		rhyolite tuffs and tuffites in the Ploužnice and Štěpánice-Čikvásky Horizon
				small effusion of basaltic andesite near Ploužnice
	B	Syřenov Fm.	U	intercalations of tuffs and tuffites (in cm) in a horizon of black claystones
			L	intercalations of tuffs and tuffites (tonsteins) (in cm) in the Syřenov Fm.
	Barr.	Kumburk Fm.	U	dacitic volcanics near Kumburský Újezd and Lužany
Cantabrian to Westphalian D			L	
MNICHOVO HRADIŠTĚ BASIN				
Autuniam		Chotěvice Fm.		uniform, areally extensive body of andesitoids with max. thickness of 130 m at Všeň
				"loaf-like" bodies of ignimbrites – max. thickness of 200 m in the neighbourhood of Český Dub
		Prosečné Fm.	U	extensive intercalatons of rhyolite tuffs and tuffites (ca. 0.1 m thick), andesite effusion between the N
			L	vicinity of Hodkovice n.M. and Bezděčín ("Upper Melaphyre Group")
		Vrchlabí Fm.	U	multiple repeated flows of andesitoids of different thickness and extent (max. total thickness
				of about 500 m – Cetenov, Bezděčín) a local body of ignimbrite at Všeň (100 m thick)
			L	effusion of andesitoids near the Lusatian Fault ("Lower Melaphyre Group")
Stephanian	C	Semily Fm.		a small body of rhyolite at Cetenov (2 m thick) with intercalations of tuffs and tuffites a few cm thick (max. 10 cm), a local body of andesitoids up to 100 m thick at Všeň
	B	Syřenov Fm.	U	intercalations of rhyolite tuffs and tuffites (tonsteins) in the horizon of black claystones and in the Mělník Group of Seams
			L	
	Barruelian	Kumburk Fm.	U	local thin bed of tuffites (volcaniclastic greywacke)
Cantabrian to Westphalian D			L	

U – Upper, L - Lower

Environmental Sciences at the Universität München using a technique described in Hegner et al. (1995) and Hegner & Kröner (2000).

Lithostratigraphy

Two volcanic suites were distinguished in the KPB based on the stratigraphic position and distribution of volcanic rocks (see Table 1):
- **the Late Carboniferous volcanic suite** comprises intermediate rocks from localities Pecka, Stav - quarry Rumchalpa, and from the Lužany area.
- **the Early Permian volcanic suite** comprises the andesitoid group (sensu Schovánková 1985b) with "melaphyre" (sensu Gotthard, 1933) composition, ranging from primitive basic and intermediate rocks to acid rocks including ignimbrites and tuffs.

Petrography

Older volcanic series

Andesites to trachyandesites (type locality of Pecka) are dark grey to pale purple in colour and almost aphyric

in appearance. Glomeroporphyritic clots (~4.5 %) of original orthopyroxene (1-3 mm in diameter) together with sparse pseudomorphs after clinopyroxene? are seen in thin sections only. Occasionally, xenocrysts of undulatory quartz (1-2 mm in diameter, ~13 vol. %) are observed, probably resulting from magmatic resorption prior to, or during, the volcanic eruption. Quartz is lined with magnetite-vermiculite symplectites, 0.05-0.2 mm thick, originally composed of small pyroxene crystals. The trachytic-textured groundmass is formed by albitized plagioclase laths (0.2-0.4 mm in size, ~55 vol.%), interstitial chlorite, hematite and carbonate. Subhedral chlorite pseudomorphs after pyroxene phenocrysts were later affected by vermiculitization (producing pale brown pleochroism) and are surrounded by clinozoisite-epidote or opacite rims. Completely opacitized amphibole (?), altered olivine (?) and apatite are accessories.

Trachydacites (type locality of Lužany) are weakly porphyritic in hand specimens, purple in colour, with hematite coatings on cracks. K-feldspar with sieve-textured rims (up to 2.5 mm in diameter), chloritized biotite (~0.5 mm in size), and minute oligoclase laths are seen in thin sections as sparse microphenocrysts. The predominance of two feldspars over partly xenocrystic drop-like quartz and altered clinopyroxene suggests rather a trachytic than dacitic composition of magma. Pseudomorphs after pyroxene have subhedral outlines and are rimmed by hematite. The quench-textured groundmass is locally red in colour (rich in hematite staining) or contains colourless fields separated by devitrified glass bands. It consists of sodic plagioclase, alkali feldspar, hematite and vitreous patches (15-30 μm in size).

Hematitized trachytic dacites with moderately porphyritic texture and strongly altered groundmass (type locality of Rumchalpa) contain glomeroporphyritic clots of sericitized plagioclase (2-3 mm in diameter, 5 vol.%), totally kaolinitized alkali feldspar mantled by albite (1.8-2.3 mm in size, 5-7 vol.%), and sparse embayed quartz (1-1.5 mm in size, 21 vol.%) as phenocrysts. Quartz is resorbed by groundmass. Hematite pseudomorphs after plagioclase laths (0.2-0.4 mm), and chloritized biotite with hematite rims (0.3-0.4 mm in size) are a part of the fluidal-textured groundmass. K-feldspar and plagioclase in groundmass, varying in size between 0.05 and 0.15 mm, are strongly kaolinitized and sericitized. Goethite, hematite, magnetite and apatite are common accessories.

Younger volcanic series

Andesitoids (basaltic andesites to basaltic trachyandesites, rarely also basalts and trachybasalts) form a group of weakly to strongly altered rocks, corresponding to former "melaphyres":

Porphyritic and locally trachytic textured rocks (type locality of Vseň) forming lava flows are mostly massive, partly amygdaloidal, black grey or brownish red in colour. The phenocryst assemblage consists of tabular and lath-shaped andesine (An_{42-48}) and pseudomorphed clinopyroxene (as much as 2 vol.%). Low-temperature albite (Pivec, in press - type locality of Benešov), chlorite and

hematite are important additional minerals, formed within spilitic-like reaction of andesine-labradorite. Locally observed traces of the original volcanic glass as well as clinopyroxene (pigeonitic augite) are affected by smectitization or chloritization. Subordinate groundmass containing also potassium feldspar is often totally altered (hematitized). Moreover, a few samples contain strongly corroded quartz xenocrysts lined with diopsidic clinopyroxene. Prismatic apatite, skeletal ilmenite and secondary iddingsite represent accessory minerals.

Rocks with intersertal to hyaloophitic textures are characterized by massive types (type localities of Studenec and Hrabačov). These rocks are generally aphanitic or amygdaloidal in hand specimens. The primary mineralogy reveals two plagioclase generations (An_{50-62} and An_{38-50}), pyroxenes (pigeonitic augite and/or orthopyroxene), and devitrified volcanic glass (commonly 20-35 vol.%). Lesser amount of alteration products such as chlorite, albite, clay minerals, calcite and hematite are also found. A high degree of devitrification is visible, passing from black-brown to yellow-brown colour and resulting from abundant magnetite, and hematite dust in the groundmass. Highly devitrified glass, especially that containing skeletal plagioclase, may be whitish grey in colour. Pseudomorphs after olivine and magnetite occur as accessory phases.

Rocks with ophitic or poikiloophitic textures are rare (type locality of Košťálov). When almost unaltered, this rock is dark grey to black in colour and massive in hand specimens. Due to oxidation, the rock colour passes into purple or red, mainly along fractures. A typical mineral assemblage comprises normally zoned plagioclase (An_{64-48}, 45-50 vol.%), both ortho- and clinopyroxenes, and pseudomorphs after olivine. Reddish-brown biotite and magnetite grains form overgrowths on pyroxenes. Subhedral pyroxenes, if only partly altered, can be recognized as very pale rose hypersthene or pale green-coloured pigeonitic augite. The size of plagioclase and pyroxene microphenocrysts ranges from 0.15 mm to 2.1 mm. Minor pseudomorphs after olivine (0-2 vol.%, up to 0.6 mm in size) are rimmed by magnetite and consist of serpentine or smectite minerals. Albitized plagioclase laths are also replaced by tiny colourless chlorite flakes. Acicular accessory apatite occurs in places.

A textural diversity is also typical for altered acid rocks, especially those including ignimbrites. Ignimbrites are often hematitized and kaolinitized, pink to pale purple in colour. They occur in two varieties:

Fine-grained rhyolite ignimbrite (type locality of Mlázovice) is usually characterized by predominance of silt-sized, moderately sorted ash with less abundant glass shards as well as broken feldspar clots or crystalloclasts, up to 2.5 mm in size. The ash particles have a spherical shape. Sieve-textured plagioclase fragments as well as areas or rims of unevenly altered glass show disequilibration. Clay minerals formed after vitreous particles and feldspars as well as hematite dust are ubiquitous. Small broken quartz crystals occur in substantial amounts.

Nevaditic rhyolite ignimbrite (type locality of Tatobity) predominantly contains subrounded and broken crystals of quartz (0.1-3 mm in size, 50-60 vol.%) and
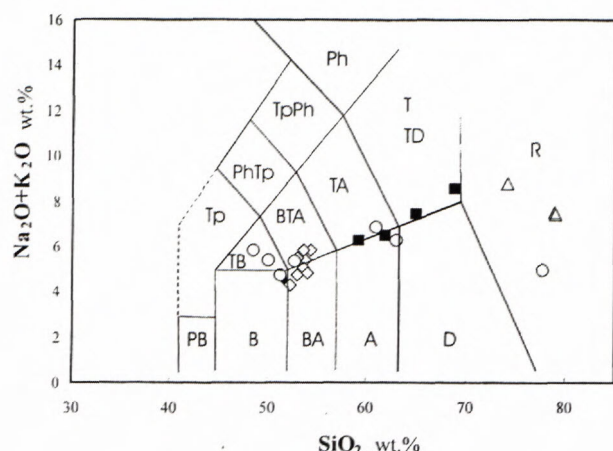
Fig. 2 Volcanics of the Krkonoše Piedmont Basin and the Mnichovo Hradiště Basin in the TAS diagram (Le Maitre ed., 2002). Altered samples (empty circles) plotted for comparison were not used for geochemical consideration.

Rock fields: B – basalt, BA – basaltic andesite, A-andesite, D – dacite, R – rhyolite, TB – trachybasalt, BTA – basaltic trachyandesite, TA – trachyandesite, T – trachyte, TD –trachydacite.

Explanations for symbol: full squares – group I (Carboniferous volcanics of the Krkonoše Piedmont Basin); diamonds – group II (empty diamonds – Permian volcanics of the Krkonoše Piedmont Basin, full diamond – Mnichovo Hradiště Basin); empty triangles – group III (Permian acid rocks of the Krkonoše Piedmont Basin and the Mnichovo Hradiště Basin); empty circles – altered samples.

alkali feldspar (0.1-2.8 mm in size, 10-20 vol.%) with subordinate but characteristic pseudofluidal banded groundmass. Otherwise fresh rock contains alternating thin bands of glass and fragments of quartz and alkali feldspar. Subordinate plagioclase grains show sieved texture or are totally sericitized. Quartz displays undulatory extinction. Secondary voids after leached plagioclase and glass occur in strongly weathered rocks. Flakes of dark brown biotite (0.1-0.7 mm in size), zircon and sphene occur as accessory minerals.

Geochemistry

Analytical data

The twenty-five samples from the KPB and 2 samples from the MHB were selected for geochemical study. The samples were selected with the purpose to cover a variety of regions and stratigraphical positions. Only a few outcrops of Carboniferous volcanics are present in the KPB, exposing highly altered rocks. For this reason, only four samples of Carboniferous volcanic rocks were included into the sample set. Samples with $H_2O>3$ wt.% were considered altered and excluded from the data set for geochemical study. Major and trace element analyses of all samples are summarized in Tables 2 a, b. Nine rock samples from the KPB and one sample from the Central Bohemian basins were chosen for Nd and Sr isotope study (Table 3).

Geochemical characteristics of volcanic rocks

The studied samples from the KPB and MHB show a wide range of SiO_2 contents (48-78 wt.% SiO_2). An uneven distribution of SiO_2 content was confirmed, with a compositional gap between SiO_2 contents of 54-59 wt.%. The rocks were subdivided into 3 groups according to their SiO_2 contents and stratigraphic positions (see Lithostratigraphy). In the TAS diagram (Fig. 2) of Le Maitre ed. (2002), the rocks can be classified as:

- **group I,** comprising four samples that plot along the trachyandesite-andesite boundary and in the trachyte-trachydacite field near the boundary with dacite. Schovánková (1985a, b, 1989) denoted all these rocks generally to dacites.
- **group II,** comprising samples that plot near the boundary of basaltic trachyandesite and basaltic andesite fields, with some scatter into the adjacent basalt and trachybasalt fields. According to Schovánková (1985a, b, 1989) these rocks are generally classified as andesitoids.
- **group III,** represented by four samples of rhyolites.

Group I volcanics of intermediate composition is of Carboniferous age, whereas groups II and III are of Permian age and reveal a basic-acid composition.

According to the $Na_2O + K_2O$ vs. SiO_2 contents, prevailing part of Carboniferous and Permian rock samples shows transitional character between subalkaline and alkaline rock series of Miyashiro (1978). The high K_2O and relatively low TiO_2 contents reflect the pertinence of the studied rocks to those of continental character (Coleman, 1977; Pearce et al., 1975). In Harker's diagrams. FeO, MgO, TiO_2, MnO, CaO and P_2O_5 correlate negatively and K_2O correlates positively with SiO_2. The contents of Al_2O_3 and Na_2O are uniform in most samples and decrease at high SiO_2 contents (>65 %) only (cf. Table 2 a, b).

The rhyolites are alumina-rich and similar to peraluminous S-type granites. However, their $Al_2O_3/(CaO + Na_2O + K_2O)$ vs. $Al_2O_3/(Na_2O + K_2O)$ molar ratios display a trend analogous to post-orogenic granites (sensu Loiselle & Wones, 1979; Maniar & Piccoli, 1989), Fig. 3. When compared to experimental data (Altherr et al., 1999), the composition of the rhyolites is similar to that of partial melts of a metapelite source (Fig. 3).

In PM-normalized multi-element variation diagrams, groups I and II show very similar patterns with negative Rb, Nb, Ta, Eu and Ti anomalies (Fig. 4). However, the groups substantially differ in Sr anomaly, which is positive in the group I and negative in the group II. Rocks of group the III differ from other groups in better pronounced negative Sr, Ti and Eu anomalies, as well as in negative P and Ba anomalies.

The medium ΣREE is a characteristic feature of groups I and II of intermediate rocks (141-385 ppm) and acid group III rocks (125-171 ppm). Chondrite-normalized REE patterns of all groups show medium to low fractionation (Fig. 5) with La_N/Yb_N ratios between 8-21 (groups I and II) and 4-7 (III group). Negative Eu anomaly is present in all samples (Eu/Eu* = 0.5-0.9), however, the expressive negative anomaly is characteristic of acid derivatives (Eu/Eu* = 0.1-0.2), indicating strong plagioclase fractionation in parental magma.

Table 2: Chemical analyses of the Late Paleozoic volcanics A55from the Krkonoše Piedmont and the Mnichovo Hradiště basins.

	Krkonoše Piedmont Basin - group I					Krkonoše Piedmont Basin group II													MHB	Krkonoše Piedmont Basin - group III			MHB
Nos.	1	2	3	4	5	6	7	8	9	10	11	12	13	14	15	16	17	18	19	20	21	22	23
Sample No.	301	312	313	379	380*	303	304	305	306*	307	308	311	331*	376*	377	381*	382	383*	335	309	310	314	334*
	Rumchalpa	Pecka	Pecka	Lužany	Lužany	Studenec	Koštálov	Lomnice n. Popelkou		Doubra-vice		Hrabacov	Koštálov	Benešov u Semil	Lomnice n. Popelkou	Bradlecká Lhota	Semily, Varta	Stará Paka	Všeň	Tatobity	Tatobity	Mlázovice	Všeň
SiO$_2$	67.33	58.39	56.63	62.72	59.41	53.12	52.70	52.10	46.52	50.72	52.23	51.64	58.46	43.75	51.65	51.06	52.07	50.06	50.51	77.99	78.01	72.79	71.71
TiO$_2$	0.51	0.88	0.78	0.72	0.75	1.54	1.45	1.35	1.51	1.55	1.62	1.61	1.11	1.35	1.61	1.54	1.59	1.46	1.62	0.11	0.10	0.10	0.11
Al$_2$O$_3$	15.03	16.67	16.16	15.68	16.88	15.84	16.21	16.41	15.57	16.27	15.95	15.85	17.74	17.36	17.31	16.26	16.51	16.10	16.33	11.33	11.42	14.66	12.23
Fe$_2$O$_3$	2.96	4.44	4.24	4.38	4.93	7.66	3.50	7.98	9.96	8.79	7.74	4.38	3.37	2.89	4.66	9.48	3.80	7.20	9.31	1.04	1.05	1.62	0.86
FeO	0.20	0.33	1.02	0.34	0.57	1.88	5.90	1.39	0.35	1.89	2.22	5.92	4.37	6.31	5.06	1.58	5.30	3.50	2.13	0.20	0.31	0.11	0.16
MnO	0.04	0.10	0.08	0.03	0.05	0.13	0.15	0.17	0.18	0.12	0.10	0.16	0.05	0.09	0.13	0.07	0.11	0.17	0.12	0.02	0.02	0.01	0.03
MgO	0.67	1.64	3.41	1.85	1.80	4.10	4.85	4.44	3.52	4.97	4.38	4.69	3.56	6.60	4.24	4.25	4.44	5.73	4.63	0.43	0.42	0.11	1.39
CaO	2.58	5.63	7.16	3.48	3.86	7.22	7.34	7.21	9.79	7.99	7.72	8.08	0.55	5.97	6.64	6.89	7.17	8.25	7.82	0.35	0.08	0.26	1.35
Na$_2$O	3.62	3.19	3.52	2.96	3.34	3.59	3.31	3.04	3.13	2.90	2.92	3.22	3.08	5.14	3.39	3.19	3.12	3.04	2.99	2.38	2.29	2.82	2.46
K$_2$O	4.73	2.92	2.49	4.25	2.57	2.11	1.94	2.63	1.87	1.24	1.96	1.37	3.48	0.09	1.94	2.00	1.50	1.58	1.28	5.03	5.04	5.82	2.09
P$_2$O$_5$	0.20	0.23	0.23	0.22	0.23	0.62	0.55	0.47	0.52	0.54	0.63	0.56	0.28	0.58	0.77	0.66	0.70	0.49	0.54	0.04	0.03	0.02	0.03
H$_2$O$^+$	0.71	1.54	1.15	1.21	1.71	0.90	0.93	1.08	2.96	1.11	0.79	1.24	3.32	4.95	1.01	1.03	1.78	1.00	1.08	0.64	0.79	1.16	2.15
H$_2$O$^-$	0.88	1.18	1.55	1.63	2.26	1.30	0.84	1.57	1.46	1.61	1.61	1.20	0.53	1.34	1.57	2.25	1.92	1.66	1.68	0.68	0.59	0.25	4.71
CO$_2$	0.77	2.73	1.76	0.55	1.53	0.00	0.00	0.00	2.50	0.03	0.00	0.00	0.00	3.08	0.00	0.06	0.09	0.00	0.01	0.09	0.00	0.09	0.15
S	100.23	99.87	100.18	100.02	99.89	100.01	99.67	99.84	99.84	99.73	99.87	99.92	99.90	99.50	99.98	100.32	100.10	100.24	100.05	100.33	100.15	99.82	99.43
As	3.3	4.8	2.3	2.4	1.7	4.6	n.d.	2.1	1.6	1.6	n.d.	2.5	9.5	8.4	0.7	0.9	63.3	1.9	4.1	15.9	26.4	15.0	11.7
Ba	841	1188	1156	837	1056	596	564	692	461	525	605	473	402	75	702	572	743	480	578	94	83	82	48
Ce	85.7	56.7	57.2	84.5	59.7	121.0	107.7	170.2	93.5	94.0	118.2	101.3	73.8	104.6	113.2	110.5	117.5	73.8	94.9	69.1	69.6	57.0	7.4
Co	5.6	n.d.	11.0	10.0	10.0	22	25	23	22	28	22	27	26	40	25	22	24	29	173	n.d.	n.d.	n.d.	10.0
Cr	11	82	83	90	96	82	103	49	111	99	80	100	117	241	48	79	156	111	19	2	2	2	25
Cs	5.89	4.50	2.04	7.19	2.68	0.40	0.46	0.76	0.34	0.53	0.39	0.46	10.61	0.48	0.68	0.39	5.58	0.48	3.13	15.47	10.09	3.81	7.36
Cu	32	35	49	n.a.	n.a.	79	94	49	80	49	97	99	n.a.	n.a.	n.a.	n.a.	n.a.	n.a.	n.a.	18	18	292	n.a.
Eu	1.19	1.40	1.42	1.47	1.40	2.53	2.40	2.30	2.25	2.30	2.55	2.43	1.35	1.95	2.77	2.56	2.71	2.13	2.44	0.19	0.22	0.27	0.20
Gd	7.0	6.8	6.0	7.0	4.6	10.6	10.5	12.2	10.0	9.6	8.1	11.8	10.1	8.3	10.6	10.2	12.8	8.8	11.0	9.8	10.7	4.5	10.4
Hf	5.4	4.5	4.4	5.7	4.3	9.7	8.7	9.0	7.6	7.8	9.6	8.3	7.3	6.9	8.5	9.1	8.7	6.2	7.5	4.5	4.4	8.4	4.3
Ho	0.76	0.52	0.58	0.77	0.65	1.22	0.93	1.06	0.82	1.15	1.16	1.39	1.83	1.62	1.70	1.48	1.60	1.41	1.45	1.91	2.24	0.82	3.09
La	53.4	32.8	33.5	51.3	32.4	65.9	58.5	99.8	51.1	50.6	64.4	54.4	38.6	59.4	61.3	64.9	67.6	40.9	50.4	35.6	35.2	32.4	37.4
Lu	0.32	0.24	0.27	0.36	0.22	0.65	0.58	0.59	0.58	0.6	0.65	0.65	0.55	0.56	0.62	0.63	0.65	0.55	0.63	0.96	0.99	0.51	1.17
Nb	17	13	14	7	n.d.	36	29	27	31	27	31	26	20	21	22	20	22	11	19	33	31	40	25
Nd	42.7	35.7	37.0	40.2	27.0	68.8	59.9	80.8	50.2	54.4	66.9	54.9	35.0	52.5	61.4	59.0	64.1	41.3	51.4	34.5	34.9	22.5	36.9
Ni	13	35	57	32	54	53	56	48	63	59	55	53	73	88	38	53	52	59	93	n.d.	n.d.	21	2
Pr	n.d.	n.d.	n.d.	n.d.	n.d.	26.3	n.d.	29.4	n.d.	n.d.	n.d.	17.4	n.d.	n.d.	n.d.	n.d.	n.d.	n.d.	n.d.	13.4	n.d.	n.d.	n.d.
Rb	158	73	61	157	62	43	32	49	33	29	36	29	131	5	35	37	20	26	39	335	328	266	86
Sc	9.4	19.6	19.2	15.3	18.9	23.7	23.6	27.6	26.6	27.7	25.2	28.7	20.1	29.0	22.8	24.9	24.6	31.5	28.5	7.1	6.7	0.6	6.9
Sm	7.0	4.9	5.2	6.7	4.8	11.5	10.3	12.1	9.6	9.5	11.5	10.0	6.8	9.0	11.0	10.5	11.5	8.0	9.7	7.7	7.8	3.1	8.4
Sr	169	465	610	256	480	260	295	257	291	248	254	236	33	63	339	292	391	221	279	19	18	28	126
Ta	0.84	0.54	0.53	0.83	0.48	1.70	1.59	1.27	1.42	1.45	1.74	1.48	1.46	1.54	1.64	1.60	1.73	1.07	1.36	2.63	2.51	1.73	2.51
Tb	0.66	0.56	0.58	0.69	0.50	1.41	1.3	1.25	1.26	1.25	1.45	1.35	0.96	1.16	1.36	1.34	1.46	1.16	1.27	1.50	1.55	0.47	1.59
Th	23.96	9.68	9.67	21.44	9.18	8.14	7.17	11.61	6.09	6.08	7.86	6.35	14.61	6.85	6.52	7.39	7.36	4.61	6.95	20.29	19.45	56.78	21.37
Tm	0.27	0.31	0.37	0.39	0.34	0.66	0.60	0.70	0.67	0.68	0.74	0.68	0.49	0.95	0.84	0.70	0.76	0.62	0.70	0.90	0.97	0.35	1.08
U	4.19	2.12	3.13	3.63	2.46	1.43	1.16	1.39	1.94	0.8	1.93	1.17	3.01	1.67	1.09	2.67	1.29	1.10	1.55	4.40	3.59	3.45	12.46
V	23	79	83	38	74	100	102	108	135	113	93	124	112	168	96	85	106	119	125	n.d.	n.d.	n.d.	n.d.
Y	32	25	26	23	16	48	42	38	41	42	45	42	35	32	36	35	36	31	33	66	72	38	64
Yb	1.85	1.46	1.67	2.13	1.37	3.93	3.79	3.72	3.78	3.71	4.16	3.89	3.51	3.63	4.13	4.01	4.29	3.63	3.96	6.41	6.58	3.12	7.53
Zn	29	56	68	57	75	122	121	115	88	130	118	128	221	217	120	98	126	115	142	34	34	36	60
Zr	176	140	140	193	143	349	290	304	263	260	320	265	236	252	304	320	324	205	255	94	86	191	82
#Mg	32.91	44.29	59.66	47.53	42.98	49.49	52.92	52.07	44.22	51.54	50.00	49.93	50.21	60.83	49.00	46.85	51.64	54.63	48.03	44.25	41.24	12.82	75.73
K/Rb	248.47	332.00	338.80	224.68	344.05	407.28	503.19	445.49	470.33	354.90	451.89	392.10	220.49	149.40	460.06	448.65	622.50	504.38	272.41	124.62	127.54	181.60	201.71
Rb/Sr	0.93	0.16	0.10	0.61	0.13	0.17	0.11	0.19	0.11	0.12	0.14	0.12	3.97	0.00	0.10	0.13	0.05	0.12	0.14	17.63	18.22	9.50	0.68
Th/U	5.72	4.57	3.09	5.91	3.73	5.69	6.18	8.35	3.14	7.60	4.07	5.43	4.85	4.10	5.99	2.77	5.69	4.18	4.48	4.61	5.42	16.46	1.72
Zr/Hf	4.10	8.26	11.35	8.25	16.33	35.91	33.45	33.74	34.56	33.46	33.47	32.08	32.51	36.50	35.92	35.22	37.03	33.03	34.23	3.48	3.23	7.92	5.79
Nb/Ta	20.24	24.07	26.42	8.39	0.00	21.18	18.24	21.26	21.83	18.62	17.82	17.57	13.70	13.63	13.44	12.51	12.74	10.27	13.97	12.55	12.35	23.12	9.96
SREE	200.90	141.32	143.64	195.47	132.97	288.08	256.43	384.70	223.66	227.80	279.79	242.82	173.03	243.65	268.88	265.86	284.86	182.31	227.84	168.51	170.72	125.01	115.04
La$_N$/Yb$_N$	20.72	16.11	14.38	17.33	16.93	12.02	11.06	19.23	9.69	9.78	11.10	10.03	7.90	11.72	10.63	11.60	11.30	8.09	9.13	3.98	3.83	7.44	3.56
Eu/Eu*	0.51	0.74	0.78	0.65	0.90	0.69	0.70	0.57	0.70	0.73	0.68	0.68	0.50	0.67	0.78	0.75	0.68	0.77	0.72	0.07	0.07	0.22	0.07

n.a. - not analysed, n.d. - not determined, below detection limit, * - altered samples excluded from the A136geochemical study, MHB - Mnichovo Hradiště Basin.
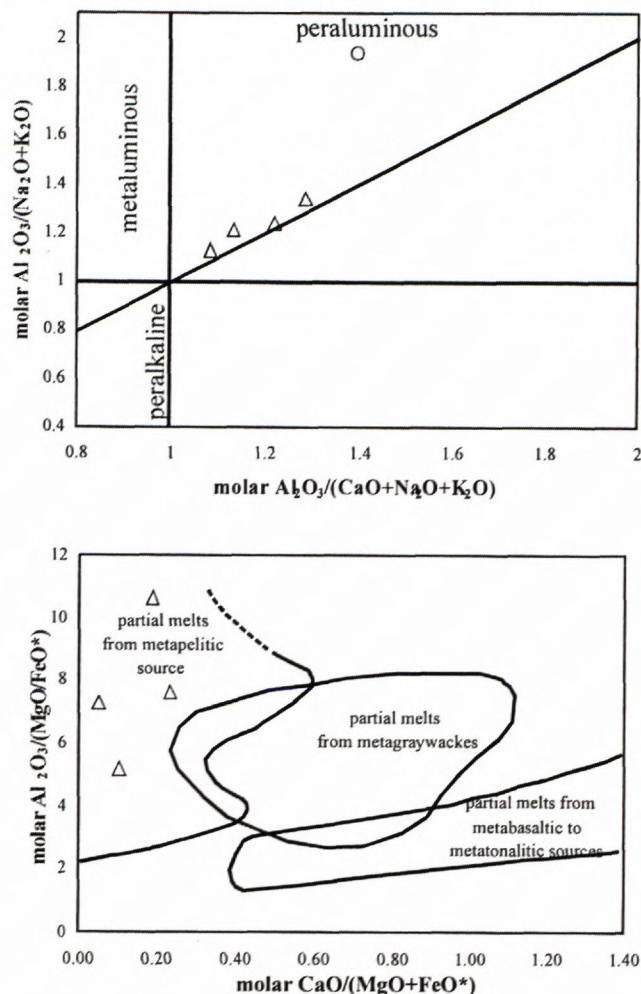
Fig. 3 Acid volcanic rocks of the Krkonoše Piedmont Basin plotted in the diagrams of Maniar & Piccoli (1989) and Altherr et al. (1999). For explanation of symbols see Fig. 2. These diagrams show the rock series affinity to peraluminous S-type granites and to partial melts from a metasedimentary source.
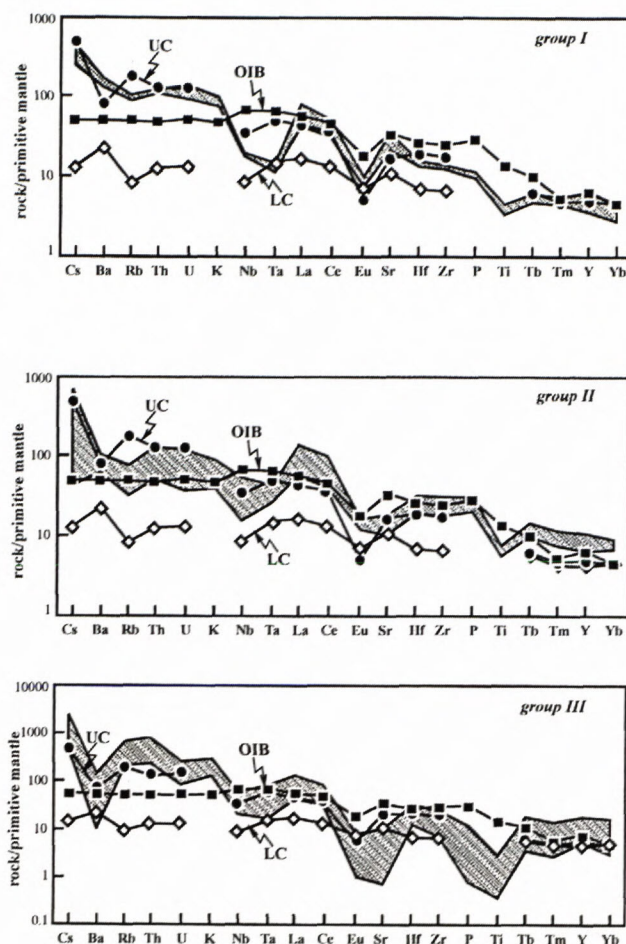
Fig. 4 Volcanics of the Krkonoše Piedmont Basin and Mnichovo Hradiště Basin in the PM-normalized multi-element variation diagram. For explanation of symbols see Fig. 2, cross-hatched areas correspond to rocks of individual groups I to III. Normalization values after Sun & McDonough (1989).

The following differences were recognized between the geochemical signature of comparable volcanics of groups I and II (see Table 3 for data):

– **Group I** of more evolved intermediate to acid volcanics is relatively impoverished in compatible elements as Ni, Sc, V and incompatible elements as Sr, REE, Zr, Ti, P, Nb and enriched in incompatible elements as K, Rb, Ba, Th and characterized with high La_N/Yb_N ratio associated with low ΣREE and low K/Rb ratio.

– **Group II** of more primitive intermediate to basic volcanics is relatively enriched in incompatible elements as Sr, REE, Zr, Nb, P and compatible elements as Ni, Sc, Ti, V, impoverished in incompatible elements as K, Rb, Ba, Th and characterized with low La_N/Yb_N ratio associated with high ΣREE and high K/Rb ratio.

Within groups I and II kindred differentiation trends in Harker's diagrams point to a fractionation of magma of similar composition. Geochemical data indicate that the rocks of the group I represent more advanced differentiates compared to the group II. The main differences are in higher K, Rb (Ba, Th), and lower Sr (REE, Zr, Ti,

P, Nb, Ta) and V (Ni, Sc) contents in the volcanics of the group I compared to volcanics of the group II. Negative Nb-Ta anomaly, depletion in P, Ti are typical features of subduction-related magmas (Bailey 1981).

Prevailing intermediate rocks of both groups were compared with geochemically similar rocks from the doubtless active continental margin and subduction regime of (i) the Andes and (ii) island arcs of the southwest Pacific (e.g. Ewart, 1982). Geochemistry of rocks of groups I and II can be paralleled to Andean andesites and basaltic andesites, respectively (Ewart, 1982). Considering the systematic increase in K, Rb, Ba, La, Ce, Th, Zr, Hf and decrease in Y along a profile from island arc to thick continental margin (Bailey 1981), the Krkonoše Piedmont Basin is herein proposed to represents a region with very thick crust. Volcanics of both groups show very similar geochemical features with the Andean volcanic rocks, primarily of the Central Active Volcanic Zone - East (Thorpe et al., 1984). In the K_2O vs. SiO_2 diagram (Peccerillo & Taylor 1976) volcanics of both groups plot into the high-K field, less commonly also to the field of shoshonitic series.

Table 3: Sr and Nd isotope ratios of the Late paleozoic volcanics from the Krkonoše Piedmont Basin.

	Sample No.	Locality	Rb*	Sr*	$^{87}Rb/^{86}Sr$	$^{87}Sr/^{86}Sr$	$^{87}Sr/^{86}Sr(t)$	Sm*	Nd*	$^{147}Sm/^{144}Nd$	$^{143}Nd/^{144}Nd$	$\varepsilon_{Nd}(t)$
Group I	303	Studenec	43	260	0,48	0.708681(11)	0,70670	10,80	56,42	0,11580	0.512331(11)	-3,0
	304	Košťálov	32	295	0,31	0.708433(11)	0,70715	9,73	50,43	0,11670	0.512303(9)	-3,6
	305	Lomnice n. P.	49	257	0,55	0.708246(11)	0,70598	11,30	69,87	0,09743	0.512316(10)	-2,6
	308	Doubravice	36	254	0,41	0.708482(11)	0,70679	10,60	54,97	0,11640	0.512334(11)	-3,0
	311	Hrabačov	29	236	0,36	0.707933(11)	0,70645	9,40	47,59	0,11940	0.512348(10)	-2,8
Group II	301	Rumchalpa	158	169	2,71	0.718442(12)	0,70726	6,11	36,29	0,10180	0.512153(11)	-6,0
	313	Pecka	61	610	0,29	0.707580(12)	0,70638	4,68	24,60	0,11500	0.512345(10)	-2,7
Group III	309	Tatobity	335	19	52	0.976319(12)	0,76174	6,71	28,10	0,14430	0.512280(10)	-5,1
	314	Mlázovice	266	28	28	0.853164(12)	0,73762	2,53	14,20	0,10780	0.512364(9)	-0,9
Central Bohemian Basins	323	Záhoří	49	272	0,52	0.709497(12)	0,70735	14,7	75,51	0,11780	0.512311(11)	-3,5

Krkonoše-Piedmont Basin

$\varepsilon_{Nd}(t)$ and $^{87}Sr/^{86}Sr(t)$ are recalculated for 290 Ma; * in ppm; data in paranthesis - standard deviation.
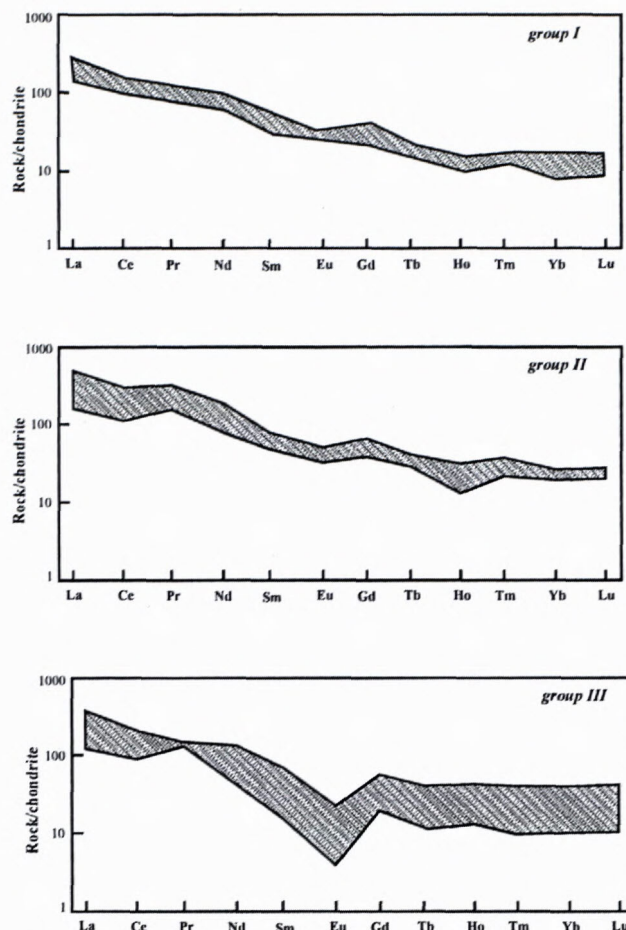

Fig. 5 Chondrite-normalized REE patterns of volcanics of the Krkonoše Piedmont Basin and Mnichovo Hradiště Basin. Normalization values after Sun & McDonough (1989).

All samples have low initial ε_{Nd} values between –1 and –6 and corresponding $(^{87}Sr/^{86}Sr)_i$ ratio of ca. 0.706 to 0.707 (Table 4). Two samples with very high Rb/Sr ratios (samples 309 and 314) yielded much higher calculated $(^{87}Sr/^{86}Sr)_i$ ratios, which is probably due to the modification of Rb and Sr concentrations during sample alteration, as suggested by a similar Sm-Nd isotopic systematics as in other samples. In the $(^{87}Sr/^{86}Sr)_i$ vs. ε_{Nd} diagram (Fig. 6), the data for samples of groups I and II produce a vertical trend whereas rhyolitic rocks of group III show higher calculated $(^{87}Sr/^{86}Sr)_i$ ratio; this is probably due to the disturbance of the Rb-Sr system in these samples. Rocks of group II show negative correlation of ε_{Nd} values with some trace element contents (Sr, Cr, Ni).

Origin and differentiation of magmas

Similar patterns in PM-normalized multi-element variation diagrams and isotopic data point to the same source material of parental magma for rocks of groups I and II. Negative Ta, Nb and Ti anomalies, high K_2O content and the position of the studied samples in the Th/Yb vs. Ta/Yb diagram (Fig. 7) are characteristic for lower crustal contamination (Pearce, 1983). Low ε_{Nd} and $(^{87}Sr/^{86}Sr)_i$ values, trending to the lower crust in the ε_{Nd}-$(^{87}Sr/^{86}Sr)_i$ diagram, and negative Rb anomaly in

Table 4 Contrasting geochemical features of the Carboniferous (I) and Permian (II) groups of volcanics in the Krkonoše Piedmont Basin

	Group I intermediate to acid volcanics		Group II intermediate to basic volcanics	
	average	range	average	range
Mg#	47	33-60	51	49-53
Ni (ppm)	34	13-57	52	38-59
Sc	15	9-19	26	23-29
V	48	23-83	105	96-124
K₂O (Wt %)	3.82	2.49-4.73	1.83	1.24-2.63
Rb	125	61-158	34	20-49
K/Rb	271	248-338	440	220-622
Sr	162	169-610	280	236-391
Ba	947	841-1156	613	473-743
REE	180	144-201	279	228-385
La$_N$/Yb$_N$	18	14-21	12	10-19
Zr	170	140-193	302	260-349
Th	18	10-24	8	6-12
TiO₂	0.67	0.51-0.78	1.54	1.35-1.62
P₂O₅	0.22	0.20-0.23	0.61	0.54-0.77
Nb	13	42917	28	22-36

Fig. 7 Volcanics of the Krkonoše Piedmont Basin and Mnichovo Hradiště Basin in the Th/Yb-Ta/Yb diagram (Pearce, 1983). Symbols as in Fig. 2.
SH – shoshonites, CA – calc-alkaline series, TH – tholeiites, ACM – active continental margins, OIA – oceanic island arcs, EM – enriched mantle, DM – depleted mantle, IPB – intra-plate basalts, MORB – mid-ocean ridge basalts, s – subduction enrichment, c – crustal contamination, w – within-plate enrichment, f – fractional crystallization.
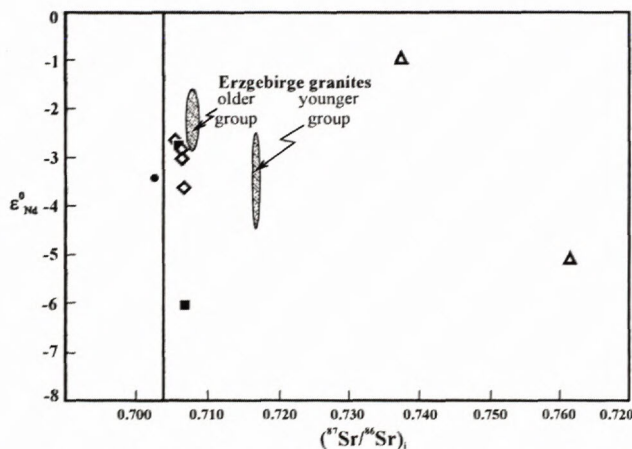
Fig. 6 Volcanics of the Krkonoše Piedmont Basin in the $(^{87}Sr/^{86}Sr)_i$ vsε_{Nd} diagram. For explanation of symbols see Fig. 2. Samples from Central Bohemian basins (full circle) and from Erzgebirge granites (Förster et al., 1999) are plotted for comparison.

PM-normalized multi-element variation diagrams point also to the contamination by lower crustal material. The samples of groups I and II, however, are enriched in most incompatible elements compared to the lower crust (Fig. 4). Such enrichment can be achieved either by a fractional crystallization or by mixing with acid partial melts or by source enrichment. Both fractional crystallization and mixing with acid partial melts should produce an increase in SiO₂ content. However, some samples of the group II are basic (of basaltic composition), and the source enrichment is therefore more probable. Affinity to the OIB (see Fig. 4) points to EM as a possible source of initial magma for groups I and II. Similar patterns in the PM-normalized multi-element variation diagram and characteristic trends in Harker's diagrams point to the fractionation of one initial magma within the individual groups. Nevertheless, variation in the Sr anomaly in the PM-normalized multi-element variation diagram cannot be explained by fractional crystallization or crustal assimilation. It is therefore probable that parental magmas
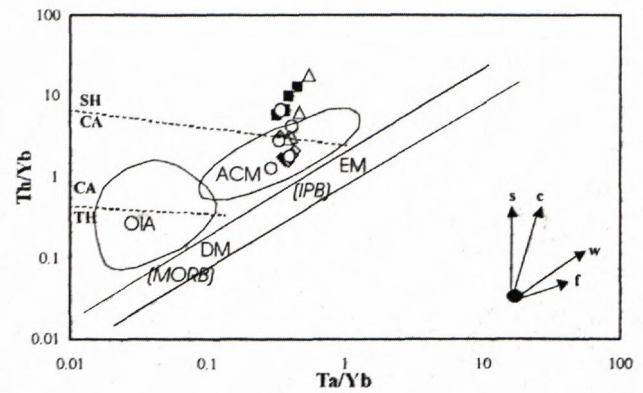
of the individual groups evolved in different ways. The presumption that the rocks of groups I and II cannot represent members of a single differentiation path is also clear from the SiO₂ contents, which are lower in younger rocks (group II) than in the older ones (group I). On the other hand, similar patterns in PM-normalized multi-element variation diagrams for rocks of groups I and II point to very similar initial magma for both groups. The evolution from more acid to basic members can be explained by replenishment of one magmatic chamber by a new basic magma, although an evolution in different magmatic chambers can be neither excluded. Although the rhyolitic magma of group III has some characteristics close to the rocks of groups I and II (negative Ti, Nb, Ta and Sr anomalies, low ε_{Nd} values), the compositional gap between coexisting intermediate and acid rocks of the same age (groups II and III), the affinity of rhyolites to the S-type granites and different $(^{87}Sr/^{86}Sr)_i$ and ε_{Nd} values point to different sources of basic and acid magmas. According to $(^{87}Sr/^{86}Sr)_i$ and ε_{Nd} values and the pattern in the PM-normalized multi-element variation diagram (Fig. 4) the parental magma of acid rocks (group III) formed by partial melting of the upper crustal material.

Compositional trends of the group II in the $(^{87}Sr/^{86}Sr)_i$ vs.ε_{Nd}, ε_{Nd} vs. Sr, ε_{Nd} vs. Cr and ε_{Nd} vs. Ni diagrams point to a typical lower crustal contamination (cf. Fig 8). Especially the increase in incompatible element contents together with decreasing ε_{Nd} values show that the magma composition was affected by assimilation as well as by fractional crystallization. However, simple mixing models of crustal assimilation cannot explain the observed trends (Fig. 8), and a combined AFC is a more probable process of magma evolution. To test this hypothesis, the evolution of ε_{Nd}, $(^{87}Sr/^{86}Sr)_i$, Sr, Ni and Cr contents in the magma during the AFC process was modelled (for methods used in modelling see the Appendix). As demonstrated by this modelling, the parental magma of the rock
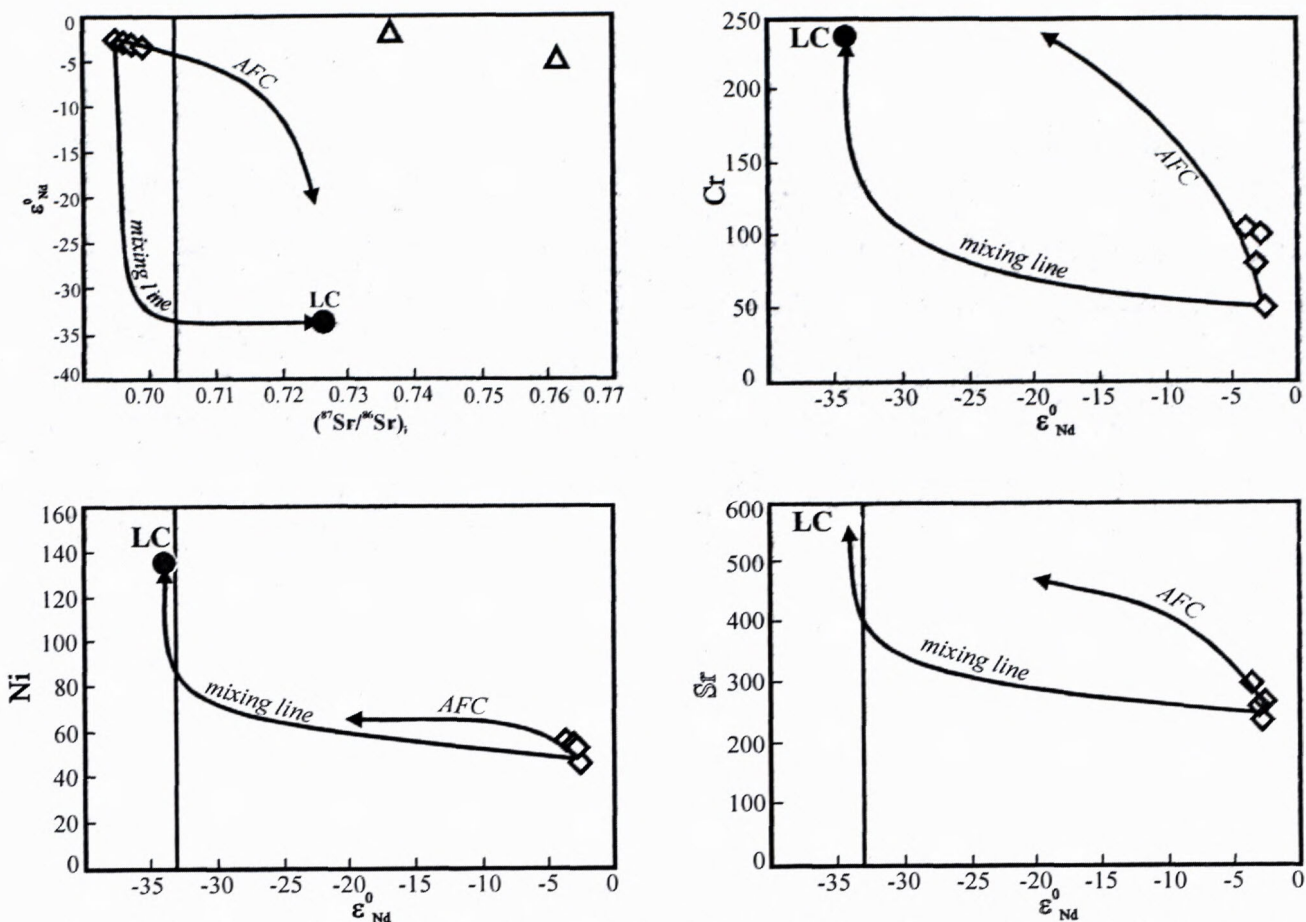
Fig. 8 Results of modelling of magma evolution. Composition of sample No. 305 was used as a starting magma composition, trace element contents in the lower crust are from Taylor & McLennan (1985), ε_{Nd} and $(^{87}Sr/^{86}Sr)_i$ were calculated for the age 290 Ma from the values of DePaolo et al. (1982). The line AFC was modelled using the following parameters: fractionated phase consists of 20 % plagioclase, 35 % olivine, 10 % clinopyroxene, 25 % orthopyroxene, 5 % Fe-oxide and 5 % apatite and r = 1 (mass assimilated/mass fractionated). Mixing line is shown for comparison; it models simple assimilation without fractionation. For the method of modelling see Appendix.

group II could have evolved by the AFC process. The contaminant was represented by the lower crust, and the fractionated phase consisted of 20 % plagioclase, 35 % olivine, 10 % clinopyroxene, 25 % orthopyroxene, 5 % Fe-oxide and 5 % apatite, while r = 1 (mass assimilated/ mass fractionated) – see Fig. 8.

Comparison to other Upper Paleozoic volcanics of the Bohemian Massif

Basic to intermediate rocks of the KPB (groups I and II) were compared to volcanic rocks of other LP basins in the Bohemian Massif (Central Bohemian basins, the Česká Kamenice Basin and the Intra-Sudetic Basin). In PM-normalized multi-element variation diagrams the rocks from the Česká Kamenice Basin and the Intra-Sudetic Basin show very similar characteristics - negative Nb, Ta, Eu and Ti anomalies (Fig. 9), enrichment in most of incompatible elements, pointing to similar sources of their parental magmas. Nevertheless, differences were found in the magnitude of Sr, Rb and Eu anomalies. Such differences can be explained by fractionation of plagioclase and by a different degree of crustal contamination. Rather unclear trends in the Harker's diagrams show that

rocks from different basins could not have formed by a continuous evolution of the same initial magma.

More differences exist between the studied rocks of groups I and II and basic to intermediate rocks of the Central Bohemian basins. In PM-normalized multi-element variation diagram, the elements from Nb to Yb show patterns similar to those of the group II with the exception of Ce anomaly in one sample from the Central Bohemian basins, whereas the elements from Cs to K show rather different patterns (Fig. 10). The similarity of the patterns for Nb to Yb may indicate a similar source of magma, however, the low number of unaltered samples of volcanics from the Central Bohemian basins makes a comparative study difficult (Pešek et al., in press).

When rocks of similar ages from different basins are compared, it is also difficult to find and explain the relationship between magma composition and the age of extrusion/intrusion. Thus the discussed rocks can hardly be linked to an evolution in one large, uniform magmatic chamber, and it is much more likely that several smaller magmatic chambers existed beneath the Bohemian Massif. Some of them could have been replenished several times by new primitive (basic) magma batches. On the other hand, the initial magma in individual chambers was
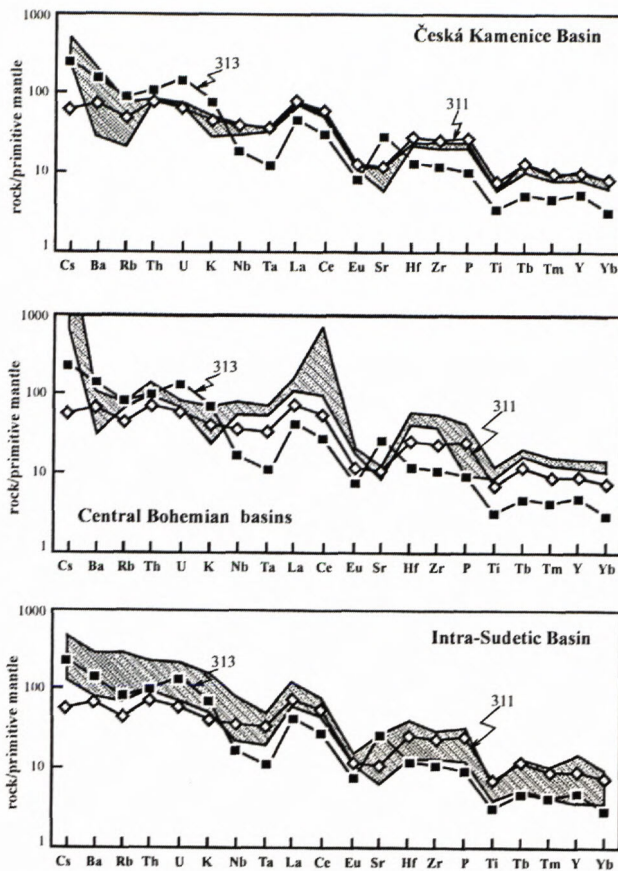
Fig. 9 Basic to intermediate volcanic products of the Česká Kamenice Basin, Central Bohemian basins and the Intra-Sudetic Basin in the PM-normalized multi-element variation diagrams. Representative samples of the group I (No. 313) and the group II (No. 311) of the Krkonoše Piedmont Basin are plotted for comparison.
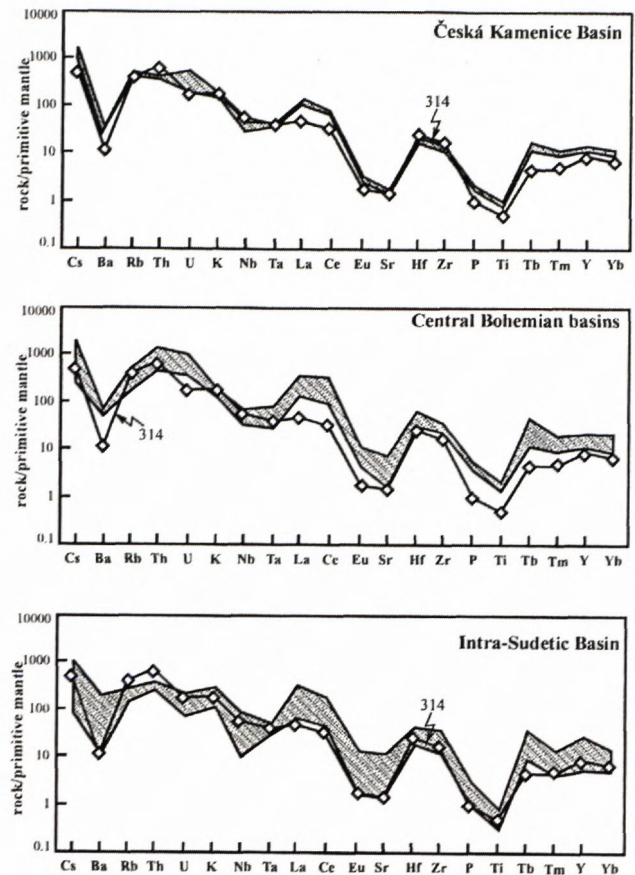
Fig 10 Acid volcanics of the Česká Kamenice Basin, Central Bohemian basins and the Intra-Sudetic Basin in the PM-normalized multi-element variation diagrams. Representative samples of the group III (No. 314) of the Krkonoše Piedmont Basin are plotted for comparison.

very similar and came from the same source. However, a separate study would be necessary to do to establish the number of the chambers and details of their evolution, but this is out of the scope of the present paper.

Basic and intermediate rocks were correlated with the published data on UP volcanic rocks from regions outside the Czech Republic – the Polish part of the Intra-Sudetic Basin (Dziedzic, 1998; Awdankiewicz 1999 b) and the Northeast German Basin (Benek et al., 1996). Rocks of the Intra-Sudetic volcanic field show similar patterns in the PM-normalized multi-element variation diagrams as those of the group II, thus possibly indicating a similar magma source. On the other hand, most of the rocks from the Northeast German Basin are rather different. Only the andesitic rocks from the Mecklenburg-Vorpommern area have similar geochemical features.

A comparison of the acid rocks of the KPB with their analogues from other basins in the Bohemian Massif shows a striking similarity in PM-normalized multi-element variation diagrams (Fig. 10), suggesting similar magma sources. Acid rocks have their equivalents in rhyolites of the Intra-Sudetic Basin (Dziedzic, 1998; Awdankiewicz, 1999a, b) and in rhyolites and microgragranitoids of the Mecklenburg-Vorpommern area of the Northeast German Basin (Benek et al. 1996).

The acid rocks of the KPB (group III) were also correlated with the late Variscan granitic rocks of the Bohemian Massif. Most of the late Variscan granitoids (Breiter & Sokol, 1997) were found to differ in their geochemical signatures from the studied acid volcanics of the KPB. A similarity was found to some granitic rocks from the Eastern Erzgebirge – the Preisselberg type only (Breiter & Sokol, 1997; Förster et al., 1999).

Discussion

The geochemical study shows that the parental magma of absolute majority of rocks of the group II evolved in a lower crustal chamber by the AFC process. This is in accordance with the conclusions of Dziedzic (1998) for volcanic rocks of the Intra-Sudetic Basin.

It is probable that the initial basic magma was derived from an enriched mantle source (see previous chapter). The similarity of the studied rocks with those of the Mecklenburg-Vorpommern region suggests analogues in their origin. Their generation was explained by the underplating of basic melts at the mantle-crust boundary (Benek et al., 1996).

Opinions on the origin of acid volcanic rocks having similar geochemical characteristics as the rhyolites of the

KPB are rather different. Benek et al. (1996) supposed that the rhyolites and microgranitoids from the Mecklenburg-Vorpommern area represent dry anatectic melts of the lower crust. However, Dziedzic (1998) assumed that the parental magma of rhyolitic rocks formed by the anatexis of the upper crust. Nd and Sr isotope signatures of the studied rhyolitic rocks and their trace element data imply the upper crustal origin. In general, the origin of UP volcanics can be explained by underplating of basic, mantle-derived melts at the mantle-crust boundary, where they were substantially affected by lower crustal material. Heat from the magma together with extension movements led to the melting of the upper crust and formation of shallow magmatic chambers of rhyolitic magma.

The LP volcanic activity in general is usually associated with the collapse of the Variscan Orogeny. Despite of the limited amount of Carboniferous volcanics (group I), a successive change in the geochemical character of volcanic rocks is evident. Volcanic activity in the KPB started with the Carboniferous intermediate volcanism (andesite to dacite), which was replaced by more basic volcanic products (basalts to basaltic andesites) in the Permian. Volcanics of both series represent products of late to post-collisional volcanism associated with the eastern part of the Variscan orogeny. The rocks of the Carboniferous group I show primarily calc-alkaline characteristics of volcanics of convergent plate margin-like setting, plotting near the discrimination boundary to alkaline series. However, the rocks of the Permian group II with similar geochemical characteristics reveal some closer affinity to transitional to mildly alkaline volcanics typical of a within-plate, post-collisional extensional setting. A similar transitional development of geochemical characteristics of the LP volcanic activity was reported by Awdankiewicz (1999b) from the Intra-Sudetic Basin. Calc-alkaline volcanic rocks with geochemical characteristics of convergent plate margins need not be always associated with the subduction at convergent plate boundaries. They can also originate in a post-collisional extensional setting, adjacent to former active continental margin, with a transition towards volcanism with alkaline affinity. An example of such a development is the Basin and Range Province, SW USA (Desonie 1992; Davies & Hawkesworth 1995).

The heat input into the crust from the primary basic magmas and from the upper mantle thermal layer led to the formation of anatectic crustal melts as represented by the group III rhyolites.

Variable evolutionary trends in volcanic activity in different basins point to the existence of several independent lower crustal magmatic chambers. The rise of basaltic magmas and their emplacement at the mantle-crust boundary (Benek et al., 1996) can well explain the variations observed in the rock suites. Formation of a number of small-scale plumes is characteristic of the passive rifting (Buck, 1986), which was probably the principal mechanism of extension in the region of LP basins in the Bohemian Massif. Rifting can be well explained by a post-orogenic collapse of the Variscan Orogeny.

Conclusions

The Late Palaeozoic volcanic activity of the KPB shows the following characteristics:
– three separate groups of volcanic products were recognized: group I consisting of trachyandesites, (andesites) and trachydacites, group II including basaltic andesites and basaltic trachyandesites (alkali basalts, trachybasalts), and group III including rhyolites only;
– volcanic activity in the KPB started in the late Carboniferous with calc-alkaline andesitic to trachyandesitic activity (group I) in the southern part of the basin, and migrated northwards during the Permian time. In the Permian, basaltic to andesitic (group II) and rhyolitic (group III) types of volcanism coexisted;
– the parental magma for basic to intermediate rocks was probably derived from an enriched mantle source and retained in lower crustal chamber(s) for a long time, where it evolved by the AFC process;
– the heat input from primary magmas (together with that from the mantle thermal layer) led to the formation of anatectic melts;
– volcanic products of different LP basins of the Bohemian Massif are principally similar in their sources and origin; however, they probably evolved in separate, lower-crustal magmatic chambers. This can be explained by the existence of a number of small-scale mantle plumes, characteristic of passive rifting;
– the origin of the LP volcanic activity in the N Bohemia can be linked with the collapse phase of the Variscan Orogeny and the tensional regime.

Appendix

Changes in the trace element contents in the magma during assimilation of lower crustal material and during combined AFC process have been modelled. The composition of a sample with relatively high ε_{Nd} (recalculated to 290 Ma) – e.g., sample No. 305 was taken as a starting magma composition. The trace element contents in the lower crustal material were taken from Taylor & McLennan (1985) and ε_{Nd} and $(^{87}Sr/^{86}Sr)_i$ were calculated from values of DePaolo et al. (1982). The used lower crustal composition is summarized in the following tables:

Ni	135
Sr	569
Nd	18.5
Cr	235

$(^{87}Sr/^{86}Sr)$	0.717	$(^{143}Nd/^{144}Nd)$	0.51071
$(^{87}Rb/^{86}Sr)$	0.056	$(^{147}Sm/^{144}Nd)$	0.0943
$(^{87}Sr/^{86}Sr)_i$	0.7168	ε_{Nd}	-33.84

Initial $(^{87}Sr/^{86}Sr)_i$ and ε_{Nd} are recalculated for 290 Ma.

Modelling of magma mixing (simple assimilation)

For the calculation of trace element evolution during simple assimilation of lower crustal material, the following mixing equation was used:

$$c^i_{mix} = X_m c^i_m + (1 - X_m)c^i_a$$

where c^i is the concentration of element **i**, indexes **m, a, mix** stand for the initial magma, the assimilant and the resulting magma affected by assimilation, X_a is the weight fraction of the resting magma expressed by the ratio of masses **M**:

$$X_m = \frac{M_m}{M_m + M_a}.$$

For the evolution of $^{87}Sr/^{86}Sr$ isotope ratio during simple assimilation, the equations of Langmuir et al. (1978) were used:

$$\left(\frac{^{87}Sr}{^{86}Sr} \right)_{mix} = \varphi_m \left(\frac{^{87}Sr}{^{86}Sr} \right)_m + \varphi_a \left(\frac{^{87}Sr}{^{86}Sr} \right)_a,$$

where

$$\varphi_m = \frac{c^{Sr}_m X_m}{c^{Sr}_m X_m + c^{Sr}_a (1 - X_m)},$$

$$\varphi_a = \frac{c^{Sr}_a (1 - X_m)}{c^{Sr}_m X_m + c^{Sr}_a (1 - X_m)}.$$

Explanation of symbols: c^{Sr} – concentration of Sr; subscripts a, m, mix stand for the assimilant, the initial magma and the resting magma affected by assimilation, respectively; X_m stands for magma fraction (see the mixing equation).

The same type of equation was used for the evolution of $^{143}Nd/^{144}Nd$ in the magma upon mixing.

Modelling of assimilation-fractional crystallization process (AFC)

The equation used for the calculation of the trace element concentrations, $^{143}Nd/^{144}Nd$ and $^{87}Sr/^{86}Sr$ ratios in the magma during the combined AFC process was taken from Allègre & Minster (1978) and DePaolo (1981).
a) trace element concentration during AFC:

$$\frac{c^i_m}{c^{i_0}_m} = F^{-z} + \left(\frac{r}{r-1} \right) \frac{c^i_a}{z c^{i_0}_m}(1 - F^{-z})$$

where

$$z = \frac{r + D - 1}{r - 1}$$

c^i is the concentration of trace element i, subscripts m, a stand for the magma and the assimilant, respectively, superscript ^{0} stands for the initial magma, r is the ratio of assimilated mass/fractionated mass, F means the magma fraction (mass of initial magma/mass of evolved magma) and D is the bulk partition coefficient of fractionated solid phase. For the calculation of the bulk partition coefficient, the following mineral-liquid partition coefficients were used:

	Plg	Ol	cpx	opx	Fe-Ti oxide	apatite
Ni	0.06[2]	4.3[6]	1.2[9]	0.79[2]	3.8[2]	
Sr	5.28[1]	0.02[4]	0.5[3]	0.01[3]	0.11[7]	1.1[12]
Nd	0.09[3]	0.02[3]	0.12[13]	0.05[2]	0.0079[13]	14[11]
Cr	0.02[2]	0.63[5]	3.5[8]	0.95[10]	6[8]	

Data source: [1]Ewart & Griffin (1994), [2]Luhr & Carmichael (1980), [3]Bacon & Druitt (1988), [4]Villemant (1988), [5]Beattie (1994), [6]Drake & Holloway (1981), [7] Burke et al. (1982), [8]Ringwood (1970), [9]Duke (1976), [10]Dunn & Sen (1994), [11]Paster et al. (1974), [12]Watson & Green (1981), [13]Fujimaki & Tatsumoto (1984)

The following equation was used for the calculation of the isotope ratio during the AFC process:

$$\frac{\alpha^i_m - \alpha^{i_0}_m}{\alpha^i_a - \alpha^{i_0}_m} = 1 - \left(\frac{c^{i_0}_m}{c^i_m} \right) F^{-z},$$

where α^i is the isotope ratio ($^{87}Sr/^{86}Sr$ or $^{143}Nd/^{144}Nd$), other symbols are the same as in the previous equation.

References

Allègre C.J. & Minster J.F., 1978: Quantitative models of trace element behavior in magmatic processes. Earth Planet. Sci. Lett., 38, 1-25.

Altherr R., Henes-Klaiber U., Hegner E., Satir M. & Langer C., 1999: Plutonism in the Variscan Odenwald (Germany): from subduction to collision. Int. J. Earth Sci., 88, 422-443.

Awdankiewicz M., 1999a: Volcanism in a late Variscan intramontane through: the Carboniferous and Permian volcanic rocks of the Intra-Sudetic Basin, SW Poland. Geologica Sudetica, 32, 13-47.

Awdankiewicz M., 1999b: Volcanism in a late Variscan intramontane through: the petrology and geochemistry of the Carboniferous and . Permian volcanic rocks of the Intra-Sudetic Basin, SW Poland. Geologica Sudetica, 32, 83-111.

Bacon C.R. & Druitt T.H., 1988: Compositional evolution of the zoned calc-alkaline magma chamber of Mt. Mazama, Crater Lake, Oregon. Contr. Mineral. Petrol., 98, 224-256.

Bailey J.C., 1981: Geochemical criteria for redefined tectonic discrimination of orogenic andesites. Chemical Geology, 32, 139-154.

Beattie P., 1994: Systematics and energetics of trace-element partitioning between olivine and silicate melts: Implications for the nature of mineral/melt partitioning. Chem. Geol., 117, 57-71.

Benek R., 1991: Aspects of volume calculation of palaeovolcanic eruptive products – the example of the Teplice rhyolite (East Germany). Z. Geol. Wiss., 19, 379-389.

Benek R., 1995: Late Variscan calderas/volcano-tectonic depressions in Eastern Germany. Terra Nostra, 7, 16-19.

Benek R., Katzung G. & Röllig G., 1976: Variszischer subsequenter Vulkanismus und tektogene Entwicklung im Gebiet der DDR. Jb. Geol., 8, 17-31.

Benek R., Kramer W., McCann T., Schenck M. Negendank J.F.W., Korich D., Huebscher H.-D. & Bayer U., 1996: Permo-Carboniferous magmatism of the Northeast German Basin. Tectonophysics, 266, 379-404.

Bouška V., 1985: Petrological and geochemical investigation of the Upper Palaeozoic volcanics. Unpublished Report, Faculty of Sci., Charles University, Praha, 81 pp (in Czech).

Breiter K., 1997: The Teplice rhyolite (Krušné hory Mts., Czech Republic) - chemical evidence of a multiply exhausted stratified magma chamber. Věst. Čes. geol. Úst., 72, 205-213.

Breiter K. & Sokol A., 1997: Chemistry of the Bohemian granitoids: Geotectonic and metallogenic implications. Sbor. geol. Věd, Ř. LG, M, 31, 75-96.

Breiter K., Novák J.K. & Chlupáčová M., 2001: Chemical evolution of volcanic rocks in the Altenberg-Teplice caldera (Eastern Krušné hory Mts., Czech Republic, Germany). Geolines, 13, 17-22.

Buck W.R., 1986: Small-scale convection induced by passive rifting: the cause of uplift of rift shoulders. Earth Planet Sci. Lett., 77, 362-372

Burger K., 1985: Die Kohlentonsteine in Niederrheinisch-Westphälischen Steinkohlrevier. Erkenntnissstand 1983. C.R. 10eme Int. Congres Stratigr. Géol. Carbon. (Madrid) 4, 211-234.

Burke W.H., Denison R.E., Hetherington E.A., Keopnick R.B., Nelson H.F. & Otto J.B., 1982: Variation of seawater $^{87}Sr/^{86}Sr$ throughout Phanerozoic time. Geology, 10, 516-53.

Cerai E. & Testa C., 1968: Separation of rare earths by means of small columns of Kel-F supporting di(2-ethyl)orthophosphoric acid. J. Inorg. Nucl. Chem., 25, 1045-1050.

Coleman R.G., 1977: Ophiolites. Springer-Verlag, Berlin.

Davies J.M. & Hawkesworth C.J., 1995: Geochemical and tectonic transitions in the evolution of the Mogollon-Datail Volcanic Field, New Mexico, U.S.A. Chem. Geol., 119, 31-53.

DePaolo D.J. 1981: Trace element and isotopic effects of combined wallrock assimilation and fractional crystallisation. Earth Planet. Sci. Lett., 53, 189-202.

DePaolo D.J., Manton W.I., Grew E.S. & Halpern M., 1982: Sm-Nd, Rb-Sr, U-Th-Pb systematics of granulite facies rocks from Fyfe Hills, Enderny Land, Antarctica. Nature, 298, 614-618.

Desonie D.L., 1992: Geologic and geochemical reconnaissance of Isla San Esteban: post-subduction orogenic volcanism in the Gulf of California. J. Volcanol. Geoth. Res., 52, 123-140.

Downes H. & Duthou J.L., 1988: Isotopic and trace element arguments for the lower-crustal origin of Hercynian granitoids and pre-Hercynian orthogneisses, Massif Central (France). Chem. Geol., 68, 291-308.

Drake M.J. & Holloway J.R., 1981: Partitioning of Ni between olivine and silicate melt: the 'Henry's Law problem' re-examined. Geochim. Cosmoch. Acta, 45, 431-437.

Duke J.M., 1976: The distribution of the period for transition elements among olivine, calcic clinopyroxene and basic silicate liquid. J. Petrology, 17, 499-521

Dunn T. & Sen C., 1994: Mineral/matrix partition coefficients for orthopyroxene, plagioclase, and olivine in basaltic to andesitic systems: A combined analytical and experimental study. Geochim. Cosmoch. Acta, 58, 717-733.

Dziedzic K., 1996: Two-stage origin of the Hercynian volcanics in the Sudetes, SW Poland. Neu. Jb. Mineral. Geol. Paläont., Abh., 199, 65-87.

Dziedzic K., 1998: Genesis and evolution of the Sudetic late Hercynian volcanic rocks inferred from the trace element modelling. Geologica Sudetica, 31, 79-91.

Eckhard F.J., 1979: Der permische Vulkanismus Mitteleuropas. Geol. Jb. Reihe D, Heft 35, 84 pp.

Eigenfeld F. & Schwab M., 1974: Zur geotektonischen Stellung des permosilischen subsequenten Vulkanismus in Mitteleuropa. Z. geol. Wiss., 2, 115-137.

Ewart A., 1982: The mineralogy and petrology of Tertiary-Recent orogenic volcanic rocks: with special reference to the andesitic-basaltic compositional range, 26-87. In Thorpe R.S. (ed.): Andesites: Orogenic Andesites and Related Rocks. Wiley & Sons, Chichester,

Ewart A. & Griffin W.L., 1994: Application of proton-microprobe data to trace-element partitioning in volcanic rocks. Chem. Geol., 117, 251-284

Fediuk F., 1965: Melaphyres in structural boreholes of the profile line Mělník-Ještěd. Sbor. Geol. Věd, Ř. G, 9, 103-108 (in Czech).

Fediuk F., 1967: Permokarbonische Vulkanite unter der Böhmischen Kreidetafel. Ber. Deutsch. Gesell. geol. Wiss., B- Mineral. Lagerstättenforsch., 12 173-179.

Fediuk F., 1972: Lower Paleozoic, Upper Paleozoic and Neoidic volcanics from the Železný Brod area. Unpublished Report, Faculty of Sci., Charles University, Praha (in Czech).

Fediuk F., 1973: Melaphyre rocks of northern margin of the Mnichovo Hradiště Depression. Sbor. Severočes. Mus., přír. Vědy, 5, 85-96 (in Czech).

Förster H.J., Tischendorf G., Trumbull R.B. & Gottesmann B., 1999: Late-collisional granites in the Variscan Erzgebirge, Germany. J. Petrology, 40, 1613-1645.

Franke D., 1995: The North Variscan Foreland. In: Pre-Permian Geology of Central and Eastern Europe, Dallmayer, R.D., Franke, W. & Weber, K. (Eds.). Springer Verlag, Berlin, 554-566.

Franke W., 1989: Variscan plate tectonics in Central Europe – current ideas and open questions. Tectonophysics, 169, 221-228.

Fuijimaki H. & Tatsumoto M., 1984: Partition coefficients of Hf, Zr and REE between phenocrysts and groundmass. Proceedings of the 14th Lunar Planetary Science Conference. J. geophys. Res., 22, 662-672

Gotthard J., 1933: Petrographic characteristic of melaphyres in the Podkrkonoši (Krkonoše Piedmont) area. Arch. přírod. Prozk. Čech, 18, 2, Praha (in Czech).

Hegner E. & Kröner A., 2000. Review of Nd isotopic data and xenocrystic and detrital zircon ages from the pre-Variscan basement in the eastern Bohemian Massif: speculations on palinspastic reconstructions. Spec. Pub. Geol. Soc. London, 179, 113-129.

Hegner E., Walter H.J. & Satir M., 1995. Pb-Sr-Nd isotopic compositions and trace element geochemistry of megacrysts and melilitites from the Tertiary Urach volcanic field: source composition of small volume melts under SW Germany. Contrib. Mineral Petrol., 122, 322-335.

Hoth, K. Huebscher H.-D., Korich D., Gabriel W. & Enderlein F., 1993: Die Lithostratigraphie der permokarbonischen Effusiva im Zentralabschnitt der Mitteleuropäischen Senke. Geol. Jb., A 131, 179-196.

Jindřich V., 1971: New views in tectonic significance of platform sediments in the Bohemian Massif, Czechoslovakia. Geol. Soc. Amer. Bull., 82, 763-768.

Kölbl-Ebert M., 1995: Paläozoische Ganggesteine (Rhyodazite/Dazite und Lamprophyre) des Südschwarzwaldes. Tübinger Geowiss. Arbeiten, Reihe A, Band 23, 206 pp.

Korich D., 1989: Zum Stoffbestand jungpaläozoischer basischer Magmatite aus dem DDR - Teil der Mitteleuropäischen Senke. Z. angew. Geol., 35, 72-78.

Korich D., 1992: Zu Stoffbestand und Genese der saueren und intermediären Vulkanite des Darss-Uckermark-Eruptivkomplexes in Mecklenburg-Vorpommern. Z. geol. Wiss., 20, 337-350.

Langmuir C.H., Vocke R.D., Hanson G.N. & Hart S.R., 1978: A general mixing equation with applications of Icelandic basalts. Earth Planet Sci. Lett., 37, 380-392.

Le Maitre, R.W. ed., 2002: Igneous Rocks A Classification Glossary of Terms. Cambridge University Press, Cambridge.

Loiselle N.C. & Wones D.R., 1979: Characteristic and origin of anorogenic granites. Geol. Soc. Amer., Abstr. 11, 468.

Lorenz V. & Nicholls I.A., 1984: Plate and intraplate processes of Hercynian Europe during the Late Palaeozoic. Tectonophysics, 107, 25-56.

Luhr J.F. & Carmichael I.S.E., 1980: The Colima Volcanic Complex, Mexico I. Post-caldera andesites from Volcan Colima. Contrib. Mineral. Petrol., 71, 343-372

Maniar P.D. & Piccoli P.M., 1989: Tectonic discrimination of granitoids. Geol. Soc. Am. Bull., 101, 635-643.

Miyashiro A., 1978: Nature of alkalic volcanic rocks series. Contrib. Mineral. Petrol., 66, 91-104.

Paster T.P, Schauwecher D.S. & Haskin L.A., 1974: The behavior of some trace elements during solidification of the Skaergaard layered intrusion. Geochim. Cosmochim. Acta, 38, 1549-1577.

Pearce J.A., 1982: Trace element characteristics of lavas from destructive plate boundaries. In: Andesites, Orogenic Andesites, and Related Rocks, Thorpe, R.S. (Ed.). J. Wiley & Sons, London, 525-548.

Pearce J.A., 1983: The role of sub-continental lithosphere in magma genesis at destructive plate margins. In: Continental Basalts and Mantle Xenoliths, Hawkesworth, C.J. & Norry, M.J. (Eds.). Shiva, Nantwich, 230-249.

Pearce J.A. & Cann J.R., 1973: Tectonic setting of basic volcanic rocks determined using trace element analysis. Earth. Planet. Sci. Lett., 19, 290-300.

Pearce T.H., Gorman B.E. & Birkett T.C., 1975: The $TiO_2-K_2O-P_2O_5$ diagram: a method of discriminating between oceanic and non-oceanic basalts. Earth Planet. Sci. Lett., 24, 419-426.

Pearce J.A, Harris N.B.W. & Tindle A.G., 1984: Trace element discrimination diagrams for the tectonic interpretation of granitic rocks. J. Petrology, 25, 956-983.

Peccerillo A. & Taylor S.R. 1976: Geochemistry of Eocene calc-alkaline volcanic rocks from the Kastamonu area, northern Turkey. Contrib. Mineral. Petrol., 58, 63-81.

Pešek J. & Tásler R.. 1989: Volcanism and volcanogenic rocks in the Upper Palaeozoic limnic basins of the Bohemian Massif. Folia Mus. Rer. Natur. Bohemia Occid. (Plzeň), 30, 3-55.

Pešek J. (Ed.), 2001: Geology and deposits of the Upper Palaeozoic limnic basins of the Czech Republic. Czech Geological Survey, Praha (in Czech).

Pešek J., Jelínek E., Bouška V. & Kühn J., in press: Geochemistry of the Late Palaeozoic volcanic rocks of the Central and Western Bohemian basins. Proccedings 9th Coal-Geology-Conference (Praha 2001). Acta Univer. Carol., Geol., 18 pp.

Pivec E., in press: Rock-forming minerals in albitization (spilitization) process in melaphyres of the Krkonoše Piedmont PermoCarboniferous Basin. Bull. mineral.-petrolog. Odd. Nár. Muz. (Praha), 10 pp (in Czech).

Ponikelská B., 1982: Melaphyres of the Levín Platform. Unpublished MSc. Thesis, Charles University, Praha (in Czech).

Prouza V., 1993: Results of new geological mapping of Permo-Carboniferous between Kozákov and Hodkovice nad Mohelkou. Proccedings 7th Coal Conference, January 26-28, 1993, Faculty of Sci., Charles University, Praha, 167-169, (in Czech).

Prouza V. & Tásler R., 2001: The Krkonoše Piedmont Basin. In: Geology and Deposits of the Upper Palaeozoic Limnic Basins of the Czech Republic, Pešek, J. (Ed.). Czech Geological Survey, Praha, 128-167 (in Czech).

Prouza V., Coubal M. & Málek J., 2000: Flow directions of lava flows of the Krkonoše Piedmont Upper Palaeozoic andesitoids and localisation of their volcanic centres. Zpr. geol. Výzk. v roce 1999, 73 (in Czech).

Řanda Z., Benada, J., Kuncíř J., Vobecký, M. & Frána J., 1970: Radio-analytical methods for nondestructive analysis of lunar samples. J. Radioanal. Chem., 11, 305-337.

Ringwood A.E., 1970: Petrogenesis of Apollo 11 basalts and implications for lunar origin. J. geophys. Res., 75, 6453-6479.

Rutšek J., 1995: Permo-Carboniferous volcanics in the basement of the Bohemian Cretaceous Basin in northern Bohemia. In: Final Report on the Activities of the Uranium Survey in the Bohemian Cretaceous Basin in 1959-1990. Part III, Basement of the Cretaceous, Team of authors, 42-67. Unpublished Report, Archive DIAMO s.p., Stráž p. Ralskem.

Schneder J. Rösler R. & Gaitzsch B., 1994: Time lines of Late Variscan volcanism, Geodynamik des Europäisches Variszikums. Bayerisches Geoinstitut, 3-4, Bayreuth.

Schovánková D., 1973: Petrography of paleorhyolites in borehole Vš-1 (a preliminary report). In: Structural borehole Vš-1 Všeň (near Turnov), Tásler, R. Unpublished Report, Geofond, Praha (in Czech).

Schovánková D., 1984: Upper Palaeozoic volcanism. In: Česká Kamenice Basin - Evaluation of Geological and Economic-Geological Conditions. Vejlupek, M. et al. (Eds.). Unpublished Report, Geofond, Praha (in Czech).

Schovánková D., 1985a: The Upper Palaeozoic volcanism of the Mnichovo Hradiště and the Krkonoše Piedmont basins. In: The Krkonoše Piedmont Basin. Evaluation of Geological and Coal Economic-Geological Conditions, Tásler, R. et al. (Eds.). Unpublished Report, Archive Czech Geological Survey, Praha (in Czech).

Schovánková D., 1985b: Petrological types and chemical trends in the Upper Palaeozoic volcanism in the Bohemian Massif. Unpublished Report, Archive Czech Geological Survey, Praha (in Czech).

Schovánková D., 1989: Petrology of the Upper Palaeozoic volcanics of the Krkonoše Piedmont Basin. Part I. Permian basaltic andesites. Unpublished Report, Archive Czech Geological Survey, Praha (in Czech).

Seckendorf v. V., 1989: Geologische, petrographische und geochemische Untersuchungen an permischen Magmatiten im Saarland (Blatt 6507 Lebach). Berichte Geol.-Paläont. Inst. Univ. Kiel, Nr. 39, Kiel.

Středa J., 1971: Geological-petrographical characteristics of the Mnichovo Hradiště Basin near Hodkovice. Sbor. geol. Věd, Ř. G, 21, 109-155 (in Czech).

Sun S.S. & McDonough W.F., 1989: Chemical and isotopic systematics of oceanic basalts: implications for mantle composition and processes. In: Magmatism in the Ocean Basins, Geol. Soc. Spec. Publ., 42, Washington, 313-345.

Taylor S.R. & McLennan S.M., 1985: The continental crust: its composition and evolution. Blackwell Scientific, Oxford.

Thorpe R.S., Francis P.W. & O'Callaghan L. 1984: Relative roles of source composition, fractional crystallisation and crustal contamination in the petrogenesis of Andean volcanic rocks. Phil. Trans. R. Soc. London, A310, 675-692.

Ulrych J., Pešek P., Martinec, Lloyd F.E. & Bosák P., in prep.: Magmatism in Late Variscan basins of the Bohemian Massif: structural setting and geochemical constraints. Chem. Erde, 35 pp.

Villemant B., 1988: Trace element evolution in the Plegrean Fields, Central Italy: fractional crystallization and selective enrichment. Contrib. Mineral. Petrol., 98, 169-183.

Watson E.B. & Green T.H., 1981: Apatite/liquid partition coefficients for the rare earth elements and strontium. Earth planet. Sci. Lett., 56, 405-421.

Wilson M., 1993: Magmatism and the geodynamics of basin formation. Sed. Geol., 86, 5-29.

Wilson M. & Downes H., 1991: Tertiary-Quaternary extension-related alkaline magmatism in western and central Europe. J. Petrology, 32, 811-849.

Ziegler P.A., 1990: Geological Atlas of Western and Central Europe. Shell Intern. Petrol. Maatschappij BV, The Hague.

Shear deformation in granodiorite: Structural, ^{40}Ar /^{39}Ar, and geotechnical data (Tribeč Mts., Western Carpathians)

Ján Kráľ[1], Jozef Hók[1], Wolfgang Frank[2], Pavol Siman[1], Pavel Liščák[1] & Vlasta Jánová[3]

[1]Geological Survey of the Slovak Republic, Mlynská dolina 1, 817 04 Bratislava, Slovakia
[2]Geozentrum, Universität Wien, Althanstrasse 14, A - 1090 Wien, Austria
[3]Ministry of the Environment of the Slovak Republic, nám. Ľ. Štúra 1, 812 35 Bratislava, Slovakia

Abstract. A shear zone in granodiorite has been studied in the Tribeč Mts. Whole rocks and mineral samples from deformed and undeformed rock types have been processed by means of structural, geotechnical and ^{40}Ar/^{39}Ar methods. The shear zone was formed by progressive simple shear in ductile to brittle-ductile conditions. The quartz isotropic microfabrics of the undeformed host rocks have been progressively transformed into anisotropic microfabrics composed of single oblique girdle indicating sinistral shear. A simple shear deformation was responsible for the formation of "s" and "c" foliations. Shear strain has been calculated for particular parts of the shear zone. Geotechnical data show the decrease of mechanical index parameters of rocks towards the centre of the shear zone. Decreasing of SiO_2, MgO and Na_2O content and increasing of Al_2O_3, CaO, K_2O and Fe_2O_3 in the same direction have been documented. ^{40}Ar/^{39}Ar data of white micas from centre of the shear zone proved its formation about 71–63 Ma ago. Obtained ages are interpreted as shear zone formation age . ^{40}Ar/^{39}Ar biotite apparent age spectra from undeformed granodiorite samples reveal significant Ar excess.

Key words: granodiorite, shear zone, structural data, ^{40}Ar/^{39}Ar dating, mechanical properties, Tribeč Mts., Western Carpathians

Introduction

Geological mapping (Ivanička et al., 1998) revealed in the Zobor part of the Tribeč Mts. (sensu Vass et al., 1988) a tectonic zone of NE-SW trend, being accompanied with intensive mylonitization of granitoid rocks. The length of the zone is app. 10 km, the width varies from several hundreds to several tens of metres. The rock deformation inside the zone is not homogeneous. A segment of this tectonic zone is exposed in the northwestern - Zobor part of the Tribeč Mts. in termination of the Malé Jastrabie Valley (Fig. 1). The mylonitic zone with transitions from deformed granitoid rocks towards undeformed ones is exposed there in the outcrop of app. dimensions 5 m x 5 m x 3 m. Mylonitic zone, resp. shear zone of the brittle-plastic character, is developed in the medium-grained biotitic granodiorites to tonalites (Ivanička et al., 1998). Broska & Petrík (1993), Petrík et al., (1994) ranked these types of granitoid rocks to allanite, resp. I-type of granitoid rocks of the Western Carpathians. In the outcrop we have distinguished three domains in relation to the intensity of rock strain from undeformed to the most intensive deformed rocks. The topic of our study included the change of rock properties in individual distinguished domains. We have observed the type and spatial arrangement of tectonic foliation and lineation as well as the change of arrangement of quartz optical axes. Isotopic research was fo-

cused prevailingly on ^{40}Ar/^{39}Ar micas dating from deformed and undeformed types of granitoid rocks. The last observed topic covered the geomechanic properties of rocks and their changes in relation of tectonic rock strain.

Methodics

Using macroscopic criteria for the evaluation of the deformation degree we have distinguish three domains in studied locality/outcrop. These differ each another prevailingly by the different intensity of tectonic foliation development (Fig. 3). The first domain is without any presence of visually recognizable tectonic overprint. The second one is characteristic with the presence of "s-planes" of tectonic foliation. Third domain manifests strong development of "c-planes" of tectonic foliation, next the intensive macroscopically observable deformation of minerals and development of definable stretching lineation.

Structural analysis consisted from identification and determination of spatial characteristics of principal structural elements (foliation, mineral lineation). Structural data were graphically analysed using tectonograms (e.g. Fig. 3). Oriented thin-sections allowed to observe the microstructures. Orientation of optical quartz c-axes was defined using standard methodics by universal stage (c.f. for instance Fediuk, 1961).
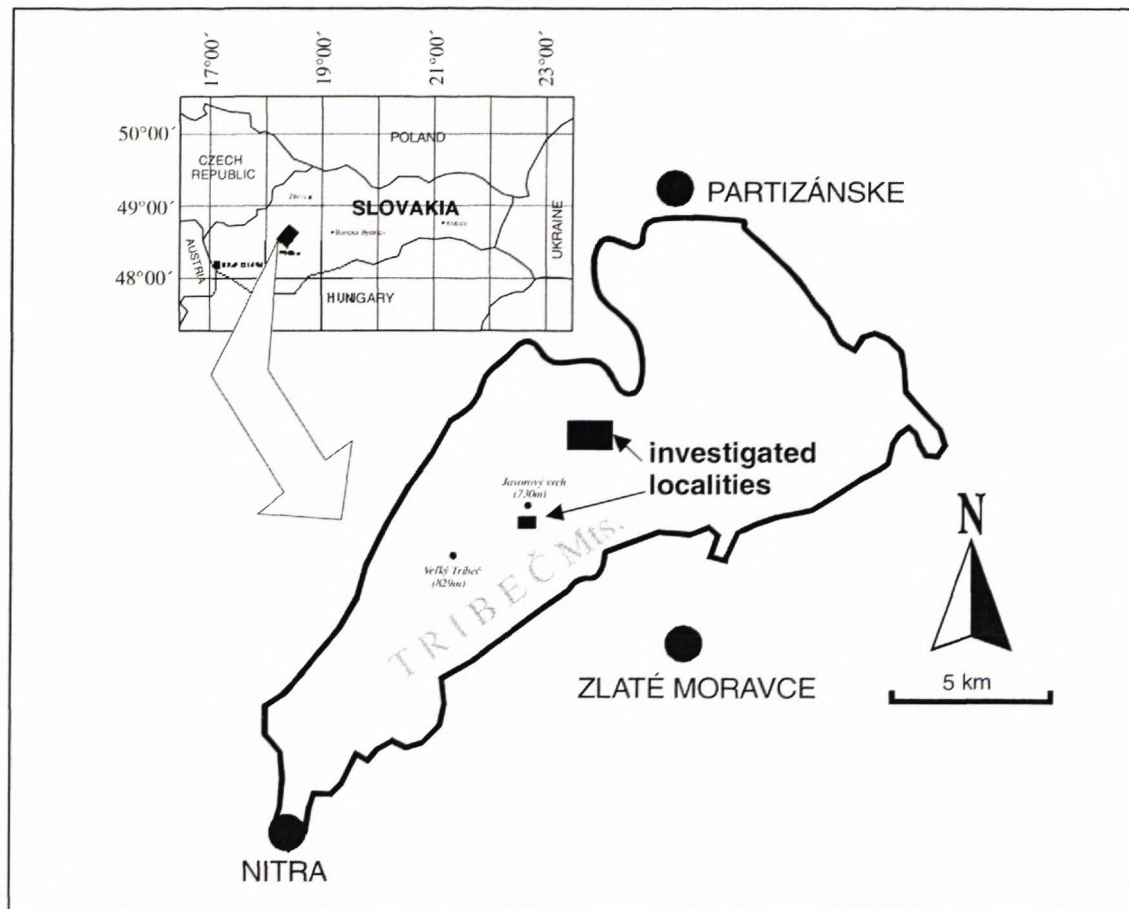
Fig. 1 Position of investigated localities in the Tribeč Mts.
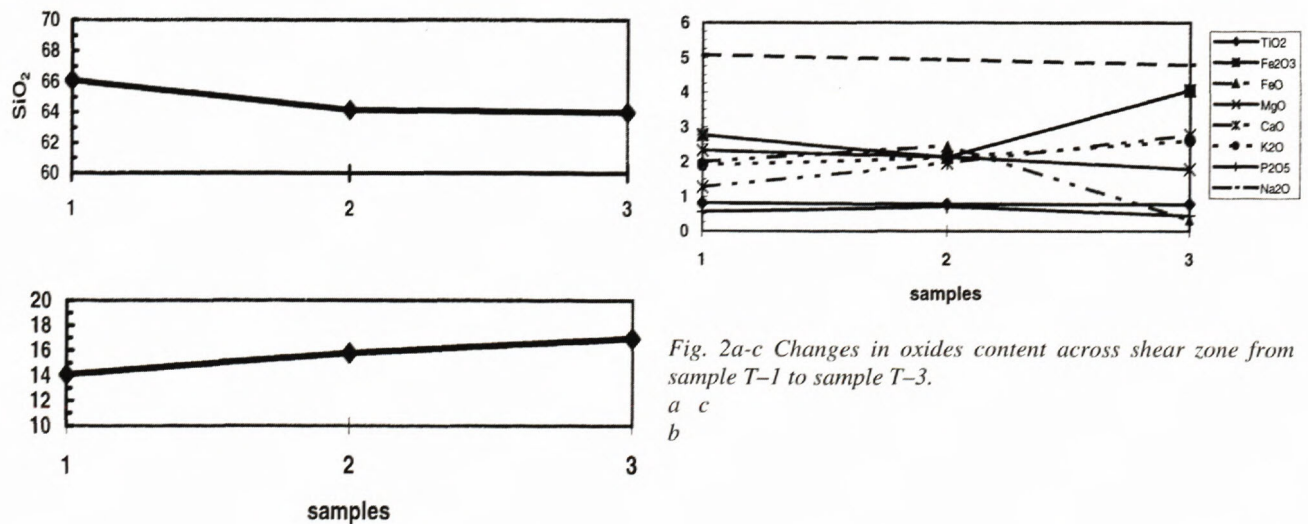
Fig. 2a-c Changes in oxides content across shear zone from sample T–1 to sample T–3.

a c

b

The index mechanical characteristics of rock massif/material were tested by the Schmidt's rebound hammer as well as the Point Load Test (PLT). To learn the resistance of rock against weathering we used the Slake Durability Test.

Schmidt's rebound hammer for simply and quick testing of rock rebound hardness allows to obtain an information on a broad physical state of rocks in the massif. Simultaneously it allows to distinguish in measured profile the horizons with differing degree of rock weathering (resp. other alterations). It is useful for qualified estimation of rock strength characteristics.

Point Load Test - PLT - $Is_{(50)}$ [MPa] allows prompt determination of rock strength. Test consists from registration of rock resistance against the imposed stress through two co-axially arranged conic platen points. The examination can be carried out on regularly shaped (square, cylindrical roller) or irregular (fragments) samples.

Slake Durability Test was used for evaluation of "rock durability". From each rock we prepared 20 fragments weighting app. 50 g (using 10 fragments into two rotating drums). Fragments were thoroughly washed and easily removable roughnesses and edges were retrieved. Consequently they were dried using temperature 105 ^{0}C till their steady weight. We placed two samples of the same rock type into the perforated steel drums with holes of 2 mm diameter. Both drums were fixed to apparatus in such a way to be submerged into the water container to the water level reaching the level approximately 2 cm beneath the drum rotation axis. The drums` rotation by velocity 20 turns per minute lasted two minutes. Afterwards the samples were taken off the drum and dried in drying-oven to steady weight. The whole cycle was repeated 3-times.

The micas for ^{40}Ar/^{39}Ar dating were separated from crushed and sieved rock using the wet shaking table and electrostatic separator. Purification was done using hand separation under binocular magnifying lens and ultrasound in distilled water. Next step was the irradiation by fast electrons together with internal laboratory standard WAP. The isotopic ratios ^{40}Ar, ^{39}Ar were measured from individual gas portions (purified in vacuum quartz equipment by gettering) in increasing temperature, applying the gas mass spectrometer VG-5400. This standard procedure, used in geochronologic laboratory Geozentrum Wien, has recently the individual analytical steps automatized. For age calculations there were used the decay constants by Steiger & Jäger (1977).

Results and disscusion

Description of investigated samples

The primary rock is represented by massive, medium-grained, equigranular light-grey granodiorite to tonalite of I-type, rich in biotite, titanite, allanite and epidote. There are typical the greenish plagioclases with basic cores, as well as bluish grains of quartz reaching dimensions 3-6 mm. The increasing deformation changed the rock character from massive to schistose with expressive foliation and often with abundant sericite, occasionally only with Fe oxides and hydroxides in foliation planes. This rock has greenish to grey-green colour with the white deformed feldspar porphyroclasts. Green character is caused by the presence of newly-formed phyllosilicate sericite and chlorite phases, eventually chloritized biotite.

The undeformed granitoid rocks have hypidiomorphic crystal shape, with modally the equal presence of quartz and plagioclase grains reaching dimensions up to 6 mm. Quartz forms the well-preserved hypidiomorphic grains with weak undulose extinction. The plagioclase is strongly sericitized to saussuritized and albitized preferably in its cores with higher basicity, around which albitic rim is developed. Biotite is abundantly present in the form of rests and aggregates being often disintegrated, recrystallized, smaller, but often even of idiomorphic shapes. It has rich green pleochroism in sections X,Y and X,Z, that could indicate the increased content of Fe-component - annite. K-feldspar, if present, forms several mm large strongly perthitized grains. Titanite has form of clearly spinning, broken crystal forms recrystallized to ilmenite. Next minerals, chlorite, rutile, magnesite, zircon and allanite are present accessorially.

Increasing degree of rock deformation markedly reduces the grain-size, mainly in quartz even below 0.1 mm. Quartz occurs in the form of bands (ribbons) with undulose extinction and even in the foamy structure. It behaves considerably plastically. It is possible to observe the grain boundaries migration. Contrary to this, the feldspars affected by the same changes, sericitization to saussuritization, eventually by perthitization, demonstrate more rigid behaviour with gaining of preferred orientation. Biotite is changed to chlorite and this one together with sericite, as the main weakened minerals became the main bearer of deformation. The rock structure gradually changes from porphyroblastic to mylonitic with clear preferred orientation and lineated phyllosilicates. In the last stage of deformation the rock became totally disintegrated, schistose and oriented. Quartz has very fine-grained polygonal structure with steeply decreasing grain-size below 0.1 mm. Feldspars and biotite are totally disintegrated into chlorite-sericite mass. Biotite is not present since. Its existence is confirmed only by the presence of chlorite with ilmenite clusters.

Described deformation is possible to consider as relatively low-temperature alteration within greenschists facies. It results from the phase change of biotite to chlorite where Eggleton & Banfield (1985 in Shelley, 1993) suppose for the chloritization the temperature 340 °C. In this case the more interesting is the strongly plastic behaviour of quartz during the rigid behaviour of feldspars. The very high strain rate could be supposed in this case.

To complete the presented data we introduce also the results of the chemical analyses of selected oxides from samples taken transversally through the mylonite zone from undeformed granodiorite (sample T-1), protomylonite (sample T-2) and mylonite (sample T-3; Fig. 2a, b, c). The graphs demonstrate the decrease of SiO_2, MgO and Na_2O content towards the centre of mylonitic zone. On the contrary, the content of Al_2O_3, CaO, Fe_2O_3 and K_2O increases.

Structural geology

From the viewpoints of tectonodeformation processes the rocks in the outcrop scale can be alternatively divided into three groups (Fig. 3): undeformed granitoids without macroscopically and microscopically visible deformation structures, medium deformed granitoids being according to the classification by Sibson (1977, 1980) denoted as protomylonites and intensively deformed granitoid rocks - mylonites (sensu l.c.).

Undeformed granitoids (Fig. 4) macroscopically do not express any tectonic overprint with exception of
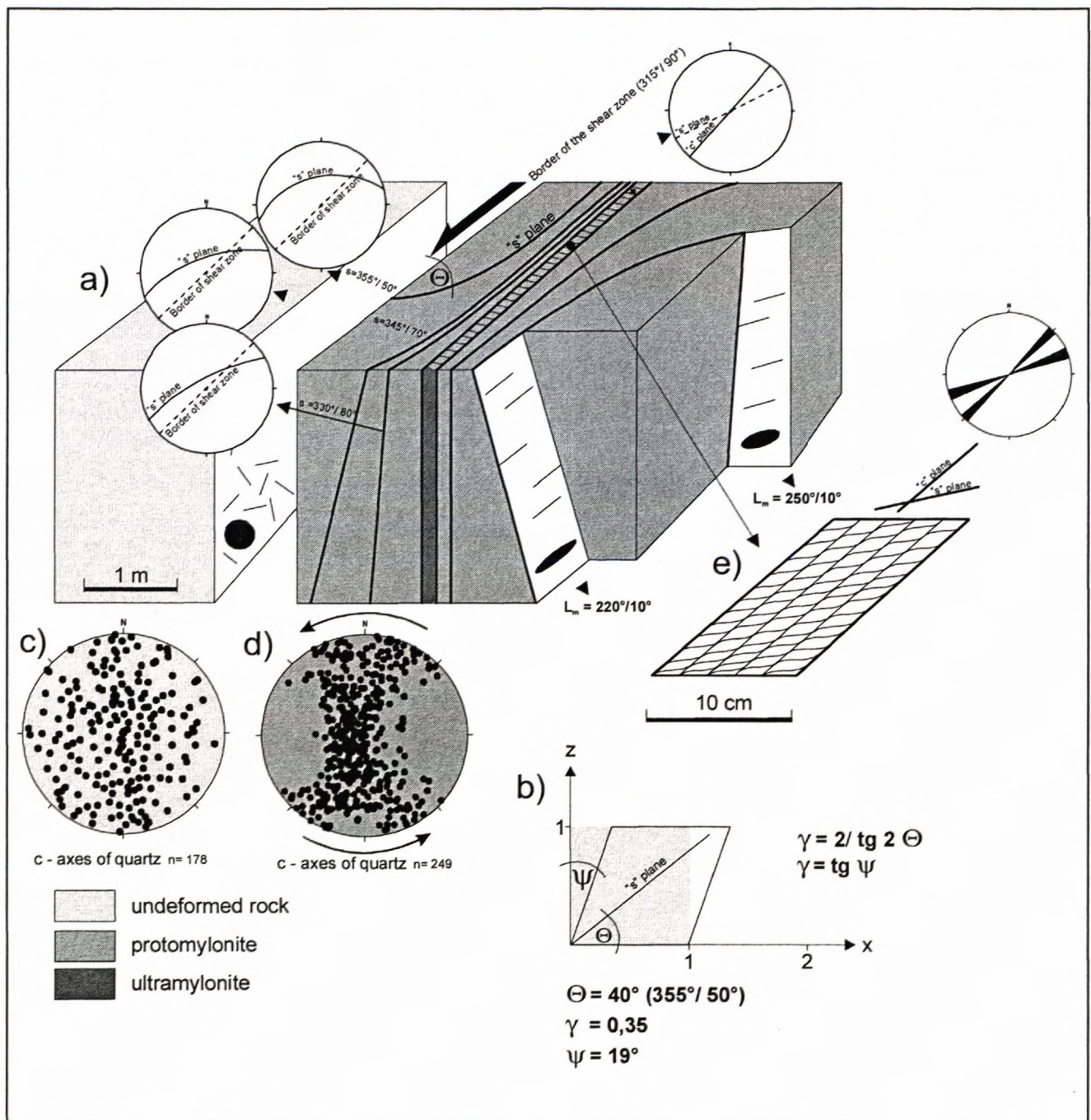
Fig. 3 Simplified sketch of the shear zone a) simplified sketch with observed structural elements, intensity of shading corresponds to intensity of deformation, arrow indicates sense of movement, diagrams display orientation of the "s" and "c" planes and shear zone border: 315°/ 90° (Lambert projection, lower hemisphere), Θ angle between "s" plane and shear zone border, L_m stretching linea-tion ; b) method of calculation and graphic demonstration of the homogeneous simple shear deformation of the unit square / circle, Θ angle between "s" plane and shear zone border, Ψ - shear angle, γ - shear strain; c) fabric of quartz diagram from undeformed granodiorite ; d) fabric of quartz diagram from protomylonite (n - number of measurements); e) simplified sketch of central part of the shear zone with rose diagram of orientation "s" and "c" planes

joints, being oriented in two general perpendicular direc-tions NW-SE and NE-SW. The orientation of optical quartz c-axes is isotropic and has no more impressive preferred orientation (Fig. 3c).

The qualitatively new planes of planar anisotropy de-scribed as schistosity or s-planes (Figs. 5 and 6) originate in deformation domain of protomylonites. These planes are parallel to the plane XY of deformation ellipsoid and originate perpendicularly to direction of the highest pres-sure. In the ideal case the first s-planes would appear in the rock under the angle 45° to the boundary of shear zone. In observed zone the macroscopically defined s-planes include the angle 40° towards the shear zone. Towards the centre of shear zone the schistosity planes

gradually change their direction and inclination (Fig. 3a). Using the orientation of s-planes it is possible to calculate the shear deformation/strain γ in the rock:

$$\gamma = 2 / \text{tg } 2\Theta \text{ (c.f. Ramsay, 1980)}$$
$$\gamma = \text{tg } \psi$$

where Θ represents the angle between the schistosity plane and the boundary of shear zones (Fig. 3b). ψ is the shear angle between the unit deformed object (square, circle) with the "z" axis of the coordinate system (Fig. 3b). On the basis of measured values it is possible to calculate the increment of the shear deformation, the shear angle (Tab. 1) and to express the deformation (Figs. 3b and 7).

Tab. 1: Relationship between the shear strain and orientation of the s–plane.

angle between s–plane and shear zone border	shear strain	shear angle
$\Theta = 40°$	$\gamma = 0{,}35$	$\psi = 19°$
$\Theta = 30°$	$\gamma = 1{,}15$	$\psi = 49°$
$\Theta = 20°$	$\gamma = 2{,}38$	$\psi = 67°$

The results of microstructural study of orientation of optical quartz c-axes demonstrate the anisotropic distribution with the origin of striking belt girdle maximum indicating the sinistral simple shear (e.g. Lister & Williams, 1979). In deformation domain of mylonites being directly in the centre of shear zone we have not succeeded to measure the representative number of quartz optical c-axes, because the quartz grains were tectonically broken into the submicroscopic aggregates.

The centre of shear zone is ca 20 cm wide and the inhomogeneity planes depicted like "c" planes (sensu Berthé et al., 1979) appear there. The "c" planes represent foliations with concentrated shear deformation. The angle between "c" and "s" planes is ca 20° (Figs. 3e and 6). In the case investigated the failure of the rock coherence occurs along the "c" planes and the rock is sheared in brittle regime. This is the reason why the mutual offset of rock blocks in the centre of shear zone is not possible to define precisely.

Physical-mechanical properties

Modified final value of the strength index by the Point Load Test is correlated with the strength in the uni-axial pressure σ_c. The mostly used conversion relation is:

$$\sigma_c = 24 . \text{Is}_{(50)} \text{ [MPa]}$$

Bieniawski (1973) for evaluation of strength suggests to use the classification scale, presented in Tab. 2.

Tab. 2: Estimation of a compressive strength of rocks according Point Load Test (Bieniawski, 1973)

Strength degree	PLT index $\text{Is}_{(50)}$ [MPa]	Compressive strength σ_c [MPa]
1. Very high	> 8	> 200
2. High	4 to 8	100 to 200
3. Medium	2 to 4	50 to 100
4. Low	1 to 2	25 to 50
5. Very low	< 1	< 25
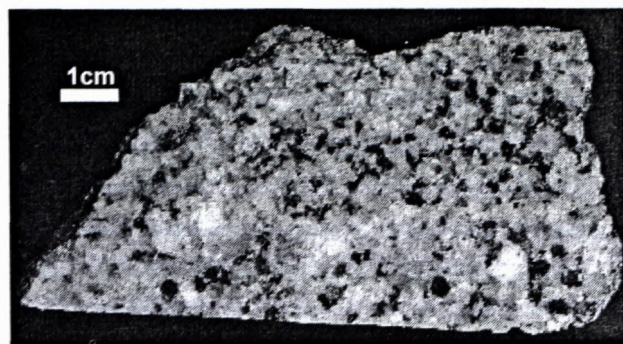
Fig. 4 Photograph of the undeformed granodiorite. Malé Jastrabie locality.

Fig. 5 Photograph of the protomylonite. Note the development of the "s" planes foliation. Malé Jastrabie locality.
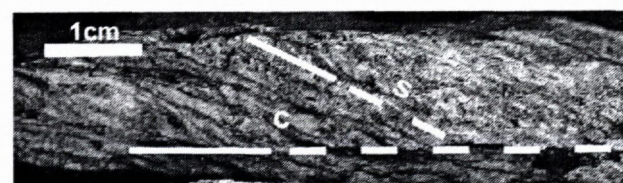
Fig. 6 Photograph of the mylonite. The "s" planes foliation is predominant structure and "c" planes are present as a new structural element. Malé Jastrabie locality.
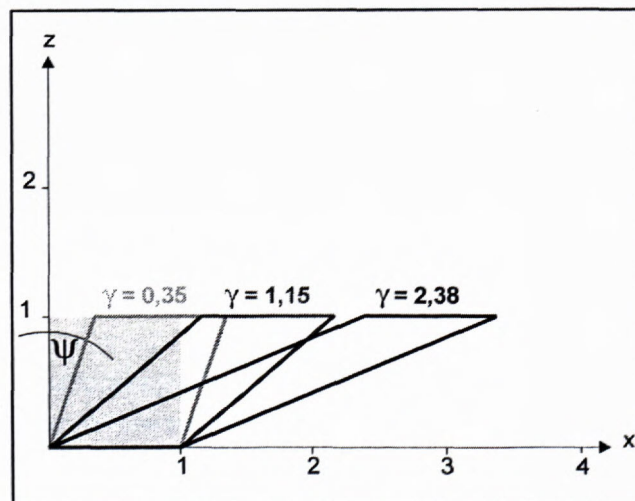
Fig. 7 Graphic plot of data from the Tab. 1, showing progressive shear strain towards the centre of the shear zone.

240

Slovak Geol. Mag., 8, 3– 4(2002), 235 – 246
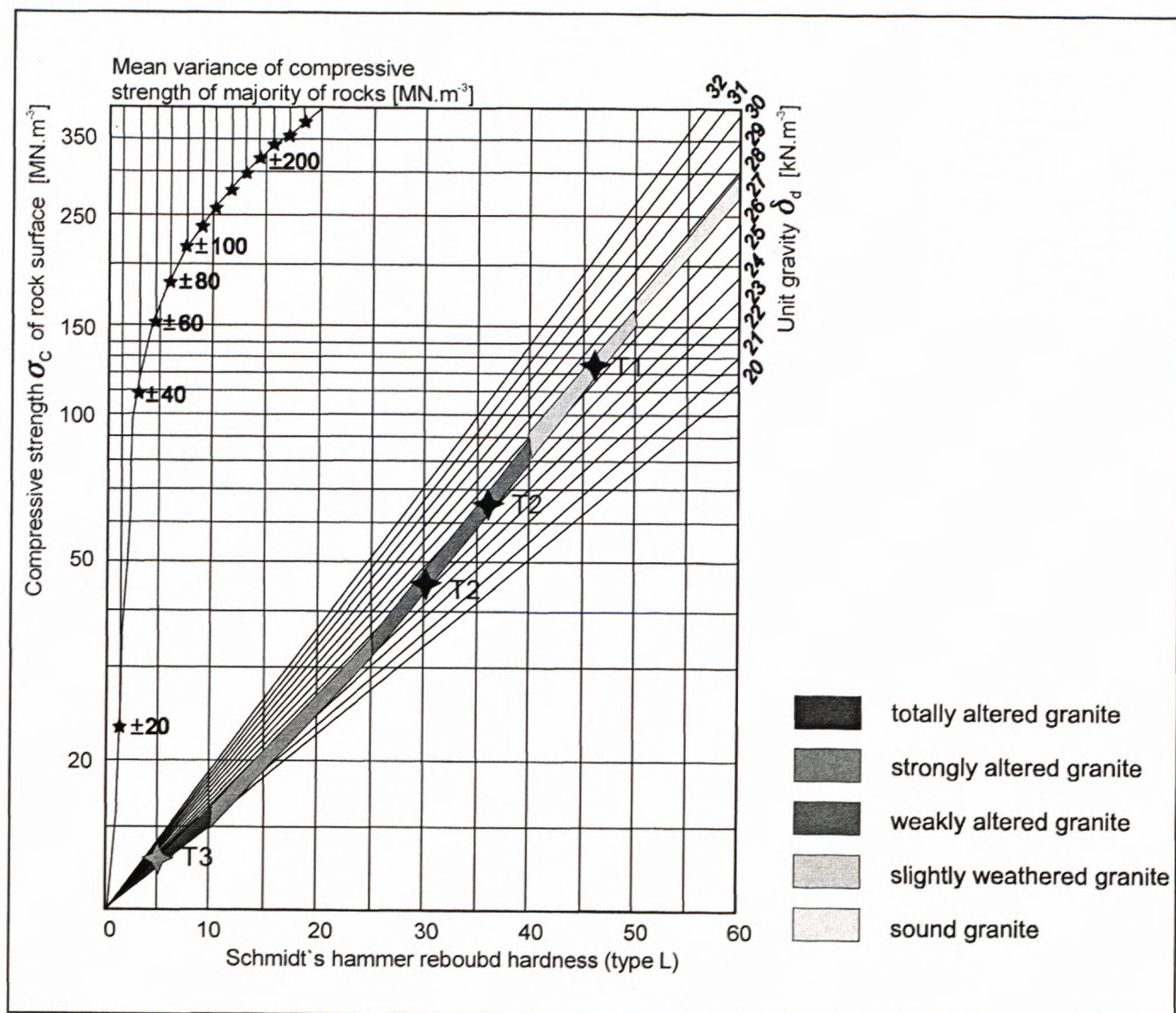
Fig. 8 Evaluation of granodiorite alteration inferred from the Schmidt's rebound hardness.

The results of measurements of rebound hardness are described in graph (Fig. 8). The measuring sample point T-3 was situated in outcrop with the strongest mylonitization. The massif weathering is here the strongest in comparison to the whole outcrop, and is manifested by decrease of strength in uni-axial pressure (value 45.67 MPa ranked the mylonite among the semisolid rocks according to STN 73 1001 Norm). From the centre of mylonitic zone (measurements in sample T-2) the strength in uni-axial pressure increases mainly due to the weakest rock deformation and smaller rock weathering. It confirms the zonality of physical-mechanical properties in mylonitic zone. The sample T-1 represents the weathered granodiorite without evident tectonic failure and it has the highest compressive strength values. The Fig. 8 confirms that derived strength in uni-axial pressure of investigated rock from the centre of mylonite zone is of low-order in comparison with the samples from its periphery.

Very similar values of uni-axial strength in pressure are shown also by the PLT test. It confirms the suitability

of the use of both methods for relatively quick and simply determination of this parameter either from technological or geotechnical viewpoints. The indicator of the rock resistance against slaking (slake durability index) is then the percentage ratio of lowered sample weight compared with its original weight.

$$\text{Slake durability index } (I_d) = \frac{\text{original weight - weight after n cycles}}{\text{original weight}} \cdot 100(\%)$$

The examination allows to classify rocks into the six groups:

a/ I_d = 95 - 100 % - rocks with extreme durability,
b/ I_d = 90 - 95 % - rocks with very high durability,
c/ I_d = 75 - 90 % - rocks with high durability,
d/ I_d = 50 - 75 % - rocks with medium durability,
e/ I_d = 25 - 50 % - rocks with low durability,
f/ I_d = 0 - 25 % - rocks with very low durability.

For comparison we list the durability of granitoid rocks also from other localities in the Tribeč Mts. (Tab. 3). In the

Tab. 3: Durability of selected granitoids from the Tribeč Mts. according to Slake Durability Test

Number of sample	Locality	Rock type	Slake durability 1. cycle (%)	Slake durability 2. cycle (%)	Classification according slaking
1	Skýcov	Leucocrate granite	99.50	99.10	Extremely high
2	Skýcov	Slightly weathered leucocrate granite	99.68	99.20	Extremely high
3	Javorový vrch	Granodiorite tonalite, coarse-grained	93.59	93.30	Very high
4	Javorový vrch	Aplitic granodiorite	97.99	97.71	Extremely high
5	Malé Jastrabie	Mylonitized granite	97.89	97.24	Extremely high
6	Malé Jastrabie	Mylonitized granite	97.68	97.10	Extremely high
7	Medvedí vrch	Leucocrate granite	99.70		Extremely high

sense of above stated classification the obtained values of slate durability indicate the durability and resistance of granitoid rocks from the Tribeč Mts. against weathering.

^{40}Ar / ^{39}Ar data

Until recent only the geochronological data from granitoid rocks were published from the crystalline basement of the Tribeč Mts.. The first age from the zircon being separated from tonalite near Janova Ves was published by Bojko et al. (1974). The U, Th/Pb model ages are concordant and vary around 290 Ma. Broska et al. (1990) refined this data from zircons of similar rock for 306 ± 10 Ma. Data can be interpreted as the intrusive age of plutonic rocks (tonalites-granodiorites) in the Tribeč Mts. Rb/Sr datings of the whole rock granodiorite samples are discordant in comparison with these data and older - the slope of published isochron corresponds to the age 352 ± 5 Ma (Bagdasaryan et al.1990). Kováč et al. (1994) published the FT age 28 ± 3 Ma on accessory apatite from tonalite.

The analysed mineral samples were separated from three sample types - undeformed granodiorite - (T-1), from partly deformed granodiorite (T-2, T-7) and from the centre of mylonite zone (T-3). Samples T-1, T-2 and T-3 were taken from the distance ca 20 m from the area of distinct mylonite zone developed in granodiorite.

The principal analytic data together with plots of apparent ^{40}Ar*/^{39}Ar ages (decay constants according to Steiger a Jäger, 1977) are given in Tabs. 4-10 and Figs. 9 - 15.

The biotite was separated and analysed from the samples of undeformed granodiorites T-1, T-8, T-9. ^{40}Ar/^{39}Ar spectra are discordant and all apparent ages of individual temperature steps are markedly higher as U-Pb data from zircons of petrographically identical rocks, limiting the intrusion age for 306 Ma (Fig. 9, 14, 15).

The only separable mineral suitable for dating of deformed granodiorite T-2 was the fine light-coloured mica because the former biotite was strongly chloritized. More than 60 % of ^{39}Ar from the sample was degassed in four last high-temperature steps (Fig. 10). This part of the spectrum gives the corresponding plateau age 155 ± 9 Ma.

From the sample T-3, representing the typical mylonite, we have separated and analysed two minerals - fine white mica (sericite) and coarse-grained muscovite. The ^{40}Ar*/^{39}Ar spectrum of apparent ages in sericite has continual staircase shape, where for the higher degassing temperature the apparent age is ca 73 Ma, and in the lowermost degassing temperature the age is 63 Ma. Apparent ^{40}Ar*/^{39}Ar ages of muscovite from the same sample (Fig. 12) have discordant character, mainly in the higher temperature part of the spectrum. The degassing of muscovite is represented by plateau age 72 ± 2 Ma, that is in the range of analytical error corresponding with the higher age from fine-grained light-coloured mica, separated from the same sample.

Biotite from deformed granodiorite T-7 has slightly concave shape, steeper in the high-temperature part of the spectrum (Fig. 13). Lowermost apparent ages in the middle part of the spectrum are forming three medium-temperature steps with data 81-82 Ma.

Though micas are widely used in K/Ar geochronology, in metamorphic terranes the obtained data are most frequently interpreted like the age of cooling, because their blocking temperatures are lower than the ages of many metamorphic, resp. plutonic processes. Therefore they are used rather for the reconstruction of temperature history of investigated area than for the identification of ages of plutonic, resp. metamorphic processes. Despite the usually well readable and interpretable spectra of e.g. phengite, the biotites manifest various types of spectra, which interpretation might be complicated. One of the reasons is the presence of the excess argon. In such cases the apparent age spectra can be smoothed in all temperature steps and the shallow-brained analyses of the data can lead to the age significant spectra of minerals untouched by temperature. Spectra obtained from biotites, resp. minerals with excess Ar might be also of convex or concave shapes (the relevant literature to this problem is discussed by McDougall & Harrison, 1988). The interpretation of such spectra is therefore necessary to be supported also by another geochronologic information in context of relating knowledge from regional geology.

From the comparison of blocking temperatures of U/Pb system in zircons and K/Ar system in micas there follows, that K/Ar ages of biotite in plutonic resp. meta-

morphic rocks will be lower than the real age of plutonic, resp. high-temperature processes. It was confirmed also by a big amount of published data from various geological areas. The magnitude of the difference in obtained U/Pb and K/Ar ages in the case of the simplest thermic history – monotonous cooling - depends on cooling rate. The comparison of data from the Western Carpathians – preferably from core Mountains, where the idea of monotonous cooling during uplift in Hercynian evolution can be accepted - confirms this model (the Malé Karpaty Mts. - Bagdasaryan et al. 1977, Shcherbak et al. 1988; the Malá Fatra, Mts. – Shcherbak et al. 1990, Hók et al. 2000; the Veľká Fatra Mts. – Kohút et al. 1998; the Strážovské vrchy Mts. – Kráľ et al. 1997; review of available K- Ar data and their new interpretation from the crystalline basement of the Western Carpathians till 1985 is available in Burchart et al. 1987), though records about Alpine influence in these rocks were documented by Maluski et al. (1993).

Tab. 4: $^{40}Ar/^{39}Ar$ analytical data from biotite, undeformed granodiorite T-1, Tribeč Mts.

Step	T(C°)	% $^{39}Ar^*$	% $^{40}Ar^*$	$^{40}Ar/^{39}Ar\pm2s.$ d.(%)	Age (Ma) ± 2s.d.
1	620	21.5	95.5	44.83 ± 0.3	348.5 ± 1.1
2	690	11.5	97.2	45.34 ± 0.6	352.1 ± 1.9
3	830	7.0	97.1	45.34 ± 0.4	352.1 ± 1.2
4	1060	45.4	97.2	45.49 ± 0.2	356.4 ± 0.7
5	1350	14.6	97.9	46.49 ± 0.3	360.3 ± 0.9

J = 0.004530 ± 0.4 %   total gas age: 354.5 ± 2.8

Tab. 5: $^{40}Ar/^{39}Ar$ analytical data from fine-grained white mica, deformed granodiorite T-2 (protomylonite), Tribeč Mts.

Step	T(C°)	% $^{39}Ar^*$	% $^{40}Ar^*$	$^{40}Ar/^{39}Ar\pm2s.$ d.(%)	Age (Ma) ± 2s.d.
1	585	11.3	54.2	13.72 ± 11.0	113.6 ± 12.2
2	605	3.9	47.0	21.46 ± 30.7	174.9 ± 51.3
3	635	5.8	55.7	18.88 ± 18.3	154.7 ± 27.1
4	670	7.1	58.9	15.37 ± 14.7	126.8 ± 18.0
5	710	7.2	67.5	16.39 ± 13.4	135.0 ±17.4
6	750	7.2	58.2	18.78 ± 2.2	153.9 ± 3.2
7	790	9.9	59.5	18.68 ± 3.1	152.6 ± 4.5
8	830	5.9	68.4	17.10 ± 6,5	140.6 ± 8.9
9	1220	41.8	74.6	19.7 ± 2.8	156.9 ± 4.2

J = 0.004530 ± 0.4 %   total gas age: 147.3 ± 15.0
65 % plateau age: 154.5 ± 8.5

Tab.. 6: $^{40}Ar/^{39}Ar$ analytical data from fine-grained white mica, mylonite T-3, Tribeč Mts.

Step	T(C°)	% $^{39}Ar^*$	% $^{40}Ar^*$	$^{40}Ar/^{39}Ar\pm2s.$ d.(%)	Age (Ma) ± 2s.d.
1	615	4.0	91.4	7.48 ± 1.1	62.8 ± 0.7
2	655	2.6	96.7	7.57 ± 1.8	63.6 ± 1.1
3	695	4.8	97.8	7.54 ± 0.7	63.3 ± 0.4
4	735	2.6	97.5	7.58 ± 1.5	63.7 ± 0.9
5	785	11.9	98.7	7.60 ± 0.5	63.8 ± 0.3
6	845	6.5	98.5	7.76 ± 0.5	65.2 ± 0.3
7	920	18.7	98.7	7.94 ± 0.3	66.6 ± 0.2
8	995	17.4	98.8	8.25 ± 0.3	69.2 ± 0.2
9	1050	21.4	98.9	8.49 ± 0.2	71.1 ± 0.1
10	1220	10.3	98.8	8.66 ± 0.5	72.6 ± 0.4

J = 0.004530 ± 0.4 %   total gas age: 67.7 ± 0.6

Tab. 7: $^{40}Ar/^{39}Ar$ analytical data from medium-grained white mica, mylonite T-3, Tribeč Mts.,

Step	T(C°)	% $^{39}Ar^*$	% $^{40}Ar^*$	$^{40}Ar/^{39}Ar\pm2s.$ d.(%)	Age (Ma) ± 2s.d.
1	620	3.3	74.4	8.09 ± 8.0	67.9 ± 5.3
2	690	6.2	88.6	8.96 ± 6.8	75.0 ± 5.0
3	790	10.5	91.7	8.67 ± 4.2	72.6 ± 3.0
4	920	47.4	96.7	8.51 ± 0.9	71.3 ± 0.6
5	1060	27.9	93.9	12.12 ± 1.2	100.8 ± 1.2
6	1350	4.8	67.0	31.02 ± 2.5	247.9 ± 5.9

J = 0.004530 ± 0.4 %   total gas age: 88.3 ± 2.6
65 % plateau age71.4 ± 0.7

Tab. 8: $^{40}Ar/^{39}Ar$ analytical data from biotite, deformed granodiorite T-7, Tribeč Mts.

Step	T(C°)	% $^{39}Ar^*$	% $^{40}Ar^*$	$^{40}Ar/^{39}Ar\pm2s.$ d.(%)	Age (Ma) ± 2s.d.
1	690	10.2	76.9	10.17 ± 2.0	88.2 ± 1.7
2	730	18.2	80.3	10.00 ± 1.4	86.7 ± 1.2
3	780	15.5	82.2	9.46 ± 1.2	82.1 ± 1.0
4	800	8.2	77.9	9.45 ± 2.4	82.0 ± 1.9
5	880	14.9	80.9	9.33 ± 1.7	81.1 ± 1.4
6	925	8.4	73.3	9.84 ± 2.8	85.4 ± 2.4
7	980	10.0	75.3	10.77 ± 2.1	93.2 ± 1.9
8	1080	9.7	77.0	12. 32 ± 2.4	106.3 ± 2.4
9	1250	4.8	65.5	12.82 ± 4.4	110.5 ± 4.7

J = 0.004530 ± 0.4 %   total gas age: 88.5 ± 3.3

Tab. 9: $^{40}Ar/^{39}Ar$ analytical data from biotite, undeformed granodiorite, T-8, Tribeč Mts.

Step	T(C°)	% $^{39}Ar^*$	% $^{40}Ar^*$	$^{40}Ar/^{39}Ar\pm2s.$ d.(%)	Age (Ma) ± 2s.d.
1	650	7.7	95.1	40.94 ± 1.1	332.2 ± 3.4
2	690	7.9	78.1	44.03 ± 2.0	355.1 ± 6.4
3	730	8.7	92.2	42.81 ± 0.9	346.1 ± 2.8
4	780	10.5	97.7	40.26 ± 0.6	327.1 ± 1.9
5	800	8.8	97.8	41.24 ± 1.0	334.5 ± 3.1
6	880	5.2	96.4	40.72 ± 1.8	330.6 ± 5.3
7	925	4.4	95.9	41.17 ± 1.0	333.9 ± 3.2
8	980	9.6	96.2	41.66 ± 1.2	337.6 ± 3.8
9	1080	23.5	97.9	41.17 ± 0.4	334.0 ± 1.1
10	1250	13.7	97.6	40.19 ± 0.8	326.6 ± 2.4

J = 0.004708 ± 0.4 %   total gas age: 335.1 ± 4.9

Tab. 10: $^{40}Ar/^{39}Ar$ analytical data from biotite (biotite–albite enclave), undeformed granodiorite, T-9, Tribeč Mts.

Step	T(C°)	% $^{39}Ar^*$	% $^{40}Ar^*$	$^{40}Ar/^{39}Ar\pm2s.$ d.(%)	Age (Ma) ± 2s.d.
1	650	22.1	98.0	47.11 ± 0.3	377.6 ± 1.1
2	690	22.5	98.1	46.35 ± 0.3	372.1 ± 1.1
3	730	4.4	96.5	48.31 ± 1.4	386.3 ± 5.0
4	780	4.4	96.6	49.59 ± 1.3	395.5 ± 4.7
5	800	22.3	97.9	49.12 ± 0.2	392.2 ± 0.7
6	880	7.4	97.7	48.70 ± 0.5	389.1 ± 1.9
7	925	13.9	97.8	46.49 ± 0.3	373.1 ± 1.2
8	980	1.1	96.7	46.63 ± 2.3	374.1 ± 7.6
9	1080	1.9	97.0	46.71 ± 2.5	374.7 ± 8.4

J = 0.004708 ± 0.4 %   total gas age: 380.9 ± 3.4
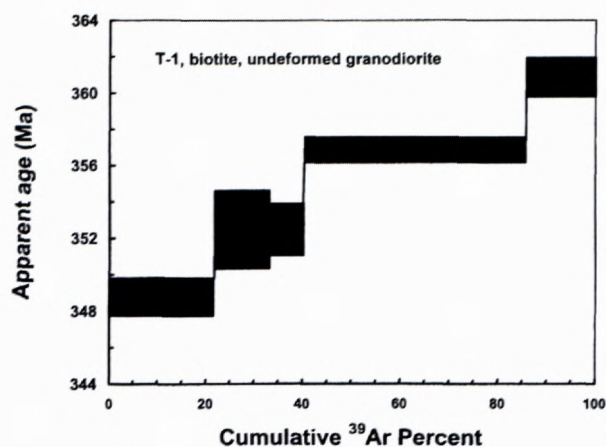
Fig. 9 ^{40}Ar / ^{39}Ar apparent age spectrum in sample T–1: Biotite from undeformed granodiorite.
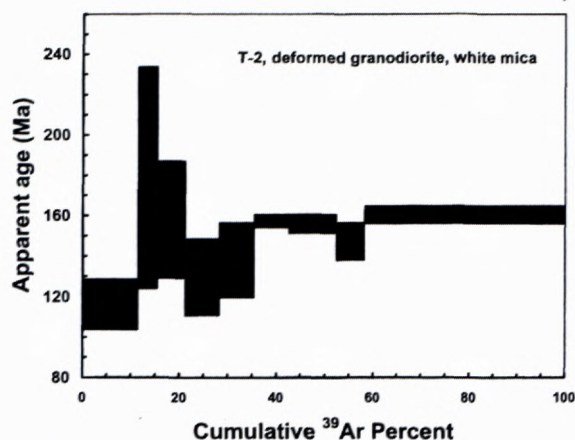
Fig. 10 ^{40}Ar / ^{39}Ar apparent age spectrum in sample T–2: medium-grained white mica from protomylonite.
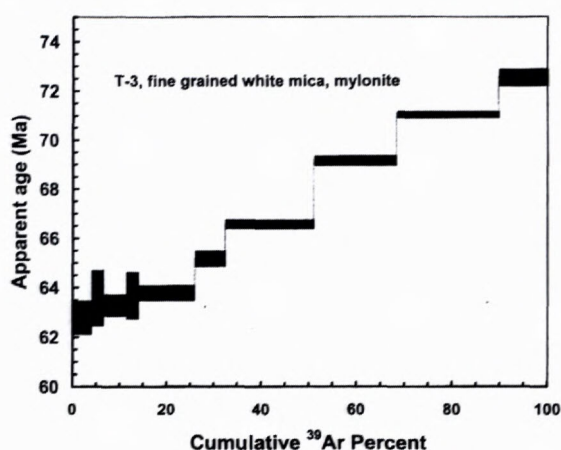
Fig. 11 ^{40}Ar / ^{39}Ar apparent age spectrum in sample T–3: fine-grained white mica from mylonite.
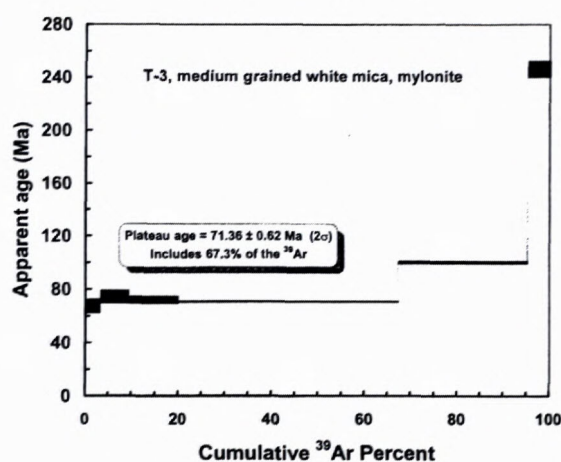
Fig. 12 ^{40}Ar / ^{39}Ar apparent age spectrum in sample T–3: medium-grained white mica from mylonite.
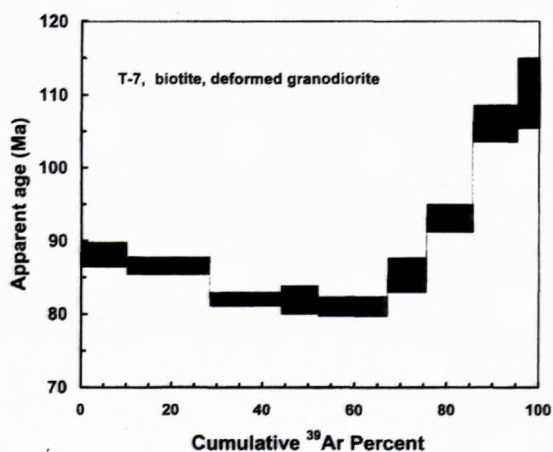
Fig. 13 ^{40}Ar / ^{39}Ar apparent age spectrum in sample T–7: biotite from deformed granodiorite
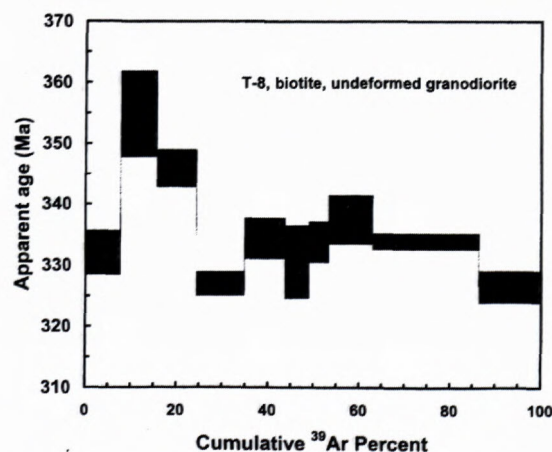
Fig. 14 ^{40}Ar / ^{39}Ar apparent age spectrum in sample T–8: biotite from undeformed granodiorite.

The variability of the shape of ^{40}Ar*/^{39}Ar spectra, obtained from differently deformed granitoids of the Tribeč Mts., as well as the apparent ages alone have to be evaluated in this context. Though it is questionable whether obtained knowledge can be generalized for the whole Tribeč crystalline basement, the found results indicate that the relation of K/Ar system to the Alpine thermal and dynamic overprint on the rocks of this basement is definitely different in comparison with other core mountains with available primary data on their Hercynian cooling. The differences in the shape of ^{40}Ar*/^{39}Ar mineral spectra, obtained from tectonically differently overprinted
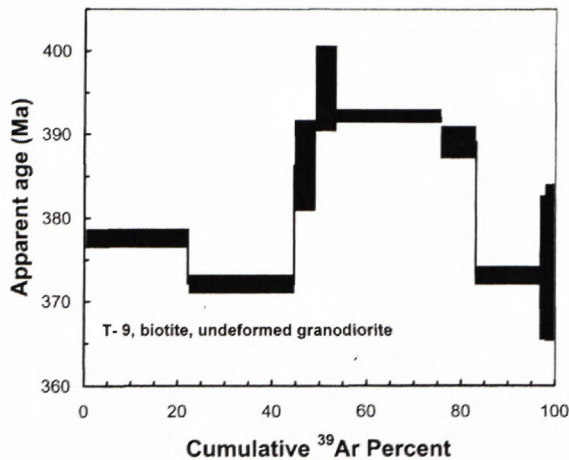
Fig. 15 $^{40}Ar / ^{39}Ar$ apparent age spectrum in sample T–9: biotite from albite–biotite enclave - undeformed granodiorite.

granitoid rocks of the Tribeč Mts. require wider analysis, preferably by control these data by Rb-Sr geochronometer.

From the sample T-3, representing typical mylonite, we have separated two kinds of white micas - medium-grained muscovite and fine-grained white mica (sericite). Light-coloured micas are the typical synkinematic minerals in rocks and can be used for dating of the mylonitization age (Figs. 4 and 5). The apparent $^{40}Ar*/^{39}Ar$ muscovite ages of sample T-3 have a discordant character only in the higher-temperature part of the spectra. Apparent $^{40}Ar/^{39}Ar$ age 248 Ma in the last temperature step cannot be interpreted unambiguously, but the decisive volume of outgassed Ar from muscovite is represented by the plateau age 72 ± 2 Ma, that is within the analytical error coincident with the higher apparent age from sericite of the same sample. $^{40}Ar*/^{39}Ar$ spectra of the apparent ages in sericite are of staircase shape proving for higher degassing temperature the apparent age ca 73 Ma and for the lowermost temperature of degassing 63 Ma. The staircase spectra of white micas from mylonitic zones are common and can be caused by the mixed mineral population of white mica different in age, next by the gradual diffusion lost of $^{40}Ar*$ in the grains of different dimensions, and by the prolonged neocrystallization during formation of mylonite zones (Kirschner et al. 1996). Comparison of obtained spectra from quantitatively different mica types from this sample and their age concordance documents, that their age is tied with the age of origin of mylonite zone.

However, it is probable, that the anomalous biotite ages from undeformed rocks (T-1, T-8, T-9 - Figs. 9, 14, 15) are caused by excess argon in analysed biotite, which can be analytically separated from radiogenic argon, produced in biotite *in situ*, e.g. by different variants of isochron analysis of analytical data. As the reason of the excess argon in biotite there is supposed the high partial pressure of argon in the rock environment, that originates by degassing of rocks from the deeper crustal parts and which in certain tectonic circumstances (thrusting) penetrates their higher parts. This phenomenon was described in the crystalline basement of the Eastern Alps by Brewer

(1969). For such argon entering into the structure of existing biotite, the temperature of environment must be higher as the blocking temperature of K-Ar system for biotite. Concerning the regional distribution of investigated samples, the argon excess in biotites from undeformed tonalites of Tribeč can be understood like characteristic phenomenon, spread at larger regional scale. It is not clear so far when the extraneous argon was captured by biotite. Because the excess argon is preserved mainly in undeformed granitoids, we suppose, that the excess origin can be joined with the deformation event and with the formation of mylonite zones.

The apparent ages spectra obtained from white fine-grained mica from the sample T-2 (Fig. 10) cannot be interpreted unequivocally. Though the Jurassic record is provable in $^{40}Ar*/^{39}Ar$ spectra of apparent ages of various minerals also in other areas of crystalline basement of the Western Carpathians (Maluski et al. 1993, Kráľ et al. 1997, Hók et al. 2000), the process related to it is questionable. The white mica analysed in this sample is also secondary in origin. For formation of new sericite there is necessary the free potassium - it can be derived from the disintegration of biotite, but can be brought into rocks also by hydrothermal processes. By this way there were interpreted the Rb/Sr and $^{40}Ar*/^{39}Ar$ Jurassic ages in the regions where the record about Alpine tectonothermal event is completely missing (e.g. Schwarzwald; Grauert et al. 1993, Lippolt and Kirsch, 1994). Potassium is deliberated during the chloritization of biotite and directly in this sample the biotite is strongly chloritized. Therefore we can suppose the temporal ties of origin of the newly-formed fine-grained mica in the sample T-2 with the strong chloritization of biotite.

The process of rock deformation in granitoids of the Tribeč Mts., being indicated by biotite from the sample T-7, had varying intensity. Presented spectra $^{40}Ar*/^{39}Ar$ of apparent ages (Fig. 13) can be the demonstration of incomplete degassing of biotite during tectonic deformation in increased temperature, as is documented by minimum apparent ages from the medium-temperature part of the spectra.

Conclusion

The results of the examination of the shear zone in granitoid rocks in the north-western segment of the Zobor part of the Tribeč Mts. can be summarized as follows:
- granitoid rocks were affected by shear deformation having the character of progressive simple shear
- the strain rate of the rock was the highest in the centre of the shear zone and it corresponded to the value γ = **2.38**
- compression during origin of the mylonite zone was oriented in N-S direction (the recent geographic orientation)
- physical and mechanical characteristics of granitoid rocks correlate with rock deformation, i.e. with the zonality of deformation
- $^{40}Ar/^{39}Ar$ ages obtained from the white micas from the centre of mylonite zones can be interpreted as the mylonitization ages

- the age of the origin of the shear zone suggests for the strong compression event, taking part at the boundary between Cretaceous and Paleogene

- the accepting of the age of tonalite intrusion 306 ± 10 Ma as well as knowledge on the crystalline basement cooling in other Core Mountains indicate, that granitoid rocks in the Tribeč Mts. were exposed to higher temperatures than the blocking temperatures in K-Ar systems in biotites. It is confirmed by excess argon in biotites from undeformed granitoid rocks, but also by the loss of radiogenic Ar from biotites of partly deformed rocks. The age of this process is not clear up till now, but we can assume, that it is related to the distinct tectonothermal event, that caused deformation and decisive metamorphic overprint in rocks of cover sequence (Lower Triassic-Lower Cretaceous, Ivanička et al. 1998), resp. mylonitization (ca 70 Ma). From this viewpoint the Tribeč Mts., as a core mountain is exceptional, because such demonstrations in the majority of Core Mountains were not documented yet in such a range.

Appendix

Location of sampling sites

T-1, undeformed granodiorite, Veľké Jastrabie Valley, ca 1300 m to SW from the holiday resort Koželužne Bošany.

T-2, partly mylonitized granodiorite, Veľké Jastrabie Valley, identical locality as T-1

T-3, central part of mylonitized zone, Veľké Jastrabie Valley, identical locality as T-1

T-7, mylonitized granodiorite, mountain ridge, 1000 m to SSW from the altitude point Medvedí (719.4 m above sea level), Tribeč Mts.

T-8, granodiorite, the Žľaby locality (520 m above sea level), ca 700 m to SSW from the altitude point Javorový vrch (730 m above sea level), rock outcrop, Tribeč Mts.

T-9, mafic enclave in granodiorite, rock outcrop, identical locality as T-8, Tribeč Mts.

References

Bagdasaryan, G.P., Cambel B. & Veselský, J. 1977: Potassium age determination of rocks of crystalline complexes from the West Carpathians and their preliminary interpretation (in Russian). *Geol. Zbor. , Geol. carpath., 28, 2, 219 –242.*

Bagdasaryan, G.P., Gukasyan, R., Kh., Cambel, B., Broska, I. 1990: Rb-Sr isochrone dating of granitoids from Tribeč Mts. Geologický zborník, Geologica Carpath., 41,4, 437-442.

Berthé, D., Choukroune, P. & Jegouzo, P. 1979: Orthogneiss, mylonite and non-coaxial deformation of granite: the example of the South Armorican shear zone. Journal of Structural Geology, 1, 31 - 42.

Bieniawski, Z.T., 1973: Engineering classification of jointed rock masses. Transact. S. Afr. Ins. Civil Eng., 15, p. 335-342.

Bojko, A.K., Kamenický, L., Semenenko, N.P., Cambel, B. & Shcherbak, N.P. 1974: Part of results of dating of absolute ages of rocks from crystalline massif of the Western Carpathians and the recent state of knowledge. *Geologický zborník, Geologica Carpath., 1, 25, 25 - 39.* (In Russian)

Brewer, M. S. 1969: Excess radiogenic argon in metamorphic micas from the Eastern Alps. *Earth Planet. Sci. Lett., 6, 321 – 331.*

Broska, I & Petrík, I. 1993: Tonalite of Sihla type sensu lato: Variscan plagioclase-biotite magmatite of I -type in Western Carpathins. Mineralia Slovaca, 25, 23 - 28. (in Slovak)

Broska, I., Bibikova, E.V., Gracheva, T.V., Makarov, V.A. & Caňo, F. 1990: Zircon from granitoid rocks of the Tribeč-Zobor crystalline complex: its typology, chemical and isotopic composition. *Geologický zborník, Geologica Carpath. 41, 4, 395 - 416.*

Burchart, J., Cambel, B., Kráľ, J. 1987: Isochron reassessment of K-Ar dating from the Western Carpathian crystalline complex. Geol. Zborn., Geol. Carpath., 38, 2, 131 – 170.

Fediuk, F. 1961 : Fiodorov microscopic method. Publishing house ČSAV, Praha. (In Czech)

Grauert, B., O'Brien, P. J. & Lork, A. 1993: Rb-Sr dating of Jurassic low-temperature potassium metasomatism in gneisses of the Schwarzwald, Germany. Abstract suppl. 1 to Terra Nova 5, p. 386.

Hók J., Siman P., Frank, W. Kráľ, J., Kotulová J. & Rakús, M. 2000: Origin and exhumation of mylonites in Lúčanská Malá Fatra Mts., the Western Carpathians. *Slovak Geol. Mag. 6,4, 325 – 334.*

Ivanička, J., Hók, J., Polák, M., Határ, J., Vozár, J., Nagy, A., Fordinál, K., Pristaš, J., Konečný, V., Šimon, L., Kováčik, M., Vozárová, A., Fejdiová, O., Marcin, D., Liščák, P., Macko, A., Lanc, J., Šantavý, J. & Szalaiová, V. 1998: Explanations to geological map of Tribeč Mts. 1 : 50 000. Geological Survey of Slovak Republic, Dionýz Štúr Publishers, Bratislava, 7 - 237.

Jánová, V., 1997: Monitoring of dynamics of weathering processes development in semi-rock environment. Proceedings from 3rd geotechnical conference. STU - Bratislava. (in Slovak)

Jánová, V., Liščák P., 1998: Monitoring of weathering processes. Supplement No. 3 to Partial monitoring system of geological factors of living environment of Slovak Republic. GS SR Bratislava. (in Slovak)

Kirschner, D. L., Cosca, M. A., Masson H. & Hunziker, J. C. 1996: Staircase $^{40}Ar/^{39}Ar$ spectra of fine grained white mica: Timing and duration of deformation and empirical constraints on argon diffusion. *Geology, 24, 8, 747–750.*

Kohút, M. Kráľ, J., Michalko, J. & Wiegerová V., 1998: Hercynian cooling of the Veľká Fatra massif – evidences from $^{40}K/^{40}Ar$ and $^{40}Ar/^{39}Ar$ thermochronometrical mineral data and the recent state of thermochronometry. *Mineralia Slovaca, 30, 253–264.* (in Slovak)

Kohút, M., Todt, W., Janák, M. & Poller, U. 1999: Rapid exhumation of the Variscan basement in the Veľká Fatra Mts. (Western Carpathians – Slovakia). In: *Alpine evolution of the Western Carpathians and related areas (eds. Plašienka D., Hók J., Vozár, J., Elečko M.). Geological Survey of Slovak republic, 21 – 22.*

Kováč, M., Kráľ, J., Márton, E., Plašienka, D. & Uher, P. 1994: Alpine uplift history of the central Western Carpathians: geochronological, paleomagnetic, sedimentary and structural data. *Geologica Carpathica, 45, 2, 83 - 96.*

Kráľ, J., Hess, J., C., Kober, B. & Lippolt, H., J. 1997: $^{207}Pb/^{206}Pb$ and $^{40}Ar/^{39}Ar$ age data from plutonic rocks of the Strážovské vrchy Mts basement, Western Carpathians. In: *Geological evolution of the Western Carpathians (Grecula, P., Hovorka, D. & Putiš, M. (eds.). Mineralia slov. - Monograph, Bratislava, 253 - 260.*

Lippolt, H., J. & Kirsch, H. 1994: Isotopic investigation of Post/Variscan plagioclase sericitization in the Schwarzwald Gneiss Massif. Chem. Erde, 54, 179 - 198.

Lister, G.S. & Williams, P.F. 1979: Fabric development in shear zones: theoretical controls and observed phenomena. Journal of Structural Geology, 1, 283 - 297.

Maluski, H., Rajlich, P. & Matte, P. 1993: ^{40}Ar-^{39}Ar dating of the Inner Carpathians Variscan basement and Alpine mylonitic overprinting. *Tectonophysics, 223, 319 - 337.*

McDougal, I. & Harrison, T. M. 1988: Geochronology and thermochronology by the $^{40}Ar/^{39}Ar$ method. Oxford University Press, New York, 212 p.

Petrík, I., Broska, I. & Uher, P. 1994: Evolution of the Western Carpathian granite magmatism: age, source rocks, geotectonic setting and relation to the Variscan structure. Geologica Carpathica, 45, 5, 283 - 291.

Ramsay, J.G. 1980: Shear zone geometry: a review. Journal of Structural Geology, 2, 1/2, 83 - 99.

246

Slovak Geol. Mag., 8, 3– 4(2002), 235 – 246

Shcherbak, N. P., Bartnitsky, E. N., Mitskievitch, N. Y., Stepanyuk, L. M., Cambel, B. & Grecula, P. 1988: U-Pb radiometric determination of the age of zircons from Modra granodiorite (Malé Karpaty) and porphyroid from Spišsko–gemerské rudohorie Lower Paleozoic, (Western Carpathians). In Russian. *Geol. Zbor. , Geol. carpath., 39, 4, 427 – 436.*

Shcherbak, N., P., Cambel, B., Bartnitsky, E., N. & Stepanyuk, L., M. 1990: U-Pb age of granitoid rock from the quarry Dubná Skala - Malá Fatra Mts. *Geol. Zborn., Geologica Carpathica, 41, 4, 407-414.*

Shelley, D. 1993: Igneous and metamorphic rocks under the microscope. *Chapman and Hall, London, 445 p.*

Sibson, R. H. 1980: Transient discontinuities in ductile shear zones. Journal of Structural Geology, 2, 1/2, 165 – 171.

Sibson, R., H. 1977: Fault rocks and fault mechanism. Journal of the Geological Society of London, 133, 190 - 213.

Steiger, R.H. & Jäger, E. 1977: Subcommision on geochronology: convention on the use of decay constant in geo- and cosmochronology. *Earth Planet. Sci. Lett. , 36, 359 – 362.*

STN 73 1001: Foundation soil beneath areal foundations

Vass, D., Began, A., Gross, P., Kahan, Š., Köhler, Lexa, J. a Nemčok, J. 1988: Regional geological division of the Western Carpathians and northern promontory of Pannonian basin in the area of CSSR. 1 : 500 000. SGÚ - GÚDŚ, Bratislava.

Variscan suture zone in Gemericum: Contribution to reconstruction of geodynamic evolution and metallogenetic events of Inner Western Carpathians

ZOLTÁN NÉMETH

Geological Survey of Slovak Republic, Jesenského 8, 040 01 Košice; nemeth@gssr-ke.sk

Abstract. The finding of Variscan geosuture in the North-Gemeric zone, as well as microtectonic proofs of its kinematics, suggested a modified model of Variscan tectonic evolution of Inner Western Carpathians, having impact also on metallogenesis.

The northward inclined ductile shear zone, dividing Early Paleozoic rocks of Gelnica and Rakovec Groups of Gemericum, manifested kinematics of south-vergent Variscan exhumation. The Rakovec Group, partly representing subducted oceanic crust (active back-arc type?), was exhumed in dextral transpression on Gelnica Group, as the former marginal lithology of the basin during the young stage of its evolution.

We suppose that thermal processes in collisional régime were sufficient for increase of thermal gradient, metamorphism and metallogenic processes. Geodynamics of Inner Western Carpathians from the time of Ordovician riftogenesis till Mesozoic is interpreted to be a product of the heat flow caused by the same linear source of convectional heat.

Key words: microtectonics, exhumation, metallogeny, geodynamic evolution, Gelnica and Rakovec Groups, Gemericum

Introduction

The research of the boundary zone between the Early Paleozoic Gelnica and Rakovec Groups of Gemericum was motivated by the multivariant interpretation of lithotectonic relations in this zone:

1. Angular discordance of rocks of Rakovec Group to those of Gelnica Group due to the Spiš phase of folding (Fusán et al., 1955).
2. Continual sedimentary and volcanic development from Gelnica Group to Rakovec Group (this finding was the reason of distinguishing the only one Volovec Group, Grecula, 1982).
3. North-vergent Variscan overthrust of the northern part of Gelnica Group, i.e. Kojšov nappe on Rakovec Group (Rakovec nappe; Grecula, 1982).
4. Finding of mylonitic zone on the boundary between both groups (Fig. 1), northern inclination of kinematically active oldest secondary foliation and proofs of the presence of higher to high-pressure metamorphic overprint of a part of Lower Paleozoic and partly Carboniferous rocks in the North-Gemeric zone (Hovorka et al., 1988; Radvanec, 1998, 1999) led to origin of subduction-exhumation model of the rocks of the Rakovec zone being interpreted like the Variscan suture zone (Németh, 1999).

The additional data of recent research, preferably about kinematics in this zone, should add arguments for or against above mentioned interpretations.

All topographic orientations, stated in the text are relative and used for simplification of mutual azimuthal relations of tectonic units of Inner Western Carpathians. The orientations "northern" and "southern" etc. is valid only for Tertiary and younger space relations. In the case of older geological events they are the relative ones, but simplify explanation of mutual relations of lithostratigraphic units in older evolution. The rotation of the crustal segments (microplates) during long-time evolution is widely known and proved with results of paleomagnetic survey.

Methodology

The result of this study are based on the regional structural/microstructural research following former regional field mapping in the Gemeric region in the scale 1 : 10 000 and assembling of the geological maps of the Nort-Gemeric zone in the scale 1 : 25 000.

The ductile shear zone dividing rocks of Lower Paleozoic Gelnica and Rakovec Groups was firstly found by the field observation. Microstructural analysis was used for finding of deformation gradient of rocks and azimuthal orientation of tectonic transport. The mylonitization of various protoliths caused the origin of the shape preferred orientation (SPO) and the lattice preferred orientation (LPO) of rheologically active minerals. The LPO was investigated by optical microscope using the gypsum plate and U-stage.

For calculation of differential stresses, causing deformation of carbonates, we have used the paleopiezometrical methods of Twinning incidence (It) and Twin density (D; Rowe and Rutter, 1990).

Legend:

▣①	Shear zone between Gelnica and Rakovec Groups [Variscan; lin. course]
⊡②	Shear zone between Gemericum and Veporicum [Alpine; linear course]
⊡③	Bôrka nappe (exhumed Meliaticum) [Alpine nappe; areal outcropping]
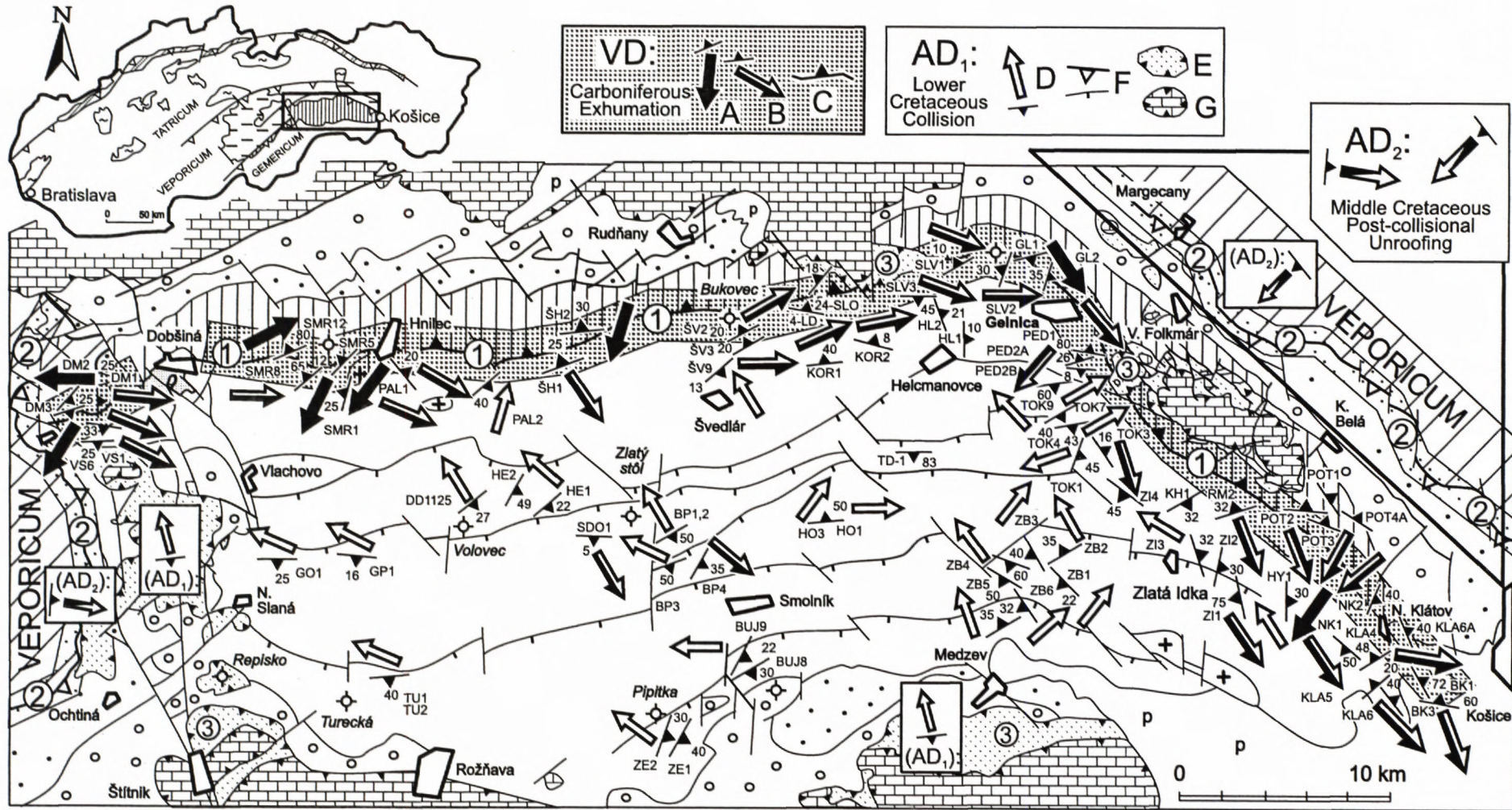
Németh, 2001, slightly modified

Obtained data

Recent areal course of boundary zone between Gelnica and Rakovec Groups (in redefined sense; Németh, 2001, Fig. 2; Németh in Mello, ed., 2000) involves a strip of tectonites passing from the wider southern vicinity of the Ostrá hill (1014) through Smrečinka (1266), Hnilec village, southern vicinity of Pálenica hill (1115), Nálepkovo, Švedlár forest, Bukovec (1127), Lacemberská valley, eastwards from Slovinky village, Krompachy hill (1025), south of Žakarovce, eastwards of Gelnica town to the Široký hŕbok elevation point (731), Vyšný Klátov and village Bukovec (the schematic course of the zone is depicted in Fig. 1).

Outcrops along the contact zone of Gelnica and Rakovec Groups demonstrate moderate dip of oldest secondary foliation to the N, NNW as well as NNE and generally subhorizontal E-W trends of lineation. In the eastern part of Gemericum, where the contact zone of both groups is bended to SE, the above described structural settings follow this bend. The foliation there dips to NE and mineral lineations have SE-NW to SSE-NNW trends. Mesostructures indicate the oblique overthrusting of the rock mélange of Rakovec Group on volcanosedimentary rock piles of Gelnica Group.

To compare the deformation gradient of rocks directly from the shear zone with character of deformation in the lower levels of the Gelnica Group and possible tectonic overprint of southermore parts of Gemericum, we firstly examined characteristics of rocks unaffected by the studied shear zone.

Tectonites from the Gelnica Group away of studies shear zone

Siliciclastic rocks and rocks of volcanic affiliation

Less deformed siliciclastic rocks are outcropping on the south of Gemericum and were sampled on the Zelená skala hill located to SE of Pipítka (1225) elevation point (**ZE1**, $S_2 = 120/40$; **ZE2**, $S_2 = 110/30$; microstructural indications of tectonic transport are to NW) and from the

Bujaková hill to the south of Smolník town (**BUJ8**, $S_2 = 150/30$; **BUJ9**, $S_2 = 118/22$, transport to the west). The quartz clasts with the low degree of deformation manifested local pressure solution, weak rotation, rare undulose extinction and the origin of subgrains. The LPO was not observed. In accordance with the mesoscopic penetrative cleavage the rough foliation planes originated in the microscale, being highlighted by the Qtz-Ser fine-grained aggregates. The sporadic plagioclases were twinned in high angle to originating rough foliation.

The next studied samples of quartzites and sandstones from the internal parts of the Gelnica Group were taken from the upper termination of the Zábava valley to the north of Medzev village. The fine/medium-grained and usually banded samples demonstrated a partial recrystallization by the grain boundary migration (GBM). In the pressure shadows we detected the onset of polygonization. Microfolds in foliation planes indicate prevailing transport either top-to-the-NE (**ZB1**, $S_2 = 225/22$; **ZB3**, $S_2 = 240/40$) or top-to-the-NW (**ZB2**, $S_2 = 330/35$), both being the product of north-vergent compression. The transport top-to-the-NNW (**ZB7**, $S_2 = 330/35$) and ENE (**ZB6**, $S_2 = 235/32$) was indicated also by synthetic shears. The banded ultramylonitic quartzites are penetrated with thin veins of Alpine type (Czo, Lxn, coarse-grained Ms). LPO of quartz in the sample **ZB7** indicated dominating medium temperature prism <a> slip, corresponding with the origin newly grown biotite as the passive marker of rough foliation.

The effects of thermal flow, related to the late Variscan granitization, have been found in quartzitic rocks from the wider eastern and northern surrounding of the Zlatá Idka village (**ZI1**, $S_2 = 258/75$, top-to-the-SE; **ZI2**, $S_2 = 102/30$; **ZI3**, $S_2 = 72/32$; **ZI4**, $S_2 = 216/45$).

The increase of dynamic recrystallization causing decreasing grain-size of the protolith (**ZI4**) was accompanied with origin of oblique foliation. The quartz c-axes orientation in **ZI4** demonstrated the prevalence of the medium temperature (300-400 °C) prism <a> slip with minor contribution of rhomb <a> slip. The pole figure asymmetry in the prism <a> slip part indicated not very distinct top-to-the-SSE shearing. Contrary to this, the

---

Fig. 1. Position of Variscan suture zone in the Alpine tectonic frame. The principal ductile shear zones are indicated with dotted areas and are numbered in circles. A-C - Variscan south-vergent exhumation of Rakovec Group on Gelnica Group, both Lower Paleozoic of Gemericum, during phase VD: A - tectonic transport demonstrated by microtectonics in mylonites of Rakovec Group in (allochthonous) hanging wall of ductile shear zone, B - tectonic transport demonstrated by tectonites of upper part of Gelnica Group in (autochthonous) footwall of shear zone, C - course of Variscan ductile shear zone, D-G - north-vergent Alpine tectonic transport: D - shearing exhibited by rocks of Gelnica Group, E - emplacement of Bôrka nappe (exhumed parts of Cimmerian Meliata-Hallstatt basin) on Gemeric rock sequences, F - Lower Cretaceous north-vergent transport of Alpine thick skinned Gemeric nappe on Veporicum produced also internal imbrication of the nappe, G - location of the Silica superficial nappe either on Bôrka nappe or Gemeric sequences. Alpine nappe piling thickened continental crust. Thermal effects caused post-collisional unroofing of Veporic core. 1 - Pieniny Klippen Belt, remnant of Late Cretaceous to Early Tertiary closure of Penninic-related oceanic domain, 2 - crystalline complexes of Tatricum, 3 - crystalline complexes of Veporicum, 4 - sedimentary and volcano-sedimentary sequences of Gemericum. 5 - lithological boundaries and faults undivided, 6 - azimuth of foliation, number indicates dip in degrees, 7-9 - Paleozoic sequences of Gemericum: 7 - Ordovician-Devonian rocks of Gelnica Group, 8 - Devonian-Lower Carboniferous? rocks of Rakovec Group; Variscan ductile shear zone divides lithologies of both lithostratigraphic units. 9 - cover sequences of Gemericum: a - Carboniferous, b - Permian. 10-11 - nappe overliers on Gemericum: 10 - Bôrka nappe, 11 - Silica nappe. 12 - Paleogene cover. 13 - Veporicum undivided.

Overthrusting of Gemericum on Veporicum is the result of Alpine compression during AD$_1$. The boundary zone between both, so-called Lubeník-Margecany line, is recently modified with post-collisional unroofing during AD$_2$.

bulk oblique foliation of Qtz + Ab + Ser ± Act aggregate, occurring in bands parallel with mesoscopic foliation, indicated top-to-the-NNW sense of shearing. In the case of tourmaline microlayers (app. 80 % of Tur and 20 % of Qtz + Ab), the bigger tourmalines as a rule crystallized in the direction of oblique foliation (top-to-the-NNW). The sample **ZI4** by this way demonstrates very complex deformation history (the first plastic deformation registered by quartz LPO indicates transport top-to-the SSE, the younger one by the oblique foliation as well as the majority of Tur grains indicate top-to-the-NNW shearing).

The dynamic recrystallization of quartz matrix of banded acid pyroclastics **KH1** (upper part of Hnilec Fm., $S_2 = 150/32$) from apical parts of the Kojšovská hoľa massif (1246) manifested the top-to-the-W shearing.

The studied lithology in continual N-S trending profile through the Tokáreň forest consisted prevailingly from banded sandstones. Rocks, mainly protomylonites, demonstrated weak fabric asymmetry. Non-penetrative tectonic overprint was reflected in differing sense of tectonic transport (**TOK1**; $S_2 = 110/45$; top-to-the-WSW; **TOK3** $S_2 = 56/16$ – ENE; **TOK4**; $S_2 = 170/43$ – ENE; **TOK7**; $S_2 = 150/40$ – NW). The ambiguity in azimuthal orientation demonstrates more probable a weak stress field occurring during deformation, than the registration of two deformational evens.

Flyschoid sandstones in the central part of the recent areal spread of the Gelnica Group (triangle among villages Vlachovo, Smolník and Helcmanovce) are outcropped in the Stará voda valley (**SDO1**; $S_2 = 182/5$; top-to-the-SSE shearing) and in the Bystrý potok valley (**BP4**; $S_2 = 120/35$; top-to-the-SE). Next outcrops in triangle demonstrated different orientation of the stress field and general vergency of shearing to NNW (green porphyroid from Dlhá dolina valley **DD1125**, $S_2 = 142/27$, top-to-the-NW; green laminated sandstone south of Pálenica elevation point **PAL2**, $S_2 = 140/40$, top-to-the NNE; porphyroid - Henclová north of Volovec elevation point **HE1**, $S_2 = 140/22$, WNW; sandstone north of the village Švedlár **SV9**, $S_2 = 140/13$, NW; green porphyroid from Bystrý potok valley **BP2**; $S_2 = 140/50$; NW). The tectonic transport to WNW was found also in the case of sandstone **GP1** from Gemerská Poloma village (Martinkov potok stream, $S_2 = 185/16$).

Contrary to the rheologically weak material (banded sandstones, volcanoclastics, pyroclastics and carbonates), more rigid and competent volcanic rocks demostrated very weak and undistinct tectonization only with primary stages of foliation development and mantled porphyroclasts being undistinctly rotated (**HL2** - rhyolite from the northern surroundings of the Helcmanovce village, $S_2 = 70/21$; **HY1** - rhyodacite outcropped to NW of Nižný Klátov village, $S_2 = 90/30$, top-to-the-NW).

Carbonates

Microstructural data from carbonates of Holec Beds demonstrate the north-vergent transpressional tectonic transport with azimuthal spread from WNW to E (outcrops north of Nižná Slaná **GO1**, $S_2 = 180/25$, top-to-the-WNW; Holec elevation point to NW of Smolník town

with two types of calcitic marbles: **HO1** $S_2 = 355/50$, top-to-the-E, but **HO3** top-to-the-NE; Bystrý potok valley **BP3**, $S_2 = 160/50$, top-to-the-WNW; Turecká massif NW of Rožňava **TU1**, $S_2 = 140/40$, top-to-the-WNW).

Differencial stresses determined by the paleopiezometry from samples **GO1** (average grain-size 253.9 $\square$m; using method Twinning incidence I_t σ = 88-110 MPa; Twin density D σ = 159-168 MPa), **HO1** (202.9 μm; It => σ = 208-210 MPa; D => σ = 231-233 MPa) and **HO3** (350.8 μm; It => σ = 141-154 MPa; D => σ = 197-203 MPa) belong to the lower part of the value range found from the ductile shear zones in Gemeric region (cf. Németh, 2001). The sample GO1 moreover demonstrated the grain boundary migration accompanied with the origin of deformation lamellae in some grains. The higher differential stress, recorded in the sample HO1 in comparison with HO3, caused the origin of microshears during the same plastic deformation of calcite grains.

Tectonites of (autochthonos) footwall of ductile shear zone

The flyschoid sandstones of the upper part of Hnilec Formation of Gelnica Group [redef. Hnilec Fm. (Németh, 2001; Fig. 2); according to the lithostratigraphy by Bajaník et al. (1981) these sandstones belong to the Smrečinka Formation of Rakovec Group] represented the suitable rheological environment for preferential strain softening and the origin of ductile shear zone dividing rock of Gelnica Group in the footwall and rock mélange of Rakovec Group in the hanging wall of the shear zone.

Mylonites of laminated flyschoid sandstones

Laminated sandstones from the northern vicinity of Švedlár (**ŠH1**, $VS_1 = 340/25$, transport to SE) demonstrate strong chloritic foliation, asymmetric structures and oblique foliation of quartzy grains. Gypsum plate indicates strong LPO of quartz aggregates. The shearing orientation of mylonites of laminated sandstones (**ŠV2**, $VS_1 = 322/20$, NE) corresponds to the transpressional deformation regime when taking into account the moderate rotation of rock block bearing studied outcrop about 30° counterclockwise. Mylonite of black laminated sandy schist, outcropping in the tight vicinity of the Bukovec (1090) elevation point (**ŠV3**, $VS_1 = 330/20$), demonstrates top-to-the-E shearing.

The LPO of quartz grains of banded flyschoid sandstones (protomylonite - Slovinky village, **SLV2**, $VS_1 = 290/30$; mylonite - Lacemberská dolina valley, **4LD**, $VS_1 = 10/5$; ultramylonite - Perlova dolina valley, **PED2A**, $VS_1 = 184/8$) demonstrated maximum in the area of low to middle-temperature prism <a> slip with contribution of basal <a> slip. The tectonic transport in the horizon of sandstones firstly occurred in their thin pelitic intercalations. According to the weak asymmetry of pole figures, but mainly according to microstructural indicators in phyllosilicates there was determined the prevailing eastern vergence of transport. The moderate shear bands and intrafoliation fold in quartzy undistinctly laminated phyllite (Perlova valley, **PED2B**, $VS_1 = 344/26$) indicated transport to SW.
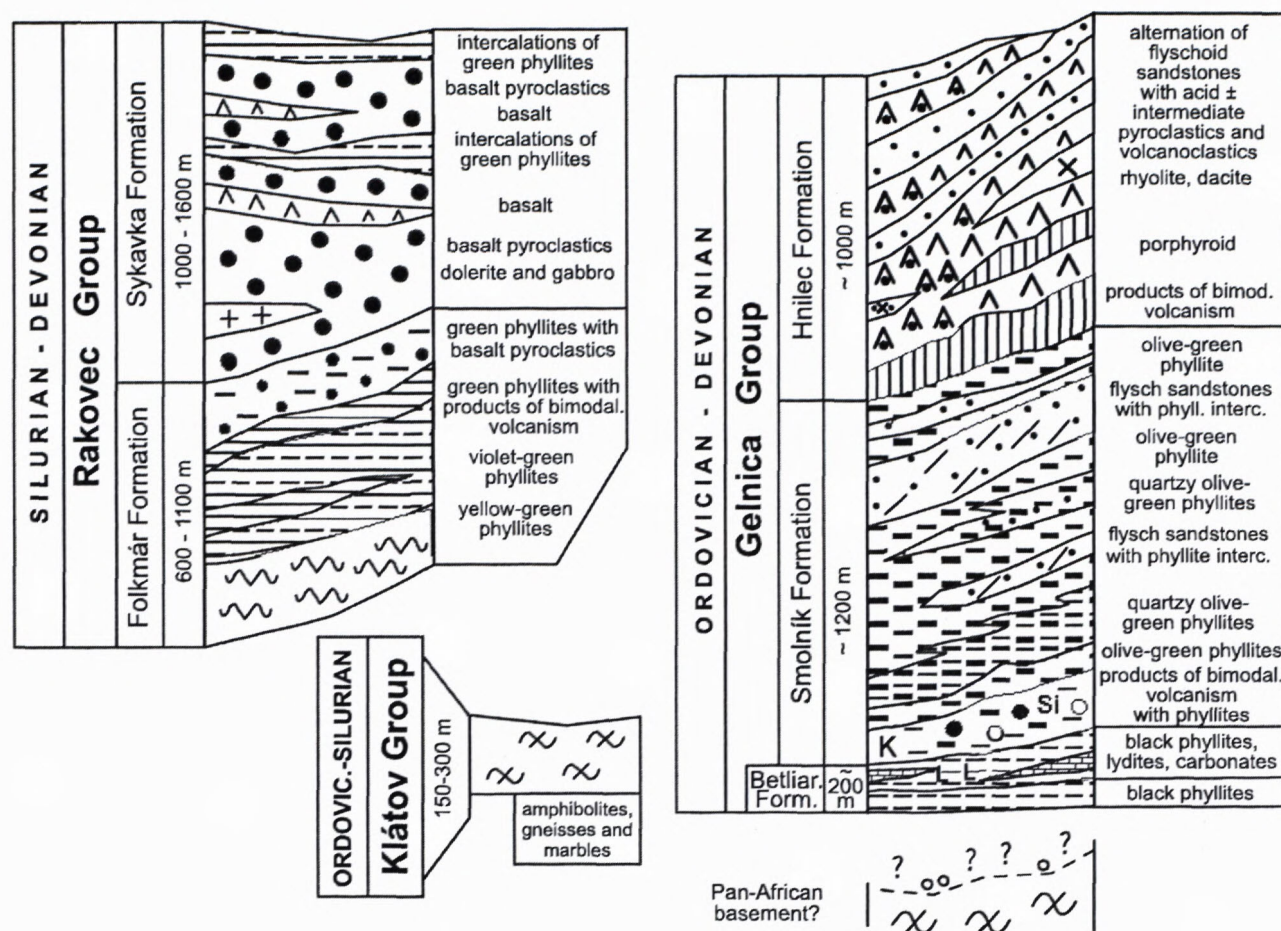
Fig. 2 Lithostratigraphy of the Lower Paleozoic of Gemericum (Németh, 1999, 2001).

The most prominent deformation process, found in banded psammites, was static recrystallization affecting the quarzy intercalations being formerly dynamically recrystallized. The first kinematic activity observed in representative samples (northern surrounding of Vyšný Klátov village ČP6, ČP7, ČP8, KLA3; N and NW surrounding of Nižný Klátov village KLA5, KLA6A, POT1, POT2, POT3; to the NE of Bukovec village BK1A, BK1B, BK2, BK3A, BK3B) was activity and recrystallization in pelitic intercalations (origin of white micas, their folding, pulling out of fragments from bordering quartzy intercalations, rotation of porphyroclasts). Next followed dynamic recrystallization of psammitic (quartzy) intercalations. The last process found from microstructures was the static recrystallization of quartzy intercalations accompanied with growth of large polygonal grains. They usually reached sizes being limited only by the distance between neighbouring pelitic intercalations. The former non-coaxial deformation was indicated by strain fringes found on pyritic grains. Oriented samples indicate top-to-the-SE and SSE shearing (KLA5, VS_1 = 320/20; POT1, VS_1 = 56/46; POT2, VS_1 = 5/28). Several samples (POT4A, VS_1 = 32/36) demonstrate the direct overthrusting of hanging wall of shear zone, and the shearing top-to-the-SW has been found there.

Deformation gradient in laminated flyschoid sandstones strongly depends on their protolith. In the samples with lower content of pelitic component and strongly

prevailing quartzy material the dynamic recrystallization has been accommodated by quartz grains. Because of lower percentage of phyllosilicates, and primarily lower amount of fluid phase liberating during phase transformation from clay minerals to phyllosilicates, the imprint of static recrystallization has been weaker (KLA2A).

Third mylonite type represents banded rock with prevailing albite in albite-quartz aggregates (having macroscopic appearance of banded keratophyre pyroclasts; KLA2B). The samples are without indications of static recrystallization with localization of deformation into penetrative foliation planes with phyllosilicates.

Mylonites of metapelites associated with flyschoid sandstones

Mylonite of grey metapelite from the Dobšinská Maša farmhouse west of Dobšiná (DM1; VS_1 = 88/25) indicates LPO of quartz aggregates under gypsum plate. Asymmetry of quartzy layer demonstrates top-to-the-E shearing. The bulk foliation of similar sample from Smrečinka hill (SMR12, VS_1 = 320/65, top-to-the-ENE) is represented with planar orientation of quartz grains flattened in XZ plane with oblique undulose extinction, corresponding with syntethic shears.

Mylonite of laminated green metapelite with younger contact metamorphic overprint (spotted shist), taken southwards of Hnilec village (PAL1, VS_1 = 50/20) con-

tains boudinaged asymmetric quartz lamines. They demonstrate top-to-the-ESE shearing, predating the contact metamorphism by Gemeric granite.

Mylonite of non-laminated metapelite (**20SLO**, $VS_1 = 15/35$) exhibits extremely strong LPO of totally dynamically recrystallized quartzy aggregates. Because of rheologically homogenous material without laminae, all strain was accommodated by quartz grains with origin of oblique foliation.

Bulk foliation of pale-coloured mylonite (Perlova valley, **PED1**, $VS_1 = 10/80$) is formed by newly formed sericite leaves. The undulose extinction of quartzy σ-porfyroclasts indicate ambiguous vergency of transport to E and W.

Mylonites of acid and intermediate pyroclastics and volcanoclastics

Volcanoclastics are present in intercalations of laminated flyschoid sandstones in the upper part of lithostratigraphic column of Hnilec Formation (intermediate rocks from the Korban altitude point west of Helcmanovce **KOR1**, $VS_1 = 354/40$ and **KOR2**, $VS_1 = 15/8$, top-to-the-ENE; **VS1** eastward of Rejdová village, $VS_1 = 178/25$, top-to-the-ESE). Acid volcanoclastics of Slovinky (**ZN-2-SLO**) demonstrate strong LPO and SPO in quartzy matrix without manifestations of static recrystallization. Feldspars are deformed by twinning.

Mylonite of coarse-grained volcanoclastics from Tokáreň mountain ridge (**TOK9**, $VS_1 = 172/60$, top-to-the-W) demonstrates SPO (flattening) of quartz and feldspar grains and wide anastomosing foliation planes with white mica.

Distinct asymmetric structures in mylonite of acid volcanoclastics with quartzy detrital bands and organic matter ("black porphyroid", Romanová valley to SW of Opátka village, **RM2**, $VS_1 = 342/18$) indicate top-to-the-SSE shearing.

Mylonites of green phyllites

Mylonites of olive-green chloritic phyllites (**VS6**, the northern vicinity of the village Vyšná Slaná, $VS_1 = 189/33$) and **SMR1**, the peak of Smrečinka hill, $VS_1 = 285/25$; both top to the SSW; **ČP5A**, southward of Košická Belá village) contain in fine-grained Chl-Ser-Qtz matrix sporadical feldspar and quartz clasts (undulose extinction, recrystallization by GBM, deformation lamellae, subgrains, linear arrangement of fluid inclusions). Quartz clasts are dynamically recrystallized, showing boudinage, intrafoliation folding and strain caps.

In banded quartzy olive-green phyllite (Slovinky, **SLV1**, $VS_1 = 330/10$, top-to-the-ESE) the phyllosilicate intercalations are transformed into bulk foliation. The intergranular spaces in quartzitic intercalations are filled with fibroidal fine-grained Qtz-Ser-Chl aggregate.

Tectonites from (allochthonous) hanging wall of ductile shear zone

For description of various types of mylonites in allochthonous part of shear zone (rocks of Rakovec Group), the different degrees of strain softening, relating mainly on protolith of mylonites, were used as a primary criterion.

Phyllitic mylonites

Sericite-chlorite phyllites (fine-grained aggregate Chl + Qtz ± Ab ± Ser) represented the softest medium of Rakovec Group. The dynamic recrystallization by GBM of thin quartzy intercalations, or sporadical clasts, caused their boudinage resp. total reduction. Recrystallized mica aggregates were usually folded and in mylonite they were present in foliation and shear bands as well as in the axial plane cleavage of microfolds. The quartz-chlorite syntectonic veins and younger pyritization and limonitization were also observed.

Oblique foliation among C-planes in violet-green phyllite (typical facies from Rakovec zone; Dobšinská Maša farmhouse, **DM3**, $VS_1 = 160/25$) indicated top-to-the-W tectonic displacement.

The increasing degree of mylonitization of violet-green phyllites caused, together with their microstructural rebuilding, also the change of their colour to yellow-green. We explain this change by their total microstructural reworking with origin of very fine-grained aggregate Qtz-Chl-Phe-Ill (e.g. **1KRI** northward from Hnilec, or **GL2** northward from Gelnica, $VS_2 = 108/76$, top-to-the-SE). The yellow-green phyllitic mylonites represent plastic environment surrounding rigid blocks (e.g. basalts). The same mylonite type we have found also in the underlier of Carboniferous conglomerates of Rudňany Fm. of Dobšiná Group.

Basalt pyrocklastics and volcanoclastics

Mylonite of basalt volcanoclastics (Dobšinská Maša farmhouse, **DM2**, $VS_1 = 130/25$) has numerous synthetic shears with newly formed white mica and chlorite indicating top-to-the-E shearing. Twinned grains between individual synthetic shears demonstrate book-shelf sliding. Decomposition of old plagioclases is accompanied with origin of epidote-zoisite and crystallization of albite.

Plagioclases of protomylonite of basalt pyroclastics (Smrečinka elevation point, **SMR5**, $VS_1 = 315/12$) are albitized, carbonatized and partly replaced by fine-grained aggregates of clinozoisite. The newly formed actinolites are a syn-tectonic product. Part of σ-porphyroclasts indicated dispacement to NE, but younger tectonic overprint top-to-the SW was indicated by crystallization of chlorite in synthetic shears and by deformation lamellae of plagioclases.

Matrix of mylonite of basalt pyroclastics (Smrečinka elevation point, **SMR8**, $VS_1 = 337/80$) consisting from flattened Qtz + Ab grains with strong SPO, represent bulk continuous foliation. Moreover, the spaced foliation by chloritic bands and boudinaged strips of newly grown carbonate have the same course. In described mylonite the top-to-the-ENE tectonic transport is indicated by synthetic shears and plagioclase σ-porphyroclasts as well as occasional book-shelf sliding of their fragments.

The protomylonite of basalt pyroclastics (northern surrounding of Švedlár village, **ŠH2**, $VS_1 = 354/30$) exhibits strong LPO of quartzy intercalations by gypsum plate. Nearly half of quartz grains demonstrates undulose extinction and origin of subgrains. According to numerous synthetic shears tectonic transport top-to-the-SSW has been distinguished.

Lenses of carbonates with oblique twinning in mylonite of basalt pyroclastics (to the north of Gelnica, **GL1**, $S_2 = 166/35$) indicate vergence of shearing top-to-the-SE. Preferred orientation of anizometric minerals contributes to planar-linear setting (SL tectonite) of rock.

Synmetamorphic deformation (fluid driven deformation) of basalt pyroclastics **NK1** (eastern surrounding of Nižný Klátov village, $S_2 = 220/20$, top-to-the-SW) is documented with segmented plagioclases having albitized fractures. Spaced foliation is formed with chlorite and elongation of newly formed actinolites.

Basalts

Outcrop of basalts (Slovinky area, **SLV3**, $S_2 = 180/45$) without any tectonization represent a rigid block, flowing in plastic phyllitic environment. The calcite rhombohedrons are the main constituents of rock together with albitized plagioclase porphyroblasts and fine-grained aggregates of chlorite and epidote-zoisite with strips of ilmenite and sporadic clinozoisite.

Discussion

Variscan geodynamic evolution

The origin of *Rakovec geosuture* of variegated lithological composition (being characterized below) is a product of Variscan evolution. The geosuture is divided from the Gelnica Group with ductile shear zone having moderate to medium northern dip. Generally, the northern inclination of the rock boundaries in this zone was proved also by the results of geophysical measurements (cf. Grecula a Kucharič, red., 1992). Moreover, the presence of the rock boundary inclined northward was in this zone indicated by seismic profiles G1a/92, G1b/92 and G2/93 (Vozár et al., 1998). The microstructural investigation of mylonites from described boudary zone proved two principal directions of tectonic transport - in autochthonous footwall of ductile shear zone, i.e. in the upper part of the Gelnica Group, the general vergency of tectonic transport to ESE prevailed (black-white arrows in Fig. 1). The allochthonous hanging wall of ductile shear zone (tectonic mélange of Rakovec Group) indicated the transport directions generally to south, but locally there was recorded also their large azimuthal spread (black arrows in Fig. 1). Our findings prove the general southern-vergency of Variscan tectogenesis. The south-vergent structures are in Gemericum common, including fold structures of this orientation.

From the evolutionary viewpoint the Lower Paleozoic rock sequences of Gemericum can be generally divided into two large groups:

A. The Lower Paleozoic rocks of Gelnica Group in "cover" position on the rigid block of the older crystalline block of "southern" Pan-African? provenience were in Upper Carboniferous deformed by generally south-vergently displaced exhuming mélange. We do not suppose the higher thickness of sediments of Gelnica Group in the pre-exhumation era than 5 km. To this corresponded the diagenesis in upper part of the rock pile of Gelnica Group and the greenschist facies in its lower part.

B. Rocks of Rakovec group were dragged into various depths of subduction zone. The age of subduction-exhumation processes (Devonian to Vestphalian) is supposed. Dating of the upper time boundary is based only on the finding of the metamorphic pressure peak of 12 kbars in a matrix of a part of sediments of the Rudňany Fm. (Radvanec, 1998). It indicates, that also part of Westphalian sediments was locally affected by metamorphism in subduction régime and consequently exhumed (cf. Chemenda et al., 1996, 1997). The Upper Devonian radiometric ages from the Klátov Group (cf. Cambel et al., 1990) which tectonometamorphism is given to relation to the early stages of subduction processes, indicate the lower time limit of subduction. The subduction slab was inclined northward below the rocks of recent Tatro-Veporic terrane (Fig. 3). The differential relative movement of rocks occurred in the subduction slab. Interpreting the kinematics in a converging terrane we suppose, that deepest position in subduction zone was reached by rocks of the "northern near-Veporic" part of a Lower Paleozoic basin, located to the north from the spreading zone. Incorporation of the mid-oceanic ridge into subduction zone meant the beginning of subduction of the Gemeric - Rakovec (southern) part of the Lower Paleozoic basin, while the source of the convectional heat was that time located below Veporicum and initiated the reverse rolling back of rock masses (occasionally also with the fragments of the mantle rocks) in subduction channel back to the surface. Approaching of crystalline rocks of (southern) basement, being present beneath the rocks of Gelnica Group, decelerated the subduction. The collision caused the origin of a geosuture. In its recent erosion cut we can find:

1. Former sediments and volcanic rocks of the Rakovec Group, in marginal parts of the basin occasionally with preserved lithostratigraphy. Their low degree of metamorphism and tectonization was the result of their position in the northern lateral continuation of the Gelnica Group, as well as the minor incorporation to the subduction zone. The transition between the Rakovec and Gelnica lithologies was documented already by Grecula (1970, 1982) and was the reason for distinguishing of the uniform Volovec Group for the whole Lower Paleozoic rocks of Gemericum. The lithological transitions are observable in the area of Perlova dolina valley eatwards of Gelnica town.

2. The subducted sediments and volcanites from the Rakovec Group, being exhumed from the deeper parts of the subduction zone. They are characteristic with higher tectonization. Metamorphism in the facies of actinolitic schists (e.g. in the strip south of the line Holý vrch hill (1016) and Suchinec (909) northward of Lacemberská dolina valley).

N ⇨ ⇦ **S**

WESTPHALIAN

Ⓒ ⓀⓁ ⓇⒶ

GE

Position of rocks of Betliar Fm. and basal part of Smolník Fm.

~ 40 km

Final stage of subduction and exhumation

PERMIAN

⇦ ⇨

Ⓟ
Ⓒ ⓀⓁ ⓇⒶ

GE

Permian extension "straightened" former tectonic setting

Granitization

Crystalline basement

Upper mantle

Axis of convectional heat is displaced southward

Post-collisional thermal consolidation, origin of ore veins

TRIASSIC-JURASSIC

⇦ ⇨

GE

Divergence in basin in South-Gemeric zone

LOWER CRETACEOUS

⇦

GE

Collision, imbrication of Gemeric rocks, Alpine overthrusting of Gemericum on Veporicum

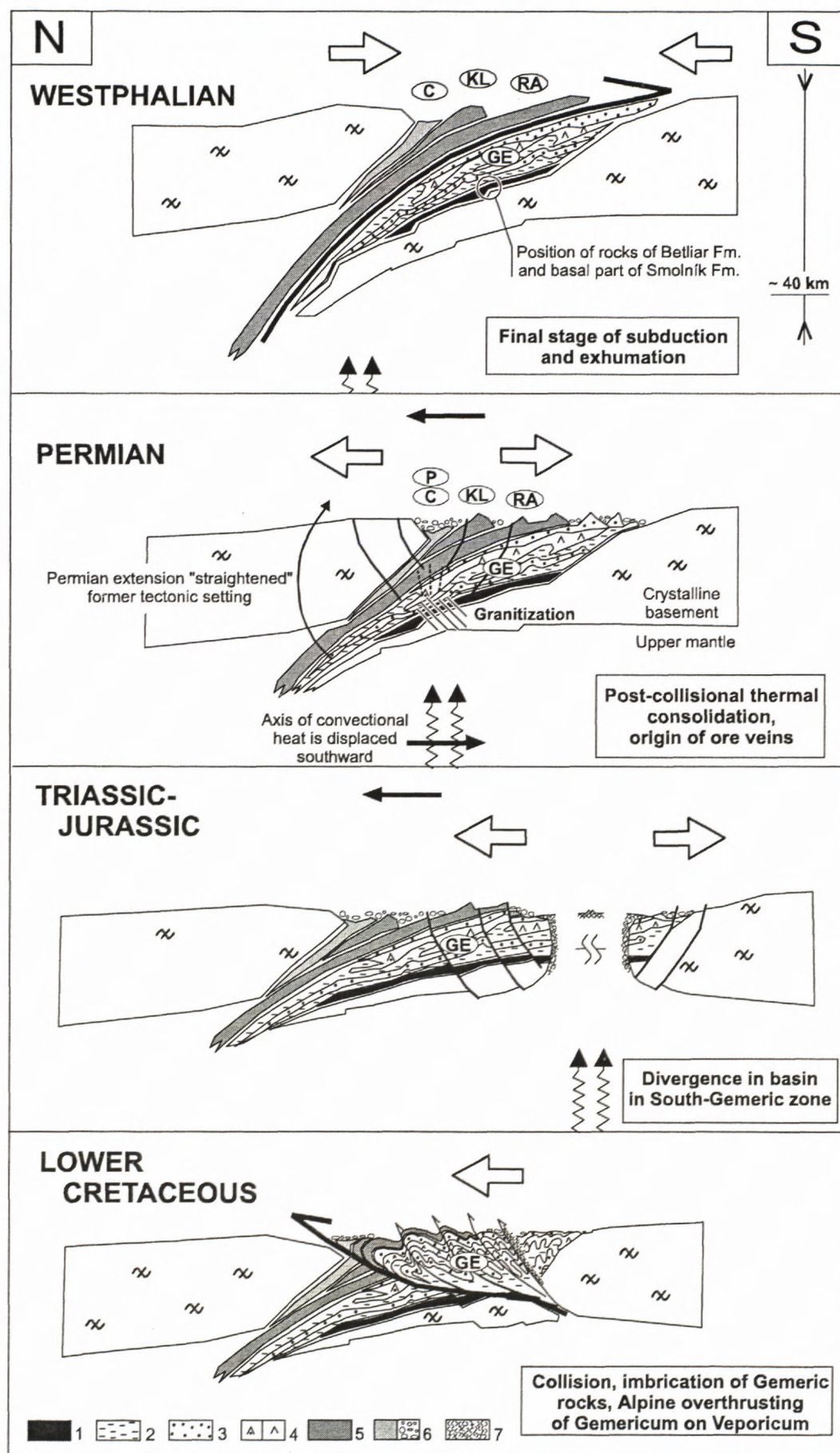■ 1 | 2 | 3 | 4 | 5 | 6 | 7

Fig. 3

3. Former sediments and volcanites of Rakovec Group exhumed from deeper parts of the subduction zone. In the case of mafic rocks there were indications of higher-pressure metamorphism (Hovorka et al., 1988; Rakovec area). Radvanec (1999) found the mantle origin and ultra-high pressure metamorphism of a part of these rocks. "Floating" rigid blocks of mafic rocks in plastic mylonitic environment of green phyllites. *[Among other indications we argue also with tectonometamorphic "transformation" of violet-green phyllitic facies into mylonites of co-called yellow-green phyllites in the zone between the altitude point Suchinec (909) and the Slovinky village northward of Lacemberská dolina valley].*

4. Part of Westphalian rocks of the Rudňany and Zlatník Formations with the demonstrations of metamorphic recrystallization recenly outcropping in segments in the zone from Sykavka to the area of Závadka village as well as in surrounding of Rudňany village (cf. Radvanec, 1998). A great deal of rocks from the Rudňany and Zlatník Fms. does not exhibit the metamorphic recrystallization because of their external sedimentation area regarding to subduction zone. They were not included into subduction process. *[For example the preservation of intercalations of black schists with well-known biostratigraphic occurrences in the area of Dobšina; review is presented by Vozárová and Vozár, 1988.]*

5. Rocks of Klátov Group with higher-temperature overprint probably represented the "near-Veporicum" part of subducted Lower Paleozoic basin with the original position northward of spreading zone. *[Rocks of recent Rakovec Group, accepting this interpretation, represented the distant - opposite part of the Lower Paleozoic basin, i.e. southward of the spreading zone.]* This former position of rocks of Klátov Group allows to suppose that they belong among the first rocks affected by tectonometamorphism in generating subduction zone at the beginning with unstable thermal regime (big dispersion of K-Ar tectonometamorphic ages from amphibolites of Vyšný Klátov and Dobšiná areas with predominance of Upper Devonian ages; Cambel et al., 1990). By the same reason, the rocks of Klátov Group belonged among first exhumed rocks and served the clastogenic material for Carboniferous sediments of Črmeľ Group, and mainly, to Rudňany conglomerates. The early exhumation of rocks ranked to Klátov Group, serving clastogenic material for sediments of Črmeľ Group in Eastern Gemericum, was sedimentologically proved by M. Grecula (1998, Fig. 24 in l.c.).

The thickness of the rock column of Gelnica Group on its footwall icreased after exhumation (south-vergent overthrusting) of Rakovec Group rocks (+ Klátov Group and part of Westphalian) sediments. Thickness of the allochthonous (exhumed) body probably did not overreach 1 km. Despite, in collided terrane we suppose a bigger thickness of hanging wall due to the partial shifting of southern margin of converged basin (i.e. Gelnica Groupon ist former crystalline basement) into subduction slab, that caused the collisional ending of subduction-exhumation process. In collisional orogen there started the resetting of thermal régime and the deeply intrenched isograds into the zone of subduction slab started to be straightened.

The Permian period is therefore the era of thermal effects, with high probability tied with the presence of elongated thermal source of convectional heat beneath the collided terrane in the North-Gemeric zone (closed Rakovec basin with geosuture and mutually approached margins of the former basin, that is "Veporic" rocks in hanging wall and Gelnica Group rocks in footwall). The linear thermal source beneath the collided terrane represent the same heat source which primarily caused in Ordovician-Devonian spreading and divergence in the Lower Paleozoic basin. Its position beneath the collided terrane is a result of convergence and later subduction of former spreading zone. It is hardly expectable that lithospheric displacement above this thermal source could locate it to the opposite ("northern") side of subduction slab. The position of thermal axis results also from the reconstruction of the Western Carpathian Permian sedimentary basin and magmatic trends in this time period (cf. Vozárová a Vozár, 1987).

The increased thermal flow caused, besides other things, the thermal erosion of lithospheric slab beneath Gelnica Group as well as the higher-grade metamorphism of the rock sequences of the Gelnica Group. These were in previous evolution protected against the income of heat (from the time of their primary sedimentaion they were localized "southward" of the spreading zone, that is besides the axis of convectional heat). We suppose, that thermal processes in collisional orogene in this internal part of the Western Carpathians were sufficient for increase of thermal gradient and served enough heat for higher-temperature metamorphism, origin of Gemeric granites and metallogenic processes.

During later Permian evolution of the terrane of Inner Western Carpathians the trend of former convergence was probably preserved and the northward relative movement of lithospheric plate continued. This is the reason, why the continual shifting of the convectional heat axis to innermost zones of Gemericum (southward) is supposed. In the Gemeric region it was confirmed by younging of Gemeric granite from the north southwards *[Hnilec - 290 Ma (Kovach et al., 1986) and 282 Ma (Cambel et al., 1989); Betliar 272 Ma; Humel 270 and*

Fig. 3. Interpretation of the geodynamics of Inner Western Carpathians. GE - Gelnica Group, RA - Rakovec Group, KL - Klátov Group, C - Carboniferous rocks, P - Permian rocks. White arrows - direction of convergence, resp. divergence, black undulating arrows - axis of convective heat, black straight arrows - relative migration of collided terrane with respect of axis of convective heat. 1 - black phyllites of Betliar Fm., 2 - green phyllites of Smolník Fm., 3 - flysch - lower bed - in Smolník Fm., upper bed - the supreme parts of Hnilec Fm., 4 - intermediate and acid volcanoclastics of Hnilec Fm., 5 - effusive and extrusive products of basalt volcanism, locally with accompanying rocks, 6 - clastics of Rudňany Fm. and further Carboniferous and Permian clastics, 7 - effusive and extrusive products of basalt volcanism of Mesozoic evolution, locally with accompanying rocks.

Slovak Geol. Mag., 8, 3– 4(2002), 247 – 257

256

246 Ma; Zlatá Idka 251 and 223 Ma (Kovach et al., 1986)]. The similar effect is indicated also by the presence of best developed siderite-sulphidic veins directly in the North-Gemeric zone. These veins penetrate the suture zone often through the bondary zone of Gelnica Group, Rakovec Group, Carboniferous formations and Permian). Towards the south the vein parameters became worst. *Conductive overheating of the Lower Paleozoic rocks of Gemericum (Gelnica Group) was the most intensive in its lowermost horizons built up with the Betliar Fm., Holec Beds and the Lower variegated volcanic horizon. These served as the metal source for originating fluids entering into extensional structures above (detail aspects of this metallogenic process are stated in works by Radvanec, 1987 and Grecula et al., 1991). The "cover" position of rocks of Betliar Formation on rigid crystalline basement and beneath the soft overlier of the Gelnica Group protected them against tectonization in previous process of exhumation and south-vergent thrusting of Rakovec Group. In Permian era before the generation of ore veins started, the rocks of Betliar Fm. had been in the same deposition like during the sedimentation in Ordovician-Silurian era, that is, they were not affected by Pre-Permian orogenesis. All Pre-Permian (south-vergent) tectogenesis was accommodated by overlying Smolník and Hnilec Formations (Fig. 3)*

Alpine geodynamic evolution

The effects of Permian extension in Gemeric terrane, owing to the displacement of lithosphere above the axis of convectional heat, were gradually shifted from the north southwards. This is the reason why we suppose in Triassic-Jurassic era the slowing down the sedimentation in the North-Gemeric zone, and, on the contrary, the new spreading activity is supposed to start in the zone of the South Gemericum. The extension in the southern zone caused gradual disintegration of the continental crust and origin of the elongated Meliata-Hallstatt basin. The relics of the former basin after its clossure are represented by obducted marginal sequences of the Meliata basin, the Bôrka nappe (cf. Németh, 1996, Fig. 4 ibid.) and origin of geosuture in the Rožňava discontinuity zone, being indicated also by magnetoteluric profile of Pawliszyn (1978) in Grecula et al. (1995).

Later Alpine evolution after Upper Jurassic? convergence has been divided into four deformation phases:

Deformation phase AD_1 is tightly related to the closure of Meliata-Hallstatt basin with following succession of events: Closure of the basin and transport of the Bôrka nappe on Gemericum. Ongoing convergence caused not only the north-vergent imbrication of Lower Paleozoic rocks of former Variscan collisional terrane, but the Lower Cretaceous displacement of several kilometers thick rock pile of Gemericum northward on Veporicum. This process of detachment was allowed by the rheologically contrast horizon of the black schists of Betliar Fm. (Németh et al., 2001a), dividing rigid crystalline basement from the rocks of Gelnica Group.

We suppose that a part of former Betliar Formation (incl. Holec Beds) remained cut in its homeland. The

north-vergent imbrication in low-temperature brittle-ductile and brittle regime caused multiple repeating the Early Paleozoic lithology of Gemericum. Next consequence of north-vergent overthrust setting (indicated by white arrows in Fig. 1) was also the recent picture of distribution of zonality of Variscan metamorphism in Gemericum (cf. Radvanec, 1989, 1992; Faryad, 1991a, b, c). The overthrust setting destructed also the courses of Late-Variscan/Early-Alpine ore veins (cf. numerous examples in Grecula et al., 1990b, 1995; Grecula, 1982).

The Alpine Lower Cretaceous nappe displacement on Veporicum during AD_1 (Fig. 1) caused:

1. Truncation of northern depth continuation of Rakovec geosuture, and "retraction" of its lower parts below Gemericum. This "bended" course of depth continuation of flat body of heavy material was indicated also by the complex geological-geophysical profiles of the Project SGR-geophysics (Grecula and Kucharič, eds., 1992).

2. Thrusting of North-Gemeric zone on "Veporic ramp" caused elevation uplift ("vent") of this area in frontal parts of the nappe, its disintegration and later erosive removal of cover carbonates of the Stratená Group.

The Alpine nappe-overthrust piling of crustal material (the basement nappe) caused thickening of continental crust in the Western Carpatians and in Middle Cretaceous the unroofing of Veporic basement during phase AD_2 (Fig. 1 upper left and right).

Deformation phase AD_3 with the origin of conjugate systems of brittle-ductile and brittle shear zones of NW-SE and NE-SW trends (cf. Grecula et al., 1990a; Németh et al., 1997) caused arc bending of Gemericum, as well as the Lubeník-Margecany line, and *sensu lato* also of the whole Western Carpathians (Németh et al., 2001b).

Deformation phase AD_4 is a gradual continuation of AD_3. It reflects an orogen parallel extension in east-west direction. The crustal indentor for the whole Western Carpathians was directed northward to the South-Gemeric zone. The brittle deformation during AD_4 takes place in shallow crustal levels and prevailing structures are those of pure-shear (faults, joints).

Conclusions

Defining of Variscan geosuture in the North-Gemeric zone and microstructural proof of kinematics of representative rock types in the Gelnica and Rakovec Groups led to suggestion of modified model of Variscan tectonic evolution of Gemericum together with new interpretation of ore-veins generation.

We suppose, that thermal processes in collisional orogen in this internal part of Western Carpathians were sufficient for increase of temperature gradient, and served sufficient heat for higher-temperature metamorphism, origin of Gemeric granites as well as metallogenic processes in Permian era.

Conductive overheating of Lower Paleozoic rocks of Gemericum (Gelnica Group) was the most intensive in its lowermost horizons, built up by the Betliar Fm., Holec Beds and the Lower variegated volcanic horizon. Their position on rigid crystalline basement and beneath the

cover of overlying rocks of Gelnica Group protected them against tectonization during exhumation and south-vergent overthrusting of rocks of Rakovec Group. The rocks of Betliar Fm., Holec Beds and Lower variegated volcanic horizon served as the metal sources for generating of fluids (cf. Radvanec, 1987; Grecula et al., 1991). Fluids entered into originating extensional structures in overlying rock sequences.

The Cretaceous Alpine tectonics destructed former Variscan structures.

Geodynamics of Inner Western Carpathians from the beginning of Ordovician riftogenesis till Mesozoic is interpreted as the product of the thermal flow of the same convective heat. The divergence, resp. the changes of kinematics of crustal segments were caused by changes of mutual position of overlying crustal segments regarding the convective heat.

References

Cambel, B., Bagdasaryan, G. P., Gukasyan, R. C. & Veselský, J., 1989: Rb-Sr geochronology of leucocratic granitoid rocks from the Spišsko-gemerské rudohorie Mts. and Veporicum. Geol. Zbor. Geol. carpath., 40, 323-332.

Cambel, B., Kráľ, J. & Burchart, J., 1990: Isotope geochronology of crystalline basement of Western Carpathians. Veda, Bratislava, 183. (in Slovak)

Faryad, S. W., 1991a: Metamorphism of mafic rocks in the Gemericum. Mineralia slov., 23, 109-122. (in Slovak)

Faryad, S. W., 1991b: Metamorpism of Lower Paleozoic acid to intermediate volcanites of Gemericum. Mineralia Slov., 23, 325-332. (in Slovak)

Faryad, S. W., 1991c: Metamorphism of Lower Paleozoic sediments of Gemericum. Mineralia Slov., 23, 315-324. (in Slovak)

Fusán, O., Máška, M. & Zoubek, V., 1955: Some problems of stratigraphy of the Spiš-Gemer Ore Mts. Geol. Práce, Zpr., 2, 3-15. (in Slovak)

Grecula, M., 1998: Carboniferous of Črmelicum terrane, Western Carpathians: relict of a fore-arc basin within Alpide Variscides. Mineralia Slov., 30, 109-136.

Grecula, P., 1970: Gelnica series as the only Early Paleozoic representant of the Spiš-Gemer Ore Mts. Mineralia slov., 2, 181-190. (in Slovak)

Grecula, P., 1982: Gemericum - segment of the Paleotethyan riftogeneous basin. Mineralia Slov.-Monogr. Alfa, Bratislava, 263. (in Slovak with extended English resume)

Grecula, P., Návesňák, D., Bartalský, B., Gazdačko, Ľ., Németh, Z., Ištván, J. & Vrbatovič, P., 1990a: Shear zones and arc structure of Gemericum, the Western Carpathians. Mineralia Slov., 22, 97-110.

Grecula, P., Návesňák, D. & Bartalský, B., 1990b: Shear zones and types of deformation of ore veins in Gemericum, Western Carpathians. Mineralia Slov., 22, 111-122.

Grecula, P., Radvanec, M. & Bartalský, B., 1991: Critical thermic isograde in metamorphic-hydrothermal model of vein mineralization on the background of the Variscan events, Gemeric unit, Western Carpathians. Mineralia Slov., 23, 403-411.

Grecula, P. & Kucharič, Ľ., eds., 1992: Partial Final report from complex geological-geophysical interpretation of northern part of SGR. Manuscript, archives of GSSR, Bratislava, 199. (in Slovak)

Grecula, P. et al., 1995: Mineral deposits of the Slovak Ore Mts. Vol 1. Geocomplex, Bratislava, 1-829.

Hovorka, D., Ivan, P., Jilemnická, L. & Spišiak, J., 1988: Petrology and geochemistry of metabasalts from Rakovec (Paleozoic of Gemeric unit, inner Western Carpathians). Geol. Zbor., Geol. Carpath., 39, 395-425.

Chemenda, A.I., Mattauer, M. & Bokun, A.N., 1996: Continental subduction and a mechanism for exhumation of high-presure metamorphic rocks: new modeling and field data from Oman. Earth Planet. Sci. Lett., 143, 173-182.

Chemenda, A.I., Matte, Ph., & Sokolov, V., 1997: A model of Paleozoic obduction and exhumation of high-pressure/low-temperature rocks in southern Urals. Tectonophysics, 276, 217-242.

Kovách, A., Svingor, E. & Grecula, P., 1986: Rb-Sr isotopic ages of granitoid rocks from the Spišsko-gemerské rudohorie Mts., Western Carpathians, Eastern Slovakia. Mineralia Slov., 18, 1-14.

Németh, Z., 1996: First discovery of the Bôrka nappe in the eastern part of the Spiš-Gemer Ore Mts. Mineralia Slov., 28, 175-184. (in Slovak with English resume)

Németh, Z., 1999: Explanations to geological maps in the scale 1 :25 000, sheets M-34-113-B-d, M-34-114-A-c, M-34-114-A-d, M-34-114-B-c, M-34-114-B-d. Stadial report. Manuscript - archives GSSR, Bratislava.

Németh, Z., 2001: Petrotectonics of the ductile shear zones of Gemericum. Ph.D. thesis. Comenius Univ., Bratislava, 1-98.

Németh, Z., Grecula, P. & Putiš, M., 2001a: Lithotectonic relations in boundary zone of Gelnica and Rakovec Groups in the North-Gemeric zone. Geol. práce, Správy 105, 67-70. (in Slovak)

Németh, Z., Putiš, M. & Grecula, P., 2001b: Origin of the arc-bended boundary zone between Gemericum and Veporicum from the viewpoint of kinematics of Alpine extensional unroofing. Geol. práce, Správy 105, 65-66. (in Slovak)

Mello, J., ed., 2000: Explanations to geological map of Slovak Paradise, Galmus and Hornád basin. Dionýz Štúr Publishers, Bratislava, 298. (in Slovak with English summary)

Radvanec, M., 1989: Metamorphism of Early Paleozoic Gemeric rocks - middle part - Partial Final report of the project SGR-geophysics. Manuscript - archives GSSR.

Radvanec, M., 1992: Zonality of low-pressure and polyphase metamorphism in open system for fluid phase in the gneiss-amphibolite complex of Gemericum. Mineralia Slov., 24, 175-196. (in Slovak with English resume)

Radvanec, M., 1998: High-pressure metamorphism of Upper Carboniferous conglomerate from the locality Rudňany-Svinský hrb on the north of Gemericum. Mineralia Slov., 30, 95-108. (In Slovak with English resume)

Radvanec, M., 1999: Eclogitized clinopyroxenic gabbro with retrograde metamorphism in pumpellyite-actinolite facies on the hills Babiná and Ostrá (Gemerikum). Mineralia Slov., 31, 467-484. (in Slovak with English resume)

Rowe, K. J. & Rutter, E. H., 1990: Paleostress estimation using calcite twinning: experimental calibration and application to nature. J. Struct. Geol., 12, 1-17.

Vozár, J., Szalaiová, V. & Šantavý, J., 1998: Interpretation of the Western Carpathian deep structures on the basis of gravimetric and seismic sections. In: M. Rakús, ed.: Geodynamic development of the Western Carpathians. Dionýz Štúr Publishers, Bratislava, 241-257.

Vozárová, A. & Vozár, J., 1987: West Carpathians Late Paleozoic and its paleotectonic development. In: H. W. Flügel, F. P. Sassi & P. Grecula (red.): Pre-Variscan and Variscan events in the Alpine-Mediterranean mountain belts. Mineralia Slov. - Monograph, Alfa, Bratislava, 469-487.

Vozárová, A. & Vozár, J., 1988: Late Paleozoic in West Carpathians. GÚDŠ, Bratislava, 1-314.

New knowledge about stratigraphy of the eastern part of the Danube basin (Želiezovce Depression)

KLEMENT FORDINÁL[1], ALEXANDER NAGY, ADRIENA ZLINSKÁ[1],
MARIANNA SLAMKOVÁ[2], EVA HALÁSOVÁ[2] and INGRID TÖRÖKOVÁ[1]

[1]Geological Survey of Slovak republic, Mlynská dolina 1, 817 04 Bratislava, Slovakia
[2]Department Geology and Paleontology, Faculty of Natural Sciences, Comenius University,
Mlynská dolina G, 842 15 Bratislava, Slovakia

Abstract: In the eastern part of the Danube basin the Middle-Miocene filling of the Želiezovce Depression, Oligocene deposits and pre-Tertiary basement composed of metamorphic carbonates were drilled through by a geothermal borehole HGŽ-3 near village Želiezovce. The basement of the Neogene filling is composed of Lower Badenian deposits (conglomerates, coarse grained sandstones, sandy claystones), which are represented by the Bajtava Formation. They are overlain by deposits (epiclastic sandstones with intercalations of tuffites, sandy tuffitic clays, claystones with silty admixture, siltstones) of the Pozba Formation of Middle to Later Badenian age. Above them there were recognized beds of sandy deposits of the Vráble Formation of Sarmatian age. The above mentioned lithostratigraphic units were defined on the basis of rock lithology and biostratigraphic classification of the deposits according to present molluscs, foraminifers, ostracods and calcareous nannoplankton. The study of sporomorph revealed that during the Middle to Later Badenian there was warm and humid climate characteristic by the presence of hydrophilous vegetation. The presence of swampy vegetation is characteristic for the period of the Early Sarmatian.

Key words: Danube basinm,,Želiezovce Depression, pre-Tertiary basement, Oligocene sediments, Neogene sediments, grain size analysis, fauna, flora, biostratigraphy

Introduction

At the end of 80s of the 20th century in Želiezovce town the geothermal borehole HGŽ-3 (Bondarenková et al., 1990) was drilled. It was located at the eastern edge of the town, in the vicinity of the Hron river (Fig. 1). It was a regulas core borehole and ran through the Middle Miocene and Oligocene deposits and reached the pre-Tertiary basement.

With respect to the regional geological division the borehole HGŽ-3 is located the Trnava – Dubník Depression, which is a partial depression of the Danube Basin. Within this partial depression the borehole is located in the Želiezovce Depression (Vass et al., 1988).

Grain size analyses were carried out on the sedimentary material from the borehole. Molluscs, foraminifers, ostracods, otoliths, palynomorphs and calcareous nanoplankton were studied from the found fossil remnants. Based on the study of the mentioned fossil groups the sediments from the borehole HGŽ-3 were stratigraphically classified.

In the area of the Želiezovce Depression there are three Badenian faciestratotypes and one Sarmatian faciestratotype.

Borehole ŠO-1 is a faciestratotype of the Lower Badenian, it was drilled near the village Chľaba (Lehotayová & Ondrejičková, 1972; Ondrejičková, 1978), borehole K-5 is a faciestratotype of the Lower and Middle Badenian located near the village Salka (Brestenská, 1978a; Gabčo, 1965; Lehotayová, 1966; Planderová, 1966,
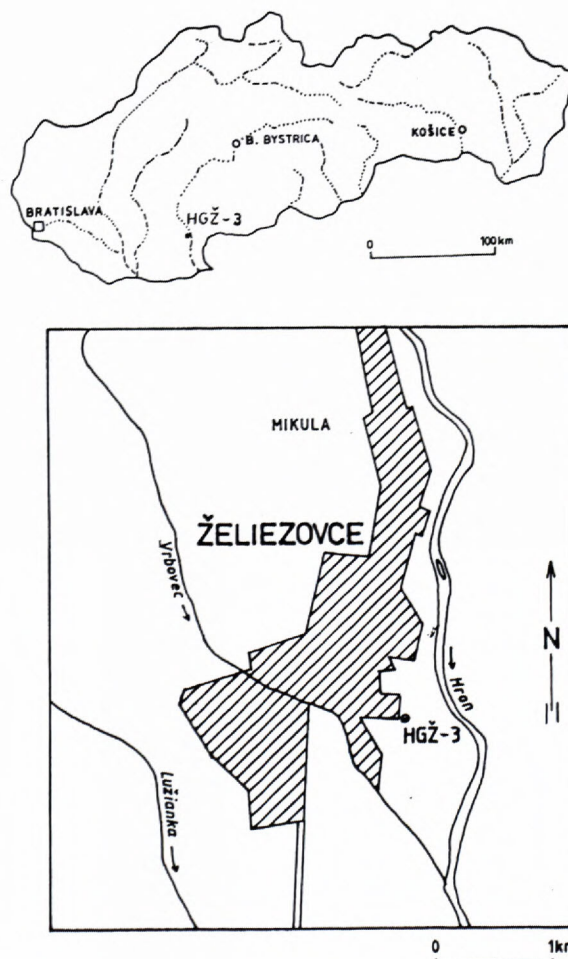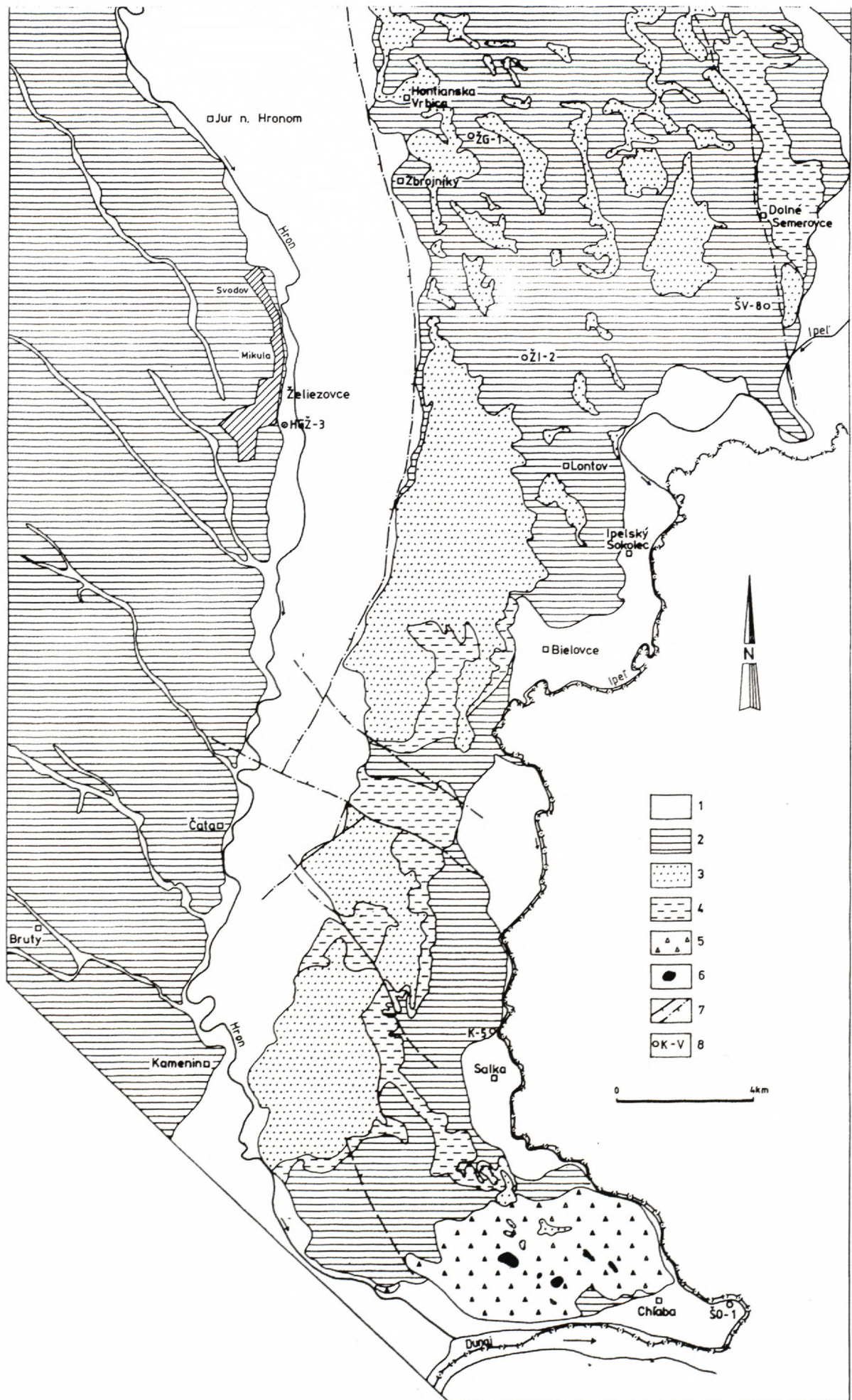

Fig. 1 Localization of the borehole HGŽ-3 ►

K. Fordinál, A. Nagy et al.: New knowledge about stratigraphy...

261

1966; Vass, 1964; 1966; Vass & Gabčo, 1966), borehole ŽI-2 is a faciestratotype of the Middle and Upper Badenian, which was located near the village Lontov (Brestenská , 1978b; Ivan, 1960; Mišík, 1958; Planderová, 1965a; Tejkal, 1968).

Borehole ŽG-1 is a faciestratotype of Sarmatian deposits. It is located near the village Hontianska Vrbica (Brestenská, 1974; Gabčo, 1969; Planderová, 1965b; Sitár, 1965; 1967; Švagrovský, 1965) (Fig. 2).

Beside the mentioned faciestratotypes also deep structural borehole ŠV-8 was sunly in vicinity of the borehole HGŽ-3 southward of the village Dolné Semerovce. The borehole was drilled through Neogene strata and it achieved the pre-Tertiary basement (Vass et al., 1981) (Fig. 2, 3).

By interpretation of the deposits from the borehole HGŽ-3 new information about rock composition and stratigraphy of the eastern part of the Danube basin (Želiezovce Depression) were obtained.

Review of geology of the Želiezovce depression

In the vicinity of borehole HGŽ-3 located in the Želiezovce Depression there are Sarmatian deposits outcropping, which are classified into so-called delta sedimentation (Nagy et al., 1998). In broader vicinity of the borehole south- and eastward there are also deposits of Badenian age (Fig. 2).

The oldest Neogene deposits of the Želiezovce Depression are of Lower Badenian age. They are represented by Turovce Member, what are pre-transgression deposits formed probably in near-shore delta environment (Marková in Vass et al., 1981). The mentioned deposits pass into marine deposits of the Bajtava Formation. In the lower part of the formation there are conglomerates, epiclastic volcanic sandstones and epiclastic volcanic claystones with layers of algal limestones representing peripheral deposits of the Börzöny stratovolcano. Toward the overlying beds these deposits pass into basin facies composed of gray slacking calcareous siltstones and claystones with shaly disintegration. The mentioned lutaceous deposits were deposited on circalittoral open shelf plain (Seneš & Ondrejičková, 1991). They are overlain by the Pozba Formation, which includes deposits of Middle to Upper Badenian age in sense of Kováč and Hók (in Hók et al. 1999). They are represented by epiclastic volcanic sandstones, gray calcareous clays with layers of fine- and medium grained sands, sandstones and in the marginal part organogenic sandy limestones (Nagy et al., 1998; Vaškovský et al., 1982).

The Sarmatian deposits from the vicinity of the village Želiezovce are characterized by the presence of coarse-detrital volcanic sedimentary rock of Baďany Formation and so-called delta sedimentation (Nagy et al., 1998), which southward are fining and pass into sandstones and calcareous lutaceous rocks of the Vráble Formation.

Eastward of the village Želiezovce the deposits overlying the Sarmatian (sands, clays, occasionally lignites) of Pannonian to Pontian age are found (Jiříček, 1982). They are represented by Ivanka and Beladice Formations (in sense of Fordinál et al., 2001).

Evaluation of the borehole HGŽ-3

The borehole HGŽ-3 penetrated through the complete Neogene sedimentary filling of the eastern part of the Želiezovce Depression resting on Paleogene (Oligocene) deposits. The borehole was finished in carbonate rocks of the pre-Tertiary basement.

Pre-Tertiary basement

The pre-Tertiary basement was reached in the depth interval 895,0-916.0 m. It consists of dark-gray slightly metamorphosed carbonate rocks with indistinct tectonic deformations which are manifested in the form of partly overslid and directed foliation planes. According to semi-quantitative analysis the groundmass is composed of Ca-Mg carbonate (Ca oxide 98.89 %, Mg oxide 30.69 %) with insignificant content of Fe (Fe oxide 0.41%). The cement is almost exclusively formed by Ca (Ca oxide 93.53 %) with little content of Fe (Fe oxide 1.47 %). Indistinct zonality that can be seen in the measured sample is probably the result of changes in pigmentatnion. A significant content of grains of pyrite reaching size from tenths of μm to 5 μm is present in the whole sample. The white veins are formed by crystalline $CaCO_3$.

The rocks, according to division of pre-Tertiary basement of the Danube Basin belong to the cover of the Southern Veporicum, in the sense of Vozár (in Matura et al., 2000).

Sedimentary filling

Paleogene (Oligocene)

Above metamorphic Mesozoic limestones in depth interval of 854.2 – 895.0 m there are firm gray organodetrical limestones to calcareous sandstones with clayey admixture and sporadical well rounded quartz pebbles. They are rich in fossil remnants. A sample from a depth 854.8-856.0 m (Fig. 4a, b) is composed of foraminifer-bryozoan microfacies. The basic (originally most likely micrite) is more or less re-crystallized. There is abundant re-crystallized detritus in it. The organic remnants are represented by common larger foraminifers, rare planktonic and thick-walled benthonic foraminifers, bryozoans or their fragments (some of them belong to rudite fraction by size), fragments of echinoderms, thick-walled bivalves, and coralinne algae. Mineral admixture is represented by quartz (occasionally with undulose extinction), pyrite, micas, and unidentified heavy mineral. There were

---

Fig. 2 Schematic map of eastern part of Želiezovce Depression with localization of faciestratotype facies boreholes and borehole ŠV-8.
Quaternary: 1 – fluvial deposits 2 – eolian deposits, **Neogene:** 3 – Sarmatian deposits (Vráble and Ladze Formations, Baďany Formation – "delta sedimentation") 4 Badenian deposits (Bajtava and Pozba Formations, Sebechleby Formation) 5 - volcanoclastics (Lower Badenian), 6 – pyroxene – amphibolic andesites, 7 – faults proved, assumed, 8 – borehole.
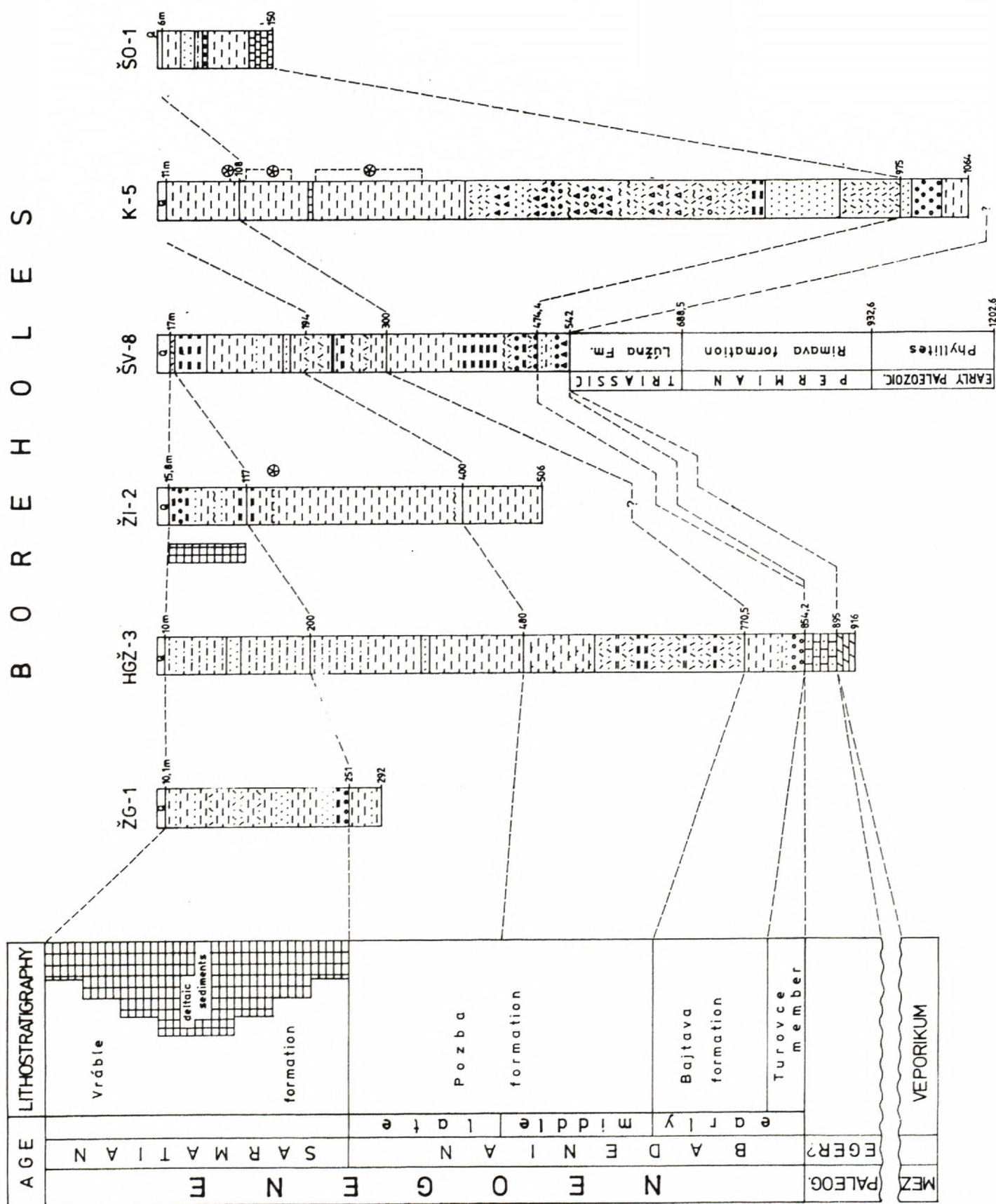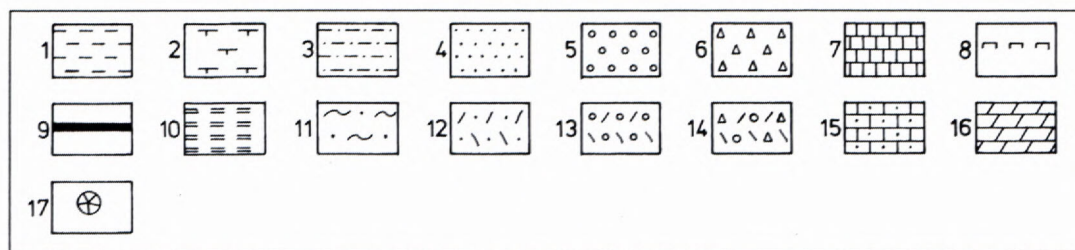
Fig. 3 Lithostratigraphy of borehole HGŽ-3 and its correlation with facie stratotype boreholes and deep structure bolrehole ŠV-8.

K. Fordinál, A. Nagy et al.: New knowledge about stratigraphy...

263

Neogene: 1 – clays, claystones, siltstones, 2 – claystones with silty admixtures, 3 – sandy clays, 4 – sands, sandstones, 5 – gravels, conglomerates, 6 – breccias, 7 – limestones, 8 – diatomite, 9 – lignite, 10 – epiclastic volcanic claystones, 11 – redeposited pyroclastics, 12 – epiclastic volcanic sandstones, 13 – epiclastic gravels with volcanic and non-volcanic material, 14 – epiclastic volcanic conglomerates, **Paleogene:** *15 – organodetrical limestones,* **Mesozoic:** *16 – metamorphosed carbonates, 17 – occurrences of diatomaceous tests*
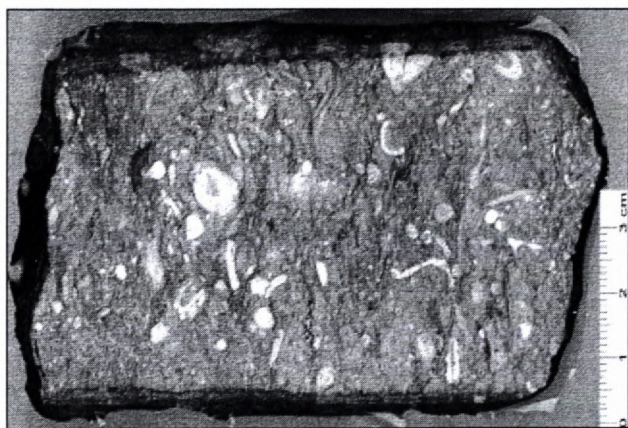
Fig. 4 Organodetrical Paleogene (Egerian?) limestone; a – borehole core from depth 854.8 – 855.0 m;
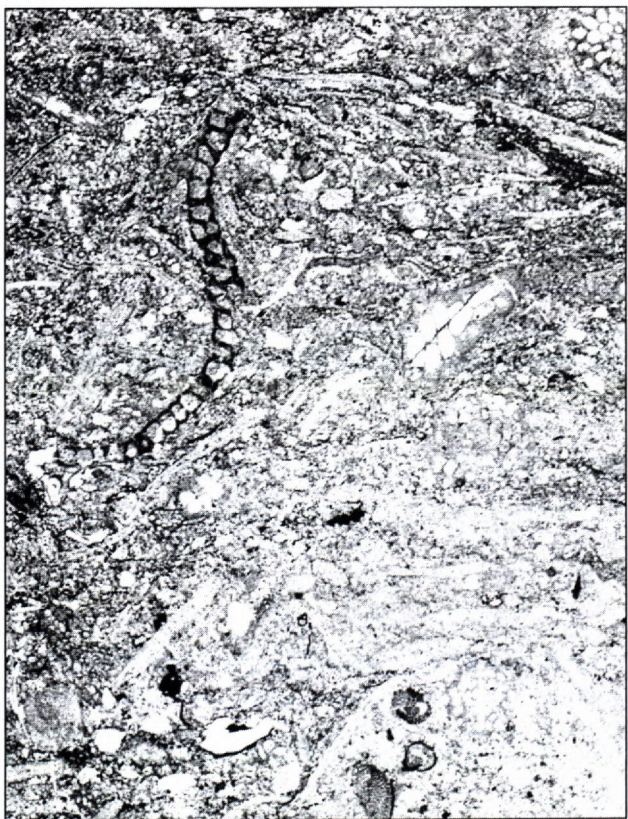
b – microphoto from the above mentioned core (dimensions of the thin section are 19.0 x 25.2 mm)

identified planktonic foraminifers of the genus *Globigerina* sp. and benthonic foraminifers *Planoperculina complanata* (DEFRANCE) and *Heterostegina* sp., which point to Oligocene, most likely Egerian age (determined by RNDr. E. Köhler, DrSc.). The occurrence of similar rocks is not known in the nearby vicinity and according to available information they do not také part are not in the complex of Štúrovo type Paleogene. Rocks of equal character and age were described as the Budikovany Member in the depressions of Lučenská kotlina and Rimavská kotlina (Vass, Elečko et al., 1989; 1992).

Neogene

The oldest Neogene deposits are located in depth interval 770.5 – 854.2 m. They are represented by the Bajtava Formation of Lower Badenian age. At the base of the formation there are conglomerates and coarse-grained sandstones, which are copying to carbonate rocks of the pre-Tertiary basement in their matter composition and they gradually pass into sandy claystones (Bondarenková et al., 1990).

Beds overlying the Bajtava Formation located in the depth interval 572.5 – 770.5 m are of Middle Badenian age. They consist of epiclastic sandstones, occasionally with intermediate layers of tuffites and sandy tuffaceous clays, and in the interval 480.0 – 572.5 of claystones with variable content of silty admixture.

The deposits of Middle-Badenian age pass without noticeable break to deposits of the Upper Badenian, which are located in depth interval 200.0 – 480.0 m. They consist of sandy clays and silts. The deposits of the Middle and Upper Badenian are part of the Pozba Formation in sense of Kováč and Hók (in Hók et al., 1999).

The deposits of the Pozba Formation are covered by deposits of the Sarmatian Vráble Formation occurring in depth interval 10.0 – 200.0 m. The base part (148.0 – 200.0 m) consists of sandy clays and silts with occasional intermediate layers of sands. In the middle part (90.0 – 148.0 m) sandstones are prevailing and the terminal part of the Vráble Formation (10.0 – 90.0 m) is formed by alternating clays, sandy clays and sandstones (Bondarenková et al., 1990).

The deposits were sampled for grain size analyses. The samples were taken from depth interval 50.2 – 552.3 m.

The samples from deeper intervals of the borehole HGŽ-3 are represented by coarse-grained silts. Upward the fractions become coarser-grained and passe to fine-

Slovak Geol. Mag., 8, 3– 4(2002), 259 – 281

264

Tab. 1 Values of grain size parameters of sediments from the borehole HGŽ-3 according to Folka and Ward (1957)

Depth (m)	Md (fí) F/W	Md (mm)	Mz (fí) F/W	So (fí) F/W	Sk (fí) F/W	Kg F/W	Characterization of sediments
50,2 - 50,3	2 903	0,027	3 562	1 856	0,524	1 061	very fine sand
56,7 - 56,8	3 641	0,018	3 966	1 114	0,330	1 127	very fine sand
151,7-152,0	3 591	0,031	3 813	1 292	0,345	1 727	very fine sand
155,0-155,3	4 466	0,0096	4 217	2 451	-0,116	0,683	coarse silt
253,5-253-6	3 763	0,023	4 160	1 577	0,366	1 412	coarse silt
350,2-350,3	2 599	0,13	2 735	1 602	0,159	1 429	very fine sand
355,8-355,9	5 048	0,0058	5 254	1 906	0,053	1 043	coarse silt
454,4-454,6	5 262	0,0041	5 458	1 701	0,126	0,859	medium silt
552,2-552,3	4 921	0,007	4 899	2 173	-0,074	0,905	coarse silt

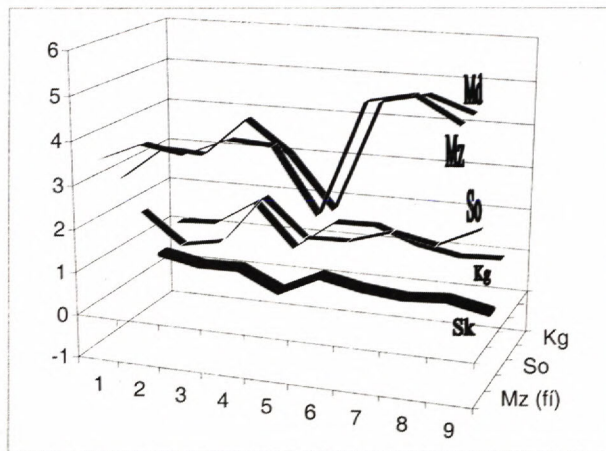*Md – median, Mz – average grain size, So – sorting coefficient, Sk – asymmetry value, Kg – kurtosis value.*

Fig. 5 Changes of grain size parameter values in the borehole HGŽ-3. Mz – average grain size, Md – median, So-sorting coefficient, Sk – asymmetry value, Kg-kurtosis value
x-axis represents depth: 1 – 50.2-50.3 m, 2 – 56.7-56.8 m, 3 – 151.7-152.0 m, 4 – 155.0-155.3 m, 5 – 253.5-253.6 m, 6 – 350.2-350.3 m, 7 – 355.8-355.9 m, 8 – 454.4-454.6 m, 9 – 552.2-552.3 m

grained sand, what generally suggests negative graded bedding of deposits (Fig. 5).

Grain size analysis (Tab. 1) of the deposits revealed that the average grain size (Mz) ranges from 2.735 (for fine-grained sand) to 5.458 (for medium-grained silt). According to Folk-Ward classification (1957) the sands and silts are slightly to weakly sorted and the sorting coefficient ranges 1.114 – 2.451.

The asymmetry of the cumulative grain size curve indicates either prevalence of fine-grained (positive values) or prevalence of coarse-grained fraction in the deposit. The asymmetry values (Sk) of the cumulative curve of the borehole HGŽ-3 are positive or near to zero in most samples, what suggests that the deposits contain a greater portion of finer-grained fraction and coarser particles are scattered in various grain size fractions. Two samples have negative values, they contain greater portion of coarser-grained fraction, what is also reflected by their very poor sorting.

The kurtosis values (Kg) suggest more on platykurtic (flat), less on very leptokuritc (steep) shapes of the cumulative curve, characterizing prevalence of fine-grained particles in the deposits.

The median (Md) ranges from 0.0041 to 0.13 mm and its values vary in the profile and at the same time increase toward the overlying part due to increasing portion of coarser grains, and so indicate a negative graded bedding.

Fauna

Mollusca

The borehole has poor content of molluscan fauna. The following fauna was identified: bivalves *Cardium* sp. (55.4 – 55.5 m; 152.8 – 153.0 m; 154.0 – 154.1 m; 154.1 – 154.5 m), *Ervilia* sp. (154.1 – 154.5 m), *Musculus sarmaticus* (GATUJEV) (152.8 – 153.0 m), and gastropods of *Mohrensternia* genus (152.8 – 153.0 m).

The presence of gastropods of *Mohrensternia* genus in depth 152.8 – 153.0 m enables to classify the fossil-bearing deposit among to the so-called Rissoa beds of the Lower Sarmatian (Papp, 1954).

Foraminifera
(Phototable I to III)

In the deposits of the borehole HGŽ-3 there was found relatively a rich association of foraminifers (Tab. 2).

In depth interval 20.0 – 55.1 m there were found siliceous and calcareous spicules of sponges (axisless, one and more axes) and re-deposited foraminifers from older Neogene stages.

A Lower Sarmatian micro-association with dominance of elfidia, however without typical form *Elphidium reginum* (ORB.), was found in depth 150.4 – 155.5 m. There are present *Elphidium flexuosum flexuosum* (ORB.), *E. rugosum* (ORB.), *Bolivina sarmatica* DIDK., "*Cibicides badenensis*" (ORB.), *Lobatula lobatula* (W.- J.), *Ammonia beccarii* (L.), for example The foraminifers are associated with centric, especially pyritizated diatoms.

In certain parts of the interval 250.4 – 457.6 m there is dominance of Bolivina-Bulimina association of foraminifers, which is typical for the Upper Badenian with occurrence of species *Bulimina elongata elongata* ORB., *Valvulineria complanata* (ORB.), *Bolivina dilatata dilatata* RSS., *Caucasina schischkinskayae* (SAMOILOVA), *Bolivina dilatata maxima* C.-Z., *Fursenkoina acuta* (ORB.), *Praeglobobulimina pupoides* (ORB.), *Praeglobobulimina ovula* (ORB.), *Bulimina elongata longa* (VENGL.), *Bolivina hebes* MACF., *Bolivina kodymi* C.-Z., *Bolivina pokornyi pokornyi* C.- Z., *Globigerina druryi*

Tab. 2 Occurrence of foraminifers in borehole HGŽ-3

Foraminifera	150,4-150,5 m	151,5-151,8 m	152,6-152,8 m	152,8-153,0 m	154 m	154,0-154,1 m	154,5-155,0 m	154,6-154,7 m	155,5 m	250,4 m	250,5-250,6 m	251,8 m	252,5-252,6 m	254,3-254,4 m	254,8 m	353,9 m	355,8 m	450,6 m	451,5 m	452,7-452,8 m	453,3 m	456,0-456,2 m	457,5-457,6m	550,2 m	551,4 m	559,1 m	650,9 m	652,4-652,6 m	654,7-654,8 m	801,5-801,6 m	852,6-852,8 m	853,4-853,6 m
	1	2	3	4	5	6	7	8	9	10	11	12	13	14	15	16	17	18	19	20	21	22	23	24	25	26	27	28	29	30	31	32
Allomorphina trigona Rss.																								x	x	x		x				
Ammonia beccarii (L.)	x	x		x		x					x	x			x		x	x											x			
Angulogerina angulosa (Williamson)											x																					
Asterigerinata planorbis (Orb.)	x									x	x	x			x															x		
Bolivina dilatata brevis C.-Z.																							x									
Bolivina dilatata dilatata Rss.										x		x			x	x	x															
Bolivina dilatata maxima C.- Z.											x				x	x	x			x		x										
Bolivina ex gr.dilatata Rss.														x							x											
Bolivina hebes Macf.															x																	
Bolivina kodymi C.- Z.															x																	
Bolivina plicatella Cush.																									x							
Bolivina pokornyi pokornyi C.- Z.																	x		x													
Bolivina sarmatica Didk.	x																															
Bolivina scalprata retiformis Cush.																								x								
Bolivina aff. vienensis Marks																									x							
Bolivina sp.																	x		x						x						x	x
Bolivina sp. / cf. B.sinuosa (Cush.) /																						x										
Budashevaella willsoni (Smith)																									x							
Bulimina aculeata Orb.																								x								
Bulimina cf.aculeata Orb.																				x												
Bulimina elongata elongata Orb.						x					x	x	x		x			x		x	x	x			x							
Bulimina elongata longa (Orb.)													x		x					x												
Bulimina elongata Orb.																		x	x			x					x					
Bulimina insignis Luczkowska																						x										
Bulimina striata striata Orb.																									x	x				x		
Bulimina striata mexicana Cush.																								x								
Cassidulina laevigata Orb.											x				x										x							
Cassidulina oblonga (Rss.)																								x								
Caucasina schischkinskayae (Samoil.)											x						x	x		x			x									
Cibicides badenensis (Orb.)	x																															
Cibicides sp.									x									x							x							
Cibicidoides pseudoungerianus (Cush.)																								x	x	x					x	
Cibicidoides ungerianus (Orb.)																								x	x		x					
Cribrostomoides columbiensis columbiensis (Cush.)														x																		
Cribrostomoides sp.																								x								
Cycloforina contorta (Orb.)																					x											
Elphidium crispum (L.)	x					x	x																									
Elphidium ex gr.flexuosum (Orb.)										x																						
Elphidium fichtelianum (Orb.)			x	x		x											x					x										
Elphidium flexuosum flexuosum (Orb.)	x			x	x																											
Elphidium granosum (Orb.)										x																						
Elphidium macellum (F.-M.)	x					x	x	x	x				x																			
Elphidium obtusum (Orb.)				x	x		x		x																							

Tab. 2 (continuation)

	1	2	3	4	5	6	7	8	9	10	11	12	13	14	15	16	17	18	19	20	21	22	23	24	25	26	27	28	29	30	31	32
Elphidium rugosum (Orb.)	x	x		x	x	x	x	x	x																							
Fissurina sp.						x					x																					
Frondicularia sp.						x																										
Fursenkoina acuta (Orb.)											x	x	x					x		x	x	x	x	x	x			x				
Globigerina aff. apertura Cush.																									x							
Globigerina apertura Cush.											x																					
Globigerina bulloides Blow										x	x	x			x	x	x	x		x	x		x		x	x						
Globigerina concinna Rss.						x					x				x		x	x						x								
Globigerina diplostoma Rss.																									x							
Globigerina druryi Akers																		x														
Globigerina nepenthes Todd																									x							
Globigerina praebulloides Blow											x					x				x					x							
Globigerina quinqueloba Natland																									x							
Globigerina regularis Orb.																							x									
Globigerina sp.														x	x												x			x		
Globigerina tarchanensis Subb.- Chutz.											x														x							
Globigerinella obesa (Bolli)										x	x					x			x						x	x						
Globigerinella regularis (Orb.)																									x							
Globigerinoides quadrilobatus (Orb.)																			x		x		x		x	x						
Globigerinoides sp.																		x														
Globigerinoides subsacculifer Cita - Premoli-Silva - Rossi																				x												
'Globigerinoides trilobus (Rss.)				x		x					x				x		x	x	x	x		x	x	x	x	x	x			x	x	x
Globoquadrina altspira (Cush.-Jarvis)																								x						x		
Globoquadrina larmeuti Akers																								x								
Globorotalia bykovae bykovae (Aisenstat)																	x															
Globorotalia sp.														x					x													
Guttulina communis Orb.																								x	x							
Hansenisca soldanii (Orb.)											x													x	x	x						x
Hanzawaia boueana (Orb.)										x	x																					
Haplophragmoides vasiceki vasiceki C.- Z.																		x	x					x		x						
Haplophragmoides ex gr. vasiceki C.-Z.												x																				
Haplophragmoides sp.																			x													
Heterolepa dutemplei (Orb.)													x					x	x	x	x	x	x		x	x			x			x
Lagena acuticosta Rss.														x																		
Lagena hispida Rss.											x																					
Lenticulina cultrata (Montf.)																								x								
Lenticulina sp.																										x						
Lobatula lobatula (W.- J.)	x	x					x												x													
Melonis pompilioides (F.-M.)																															x	
Nodosaria sp.																			x													
Nonion commune (Orb.)						x					x	x	x		x		x	x		x		x	x				x	x	x	x		
Nonion sp.										x																						
Orbulina suturalis Broenn.						x												x	x	x			x							x		x
Pappina bononiensis compressa (Cush.)											x													x								
Pappina bononiensis primiformis (P.-T.)											x																					
Paragloborotalia? mayeri (Cush.-Ell.)												x																				
Plectofrondicularia digitalis (Neugeb.)											x						x															
Praeglobobulimina ovula (Orb.)											x	x																				
Praeglobobulimina pupoides (Orb.)											x							x		x	x	x		x	x	x						
Praeglobobulimina pyrula (Orb.)													x							x			x									

K. Fordinál, A. Nagy et al.: New knowledge about stratigraphy...

267

Tab. 2 (continuation)

	1	2	3	4	5	6	7	8	9	10	11	12	13	14	15	16	17	18	19	20	21	22	23	24	25	26	27	28	29	30	31	32
Praeorbulina glomerosa (Blow)																										x				x		
Protelphidium bogdanowiczi (Volosh.)			x																												x	
Pullenia bulloides (Orb.)											x						x							x	x	x		x	x			x
Pullenia quinqueloba (Rss.)																								x								
Quinqueloculina sp.												x							x													
Reophax sp.																			x					x								
Reticulophragmium venezuelanum (Maync)																									x							
Sphaeroidina bulloides Orb.																			x			x			x	x						
Spiroloculina canaliculata Orb.																									x							
Spiroplectinella acuta (Rss.)																										x						
Spiroplectinella carinata (Orb.)																						x			x	x						
Stilostomella adolphina (Orb.)											x																					
Stilostomella advena (Cush.- Laim.)											x																x					
Stilostomella sp.														x	x																	
Melonis pompilioides (F.-M.)														x	x																	x
Subbotina aff.cognata (Pishv.)																			x			x										
Trifarina bradyi Cush.																																
Uvigerina aculeata aculeata Orb.																			x													
Uvigerina aculeata orbignyana Czjz.																									x				x			
Uvigerina ex gr.semiornata Orb.																																
Uvigerina macrocarinata P.-T.																															x	
Uvigerina semiornata brunensis Karrer																										x						
Uvigerina semiornata kusteri von Daniels-Spiegler																x										x						
Uvigerina semiornata semiornata Orb.																x									x	x					x	
Uvigerina sp.										x										x												
Valvulineria complanata (Orb.)												x					x					x			x	x	x					
Valvulineria marmaroschensis Pischv.																			x	x							x					x

AKERS, *Valvulineria marmaroschensis* PISHV., *Bolivina dilatata brevis* C.-Z., *Bulimina insignis* LUCZKOWSKA.

In depth 551.4 m the calcareous plankton is represented by *Globigerina nepenthes* TODD, limited to the Middle Badenian (Wieliczkan) and the calcareous benthos is represented by *Uvigerina aculeata orbignyana* CZJZ.

In depth 801.5 – 801.6 m *Praeorbulina glomerosa* (BLOW) was determined in the central Paratethys, which was extended only in the lower part of the Lower Badenian (Moravian) and in depth 852.6 – 852.8 m *Uvigerina macrocarinata* P.-T., the range of which in the central Paratethys is limited to the Lower Badenian only.

In depth 453.3 m the planktonic constituent has 98 % abundance in the microfauna, what suggests very good communication between deposition the sedimentation area basin and open sea.

Ostracods
(Phototab III, fig. 1)

Only scattered ostracod shells were identified in the borehole sediments. *Cytheridea hungarica* ZÁLANYI (154.0 m; 154.5 – 155.0 m) and *Henryhowella asperrima* (REUSS) (551.4 – 551.5 m).

The presence of species *Cytheridea hungarica* ZÁLANYI indicates the Lower Sarmatian age of the deposits (biozone Cytheridea hungarica - Aurila mehesi, Zelenka, 1990) and the species *Henryhowella asperrima* (REUSS) on Karpathian to Badenian age (Brestenská & Jiříček, 1978).

Calcareous nannoplankton
(Phototable IV)

In the deposits of the borehole HGŽ–3 there were determined association of calcareous nannoplankton, which are characteristic by poor preservation and content of redeposited species (of Upper Cretaceous, mainly Eocene age). The Miocene forms are rare, however, their redeposition into younger Miocene deposits was established (for example *Sphenolithus heteromorphus* DEFLANDRE in depth 250.5 – 250.6 m, *Cyclicargolithus floridanus* (ROTH & HAY) BUKRY in depth 52.5 – 52.6m, *Helicosphaera waltrans* THEODORIDIS in depth interval 154.6 – 154.7 m). In the samples from this borehole there was observed the presence of abundant diatoms and silicisponges (Tab. 3).

The individual positive samples can be evaluated as follows:

In sample from depth 52.5 – 52.6 m there was found a mixture of poorly preserved nannofossils. There were determined redeposited specimens of Eocene? – Miocene age.

The deposit from depth interval 154.6 – 154.7 m contains calcareous nannofossils occurring in Eocene and Lower Miocene horizons. Only one etched specimen of *Discoaster* sp. (resembling *Discoaster bollii* BRAMLETTE & MARTINI) was found.

The deposit is rich in diatoms and silicisponges. The sample from the depth interval 250.5 – 250.6 m is the In the samples from the depth 250.5 – 250.6 m and 251.8 m, 254.8 m there were determined nannofossils of Upper Cretaceous, Eocene and Lower Badenian age – *Helicosphaera waltrans* THEODORIDIS (NN5), *Sphenolithus*

Tab. 3 Occurrence of calcareous nannoplankton in borehole HGŽ-3

Calcareous nannofossils	52,6-52,7 m	154,6-154,7 m	250,5-250,6 m	251,8 m	254,8 m	457,5-457,6 m	652,4-652,6 m	654,7-654,8 m	704,8-704,9 m	801,5-801,6 m	852,6-852,8 m	853,4-853,6 m
Braarudosphaera bigelowi (Gran & Braarud) Deflandre		x	x	x								x
Calcidiscus leptoporus (Murray&Blackmann) Loeblich & Tappan	x	x	x	x		x	·	x	x			x
Coccolithus miopelagicus Bukry	x	x	x	x	x	x			x	x		
Coccolithus pelagicus (Wallich) Schiller	x	x	x	x	x	x	x	x	x	x	x	x
Coccolithus sp.	x		x						x			
Cyclicargolithus floridanus (Roth & Hay) Bukry	x	x	x	x	x	x	x	x	x			
Umbilicosphaera rotula (Kamptner) Varol	x	x	x	x	x	x	x	x				
Dictyococcites bisectus (Hay, Mohler & Wade) Bukry & Percival	x	x	x	x	x	x	x		x			
Discoaster deflandrei Bramlette & Riedel		x										
Discoaster sp.		x	x									
Helicosphaera obliqua Bramlette & Wilcoxon			x									
H. scissura Miller			x	x								
Helicosphaera carteri (Wallich) Kamptner	x	x	x	x	x	x	x	x	x			
Helicosphaera waltrans Theodoridis			x									
?Litostromation perdurum Deflandre			x									
Micrantholithus vesper Deflandre			x	x		x						x
Pontosphaera multipora (Kamptner) Roth		x	x	x	x	x	x					
Pontosphaera sp.		x	x	x	x		x					
Reticulofenestra pseudoumbilicus (Gartner) Gartner	x	x	x	x	x	x	x	x	x	x		
Reticulofenestra sp.		x	x			x	x					
Sphenolithus abies Deflandre			x			x						
S. heteromorphus heteromorphus Deflandre			x					x	x		x	x
Sphenolithus moriformis (Brönnimann & Stradner) Bramlette & Wilcoxon		x	x			x		x	x	x	x	x
Syracosphaera pulchra Lohmann			x			x			x			
Thoracosphaera sp.	x											
Reworked Paleogene nannofossils												
Cruciplacolithus tenuis (Stradner) Hay & Mohler			x	x								
Cribrocentrum reticulatum (Gartner & Smith) Perch-Nielsen		x										
Coccolithus formosus (Kamptner) Wise	x	x	x	x		x		x	x			x
Lanternithus minutus Stradner			x									
Pontosphaera enormis (Locker) Perch-Nielsen			x									
Reticulofenestra umbilica (Levin) Martini & Ritzkowski		x				x						
Tribrachiatus orthostylus Shamrai		x										
Transversopontis sp.		x										
Zygrhablithus bijugatus (Deflandre) Deflandre		x				x		x	x			x
Reworked Cretaceous nannofossils												
Arkhangelskiella cymbiformis Vekshina			x									
Broinsonia parca parca (Stradner) Bukry						x						
Micula decussata Vekshina			x	x		x						
Octolithus multiplus (Perch-Nielsen) Romein			x	x	x							
Quadrum gartneri Prins & Perch-Nielsen									x			
Reinhardtites anthophorus (Deflandre) Perch-Nielsen						x						
Zeugrhabdotus embergeri (Nöel) Perch-Nielsen			x									
Diatemecea			x					x	x			

K. Fordinál, A. Nagy et al.: New knowledge about stratigraphy...

269

heteromorphus DEFLANDRE (NN4-NN5), which in autochthonous position are present together in zone NN5. richest fromf the whole profile; it has the best degree of preservation.

Deposits from the depth 457.5 – 457.6 m contain nannofossils of Upper Cretaceous, Eocene and Miocene age. The prevailing species is *Coccolithus pelagicus* (WALLICH) SCHILLER. From Miocene species were determined: *Calcidiscus leptoporus* (MURRAY & BLACKMANN) LOEBLICH & TAPPAN, *Umbilicosphaera rotula* (KAMPTNER) VAROL, *Reticulofenestra pseudoumbilicus* (GARTNER), *Sphenolithus abies* DEFLANDRE.

In depth 652.4 – 652.6 m there was determined a poor association of calcareous nannoplankton with forms that are known since the Eocene and Oligocene and which become extinct in the Miocene. The only determined Miocene specie were *Umbilicosphaera rotula* (KAMPTNER) VAROL, of which the stratigraphic range is NN2-NN16 and *Reticulofenestra pseudoumbilicus* (GARTNER) GARTNER (NN4-NN15).

Similarly it is with the sample from the depth 654.7 – 654.8 m, which contained the species *Sphenolithus heteromorphus* DEFLANDRE indicating the zone NN5. The deposit contains a large amount of diatoms.

The sample from the depth interval 704.8 – 704.9 m reveals a poor association with low degree of preservation, with Miocene elements as *Calcidiscus leptoporus* (MURRAY & BLACKMANN) LOEBLICH & TAPPAN, *Sphenolithus heteromorphus* DEFLANDRE, *Reticulofenestra pseudoumbilicus* (GARTNER) GARTNER, which suggest the presence of nannoplankton zone NN5.

In the depth interval 801.5 – 801.6 m there was observed a very poor association of nannoflora, which was insufficient for stratigraphic classification.

The sample from the depth 852.6 – 852.8 m, 853.4 – 853.6 m was poor in association of calcareous nannoplankton. The most numerous species is *Coccolithus pelagicus* (WALLICH) SCHILLER and other Paleogene forms. From the biostratigraphic point of view the most significant species is *Sphenolithus heteromorphus* DEFLANDRE, pointing to zone NN5, as no specimens of *Helicosphaera ampliaperta* BRAMLETTE & MARTINI, *H. mediterranea* MÜLLER, *H. scissura* MILLER etc. were found.

In the interval 853.6 m – 654.7 m the associations of calcareous nannoplankton correspond to zone NN5. It is confirmed by occurrences of biostratigraphically most significant nannofossil *Sphenolithus heteromorphus* DEFLANDRE, without accompaniment of nannofossils typical for zone NN4. This index nannofossil was redeposited also to younger horizon (interval 250.5 – 250.6 m).

In smaller depth intervals there were not found any index nannofossils, which would allow stratigraphic classification of the deposit to the Middle of Upper Badenian. In the samples no discoastersy, were found which are common in zones NN5 and NN6 and are typical for the environment of open ocean. On the other hand, the identified foraminifer associations make possible to establish of the Middle and Upper Badenian and in the Upper Badenian there were recognized up to 98 % of planktonic constituent constituent contact with the open sea. It means, that nannoflora association could have been decimated by the influence of diagenesis in lithologically unsuitable
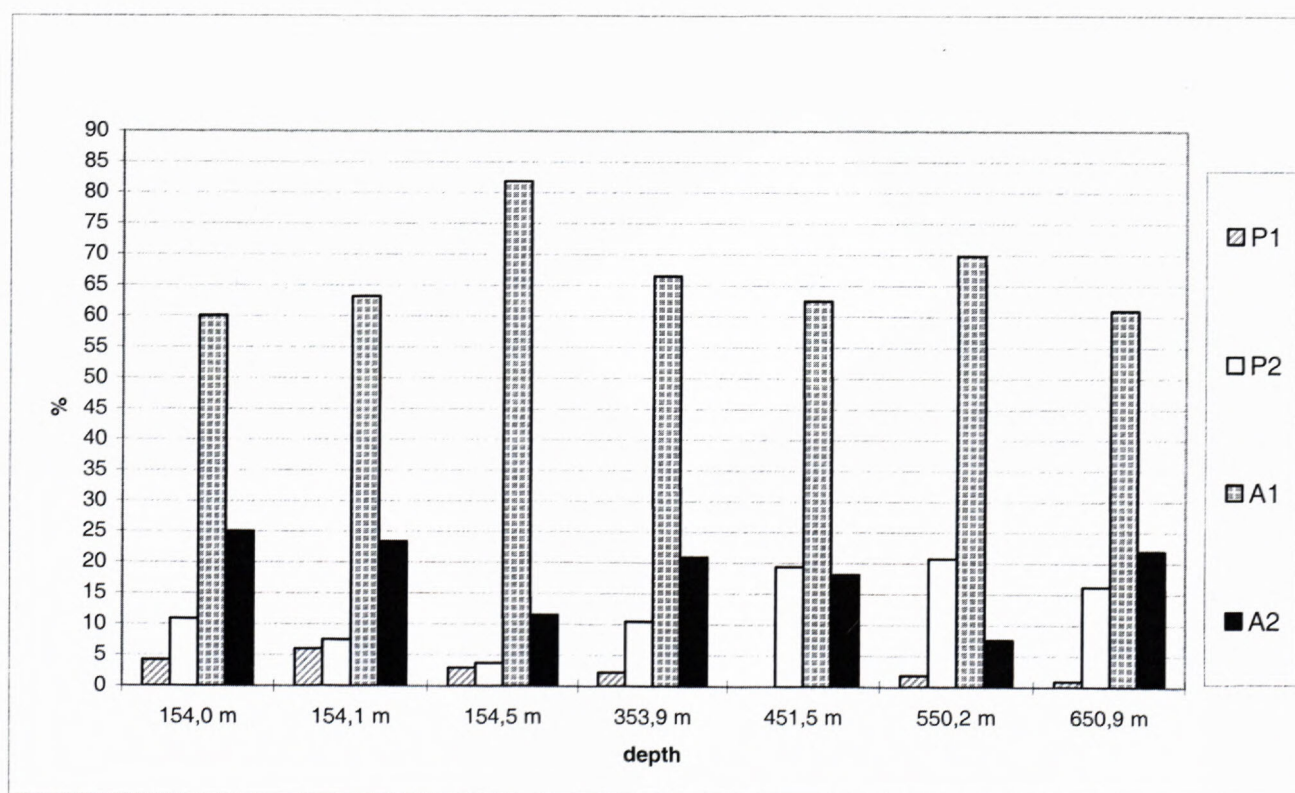

Fig. 6   Share of arctotertiary and paleotropic elements in palynospectrum of the borehole HGŽ-3
P1- paleotropic geoflora (tropical zone) P2- paleotropic geoflora (sub-tropic zone) A1 – arctoctertiary geoflora (warm temperature zone) A2 – arcoictertiary geoflora (cold temperature zone)

270

Slovak Geol. Mag., 8, 3– 4(2002), 259 – 281

environment (high in Si content in deposits – as proved by the presence of abundant of diatoms and silicisponges in preparations used for the study of calciferous nanno-plankton.

Otoliths

In the borehole there were found also remains of fish in form of otoliths (determined by Prof. RNDr. R. Brzobohatý, CSc.) The identified species were *Gadiculus* sp. (juv.), *Physiculus* sp. (juv.) from depth 452.7 – 452.8 m and *Diaphus* ex. gr. *debilis* (KOK.), *Photichtys* sp., *Bregmaceros* sp. from depth 551.4 – 551.5 m.

Sporomorphs
(Phototable V – VII)

Sporomorphs from the borehole HGŽ-3 were also studied. Relatively poor palynospectrum was obtained (Tab. 4).

In assignment of the taxons into individual geoflora type and into their corresponding climatic zones the terminology by Engler (1879; 1882) was used. He introduced the terms paleotropical (P) and arctotertiary (A) geoflora. According to terminology by Mai (1981; 1991) a paleotropic elements are considered evergreen plants genetically belonging into tropical (P1) and subtropical (P2) climatic zones in which their recent equivalents can be found. The arctotertiary type geoflora is characterized by coniferous and deciduous species partly defoliating, genetically belonging to warm temperate (A1), or cold temperate (A2) zones in which their recent equivalents can be found. Expression of the proportion between tree (AP) and non-tree (NAP) plant forms can suggest much about degree of afforestation of the studied locality in the given time sedion.

In depth 154.0 m the palynospectrum of sample is dominated by elements of arctoctertiary geoflora, mainly representatives of the group A1 (*Taxodium, Alnus, Pinus, Carya, Junglans, Nyssa*), less from the group A2 (*Picea, Ulmus, Corylus, Salix, Tilia*). Paleotropical geoflora is present in less amounts, in greater proportion there are present only subtropical elements of the group P2 (*Castanea, Myrica, Ilex*). Tropical plants from group P1 (*Engelhardtia*) have minimum extent (Fig. 6). It is obvious from the ratio of AP/NAP forms that the tree species were prevailing.

The sample from the depth 154.1 m contains dominantly elements form arctotertiary geoflora, the portion of elements from group A1 slightly increased and the portion of elements from group A2 slightly decreased. The share of paleotropical geoflora was reduced by half. A slight increase was recorded in herbaceous forms at the expense of wood plants. Beside sporomorphs also a representative of phytoplankton was present: (Dinoflagellata) species *Deflandrea spinulosa*, typical for Oligocene (Hudáčková in Halásová et al., 1996).

The sample from the depth 154.5 m is interesting by extraordinary high portion of arctotertiary geoflora of group A1 (*Taxodium, Pinus, Chenopodium, Alnus*), from group A2 there were determined *Picea, Abies* and *Ulmus*. Representation of paleotropical geoflora of groups P1 and P2 was minimum. In this depth, in comparison with other

samples, there was determined the largest portion of herbs from NAP (Chenopodiaceae, Gramineae). In the sample there was also a representative of dinoflagellates *Achomosphaera* sp.

In the sample from the depth 353.9 m the portion of arctotertiary geoflora of group A2 (*Ulmus, Salix, Fagus*) increased by one third in comparison to the preceding sample (154.5), on the contrary, the group A1 recorded lower percentage. The elements of paleotropical geoflora of group P2 (*Castanea, Myrica*) are more abundant than in the preceding sample. From the ratio AP/NAP the significant dominance of AP forms is obvious. The portion of the herbal part significantly decreased in comparison with the preceding sample. The dinoflagellates are represented by *Achomosphaera* sp. and *Spiniferites* cf. *bentori*.

In the palynospectrum from the depth 451.5 m there were dominating elements from arctotertiary geoflora, mainly from group A1. Groups P2 and A2 were represented quantitatively nearly equally.

Absence of elements from group P1 (tropical flora) is interesting. The genera *Ulmus, Pinus, Alnus, Myrica, Castanea* were abundant to very abundant. *Salix, Carya* were common. The portion of herbal component increased only slightly (Gramineae).

In depth 550.2 m the portion of elements from the group A2 decreased and representatives of tropical flora P1 there occur again in minium amount. The abundance of the paleotropical geoflora of the group P2 increased only slightly, similarly was increased the portion of arctotertiary elements from the group A1. Portion of the herbal component of the spectrum was increased again insignificantly only. The dinoflagellates are represented by the genus *Distatodinium*.

In the sample from the depth 650.9 m the relative portion of AP/NAP has not changed. However, the increase of portion of the arctotertiary elements of group A2 along with decrease of portion of elements from the groups P1 and P2 is interesting. The genera *Pinus, Alnus, Myrica, Salix* and *Ulmus* were very abundant here.

According to the mentioned paleoflora data we can conclude that during the formation of the studied deposits there was warm subtropic climate.

Macroflora

In the deposits from the depth of 52.5 – 52.6 m an imprint of a leaf *Carpinus grandis* UNGER (determined by Doc. RNDr. V. Sitár, CSc) was found.

Characteristics of the neogene lithostratigraphic units

The results of the study of the individual fossil groups of organisms served for classification of the Neogene deposits from the borehole HGŽ-3 into the defined lithostratigraphic units (Priechodská in Harčár et al., 1988; Vass in Keith et al., 1994; Kováč & Hók in Hók et al., 1999).

The presence of foraminifers *Praeorbulina glomerosa* (BLOW), and *Uvigerina macrocarinata* P.-T. is characteristic for the oldest Neogene deposits from the borehole

K. Fordinál, A. Nagy et al.: New knowledge about stratigraphy...

271

Tab. 4 Representation of the individual palynomorph species (genera) in borehole HGŽ-3

Taxon/depth	154,0 m	154,1 m	154,5 m	353,9 m	451,5 m	550,2 m	650,9 m
Osmunda sp.							
Leiotriletes sp.							
Laevigatosporites sp.							
Taxodium sp.							
Sciadopytis type							
Abies type							
Cedrus sp.							
Picea type							
Pinus type sylvestris							
Pinuspollenites type haploxylon							
Tsuga type							
Podocarpus type							
Chenopodiaceae							
Liquidambar type							
Castanea sp.							
Fagus sp.							
Quercus sp.							
Alnus sp.							
Betula sp.							
Carpinus sp.							
Corylus sp.							
Myrica type							
Carya sp.							
Engelhardtia sp.							
Momipites sp.							
Juglans sp.							
Pterocarya type							
Salix type							
Tilia sp.							
Ulmus sp.							
Zelkova sp.							
Acer type							
Rhus type							
Ilex sp.							
Nyssa sp.							
Asteraceae							
Poaceae							

Occurence: rare
common
abundant
very abundant

HGŽ-3 (770.5-916.0 m), representing the Bajtava Formation, and restricted only to the Lower Badenian (Moravian), in the central Paratethys. From the calcareous nannoplankton the most abundant was the species *Coccolithus pelagicus* (WALLICH) SCHILLER and biostratigraphically interesting *Sphenolithus heteromorphus* DEFLANDRE indicating zone NN5.

They are averlain (200.0 – 770.5 m) by Middle and Upper Badenian deposits representing the Pozba Formation.

In the depth interval 572.5 – 770.5 m there are deposits of Middle Badenian age, for which presence of foraminifers of species *Globigerina nepenthes* TODD and *Uvigerina aculeata orbignyana* CZJZ., indicating a Middle Badenian age is typical. Only a poor association of the calcareous nannoplankton was obtained there. Forms with a wide stratigraphic range were established there and except of them also *Sphenolithus heteromorphus* DEFLANDRE indicating zone NN 5 was determined. Also large amount of diatoms was identified. In these deposits also otoliths *Diaphus* ex. gr. *debilis* (KOK.), *Photichtys* sp. and *Bregmaceros* sp. were found. The presence of deep-water species *Photichtys* sp. suggests the deposition environment at the boundary between sublittoral and bathyal zone (by Brzobohatý, oral information).

In the palynospectrums of Middle Badenian deposits there are abundant forms of needles of genus *Pinus*, which abundant by continues gradually up to the Upper Badenian. Obvious occurrences of hydrophilous vegetation with representatives of *Myrica, Alnus, Salix* type are interesting. Despite the higher percentage of hydrophilous taxons we cannot speak about the existence of swamps in the area. The climate must have been very warm and humid, because in the palynospectrum more abundant of representatives of paleotropic geoflora (*Castanea*) were present.

In strata overlying Middle Badenian deposits, in depth interval 200.0 – 572.5 m there are Upper Badenian deposits.

The composition of the Upper Badenian palynospectrums was in comparison with the Middle Badenian not distinctly different on the contrary, it seems to be, insignificant differences are in sporadical to common occurrence of some taxons in depth 353.9 m, in comparison with samples from greater depths (*Cedrus, Picea, Quercus, Tilia, Zelkova, Acer* type, *Rhus*). The dominance of hydrophilous vegetation is obvious also here (*Alnus, Myrica, Salix* type). Abundant are also *Carya, Ulmus* and mainly *Pinus*. Also in this depth interval there is dominance of arctotertiary elements over paleotropical, which occured only rarely, is unambiguous.

For Upper Badenian deposits from borehole HGŽ-3 the Bolivina-Bulimina association is characteristic. The present species are: *Bulimina elongata elongata* ORB., *B.* elongata longa (VENGL.), *B. insignis* LUCZKOWSKA. *Bolivina dilatata dilatata* RSS., *B. dilatata maxima* C.-Z., *B. dilatata brevis* C.-Z., *B. kodymi* C.-Z., *B. pokornyi pokornyi* C.-Z., *B. hebes* MACF., *Fursenkoina acuta* (ORB.), *Praeglobobulimina pupoides* (ORB.), *Praeglobobulimina ovula* (ORB.), *Valvulineria marmaroschensis* PISHV. and *Globigerina druryi* AKERS. In the mentioned deposits there was identified a mixture of redeposited nannofossils coming from Upper Cretaceous, Paleogene and Neogene deposits.

Pozba Formation is overlain by the Vráble Formation in the depth interval 10-200 m. The presence of gastropods of genus *Mohrensternia* that indicates Lower Sarmatian age, bivalves of species *Musculus sarmaticus* (Gatujev) and genus *Cardium* was established in the lower part of the formation. From foraminifers there were found *Elphidium flexuosum flexuosum* (ORB.), *E. rugosum* (ORB.), *Bolivina sarmatica* DIDK., "*Cibicides badenensis*" (ORB.), *Lobatula lobatula* (W.- J.), *Ammonia beccarii* (L.). Foraminifers are accompanied by centric, mostly pyritized diatoms. From the microfauna ostracods of species *Cytheridea hungarica* ZÁLANYI were also found there. Their occurrence indicates the Lower Sarmatian ostracod biozone Cytheridea hungarica - Aurila mehesi (Zelenka, 1990).

Redeposited associations of calcareous nannoplankon, consisting of forms coming from Eocene and older Miocene horizons, were found in the mentioned deposits.

Representatives of arctotertiary geoflora of group A1 and from paleotropic group P2 (*Engelhardtia*) are prevailing in the palynospectrums of Lower Sarmatian deposits. By presence of swampy vegetation elements the

composition of the palynospectrum in this depth interval is different from the Middle to Upper Badenian deposits. In the first place there are autochthonous elements of the association Taxodium – Alnus – Myrica – Nyssa, along with abundant occurrences of *Ulmus, Carya, Juglans, Corylus* type. The herbal portion of the growth was represented by halophytes from the family Chenopodiaceae and grasses Gramineae (Poaceae).

Conclusions

The borehole HGŽ-3 contributed to closer understanding of the geological and stratigraphic settings of the Želiezovce Depression.

In the basement of the Tertiary deposits there were metamorphosed Mesosoic carbonates belonging to the South Veporicum envelope encountered in borehole. Overlying them were identified organodetrital limestone of Oligocene (? Egerian) age, which resemble in their appearance position and presence of foraminifers to Budikovany Member from depressions of Lučenecká kotlina and Rimavská kotlina.

Overlying Oligocene deposits there were identified Middle Miocene deposits of the Neogene filling of the Želiezovce Depression. Deposits of the Bajtava (Lower Badenian), Pozba (Middle to Upper Badenian) and Vráble (Sarmatian) Formations were identified here.

The Neogene deposits from the borehole HGŽ were correlated with deposits of faciestratotype boreholes in the area of the Želiezovce Depression and deep borehole ŠV-8 (Fig. 3).

Determination of the stratigraphic stages was based on stratigraphic range of the individual fossil groups.

The Lower Badenian deposits were identified on the basis of foraminifers (*Praeorbulina glomerosa* (BLOW), *Uvigerina macrocarinata* P.-T.) and calcareous nannoplankton of zone NN5 (*Sphenolithus heteromorphus* DEFLANDRE).

The deposits of the Middle Badenian age were determined according to foraminifers *Globigerina nepenthes* TODD and *Uvigerina aculeata orbignyana* CZJZ. similarly as Upper Badenian deposits, for which the presence of Bolivina-Bulimina association was characteristic.

The Sarmatian deposits were identified according to molluscs (*Mohrensternia* sp., *Musculus sarmaticus* (GATUJEV)), foraminifers, (*Elphidium flexuosum flexuosum* (ORB.), *E. rugosum* (ORB.), *Bolivina sarmatica* DIDK.) and ostracods (*Cytheridea hungarica* ZÁLANYI).

According to presence of deepwater fish type of genus Photichtys we assume that the deposits of Middle Badenian age were sedimented on the boundary between sublittoral and bathyal zone.

Sporomorphs found in the Middle to Upper Badenian deposits indicate the presence of hydrophilous flora represented by forms of *Myrica, Alnus, Salix* type. The mentioned association testifies to a warm and humid climate. The sediments of Lower Sarmatian age are characterized by the presence of palustrine vegetation element. In first order there are autochthonous elements of the association Taxodium – Alnus – Myrica – Nyssa, and simultaneous abundant occurence of *Ulmus, Carya, Juglans, Corylus* type.

References

Bondarenková, Z., Michalič, J., Michalíček, M. & Procházková, V., 1990: Želiezovce - kúpalisko. Manuskript – archív ŠGÚDŠ, Bratislava (in Slovak).

Brestenská, E., 1974: 8. Faziostratotypus: Hontianska Vrbica bei Levice, Bohrung ŽG-1. Westslowakische Donautiefebene, Tschechoslowakei. In: Papp, A., Marinescu, F., Seneš, J., 1974: Chronostratigraphie und Neostratotypen, Miozän der Zentralen Paratethys IV, M5, Sarmatien, Veda, Bratislava, 192-195.

Brestenská, E., 1978a: 6. Faziostratotypus: Salka bei Štúrovo, Bohrung K-5, Westslowakische Donautiefebene, Tschechoslowakei (Unter/Mittelbaden; Moravien/Wielicien; Lageniden/Sandschalerzone). In: Papp, A., Cicha, I., Seneš, J., Steininger, F.: Chronostratigraphie und Neostratotypen, Miozän der Zentralen Paratethys IV, M4 Badenien (Moravien, Wielicien, Kosovien), Veda, Bratislava, 175-184.

Brestenská, E., 1978b: 7. Faziostratotypus: Lontov bei Želiezovce, Bohrung ŽI-2, Westslowakische Donautiefebene, Tschechoslowakei (Mittel/Oberbaden; M4cd; Wielicien/Kosovien; Sandschaler/ Buliminen-Bolivinen Zone). In: Papp, A., Cicha, I., Seneš, J., Steininger, F.: Chronostratigraphie und Neostratotypen, Miozän der Zentralen Paratethys IV, M4 Badenien (Moravien, Wielicien, Kosovien), , Veda, Bratislava, 184-188.

Brestenská, E. & Jiříček, R., 1978: Ostrakoden des Badenien der Zentralen Paratethys. In: Papp, A., Cicha, I., Seneš, J., Steininger, F.: Chronostratigraphie und Neostratotypen, Miozän der Zentralen Paratethys IV, M4 Badenien (Moravien, Wielicien, Kosovien), Veda, Bratislava, 405-439.

Engler, A., 1879: Versuch einer Entwicklungsgeschichte der Pfflanzenwelt seit der Tertiärperiode. Leipzig W. Engelmann, 203 p.

Engler, A., 1882: Versuch einer Entwicklungsgeschichte der Pfflanzenwelt seit der Tertiärperiode. Leipzig W. Engelmann, 333 p.

Folk, R. L. & Ward, W., 1957: Brazos river bar: a study in the significance of grain size parametres. Journal of sedimentary petrology, 27, 1,

Fordinál, K., Nagy, A. & Vass, D., 2001: Problémy stratigrafie a litostratigrafie vrchného miocénu dunajskej panvy. Mineralia Slovaca 33, 1, 7-14 (in Slovak, English resume).

Gabčo, R., 1965: Sedimentárno-petrografické vyhodnotenie sedimentárneho komplexu vrtu K-V pri Salke. Manuskript – archív ŠGÚDŠ Bratislava (in Slovak).

Gabčo, R., 1969: Správa o sedimentárno-petrografickom výskume pliocénnych a miocénnych sedimentov vo vrte ŽG-1 na liste Želiezovce. Manuskript – archív ŠGÚDŠ Bratislava (in Slovak).

Halásová, E., Hudáčková, N., Holcová, K., Vass, D., Elečko, M. & Pereszlényi, M., 1996: Sea ways connecting the Fiľakovo/Pétervására Basin with the Eggenburgian/Burdigalian open sea. Slovak Geol. Mag., 2, 351-362.

Harčár, J., Priechodská, Z., Karolus, K., Karolusová, E., Remšík, A. & Šucha, P., 1988: Vysvetlivky ku geologickej mape severovýchodnej časti Podunajskej nížiny 1: 50 000. Geol. Úst. D. Štúra, Bratislava, 114 s. (in Slovak, English resume).

Hók, J., Kováč, M., Kováč, P., Nagy, A. & Šujan, M., 1999: Geology and tectonics of the NE part of the Komjatice Depression. Slovak Geol. Mag., 5, 3, 187-199.

Ivan, Ľ., 1960: Zpráva o geologickom mapovaní na top. pláne Želiezovce. Geol. práce, Zpr. (Bratislava), 20, 177-182 (in Slovak, Deutsch resume).

Jiříček, R., 1982: Stratigrafické pomery v neogéne žitavského zálivu. In: Slovák, Ľ., Hromada, J., Tabak, J., Jezný, M., Urban, V. & Bondarenková, A., 1983: Žitavský záliv – lignit. Manuskript – archív ŠGÚDŠ, Bratislava (in Slovak)

Keith, J. F., Vass, D. & Kováč, M., 1994: The Danube Lowland basin. ESRI Publication, new series, No 11A Slovakian Geology, Memorial to T. Koráb, 63-86.

Lehotayová, R., 1966: Zpráva zo štruktúrneho vrtu K-V - Salka (mikrobiostratigrafia). Manuskript – archív ŠGÚDŠ Bratislava, (in Slovak).

Lehotayová, R. & Ondrejičková, A., 1972: Mäkkýše a mikrofauna z vrtu ŠO-1 (Chľaba). Manukript – archív ŠGÚDŠ Bratislava (in Slovak).

Mai, D. H., 1981: Entwicklung und klimatische Differenzierung der Laubwaldflora Mitteleuropas in tertiär. Flora , Jena, 171, 525-582.

Mai, D. H., 1991: Paleifloristic changes in Europe and the confirmation of the Arctotertiery-Paleotropical concept. Rev. Palaeob. Palyn. (Amsterdam) 68, 1, 29-36.

Matura, A., Czászár, G., Kröll, A., Vozár, J., Wessely, G., 2000: Map of the pre-tertiary basement. Danube Region Environmental Geology Programme DANREG, Explanatory notes. Jb. Geol., 142,4, Wien, 465-482.

Mišík, M., 1958: Sedimentárno-petrografické vyhodnotenie vzoriek z vrtu ŽI-2 (Lontov, okres Želiezovce). Manuskript – archív ŠGÚDŠ, Bratislava (in Slovak).

Nagy, A., Halouzka, R., Konečný, V., Lexa, J., Fordinál, K., Havrila, M., Vozár, J., Liščák, P., Stolár, M., Benková, K. & Kubeš, P. 1998: Vysvetlivky ku geologickej mape Podunajskej nížiny, východná časť 1: 50 000. Geologická služba Slovenskej republiky, 187 s. (in Slovak, English resume).

Ondrejičková, A., 1978: Chľaba bei Štúrovo, Bohrung ŠO-1, Westslowakische Donautiefebene, Tschechoslowakei. In: Chronostratigraphie und Neostratotypen, Miozän der Zentralen Paratethys IV, M4 Badenien (Moravien, Wielicien, Kosovien), Veda, Bratislava, 173-175.

Papp, A., 1954: Die Molluskenfauna im Sarmat des Wiener Beckens. Mitt. Geol. Ges. in Wien 45, 112 s.

Planderová, E., 1965a: Palynologický výskum na liste Šahy. Manuskript - archív ŠGÚDŠ Bratislava (in Slovak).

Planderová, E., 1965b: Palynologické vyhodnotenie vzoriek z vrtov ŽG-1 a ŽG-4 z Hontianskej Vrbice. Manuskript – archív ŠGÚDŠ Bratislava (in Slovak).

Planderová, E., 1966: Dielčia záverečná zpráva zo štruktúrneho vrtu K-V - Salka (palynologické zhodnotenie vrtu). Manuskript – archív ŠGÚDŠ Bratislava (in Slovak).

Seneš, J. & Ondrejičková, A., 1991: Proposal for the terminology of fossil marine benthic shelf ecosystem. Geologica Carpathica 42, 4, 231-240.

Sitár, V., 1965: Základný geologický výskum severných a sv. výbežkov Podunajskej nížiny. Manuskript – archív ŠGÚDŠ Bratislava (in Slovak)

Sitár, V., 1967: Tertiärflora aus der Umgebung von Levice. Acta geol. et geogr. Univ. Com. 12, Bratislava, 155-162.

Švagrovský, J., 1965: Biostratigrafické rozčlenenie súvrství preniknutých vrtom ŽG-1 podľa fauny mäkkýšov. Manuskript – archív ŠGÚDŠ, Bratislava (in Slovak).

Tejkal, J., 1968: Fauna měkkýšu a vývoj biotopu v tortonu okolí Želiezovcu (Podunajská nížina). Folia Přír. fak. Univ. J.E. Purkyně v Brne, 9, Geologia (Brno) 13,1, 1-58 (in Czech, Deutsch resume).

Vass, D., 1964: Vyhodnotenie fauny molluskov z vrtu K-V Salka. Manuskript-archív ŠGÚDŠ Bratislava, (in Slovak).

Vass, D., 1966: Dielčia záverečná zpráva zo štruktúrneho vrtu K-V - Salka (vyhodnotenie fauny molluskov). Manuskript – archív ŠGÚDŠ, Bratislava, (in Slovak).

Vass, D., Began, A., Gross, P., Kahan, Š., Krystek, I., Köhler, E., Lexa, J., Nemčok, J., Ružička, M. a Vaškovský, I. 1988: Vysvetlivky k mape Regionálne geologické členenie Západných Karpát a severných výbežkov Panónskej panvy na území ČSSR. Geol. Úst. D. Štúra, Bratislava, 65 s. (in Slovak, English resume).

Vass, D., Brestenská, E., Fejdiová, O., Franko, O., Gazda, S., Lehotayová, R., Marková, M., Ondrejičková, A., Planderová, E., Reichwalder, P. a Vozárová, A., 1981: Štruktúrny vrt ŠV-8 (Dolné

274

Semerovce, Ipeľská pahorkatina). Reg. geológia Západných Karpát 14, 106 s. (in Slovak).

Vass, D., Elečko, M., Pristaš, J., Lexa, J., Hanzel, V., Modlitba, I., Jánová, V., Bodnár, J., Husák, Ľ., Filo, M., Májovský, J. & Linkeš, V., 1989: Geológia Rimavskej kotliny. Geol. Úst. D. Štúra Bratislava, 162 s. (in Slovak, English resume).

Vass, D. & Elečko, M. (ed.), Bezák, V., Bodnár, J., Pristaš, J., Konečný, V., Lexa, J., Molák, B., Straka, P., Stankovič, J., Stolár, M., Škvarka, L., Vozár, J. & Vozárová, A.,1992: Vysvetlivky ku geologickej mape Lučenskej kotliny a Cerovej vrchoviny 1 : 50 000. Geol. Úst. D. Štúra Bratislava,196 s. (in Slovak).

Vass, D. & Gabčo, R., 1966: Záverečná zpráva zo štruktúrneho vrtu K-V - Salka (geologická časť). Manuskript – archív ŠGÚDŠ Bratislava, (in Slovak).

Vaškovský, I., Bárta, R., Hanzel, V., Halouzka, R., Harčár, J., Karolus, K., Pristaš, J., Remšík, A., Šucha, P., Vass, D. & Vaškovská, E., 1982: Vysvetlivky ku geologickej mape juhovýchodnej časti Podunajskej nížiny. Geol. Úst. D. Štúra Bratislava, 115 s. (in Slovak, English resume).

Zelenka, J., 1990: A rewiew of the Sarmatian Ostracoda of the Vienna Basin. In: Ostracoda and Global Events. British Micropaleont. Soc. Publ. London, Chapman and Hall, 263-270.

K. Fordinál, A. Nagy et al.: New knowledge about stratigraphy...

275
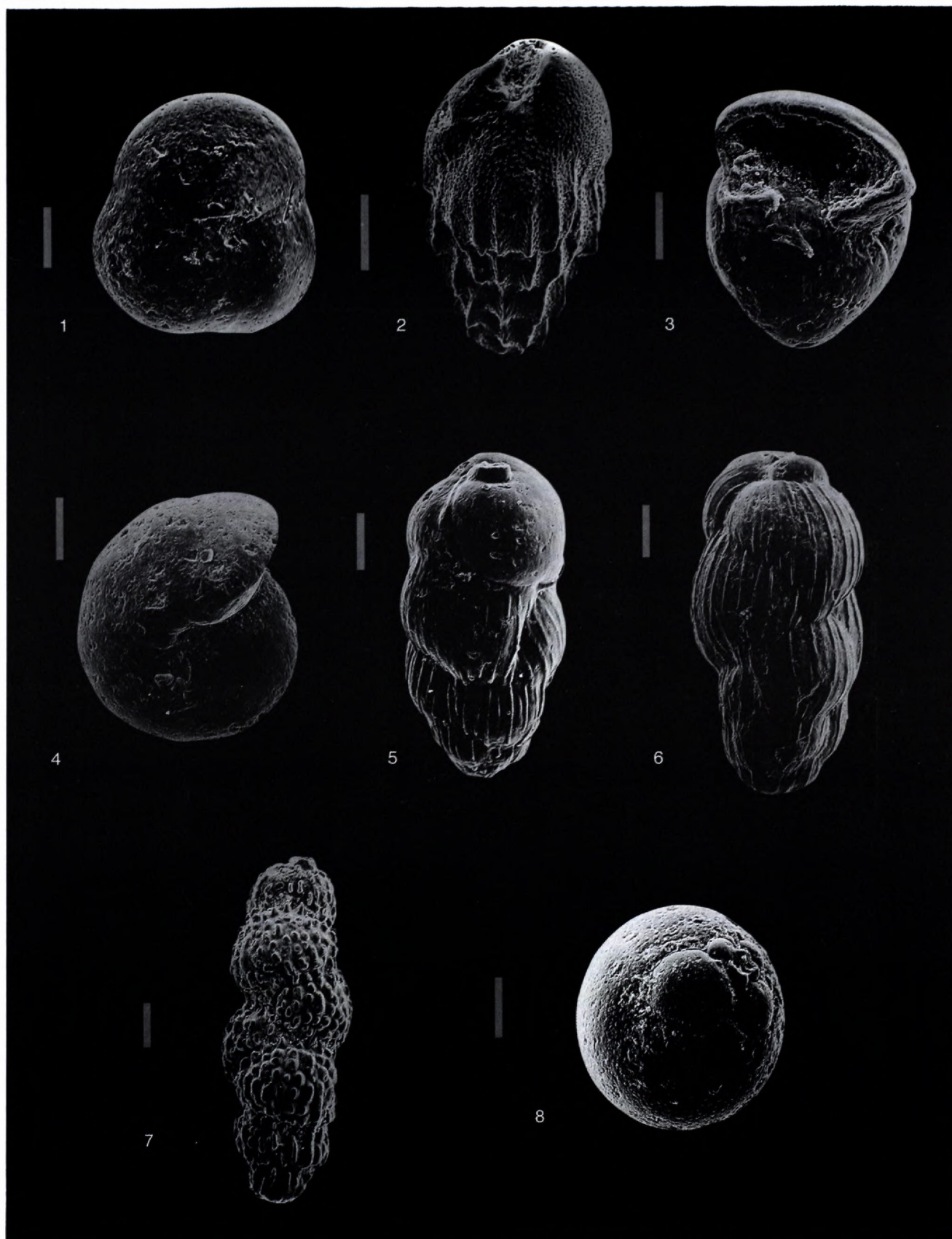
PHOTOTABLE I
1 – *Sphaeroidina bulloides* Orb., 550.2 m; 2 – *Bulimina striata mexicana* Cush., 550.2 m; 3-4 – *Hansenisca soldanii* Orb., 550.2 m; 5-6 – *Uvigerina semiornata semiornata* Orb., 550.2 m; 7 – *Uvigerina semiornata kusteri* Daniels-Spiegler, 559.1 m; 8 – *Orbulina suturalis* Broenn., 801.3 m.

PHOTOTABLE II
1 – *Globigerina praebulloides* Blow, 250.5 m; 2 – *Haplophragmoides* ex. gr. *vasiceki* C.-Z., 251.8 m; 3 – *Praeglobobulimina pupoides* (Orb.), 251.8 m; 4 – *Nonion commune* (Orb.), 251.8 m; 5 – *Bulimina elongata elongata* Orb., 254.8 m; 6 – *Bolivina dilatata maxima* C.-Z., 254.8 m; 7 – *Orbulina suturalis* Broenn., 453.3 m; 8 – *Globigerinoides trilobus* (Rss.), 453.3 m; 9 – *Globigerinoides subsacculifer* Cita-Premoli-Silva-Rossi.

K. Fordinál, A. Nagy et al.: New knowledge about stratigraphy...

277
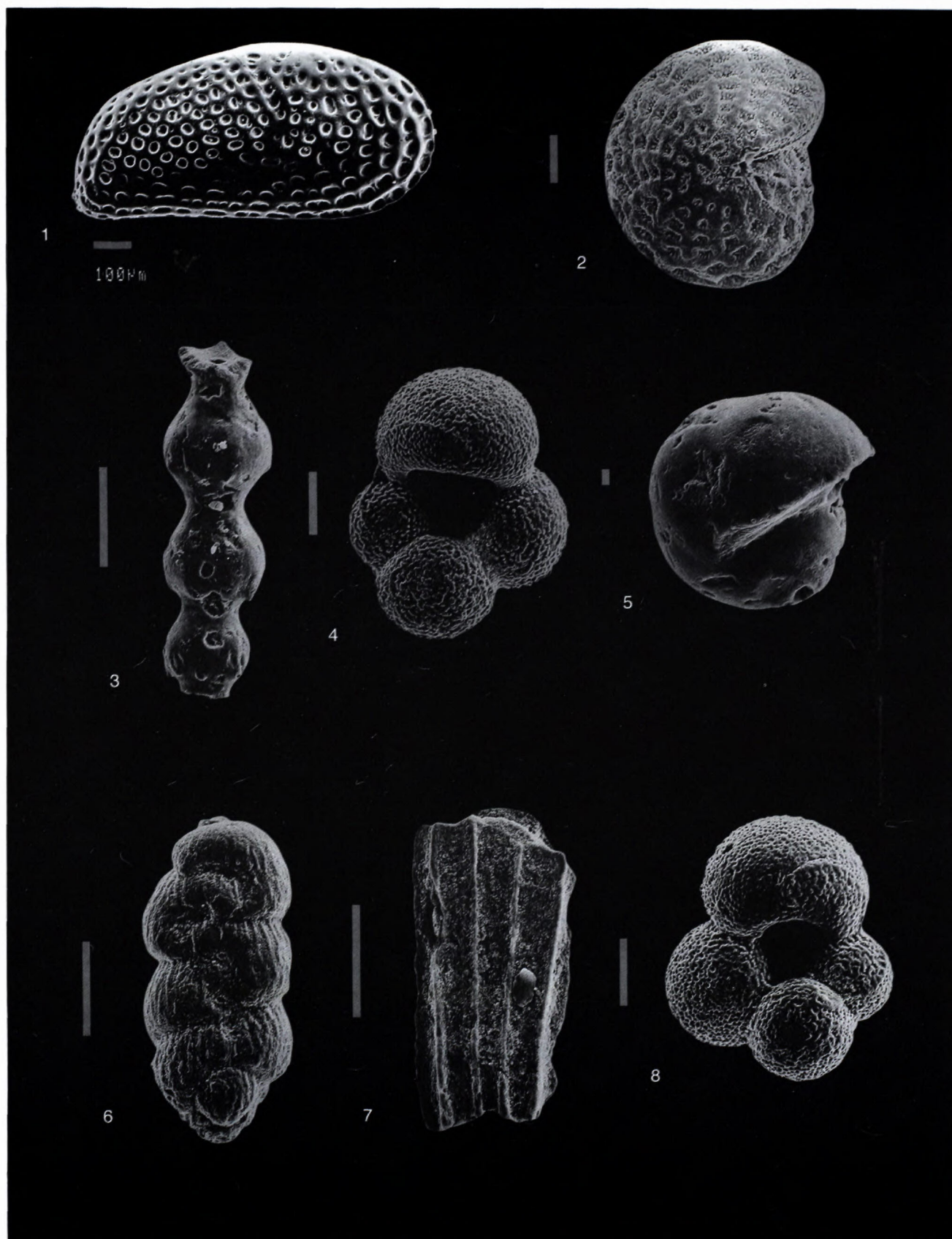
PHOTOTABLE III

1 – *Cytheridea hungarica* (ZAL.), 154.0 m; 2 – *Elphidium flexuosum flexuosum* (ORB.), 154.0 m; 3 – *Stilostomella adolphina* (ORB.), 250.5 m; *Globigerina praebulloides* BLOW, 250.5 m; 5 – *Pullenia bullodes* (ORB.), 250.5 m; 6 – *Pappina bononiensis primiformis* (P.-T.), 250.5 m; 7 – *Plectofrondicularia digitalis* (NEUGEB.), 250.5 m; 8 – *Globigerina praebulloides* BLOW, 250.5 m.

278

Slovak Geol. Mag., 8, 3– 4(2002), 259 – 281
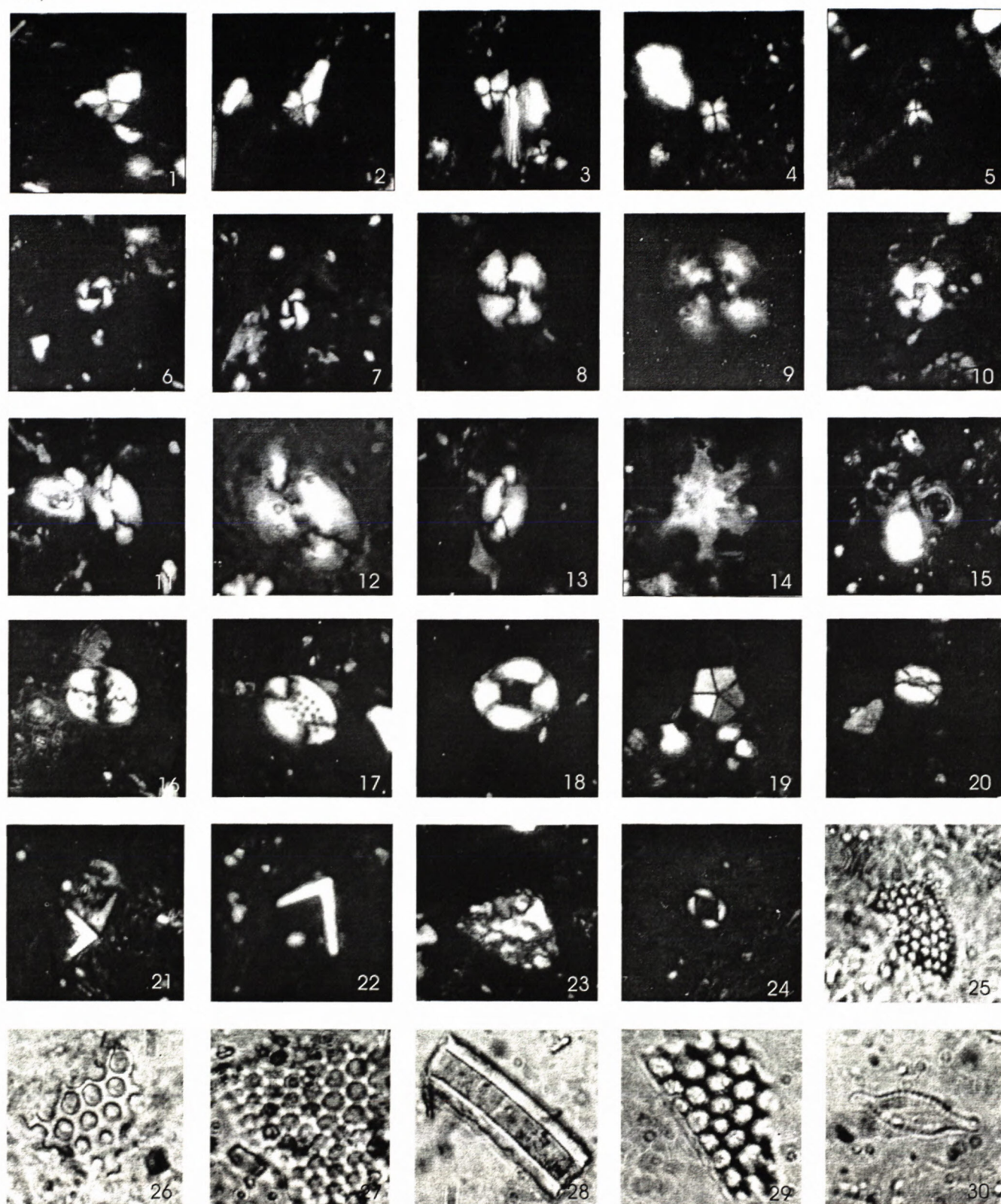
PHOTOTABLE IV

1 – 3 *Sphenolithus heteromorphus* DEFLANDRE, 250.5 – 250.6 m; 4 – *Sphenolithus abies* DEFLANDRE, 250.5 – 250.6 m; 5 – *Sphenolithus moriformis* (BRÖNNIMANN & STRADNER), 250.5 – 250.6 m; 6 – 7 *Reticulofenestra pseudoumbilicus* (GARTNER) GARTNER, 250.5 – 250.6m; 8 – 10 *Cyclicargolithus floridanus* (ROTH & HAY) BUKRY, 250.5 – 250.6 m;,154.6 — 154.7m; 11 – *Helicosphaera waltrans* THEODORIDIS, 250.5 – 250.6 m; 12 – *Helicosphaera* cf. *waltrans* THEODORIDIS, 154.6 – 154.7 m; 13 – *Helicosphaera carteri* (WALLICH) KAMPTNER, 457.5 – 457.6 m; 14 – *Discoaster* sp., 154.6 – 154.7 m; 15 – *Umbilicosphaera rotula* (KAMPTNER) VAROL, 250.5-250.6 m; 16 – *Pontosphaera enormis* (LOCKER) PERCH-NIELSEN, 250.5 –250.6 m; 17 – *Pontosphaera multipora* KAMPTNER (ROTH), 250.5 – 250.6 m; 18 – *Pontosphaera latelliptica* (BÁLDI-BÉKE) PERCH-NIELSEN, 250.5 –250.6 m; 19 – *Braarudosphaera bigelowii* (GRAN & BRAARUD) DEFLANDRE, 250.5 – 250.6 m; 20 – *Lanternithus minutus* STRADNER, 250.5 – 250.6 m; 21 – *Micrantholithus vesper* DEFLANDRE 250,5 – 250.6 m; 22 – *Micrantholithus flos* DEFLANDRE (GRAN & BRAARUD) DEFLANDRE, 250.5-250.6 m; 23 – ?*Litostromation perdurum* DEFLANDRE, 250.5 – 250.6 m; 24 *Syracosphaera pulchra* LOHMANN, 250.5 – 250.6m; 25 – 30 diatom, 154.6 –154.7 m; 30 *Fragilaria construens* (Ehrenberg) Grün. Photo by : E. Halásová; Photo n. 25, 26, 27, 28, 29, 30 magnification 1500x ; the rest magnification 1900x

K. Fordinál, A. Nagy et al.: New knowledge about stratigraphy...

279
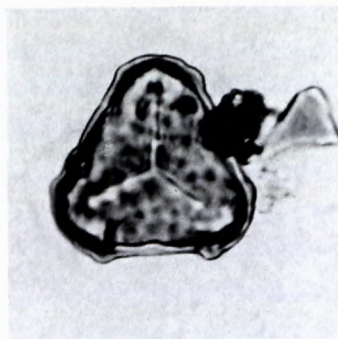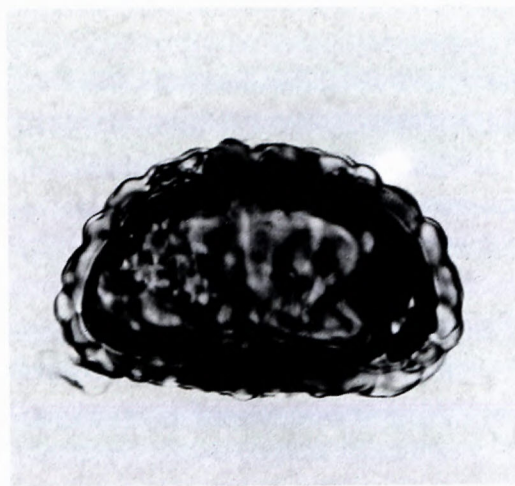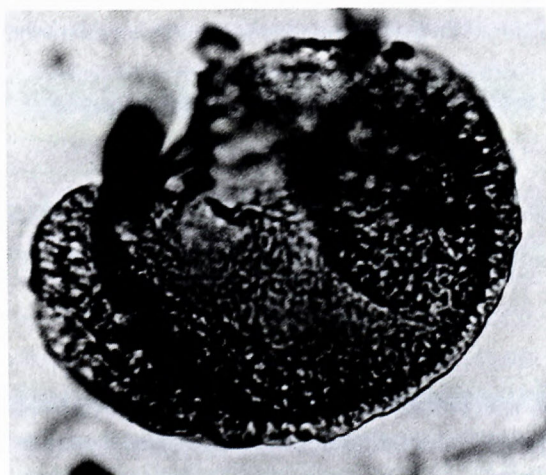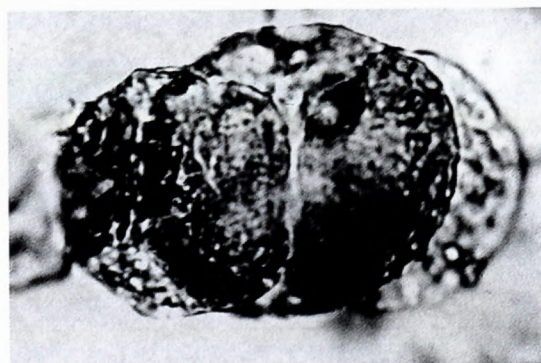
PHOTOTABLE V

1 – *Leiotriletes* sp., 650.9 m; 2 – Polypodiaceae, 650.9 m; 3 – *Laevigasporites* sp., 451.5 m; 4 – *Pinuspollenites* type haploxylon, 154.5 m; 5 – *Cedrus* sp. 154.5 m; 6 – *Pinus* type *sylvestris.*, 550.2 m,
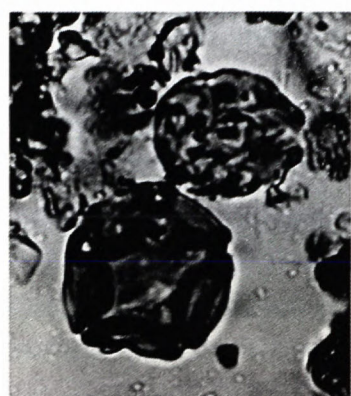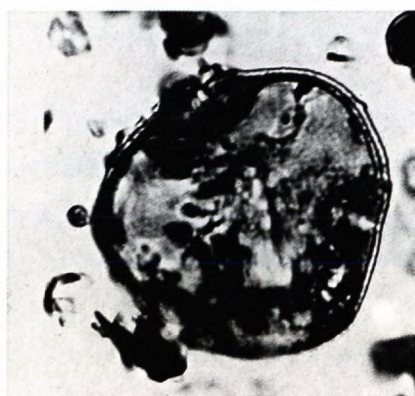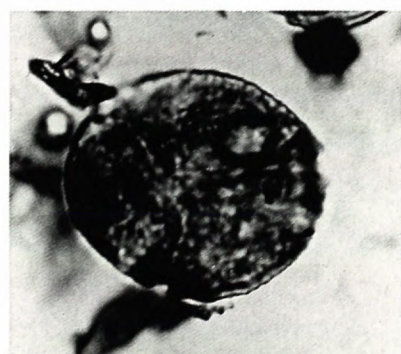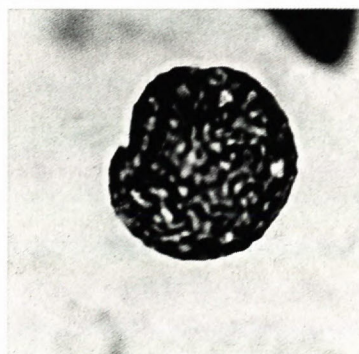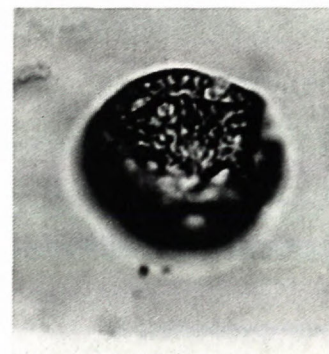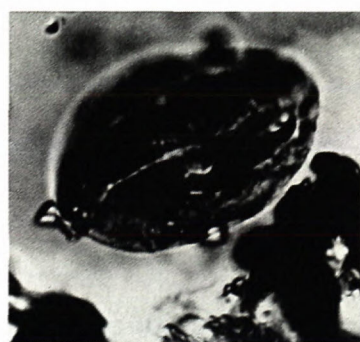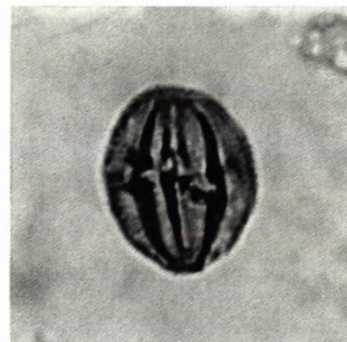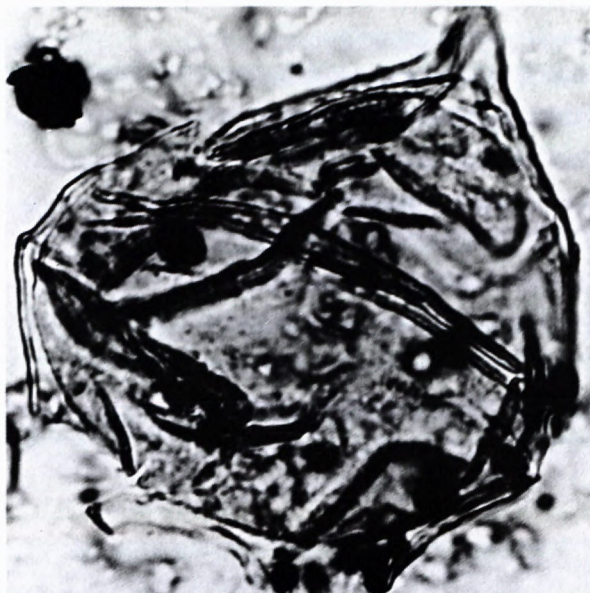
Slovak Geol. Mag., 8, 3–4(2002), 259–281

280
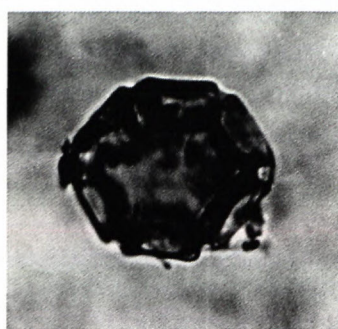
PHOTOTABLE VI

1 – *Pterocarya* type, 154.5 m; 2 – *Alnus* sp., 154.5 m; 3 – *Alnus* sp., 650.9 m; 4 – *Alnus* sp., 154.5 m; 5 – *Tilia* sp., 353.9 m; 6 – *Tilia* sp., 451.5 m; 7 – *Fagus* sp, 353.9 m; 8 – *Ulmus* sp., 451.5 m; 9 – *Liquidambar* type, 650.9 m; 10 – *Rhoipites* sp. 353.9 m; 11 – *Castanea* type, 650.9 m; 12 – *Castanea* type, 550.2 m..
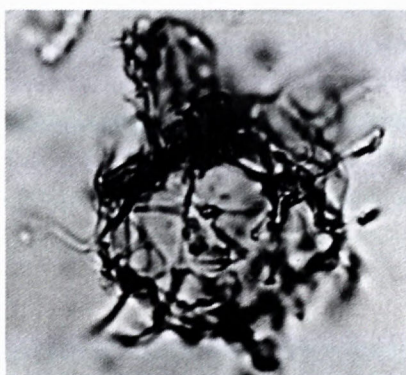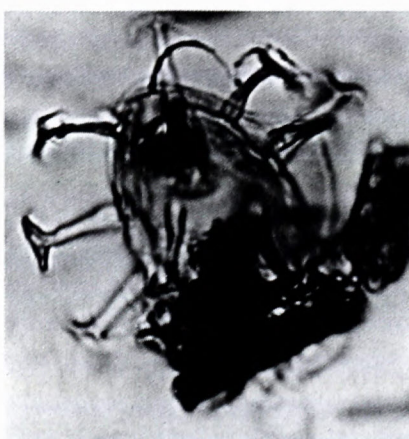
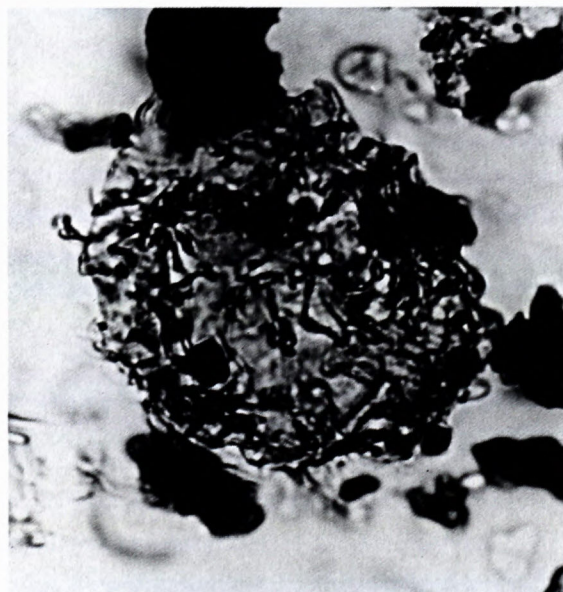K. Fordinál, A. Nagy et al.: New knowledge about stratigraphy...

281

FOTOTABLE VII
1 – *Defrandrea spinulosa* (redepozit), 154.1 m; 2 – *Spiriferites* cf. *bentori*, 353.9 m; 3 – *Achomospaera* sp., 154.5 m; 4 – *Distatodinium* sp., 550.2 m; 5 – *Cyclonephelium* cf. *vicinum* s EATON (redepozit), 353.9 m.
Photo by: M. Slamková; Magnification: 1000 x

Study of the Hokusho landslides in northern Kyushu, Japan and similar failures in the region of neogene volcanics, Slovakia

RÓBERT JELÍNEK[1], HIROSHI OMURA[2] and YUURI YAMAGUCHI[2]

[1]Geological Survey of Slovak Republic, Kynceľovská 10, 974 01 Banská Bystrica
[2]Kyushu university, Faculty of Agriculture, Department of Forestry, 812-8581 Fukuoka, Higashi-ku, Hakozaki 6-10-1, Japan

Abstract. Specific geologic, hydrologic, morphologic conditions together with a combination of high precipitation in northern Kyushu make this area prone to various types of slope movements. For example, the recent large-scale disaster caused by torrential downpours in July 1972 around Kumamoto and Nagasaki or in 1982 in Nagasaki and many others, included numerous debris flows and also human casualties: 543 deaths in the 1972 event and 493 deaths in the 1982 event (Japan Landslide Society, 2001). According to the Slope Conservation Division (1997), the Nagasaki prefecture has 135 designated landslide-treated areas of 2,788.16 ha under the jurisdiction of the Ministry of Land, Infrastructure and Transport.

In the present paper common slope movements that occur in northwestern Kyushu, so called the *Hokusho* landslide in Japanese literature, are studied. Moreover, a practical example of the Shiraidake landslide in Nagasaki prefecture is discussed. The main causes and factors influencing the slope stability of the landslide are summarized. It can be concluded that a combination of geology, hydrogeology with heavy rainfall are the main causes for landslides in this area.

Finally, a comparison between the *Hokusho* landslides and similar types of slope movements, developed in the region of *Neogene volcanics* in Slovakia, is also presented. Whereas the material of underlying rocks is almost the same in both areas, the cap rocks of the *Hokusho* landslides are composed of basalts, while in the region of *Neogene volcanics* these rocks are usually andesites and their pyroclastics. In the case of morphologic features, the landslides in the *Neogene volcanics* occur in higher altitudes with high relative relief.

Key words: Hokusho-type landslide, Matsuura Basalt, landslides in the region of Neogene volcanics

1. Introduction

Japan has suffered from many landslides and natural disasters since ancient time. The country is predominantly mountainous - about three-fourths of the national land are mountains. The mountain region displays a wide variety of topography with steep terrain in the stage of maturity. Furthermore, the islands are located within a monsoon zone of abundant rainfall. The combination of steep terrain and intensive rainfall often leads to landslides (Japan Landslide Society, 2001).

A number of authors, e.g. Varnes (1978), Nemčok (1982), Dikau et al. (1997) have classified landslides according to their material composition, type, velocity of movement, etc. Based on the velocity, landslides in Japan are classified into two categories: *Jisuberi* represents sliding and *Hokai* rapid failure. The occurrence of landslides in Japan is closely related to the geological conditions. Therefore, depending on the geological features, classically according to Koide (1955) landslides are classified into three categories: *Tertiary system, fracture zone* and *hydrothermal zone* landslides.

The *Tertiary system* represents the areas of the highest frequency of landslide occurrence on the Japanese islands. They are distributed mainly along the Sea of Japan and are rather dominant in the Tohoku, Hokuriku, northern Kyushu and San in, as shown in Fig. 1.

These landslides consist mostly of Neogene and some Paleogene semi-consolidated clastic materials and volcanic rocks, which overlie Mesozoic and Paleozoic sedimentary rocks, metamorphic rocks, intrusive rocks and plutonic rocks. Non-siliceous mudstones easily weather or decay into clays due to increased water content. Alteration of volcanic rocks ejected from the sea bottom changes the color to a greenish appearance, and thereafter they are called "green tuff". Tuffaceous mudstones contain abundant smectite clays, and contribute to one of the primary causative factors of landslides (Japan Landslide Society, 2001). Tertiary landslides often occur on gentle slopes and the movement velocity tends to be slow. According to Shuzui (2001), recurrent movement can be found in these types of landslides. The Ishikura landslide, Nagasaki prefecture, can be used as an example where the movement was first activated in 1952-53 and reoccurred in 1990.

The present work deals with a study of common type of landslides in the *Tertiary system* named the *Hokusho-type* in general. Furthermore, a practical example of the *Hokusho-type*, the Shiraidake landslide in Nagasaki prefecture, has been selected for a detailed study. To under-
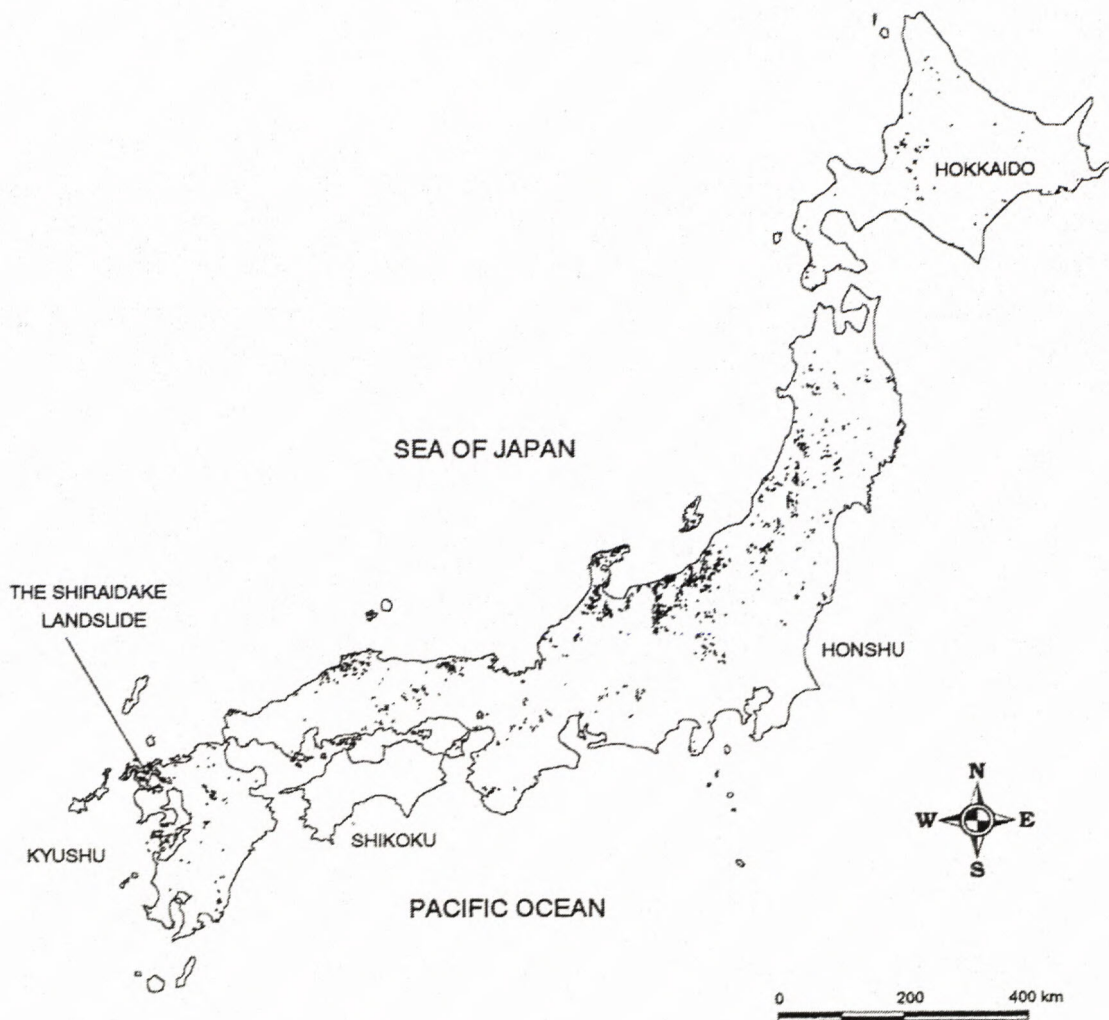
SEA OF JAPAN

THE SHIRAIDAKE
LANDSLIDE

HOKKAIDO

HONSHU

KYUSHU

SHIKOKU

PACIFIC OCEAN

N
W E
S

0   200   400 km

Fig. 1: Distribution of the Tertiary landslides in Japan (according to the Slope Conservation Division 1997)

stand the mutual relationship of the studied *Hokusho* landslides and the similar types of slope movements on the border of *Neogene volcanics* in Slovakia, a review and comparison of the above was carried out.

2. Geological background and history of the Hokusho landslide

The *Hokusho* landslides developed along the boundary between northern Nagasaki prefecture and Saga prefecture. They are named after Hokusho region in the northwest part of Matsuura, Kyushu. Landslides in this area are very frequent. The famous sites are for example: the Ishikura landslide, the Ningyooishiyama landslide, the Hirakoba landslide, the Koba landslide, the Washiodake landslide and many others.

Northwestern Kyushu is characterized by a remarkable volcanism that produced the alkali *Matsuura Basalt* during the Late Miocene and Pliocene with subsidiary andesite and rhyolite volcanism occurring nearby. The basaltic lava flows occurred repeatedly, in period be-

tween 10.6 and 2.7 Ma (Kimura et al. 1991). When molten basalt flow cools rapidly on the earth's surface, systematic cooling joints develop vertically. The basalt is further disintegrated by morphological processes. This disturbed material assists water infiltration into deep cracks along joints and subsequently promotes weathering. Moreover, presence of the discontinuous *Hatinokubo Gravel Formation,* inserted between igneous cap rocks and underlying sedimentary rocks serves, as an aquifer system. As generally accepted, ground water is the dominant inducting factor and the driving force of a landslide. An increasing ground water level increases pore water pressure within a slope and consequent reduction of shear strength can often lead to a landslide. Furthermore, the rigid basaltic body overloads the upper parts of slopes. The load may increase the shear stress and the pore water pressure, which induces a decrease in the strength and cause deep landslides in the underlying soft sedimentary rocks. The *Matsuura Basalt* flows overlie the early Tertiary sedimentary rocks, the *Kishima* and the *Sasebo Groups*, dominated by sandstone, mudstone, shale and
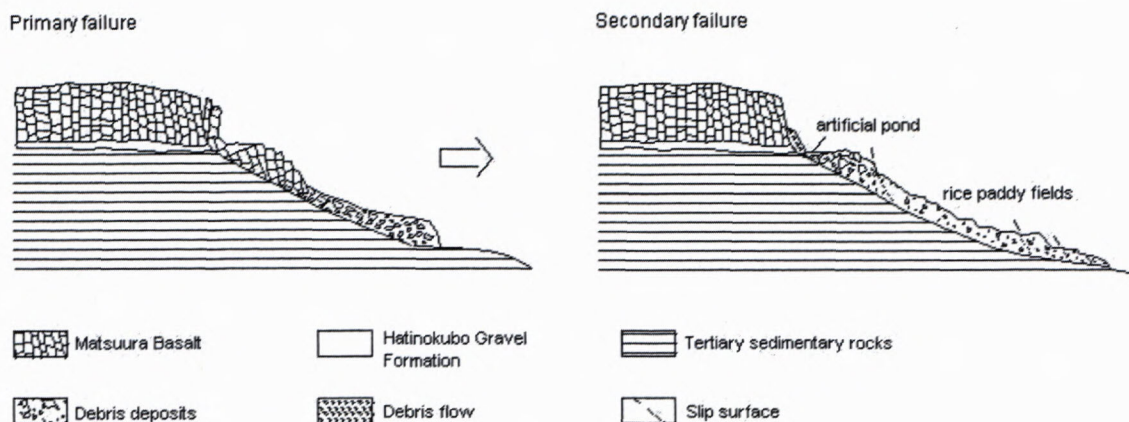
Primary failure

Secondary failure

artificial pond

rice paddy fields

Matsuura Basalt

Hatinokubo Gravel Formation

Tertiary sedimentary rocks

Debris deposits

Debris flow

Slip surface

Fig. 2: Development of the Hokusho-type landslide (modified after Yamazaki 1980 in Karakida et al. 1992)

gravel. Sandstone and shale/mudstone layers consist of 2-3 thick tuffaceous layers accompanied by thin coal seams. This tuffaceous layers with clay prepare typical environment for the development of a slip surface. Therefore, landslides occur over much of the area.

The *Hokusho* landslides start to slide in front of block failures and block fields, which spread laterally on the marginal parts of the capped basalt layers as primary failures. They are combined with slides or debris flows as secondary failures, as shown in Fig. 2. The secondary failures often developed after agricultural utilization of their gentle slopes. These are usually cultivated as rice paddy fields, which require a lot of water. To supply water for the paddy fields an artificial pond is often built in the upper part of a landslide, which of course can support underground water.

3. The Shiraidake landslide

3.1 Location and general characteristics

The Shiraidake landslide is located in the Nagasaki prefecture, northwestern part of Kyushu. The landslide developed on the west-side slope of the Shiraidake Mountain, which elevation is 358.8 m, on the right bank of the Tsukinokawa River. The type of movement is a moderately deep-seated secondary slide, the *Hokusho* landslide. Some general views of the Shiraidake landslide are shown on Photos 1 and 2. The former shows the landslide area with the cross section 1-1' on the left, whilst the later shows detailed view of the landslide on the right side of the photograph. Fig. 3 illustrates the Shiraidake landslide and the cross section 1-1'.

The size of the investigated area is about 1.4 x 1.75 km. Terrain elevation ranges from 60 to 190 m asl. (above sea level), the slope is generally gentle up to 10°. Due to Japanese geographical location between North latitude 45° 33' and 20° 25', the climate varies considerably from north to south, with marked seasonal change. Japan, except of Hokkaido, is generally a rainy country with high humidity in summer. The studied area can be characterized as warm climate with mild dry winters and hot humid summers. According to the nearest meteorological station in Sasebo city, the annual precipitation

varies between 2,000 and 2,500 mm (Bulletin, 1995-1999). However, it is necessary consider that the annual evaporation is about one third of the annual precipitation. Fig. 4 illustrates monthly precipitation in this area during five years starting from January 1995 till December 1999.

As can be seen, up to 70 % of the annual precipitation falls during 4 months between June and September. The monthly precipitation culminates in June and July, when the seasonal rain front moves progressively from the southernmost island toward the north. These rains often cause landslides and debris flow disasters. Typhoons usually generate strong winds and heavy rainfall, which cause flooding, sedimentation disasters and landslides. In the spring, numerous landslides are triggered by underground water, supplied from snowmelt on the slopes facing the Sea of Japan (Japan Landslide Society, 2001). The average annual temperature in the investigated area is about 16.2°C with an average minimum temperature 5.8°C in January and an average maximum temperature of 26.4°C in July (Bulletin, 1995-1999).

A comprehensive survey of the landslide area from geologic, geomorphologic and hydrologic points of view was done during the sliding activity between years 1952 and 1997. According to the activity of landslide at Shiraidake, the whole area was divided into five blocks A, B, C, D and E (Report, 1997). The investigation works were mainly conducted in the most active B and E blocks, where all the boreholes are concentrated. The data were collected from the surveys, and a simple spatial database was created. The database provided some general information about the investigated landslide and was also used as input data layers to calculate the slope stability. According to the records, the depth of the slip surface varies from 4.7 m at foot and head up to 23.0 m in the middle part of the landslide. Likewise, the ground water level through the landslide area varies from 1.0 m at foot to 9.5 m at head, corresponding to about 40 % of depth.

3.2 Geological setting and mechanism of the Shiraidake landslide

Tertiary sedimentary rocks of the *Fukui Formation* and the *Kase Formation* underlie the landslide. Both formations belong to the *Sasebo Group*, which is about

Photo 1: The Shiraidake landslide with longitudinal profile 1-1' illustrated on the left
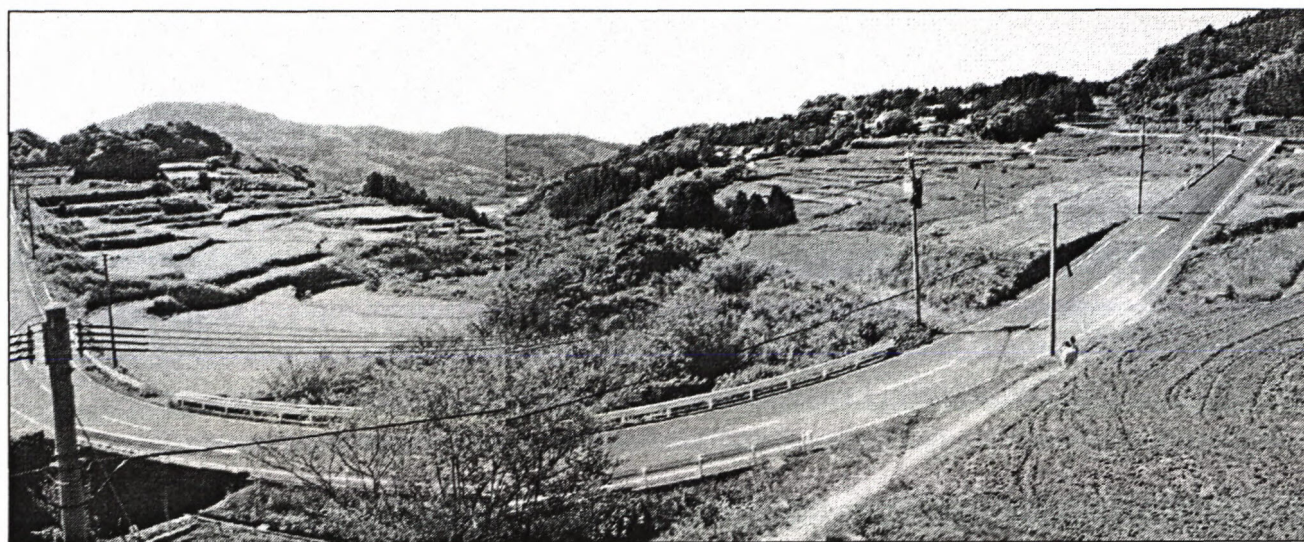

Photo 2: Detailed photo of the Shiraidake landslide (right side)

Photo 3: Gentle slopes of the Shiraidake landslide cultivated for rice paddy fields, which are sometimes full of water

1,000 to 1,600 m thick and composed of eight formations. The uppermost *Kase Formation* cosist of marine mudstone. Each of the other formations is composed of a single cyclothem that begins with a layer of marine or brackish facies and ends with a non-marine coal seam. All the strata consist of monocline structures, which are inclined gently towards the northwest. Near the summit these sedimentary rocks are overlain by the *Matsuura Basalt* as well as by the Quaternary deposits. According

to the Geological map of the Saga prefecture (Kinoshita et al. 1954) the thickness of the basalt flow is between 50 and 150 m, occasionally 300 m.

The Shiraidake landslide belongs to the *Tertiary system* of landslides, representing the highest frequency of landslide occurrence in Japan. Landslides are usually caused by complex factors. In the Shiraidake landslide the following causal factors can be summarized:
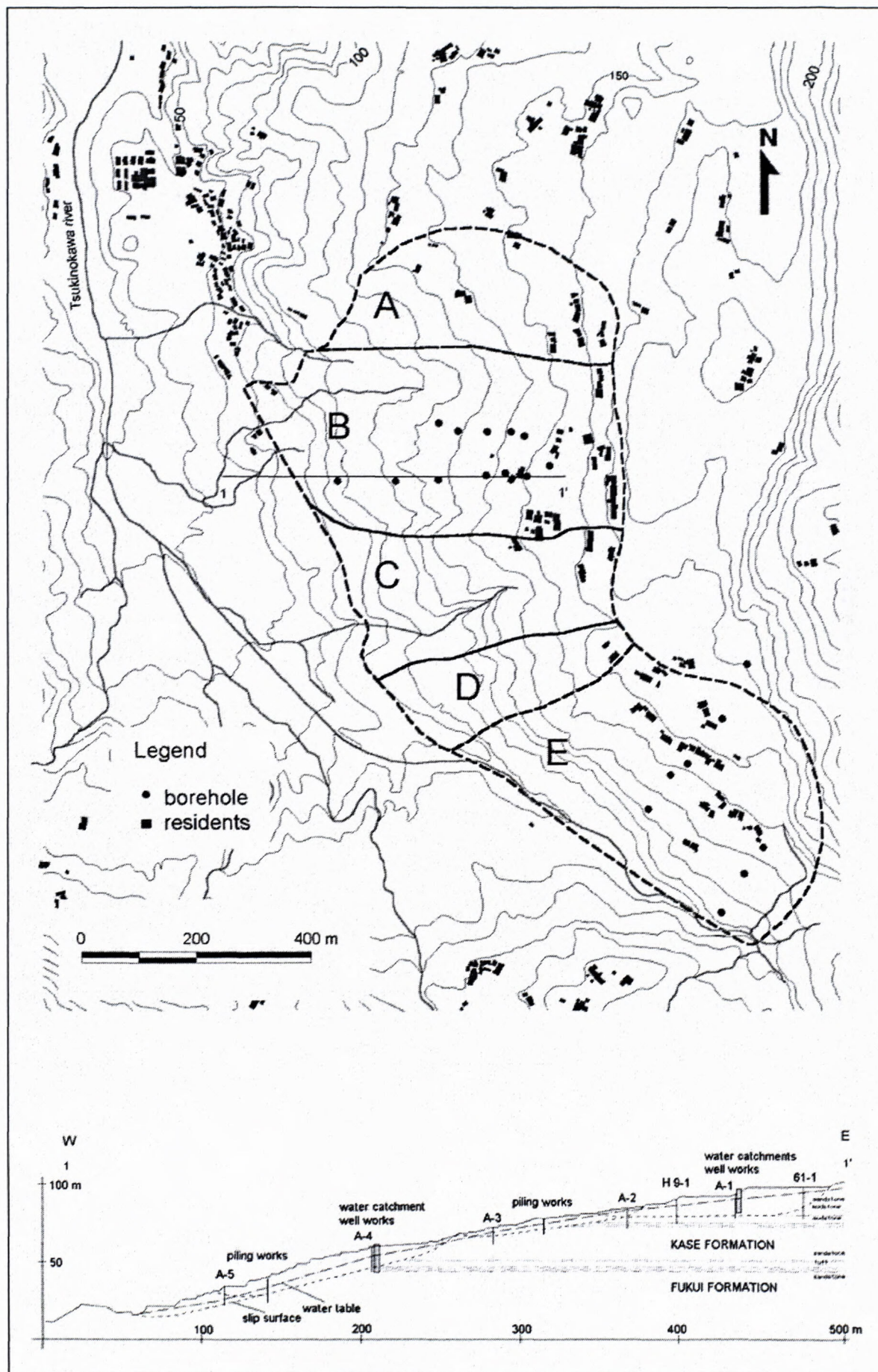
Fig. 3: The Shiraidake landslide with the cross section 1-1' through the B block
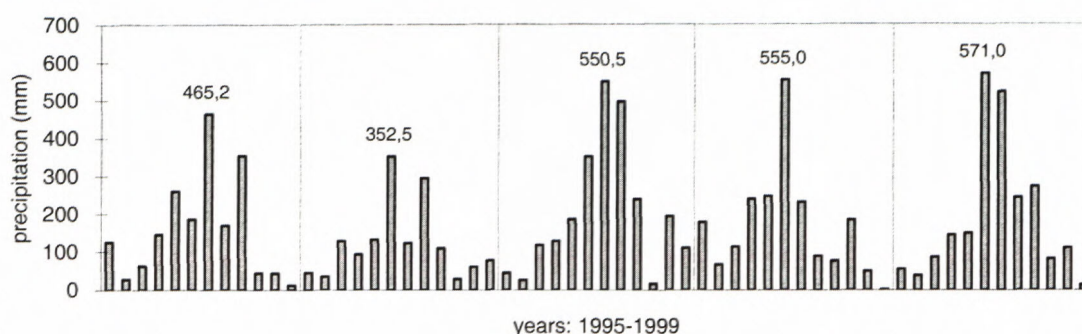
288

Slovak Geol. Mag., 8, 3 – 4(2002), 283 – 290

Fig. 4: Monthly precipitation chart for Sasebo city during the period 1995-1999

Table 1: Comparison of some general characteristics of the Hokusho landslides in the Tertiary covering sediment zones in Japan and the landslides in the region of Neogene volcanics in Slovakia

Parameters	Hokusho-type landslide in the Tertiary covering sediment zones in Japan	Landslides in the region of Neogene volcanics in Slovakia
Cap rock/era	Matsuura Basalt, Late Miocene, Pliocene	Andesite and their pyroclastics, rhyolite, basalt and their tuffs, Tortonian (Middle Miocene) Sarmatian (Upper Miocene)
Underlying rock/era	Semiconsolidated Tertiary sedimentary rocks: tuffaceous mudstones, shale, sandstone, coal seams, pyroclastic rocks	Pelitic and aleuric shales of Paleogene or semicon-solidated fine-grained strata, i.e. clayey-silty-sand rocks of Neogene
Climate	Warm temperate climate with four seasons, rainy season and typhoons; mild dry winters and hot humid summers	Continental climate with four distinct seasons; warm and mild, dry to moderately warm and humid
Average annual precipitation	2,000-2,500 mm	650-1,000 mm
Relief type	Hilly mountains with moderately steep slopes dissected by valleys	Intensively structured upland and highland type
Height	200-400 m asl.	900-1,490 m asl.
Relative relief	50-300 m	150-600 m
Slope angle	<10 °	6-8 °
Maximum landslide's dimensions	Width 4 km, length 5 km	Width 5.5 km, length 2 km (continuous landslide's ranges)
Maximum depth of slip surface	100 m	40 m
Failure types	Lateral spreading, block failures, block fields, landslides, debris flow, rock fall	Block failures, block fields, sliding of blocks, land-slides, flow, surficial and deep seated creep, rock fall

(1) Favorable geological structure and lithology, i.e. the sliding surface forms along a bedding plane and along intercalation of coal seams between tuff layers, where the contact of strata can act as a slip plane.

(2) Intensive weathering. Geographical regions with much rainfall and warm temperatures such as Japan have led to weathering of natural materials. This usually implies that these regions also have the deepest soils, which can be a potential risk of a landslide.

(3) Formation of smectite in the slip-surface mudstone (Yagi et al. 1999). Smectite can originate as an alterion product of tuff, contacted with groundwater. In particular, smectite is one of the clay minerals with lower frictional resistance, and supply for slip surface in fine clastic sedimentary rocks, such as mudstone (Shuzui 2001).

(4) Interbedded impermeable and permeable rocks, Quaternary gravel layer with the possibility of formation of a perched aquifer system.

(5) Much and extremely intensive precipitation in the area (the annual precipitation up to 2,500 mm).

(6) The undulating relief terrain of the area. A gentle dip slope (up to 10°) is typical for the occurrence of such landslides.

The slope has been stabilized by the effective retaining structures. The area is covered by vegetation; the gentle slopes are cultivated by rice paddy fields (Photo 3). There are also some residences in upper parts of the slope. The last landslide activity was recorded in the 1990's (Report, 1997).

Table 1

Parameters	Hokusho-type landslide in the Tertiary covering sediment zones in Japan	Landslides in the region of Neogene volcanics in Slovakia
Cap rock/era	Matsuura Basalt, Late Miocene, Pliocene	Andesite and their pyroclastic, rhyolite, basalt and their tuffs, Tortonian (Middle Miocene) Sarmatian (Upper Miocene)
Underlying rock/era	Semiconsolidated Tertiary sedimentary rocks: tuffaceous mudstones, shale, sandstone, coal seams, pyroclastic rocks	Pelitic and aleuric shales of Paleogene or semi-consolidated fine-grained strata, i.e. clayey-silty-sand rocks of Neogene
Climate	Warm temperate climate with four seasons, rainy season and typhoons; mild dry winters and hot humid summers	Continental climate with four distinct seasons; warm and mild, dry to moderately warm and humid
Average annual precipitation	2,000-2,500 mm	650-1,000 mm
Relief type	Hilly mountains with moderately steep slopes dissected by valleys	Intensively structured upland and highland type
Height	200-400 m asl.	900-1,490 m asl.
Relative relief	50-300 m	150-600 m
Slope angle	$<10°$	$6-8°$
Maximum landslide's dimensions	Width 4 km, length 5 km	Width 5.5 km, length 2 km (continuous landslide's ranges)
Maximum depth of slip surface	100 m	40 m
Failure types	Lateral spreading, block failures, block fields, landslides, debris flow, rock fall	Block failures, block fields, sliding of blocks, landslides, flow, surficial and deep seated creep, rock fall

4. Slope movements in the region of neogene volcanics in Slovakia

Similar features and subsequently the types of the slope movements such as the *Hokusho* landslides in northwestern Kyushu, where the cap rock formations of hard component overly soft incompetent formations, are common in recent or past volcanic regions, as for example in Italy, Irkutsk and Siberian Plain in Russia, Washington, Oregon, Idaho, Colorado, Arizona and New Mexico in the USA, New Zealand (Nemčok, 1982), Konkan coast in India and Cooee in north-west Tasmania (Nagarajan et al. 2000). Likewise, these type of slope movements are developed in the region of *Neogene volcanics* in Slovakia, where rigid volcanic materials, predominantly andesites and their pyroclastics, rhyolites and basalts, overly soft, plastic and weakly cemented sedimentary rocks, i.e. pelitic and aleuritic shales of Paleogene or clayey-silty-sand rocks of Neogene (Nemčok, 1982). In order to understand the relationship between the *Hokusho* landslides in Japan and the landslides in *Neogene volcanics* in Slovakia, a literature review (Japan Landslide Society, 2001; Shuzui, 2001; Nemčok, 1982; Matula & Pašek 1996 and many other unpublished data) and subsequent comparison of some general features was carried out (Table 1).

By comparing the above sites it was found that the cap rocks of the *Hokusho* landslide are composed of basalt, while andesite and their pyroclastics are dominant rocks in the region of *Neogene volcanics*. Underlying rocks are built by quite similar units of semiconsolidated Tertiary sedimentary rocks. The climate shows considerable variation, it is warm and continental. The average precipitation is 2-3 times higher in the area of the *Hokusho* landslide than in Slovakia. From geomorphologic point of view, the landslides in the *Neogene volcanics* occur in higher altitudes with high relative relief, while the area in the *Hokusho* landslide shows a softer relief with smaller variation in relative relief. The dimensions of landslide and the slip surface depth are a little bit larger in the *Hokusho* landslides. It is likely that many failures are combinations of several different failure modes: slides or debris flows are linked to lateral spreads; a slide can also develop into a flow form at the toe, or a deep-seated creep on the margin of the highlands can transform into a rock fall.

5. Conclusions

This paper presented some of the general features and factors contributing to the slope stability in the *Hokusho-type* landslides in northern Kyushu. Based on the infor-

Slovak Geol. Mag., 8, 3 – 4(2002), 283 – 290

290

mation obtained, it can be concluded that the main causes of the Shiraidake landslide are a combination of hydrological and geological settings of the area, deep and intensive weathering. The triggering factor was probably an increase in the ground water level after heavy rainfall during the rainy season from early June up to middle of July or during typhoon season in September. This is supported by very high monthly precipitations up to 571 mm.

Comparison between the *Hokusho* landslide and the slope movements in the region of *Neogene volcanics* showed some similarities between the studied sites. Some similar characteristics are related to the material of the underlying rock. The main differences are in the composition of cap rocks, which are basalts in the *Hokusho* landslides and andesites with their pyroclastics in the *Neogene volcanics.* From the morphological point of view, the landslides in the *Neogene volcanics* occur at higher altitudes with high relative relief, while areas in the *Hokusho* landslide show a softer relief with smaller variation in relative relief.

Acknowledgements

References

Bulletin, 1995-1999: Monthly bulletin of weather in Nagasaki prefecture. Nagasaki Ocean Weather Association, MS - Kyushu University, Fukuoka, (in Japanese).

Dikau, R., Brundsen, D., Schrott, L. & Ibsen, M.L., 1997: *Landslide recognition. Identification, movement and causes,* John Wiley & Sons, Chichester-New York-Brisbane-Toronto-Singapore, 251 p.

Japan Landslide Society, 2001: *Landslides in Japan.* Published by Japan Landslide Society, National Conference of Landslide Control, URL: http://www.cc.tuat.ac.jp/~sabo/lj/index.htm

Karakida, Y., Hayasaka, S. & Hase, Y., 1992: *Regional Geology of Japan.* Part 9 Kyushu, Published by Kyoritsu Shuppan CO., LTD., (in Japanese).

Kimura, T., Hayami, I. & Yoshida, S., 1991: *Geology of Japan.* University of Tokyo Press, 287 p.

Kinoshita, K., Tanaka, S., Matsukuma, T. (1954) Geology and Natural Resource in Saga prefecture and Geologic map of Saga prefecture, 1:100 000, Saga prefecture government, 141 p. (in Japanese).

Koide, H., 1955: *Landslides in Japan.* Toyokeizai Tokyo, Japan, 256 p. (in Japanese).

Matula, M. & Pašek, J., 1996: *Regional enginnering geology of Czechoslovakia.* ALFA Bratislava, Slovakia, 295 p. (in Slovak).

Nagarajan, R., Roy, A., Vinod Kumar R., Mukherjee A. & Khire, M.V., 2000: Landslide hazard susceptibility mapping based on terrain and climatic factors for tropical monsoon regions. Springer-Verlag, *Bull Eng Geol Env,* vol. 58, p. 275-287.

Nemčok, A., 1982: *Landslides in the Slovak Carpathians.* VEDA Bratislava, Slovakia, 319 p. (in Slovak, English summary).

Report, 1997: Shiraidake landslide area counter-plan construction work. Fujinagatiken Company and Nagasaki prefecture, northern area promotion affair, Tabira public work office, Investigation report. (in Japanese).

Shuzui, H., 2001: Process of slip-surface development and formation of slip-surface clay in landslides Tertiary volcanic rocks, Japan. *Engineering Geology,* vol. 61, p. 199-219.

Slope Conservation Division, 1997: Landslides in Japan. Published by Sabo Publicity Center, Editorial Supervision, Sabo Department River Bureau, Ministry of Land, Infrastructure and Transport

Varnes, D.J., 1978: *Slope movement type and processes.* In: Landslides analysis and control, Schuster, R.L. and Krizek, R.J., (eds) National Research Council, Transportation Research Board, Special Report 176, pp. 11-33.

Yagi, N., Yatabe, R., Yokota, K. & Bhandary, N.P., 1999: Strength of landslide clay from mineralogical point of view. In: *Proceedings Slope stability engineering,* Yagi, N., Yamada, T. & Jiang, J., (eds) Balkema, Rotterdam, pp. 701-704.

Instructions for authors

Slovak Geological Magazine – periodical of the Geological Survey of Slovak Republic is quarterly presenting the results of investigation and researches in wide range of topics: regional geology and geological maps, lithology and stratigraphy, petrology and mineralogy, paleontology, geochemistry and isotope geology, geophysics and deep structure, geology of deposits and metallogeny, tectonics and structural geology, hydrogeology and geothermal energy, environmental geochemistry, engineering geology and geotechnology, geological factors of the environment, petroarcheology.

The journal is focused on problems of the Alpine-Carpathian-Balkan region

General instructions

The Editorial Board of the Geological Survey of Slovak Republic – Dionýz Štúr Publishers accepts manuscripts in correct English. The papers that do not have sufficient accuracy in language level will be submitted back for language correction.

The manuscript should be addressed to the Chief Editor or the Managing Editor.

Contact address:

Geological Survey of Slovak Republic – Dionýz Štúr Publishers, Mlynská dolina 1, 817 04 Bratislava, Slovak Republic

e-mail addresses: hok@gssr.sk
gabina@gssr.sk
http://www.gssr.sk

The Editorial Board accepts or refuses a manuscript with regard to the reviewer's opinion. The author is informed of the refusal within 14 days from the decision of the Editorial Board. Accepted manuscript is prepared for publication in an appropriate issue of the Magazine. The author(s) and the publishers enter a contract establishing the rights and duties of both parties during editorial preparation and printing, until the time of publishing of the paper.

Text layout

The manuscript should be arranged as follows: TITLE OF THE PAPER, FULL NAME OF THE AUTHOR(S); NUMBER OF SUPPLEMENTS (in brackets below the title, e.g. 5 figs., 4 tabs.), ABSTRACT (max. 30 lines presenting principal results) – KEY WORDS – INTRODUCTION – TEXT – CONCLUSION – ACKNOWLEDGEMENTS – APPENDIX – REFERENCES – TABLE AND FIGURE CAPTIONS – TABLES – FIGURES. The editorial board recommends to show a localisation scheme at the beginning of the article.

The title should be as short as possible, but informative, compendious and concise. In a footnote on the first page, name of the author(s), as well as his (their) professional or private address.

The text of the paper should be logically divided. For the purpose of typography, the author may use a hierarchic division of chapters and sub-chapters, using numbers with their titles. The editorial board reserves the right to adjust the type according to generally accepted rules even if the author has not done this.

Names of cited authors in the text are written without first names or initials (e.g. Štúr, 1868), the names of co-authors are divided (e.g. Andrusov & Bystricky, 1973). The name(s) is followed by a comma before the publication year. If there are more authors, the first one, or the first two only are cited, adding et al. and publication year.

Mathematical and physical symbols of units, such as %, ‰, °C should be preceded by a space, e.g. 60 %, 105 °C etc. Abbreviations of the units such as second, litre etc. should be written with a gap. Only SI units are accepted. Points of the compass may be substituted by the abbreviations E, W, NW, SSE etc. Brackets (parentheses) are to be indicated as should be printed, i.e. square brackets, parentheses or compound. Dashes should be typed as double hyphens.

If a manuscript is typed, 2 copies are required, including figures. The author should mark those parts of a text that should be printed in different type with a vertical line on the left side of the manuscript. Paragraphs are marked with 1 tab space from the left margin, or by a typographic symbol. Words to be emphasized, physical symbols and Greek letters to be set in other type (e.g. *italics*) should be marked. Greek letters have to be written in the margin in full (e.g. *sigma*). Hyphens should be carefully distinguished from dashes.

Tables and figures

Tables will be accepted in a size of up to A4, numbered in the same way as in a text.

Tables should be typed on separate sheets of the same size as text, with normal type. The author is asked to mark in the text where the table should be inserted. Short explanations attached to a table should be included on the same sheet. If the text is longer, it should be typed on a separate sheet.

Figures should be presented in black-and-white, in exceptional cases also in colour which must be paid approx. 100 EUR per 1 side A 4. Figures are to be presented by the author simultaneously with the text of the paper, in two copies, or on a diskette + one hard copy. Graphs, sketches, profiles and maps must be always drawn separately. High-quality copies are accepted as well. Captions should be typed outside the figure. The graphic supplements should be numbered on the reverse side, along with the orientation of the figures. Large-size supplements are accepted only exceptionally. Photographs intended for publishing should be sharp, contrast, on shiny paper. High quality colour photographs will only be accepted depending on the judgement of the technical editors.

If a picture is delivered in a digital form, the following formats will be accepted: *.cdr, *.dxf, *.bmp, *.tiff, *.wpg, *.fga., *.jpg *.gif, *.pcx. Other formats are to be consulted with the editors.

References

Should be listed in alphabetical and chronological order **according to annotation in the text** and consist of all references cited.

Standard form is as follows: 1. Family name and initials of author(s), 2. Publication year, 3. Title of paper, 4. Editor(s), 5. Title of proceedings, 6. Publishers or Publishing house and place of publishing, 7. Unpublished report – manuscript should be denoted MS. Unpublished paper can appear as personal communications only. 8. Page range

Quotations of papers published in non-Latin alphabet or in languages other than English, French, Italian, Spain or German ought to be translated into English with an indication of the original language in parentheses, e.g.: (in Slovak).

Example:

Andrusov, D., Bystrický, J. & Fusán, O., 1973: *Outline of the Structure of the West Carpathians.* Guide-book for geol. exc. of Xth Congr. CBGA. Bratislava: Geol. Úst. D. Štúra, 44 p.

Beránek, B., Leško, B. & Mayerová, M., 1979: Interpretation of seismic measurements along the trans-Carpathian profile K III. In: Babuška, V. & Plančár, J. (Eds.): *Geodynamic investigations in Czecho-Slovakia.* Bratislava: VEDA, p. 201-205.

Lucido, O., 1993: A new theory of the Earth's continental crust: The colloidal origin. *Geol. Carpathica,* vol. 44, no. 2, p. 67-74.

Pitoňák, P. & Spišiak, J., 1989: Mineralogy, petrology and geochemistry of the main rock types of the crystalline complex of the Nízke Tatry Mts. MS – Archiv GS SR, Bratislava, 232 p. (in Slovak).

Proofs

The translator as well as the author(s) are obliged to correct the errors which are due to typing and technical arrangements. The first proofs are sent to author(s) as well as to the translator. The second proof is provided only to the editorial office. It will be sent to authors upon request.

The proofs must be marked clearly and intelligibly, to avoid further errors and doubts. Common typographic symbols are to be used, the list and meaning of which will be provided by the editorial office. Each used symbol must also appear on the margin of the text, if possible on the same line where the error occurred. The deadlines and conditions for proof-reading shall be stated in the contract.

Final remarks

These instructions are obligatory to all authors. Exceptions may be permitted by the Editorial Board or the managing editor. Manuscripts not complying with these instructions shall be returned to the authors.

1. Editorial Board reserves the right to publish preferentially invited manuscript and to assemble thematic volumes,

2. Sessions of Editorial Board – four times a year and closing dates for individual volumes will be on every 31th day of March, June, September and December.

3. To refer to one Magazine please use the following abbreviations: *Slovak Geol. Mag.,* vol. xx, no. xx. Bratislava: D. Štúr. Publ. ISSN 1335-096X.